Marine silicon cycle through the Cenozoic

Fontorbe, Guillaume

2016

LUNDQUA THESIS 82

Marine silicon cycle through the Cenozoic

Guillaume Fontorbe

LUND
UNIVERSITY

Quaternary Sciences
Department of Geology

DOCTORAL DISSERTATION
by due permission of the Faculty of Science, Lund University, Sweden.
To be defended at Pangea, Geocentrum II,Sölvegatan 12. Date 2016.05.13 and time 13.15.

Faculty opponent
Martin Frank
GEOMAR Kiel, Germany

Quaternary Sciences
Department of Geology
Faculty of Science

ISBN 978-91-87847-18-9 (print)
ISBN 978-91-87847-19-6 (pdf)
ISSN 0281-3033

Printed in Sweden by Media-Tryck, Lund University, Lund 2016

Organization	Document name
LUND UNIVERSITY Department of Geology Sölvegatan 12 SE-223 62 Lund Sweden	DOCTORAL DISSERTATION
	Date of issue: 2016.05.13
Author(s): Guillaume Fontorbe	Sponsoring organization

Title and subtitle: Marine silicon cycle through the Cenozoic

Abstract

Silicon (Si) cycle is one of Earth's major biogeochemical cycles. Furthermore, the dissolved form of Si (DSi) is an essential nutrient for both terrestrial and marine ecosystems. DSi ultimately derives from the slow process of chemical weathering of silicate minerals, a mechanism that consumes carbon dioxide, and therefore participates in regulating Earth's climate over geologic timescales. Si is delivered to the ocean mostly by rivers and will be used by a variety of organisms (e.g. diatoms, siliceous sponges, radiolarians, and silicoflagellates) that precipitate DSi into an amorphous form (biogenic silica, BSi) and control the export of Si out of seawaters. While the modern Si cycle and the processes controlling it are becoming better and better understood, its evolution through Earth's history are still poorly constrained.

Hence, this thesis aims at shedding more light on the evolution of the marine Si cycle on millennial to million-years timescales. To do so, we investigated the Si isotopic composition (expressed as $\delta^{30}Si$) of siliceous microfossils recovered from marine sediments. The analysis of $\delta^{30}Si$ from the remains of marine diatoms, radiolarians, and siliceous sponges is a powerful tool to reconstruct several facets of the oceanic Si cycle in the past.

On millennial timescales, the marine Si cycle is mostly dominated by variations in biologic productivity in the surface ocean and riverine inputs of DSi. On the other hand, on million-years time scales, the marine Si cycle appears to be mostly controlled by oceanic circulation. Further, the analysis of sponge $\delta^{30}Si$, performed during this thesis, allowed us to reconstruct the concentrations of DSi in the bottom waters in the North Atlantic and Equatorial Pacific. Our results indicate that contrary to previous hypotheses, the ocean did not experience a rapid decline in oceanic DSi content during the Paleogene (65.5 to 23.03 Ma). Conversely, we show that the North Atlantic already had low DSi concentrations, similar to today, during the early Cenozoic, whereas the Equatorial Pacific has become progressively enriched in DSi since at least 35 Ma.

Overall, although research into the evolution of the ocean Si cycle is still at an early stage, the work carried out in this thesis fills some of the existing knowledge gaps regarding the development of the marine Si cycle through geologic times

Key words: Si isotopes, Paleogene, PETM, glacial-interglacial, ocean circulation

Classification system and/or index terms (if any)

Supplementary bibliographical information	Language: English
ISSN and key title: 0281-3033 LUNDQUA THESIS	ISBN 978-91-87847-18-9

Recipient's notes	Number of pages: 107	Price
	Security classification	

Signature: Date: 2016.04.04

"There's always at least two solutions to one problem"
- Élias de Kelliwic'h -

Contents

SS

List of papers

This thesis is based on four papers listed below, which have been appended to this thesis. Paper I has been submitted to *Earth and Planetary Science Letters* and is in revision, Paper II and Paper III are manuscripts,and Paper IV is published in *Chemical Geology.*

Paper I

Fontorbe G., Frings P.J., De La Rocha C.L., Hendry K.R., Conley D.J. (in revision). A silicon depleted North Atlantic since the Palaeogene: evidence from sponge and radiolarian silicon isotopes. Submitted to *Earth and Planetary Science Letters,* in revision.

Paper II

Fontorbe G., Frings P.J., De La Rocha C.L., Hendry K.R., Conley D.J. (manuscript). Enrichment of dissolved silica in the deep Equatorial Pacific during the Eocene-Oligocene. In preparation for *Paleoceanography.*

Paper III

Fontorbe G., Frings P.J., De La Rocha C.L., Hendry K.R., Conley D.J. (manuscript). Marine silicon cycle response to the Paleocene-Eocene Thermal Maximum. Manuscript.

Paper IV

Frings P.J., Clymans W., Fontorbe G., De La Rocha C.L., Conley D.J. (2016). The continental Si cycle and its impact on the ocean Si isotope budget. Chemical Geology 45.

Acknowledgement

As they say, it's not about the destination but the journey. The past four years have been quite an adventure, with loads of ups and very few downs. If it weren't for the contributions, in many forms, from many people, you wouldn't be holding this thesis in your hands right now.

First, I would like to thank my team of supervisors. Daniel, many thanks for giving me the opportunity to live this experience, for all your inputs and constant support, and for copping with my lack of organizational skills. Christina, I have to thank you (or maybe blame you?) for dragging me, six years ago, into the wonderful world of silicon biogeochemistry and turning a clueless student into an isotope nerd. Kate, thanks for all the time you put into our discussions at various meetings and for all the inspiring ideas. Helena and Svante, thank you for your help, inputs and enthusiasm during all these years. I should also thank all the past and present members of the SiCON group for sharing all these scientific and non-scientific times.

Doing a PhD is also a social experience, and I'm happy I could meet so many new people that I can call friends.

To Patrick, my putative mentor, thanks for all the time and effort you put into helping my verbally-challenged self and for all the fun outside of work. Wim, thank you for your immutable sympathy, I think it's the first time I meet somebody who can look so happy 24/7. Florian, thanks for all the deep conversations about the meaning of science and music, and for providing me with a roof during my homeless winter (and sorry for the food poisoning, I should have seen that coming!). To the three of you, I'll only add one thing: So long, and thanks for all the booze!

Nathalie, my favourite Belgian (sorry Wim), thank you for all the smoke breaks, very nice Belgian barbecues, Belgian beers and for all the tipsy fun. Billy, thanks for all the not-so-fast food, I think my cholesterol level has risen drastically since you started your PhD, for your ice hockey obsession (Habs suck by the way), and for your crazy moves on the dance floor. Lorraine, thank you so much for all the fun on Friday nights, the late working evenings during the last few months, for the soups and the crêpes, and for getting all the references to Kaamelott! Jesper, I still need your guitar lessons so I can become a rock star before I turn 28. Laurie, thanks for being you, even when it's clearly better to be a number 7 than a number 1. Tom, thank you for your britishness, even if the empire is clearly not what it used to be. Claire, the Goonies are still waiting for you, hope we can go to a gig soon. Hanna and Carolina, thanks for providing this very enjoyable atmosphere in Silicon Valley.

This list could go on and on, Bryan, Maria, Petra, Nadine, Wenxin, Emma, Anton, Martin, Carla, and many others. So, if you ever held a glass of alcoholic beverage in Ariman shouting "SKÅL" in my company, thank you very much and you're all welcome on my island.

Pour les copains de Brest, Ju, Thomas l'animologue, Thomas Jaud Photographie, Gaspard, Manon, JiKa, Gwenn, Loïc, et tous les autres, merci d'avoir fait en sorte qu'un expat' se sente à la maison le trop peu de fois où j'ai eu la chance de passer faire un petit coucou. Nos chemins se croiseront peut-être à nouveau en Armorique autour d'une Coreff Bio ou d'une bolée d'cid', ou à 5h du mat' passablement éméchés au Vauban.

Jo, Pauline, JiBé, Adèle, Tibo, les grands, et tous ceux dont l'âme s'est un jour égarée entre les murs jaunes de cette noble bâtisse, merci pour avoir été là depuis toutes ces années. Même si les murs ont été repeints, l'esprit n'a jamais changé. Je reviens au plus vite pour refaire le monde autour d'une bonne salade maison et d'un grand verre de nectar malté. Merci à tous, c'est principalement grâce à vous que j'en suis là aujourdhui.

Pour finir cette tirade en français, merci à mes parents et mon piti frère pour m'avoir soutenu et avoir toujours cru en moi, vous êtes super cool.

To conclude, I'll use my wide knowledge of the Swedish language: tack allihop!

Introduction

Silicon cycling results from a complex interplay between physical, chemical and biological processes. The biggest reservoir of silicon on Earth is the continental crust where Si accounts for about 29% by mass (Rudnick and Gao, 2003; Wedepohl, 1995). The chemical weathering of silicate minerals releases solutes such as dissolved silica (DSi, $Si(OH)_4$), the only bioavailable form of silica. For example, the weathering reaction of K-feldspar yields secondary minerals, bicarbonate and DSi:

$$11H_2O + 2CO_2 + 2KAlSi_3O_8 = Al_2Si_2O_5(OH)_4 + 2HCO_3^{2-} + 4Si(OH)_4 + 2K^+$$

This slow weathering process consumes carbon dioxide, hence couples the silicon and the carbon cycles on geologic time scales. Part of this newly formed DSi will react to form secondary silicate minerals (e.g. clays) or be adsorbed onto oxides. Another part will be directly transferred to rivers. The remaining part will be used by organisms such as plants and be transformed into biogenic silica (BSi), an amorphous Si phase (ASi) biologically produced during the uptake of DSi. The BSi formed will be returned to soils with the death of the organisms and be remineralized as DSi or be diagenetically altered. Ultimately, DSi will be transferred to the riverine system and delivered to the oceans (Fig. 1).

The modern ocean Si cycle

The oceanic component of the Si cycle is commonly viewed as a closed system where sources and sinks are in balance on relatively short time scales (Treguer et al., 1995; Treguer and De La Rocha, 2013). The major input of Si in the ocean is from the fluvial system, accounting for about 80% of the total Si delivery. The riverine input is composed of a dissolved component (~60%) and of a particulate part (~20%), which will dissolve in the water column. The remaining 20% of the total Si transferred to the ocean is from atmospheric deposition and dissolution of dust (~3%), groundwater discharge (~7%), and hydrothermalism and weathering of the ocean crust (~10%). A schematic of the modern ocean cycle can be found in Fig. 1. Fluxes of DSi to the ocean have been recently reviewed in Paper IV of this thesis.

The cycle of Si in the water column and burial into sediments is widely dominated by biological processes (e.g. Nelson et al., 1995). Diatoms, the main contributors to the marine biological Si cycle, take up DSi in surface waters and precipitate it into BSi during the formation of their shell (i.e. frustule). Being photosynthetic microalgae, the growth of diatoms, possible only in the presence of DSi, represents a coupling between the Si and C on short time scales. The flux of DSi transformed into BSi in the surface layer by diatoms exceeds by far the yearly input flux of Si. This is possible because diatoms have a high affinity for DSi and are able to grow at maximum rates even at DSi concentrations near depletion (e.g. Paasche, 1973).

However, DSi concentrations in the modern ocean are not rapidly decreasing. The system is sustainable solely because the major part of the BSi formed will be remineralized within the water column and be available for new diatom growth (e.g. Nelson et al., 1995; Treguer et al., 1995; Treguer and De La Rocha, 2013). Other organisms, such as radiolarians, siliceous sponges and silicoflagellates, also contribute to the transport of Si into the sediments but the fluxes related to their uptake of DSi are poorly constrained. This is due to poorer knowledge about their ecology, compounded by the difficulty of conducting successful culture experiments (e.g. Krabberød et al., 2011).

The oceanic distribution of DSi is controlled by the general ocean circulation and dissolution of BSi (de Souza et al., 2014). The general pattern consists of surface waters with low concentrations of DSi due to substantial biological uptake, mostly attributed to diatoms. Some regions are exceptions to this pattern, with relatively high concentrations of DSi even in the surface waters. This is the case for High Nutrient Low Chlorophyll (HNLC) areas such as the Southern Ocean and the North Pacific, where higher DSi concentrations are often linked to limitation of diatom production due to the low

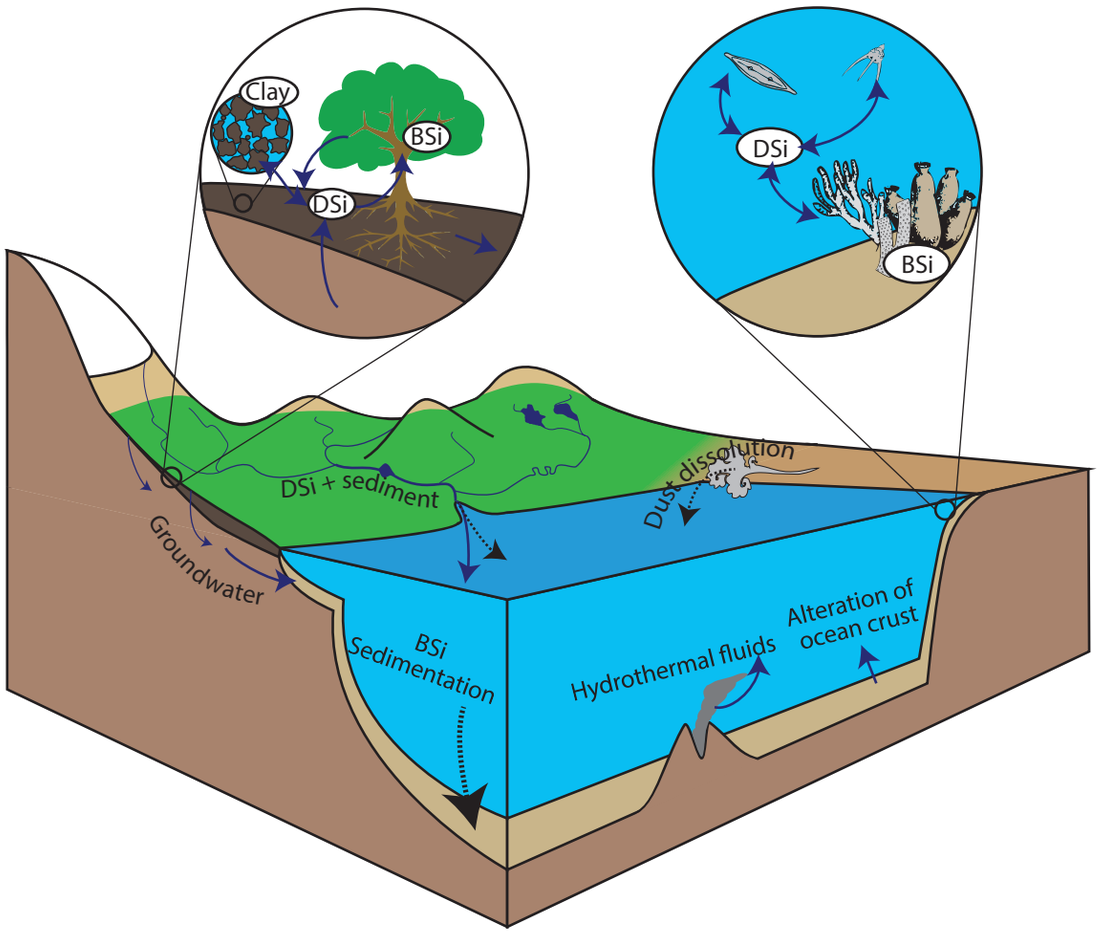

Figure 1: Cartoon schematic of the modern Si cycle. Dotted lines indicate particulate fluxes whereas solid lines indicate solute fluxes or transformations. Modified from Frings et al. (2016).

availability of other (micro)nutrients such as iron (e.g. Wells, 2003). Treguer et al. (1995) estimated that less than 5% of the BSi exported deeper than the surface layer were permanently trapped into sediments. The vast majority of this BSi will dissolve, progressively enriching the deeper layers, thus resulting in a vertical gradient of DSi concentration in the water column with increasing concentrations with depth (Fig. 2), similarly to other nutrient profiles.

A bottom water basinal gradient also exists, related to the overturning circulation. de Souza et al. (2014) showed that the interbasinal distribution of DSi concentration is controlled by dispersion of Antarctic bottom waters towards the other ocean basins. At depth, the North Atlantic has significantly lower DSi concentrations than the rest of the ocean (Fig. 2). This is the result of formation of deep waters in the North Atlantic from depleted surface waters, and the circulation of these newly formed deep waters southwards, thus reducing the influence of high DSi deep waters from the Southern Ocean.

Evolution of the marine Si cycle through geologic times

While the modern Si cycle is becoming better and better understood, its evolution over geologic times has remained at a consensus for many years. The proposed narrative is a transition from an abiotic control on DSi concentration in the ocean towards a biologically controlled one (Maliva et al., 1989; Siever, 1991). Before the evolution of the first silica secreting organisms at the end of the Precambrian, inputs of DSi to the ocean were not counterbalanced by biological uptake and sedimentation of BSi. Thus, the ocean was saturated in regard to Si and the DSi in excess was abiotically precipitated and stored in sediments. Evolution of first silica secreting

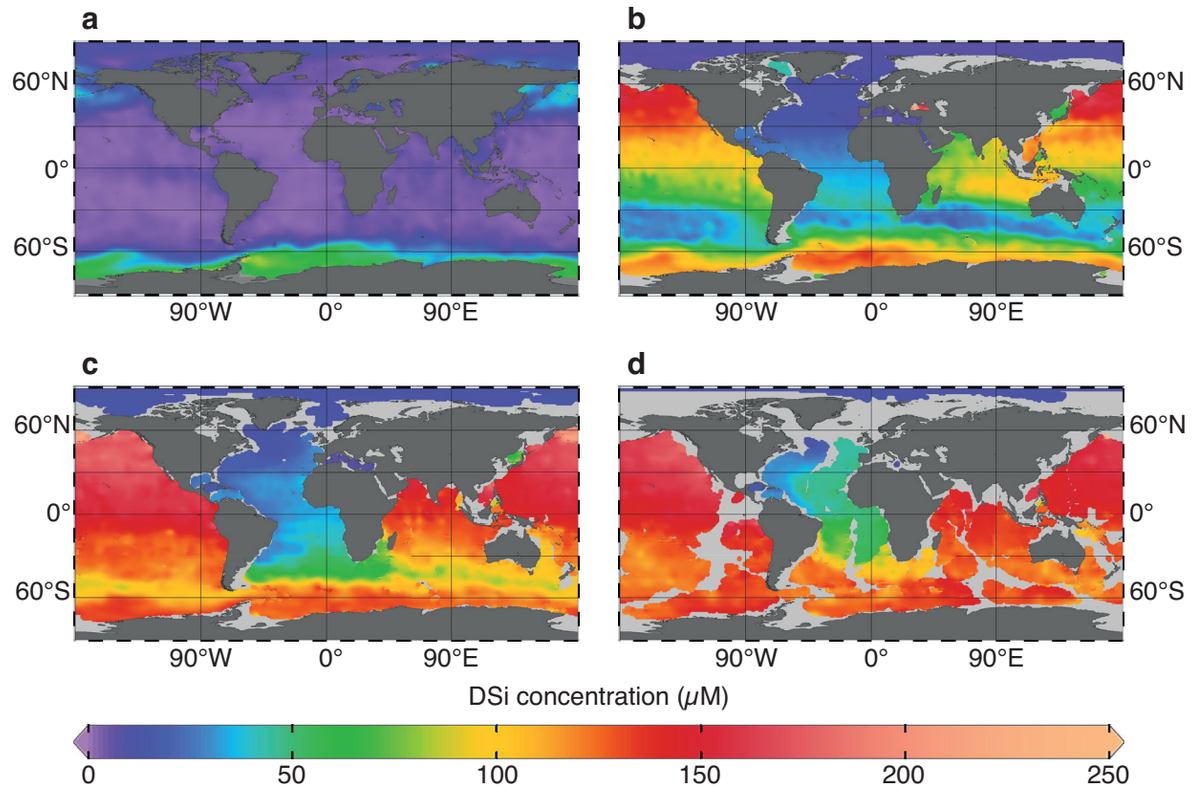

Figure 2: Modern distribution of DSi concentrations at (a) surface, (b) 1000 m, (c) 2500 m, and (d) 4000 m. Generated using Ocean Data View (Schlitzer, 2015) with DSi concentrations from Garcia et al. (2014).

organisms (e.g. radiolarian and sponges) at the end of the Precambrian and early Cambrian brought the oceanic DSi concentrations below saturation and under weak biological control. From the early Cambrian to the mid/late Cretaceous, concentrations of DSi are believed to have remained considerably high compared to present (Fig. 3).

The most striking feature in the conceptual evolution of the marine Si cycle is the drawdown of DSi concentration at the end of the Cretaceous and during the Paleogene due to the rise of diatoms (Fig. 3). The hypothesis that diatom proliferation led to decreasing DSi concentrations in the surface waters is reinforced by studies investigating the degree of silicification of radiolarians over the Cenozoic. Lazarus et al. (2009) showed that the degree of silicification of radiolarian tests at low latitudes decreases while the diatom diversity increases, attributing this phenomenon to reduced DSi availability. However, to our knowledge, a direct relationship between the proliferation of diatoms and a rapid drawdown of DSi concentrations in the surface waters has yet to be confirmed.

More emphasis has been put on investigating the evolution of the marine silicon cycle on shorter timescales such as glacial-interglacial periods (e.g. Abelmann et al., 2015; Ehlert et al., 2013; Hendry et al., 2014; Maier et al., 2013). Several studies have suggested that ocean DSi $\delta^{30}Si$ is weakly sensitive to changes in DSi input fluxes but very sensitive to changes in $\delta^{30}Si$ of the inputs (De La Rocha and Bickle, 2005; Georg et al., 2006a; Georg et al., 2009). The magnitude of changes in marine $\delta^{30}Si$ during glacial interglacial cycles, as recorded in sedimentary BSi, are possible to explain via changes in riverine $\delta^{30}Si$ (Frings et al., 2016). This is also reflected on continental systems. For example, Opfergelt et al. (2013) showed higher $\delta^{30}Si$ in non-glaciated streams than in glaciated ones in Iceland, attributed to greater formation of secondary minerals in non-glaciated areas. Therefore, changes in riverine input $\delta^{30}Si$ also play a major role in the control of mean $\delta^{30}Si$ of the ocean.

Another aspect of rapid climate change to look at is the influence on Si cycling of transient increases in global temperatures, occurring in the

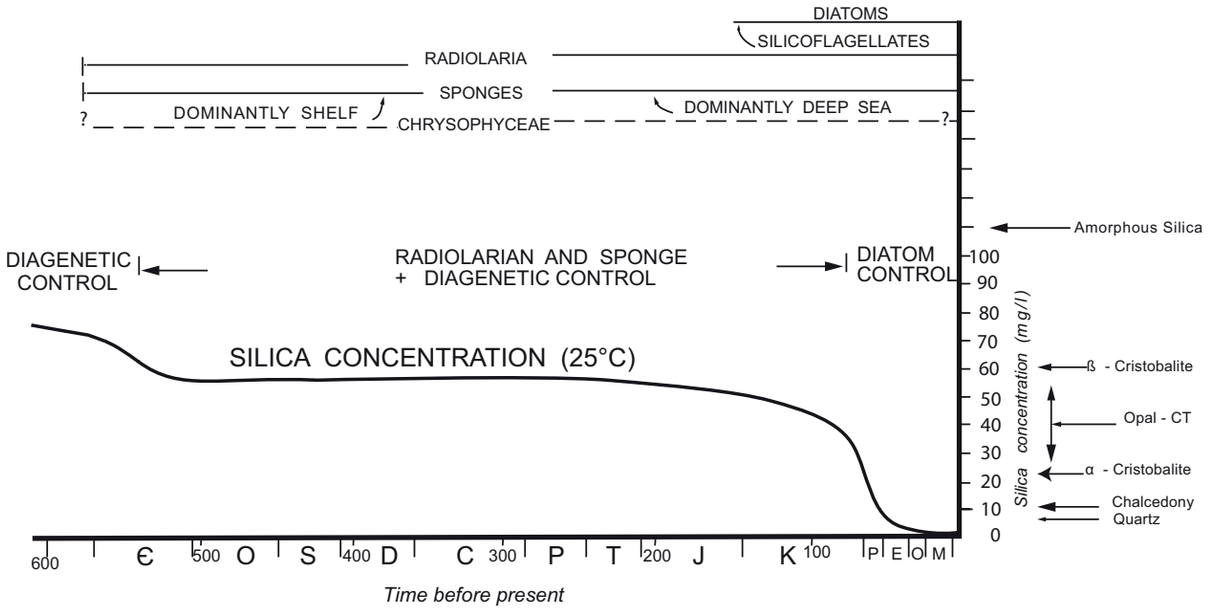

Figure 3: Variations of surface DSi concentrations over geologic time. From Siever (1991).

early Cenozoic (e.g. Lourens et al., 2005; Zachos et al., 2001). The recovery phase of early Cenozoic hyperthermals are often attributed to increased silicate weathering intensity and/or enhanced biological productivity; both processes decreasing the atmospheric concentrations of carbon dioxide and participating in global cooling. Such mechanisms have the potential to substantially impact the Si cycle (discussed further in Paper III). However, to our knowledge, no study has investigated the behavior of silicon isotopes during hyperthermals such as the Paleocene-Eocene Thermal Maximum (PETM) and similar events happening during the early Cenozoic.

Si stable isotope toolkit

Silicon has three stable isotopes of atomic masses of 27.97693 (^{28}Si), 28.97649 (^{29}Si) and 29.97377 (^{30}Si) with global natural relative abundances of 92.22%, 4.69% and 3.09% respectively (Rosman and Taylor, 1998). Si isotopes ratios are most often reported as delta values (i.e. δ^{30}Si or δ^{29}Si), which correspond to the variation in permil between a sample and a standard. The transfer of Si from one phase to another leads to a fractionation enriching or depleting the product phase in heavier Si isotopes compared to the source phase.

This fractionation mechanism leads to a wide range of δ^{30}Si values in terrestrial and oceanic materials (Fig. 4). Here, I focus on the fractionation of Si stable isotopes during the formation of BSi by marine biosilicifiers. It is well known that diatoms discriminate against the heavier isotopes of Si during the formation of their frustule (De La Rocha et al., 1997). The fractionation of Si isotopes by diatoms can be modeled following a Rayleigh or a steady-state approach (Fig. 5a). Rayleigh processes imply that the diatom take up DSi from a finite pool, whereas steady-state processes consider a constantly replenished DSi pool The diatom δ^{30}Si is dependent of the fraction of DSi remaining in solution (i.e. the degree of DSi utilization), its initial isotopic composition, and the magnitude of the fractionation. Therefore, variations of diatom δ^{30}Si values from sediment archives can be used to explore the variation in DSi utilization in the surface waters over various time-scales (De La Rocha et al., 1998; Egan et al., 2012). Recently, Sutton et al. (2013) investigated the role of diatom species-dependent fractionation and showed that inter-species variations could explain up to 67% of their sediment record variability.

Siliceous sponges also discriminate against the heavier isotopes of Si during the formation of their siliceous spicules. The magnitude of

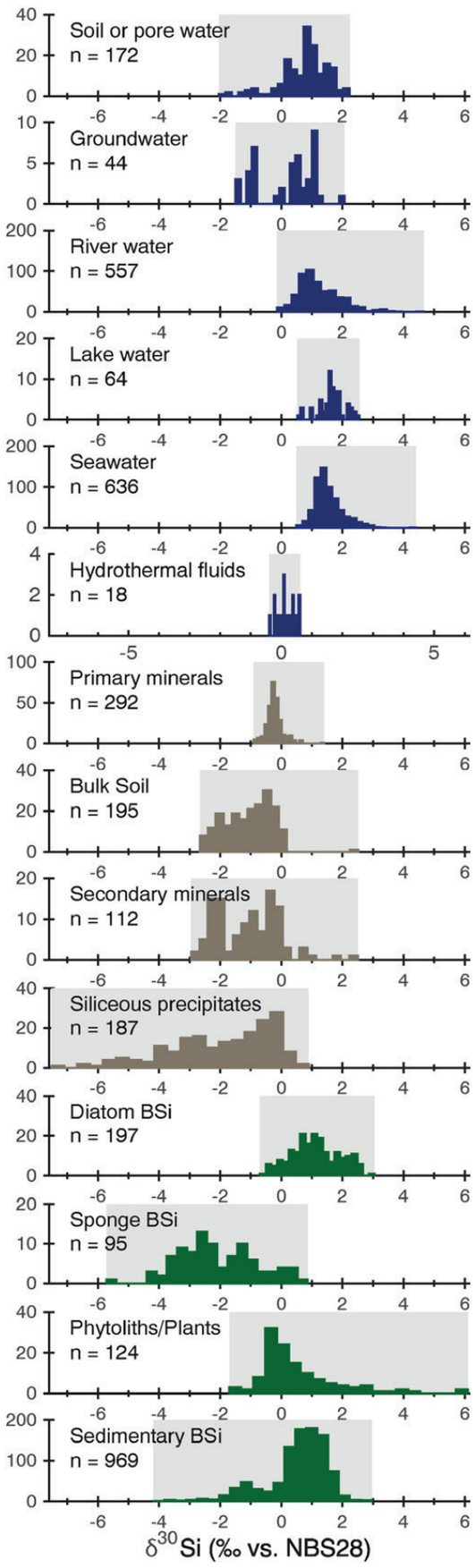

Figure 4: Compilation of silicon isotopes in natural materials. The gray shaded area shows the range of values, while the vertical bars show their distribution. From Frings et al. (2016).

this fractionation is dependent on the ambient concentration of DSi (Fig. 5b), due to the ratio of Si influx and efflux in the sponge cells (Wille et al., 2010), and has been empirically defined by Hendry and Robinson (2012) as:

$$\Delta\delta^{30}Si = -6.54 + 270/(53+[DSi])$$

where $\Delta\delta^{30}Si$ is the offset between sponge $\delta^{30}Si$ and DSi $\delta^{30}Si$ (i.e. $\Delta\delta^{30}Si = \delta^{30}Si_{sponge} - \delta^{30}Si_{DSi}$).

This relationship between Si isotope fractionation in sponges and the concentration of DSi in the bottom waters can be used, given estimations on the initial $\delta^{30}Si$ of DSi, to reconstruct oceanic DSi concentrations over geological times. Few studies have measured sponge $\delta^{30}Si$ (De La Rocha, 2003; Douthitt, 1982; Egan et al., 2013; Hendry et al., 2015; Hendry et al., 2010a; Hendry et al., 2010b; Hendry and Robinson, 2012; Wille et al., 2010) and even fewer of them focused on paleoreconstruction.

Knowledge regarding the extent of Si isotope fractionation by radiolarians is still at an early stage, mostly due to difficulties involved with bringing radiolarians through their reproductive cycle during culture experiments (Krabberød et al., 2011). Their silicification is poorly understood but thought to be controlled by internal regulation of Si concentrations and precipitation, as is the case with diatoms (Wallace et al., 2012). Two studies have estimated the magnitude of the fractionation of Si isotopes by radiolarians to fall between -2.1 and -1.1‰ (Hendry et al., 2014), or between -0.8 and -1.5‰ (Abelmann et al., 2015). Overall, it seems that the radiolarian $\delta^{30}Si$ values are more directly related to $\delta^{30}Si$ of DSi and unaffected by changes in DSi concentration.

Scope of the thesis

The general scope of this thesis is to shed light on the variation of oceanic DSi concentrations over various time-scales, primarily by the use of sponge $\delta^{30}Si$. Special focus has been put on the early Cenozoic to try to retrieve the magnitude and assess the ubiquity of the putative drawdown of ocean DSi concentrations. The working hypotheses were that 1) sponge spicule

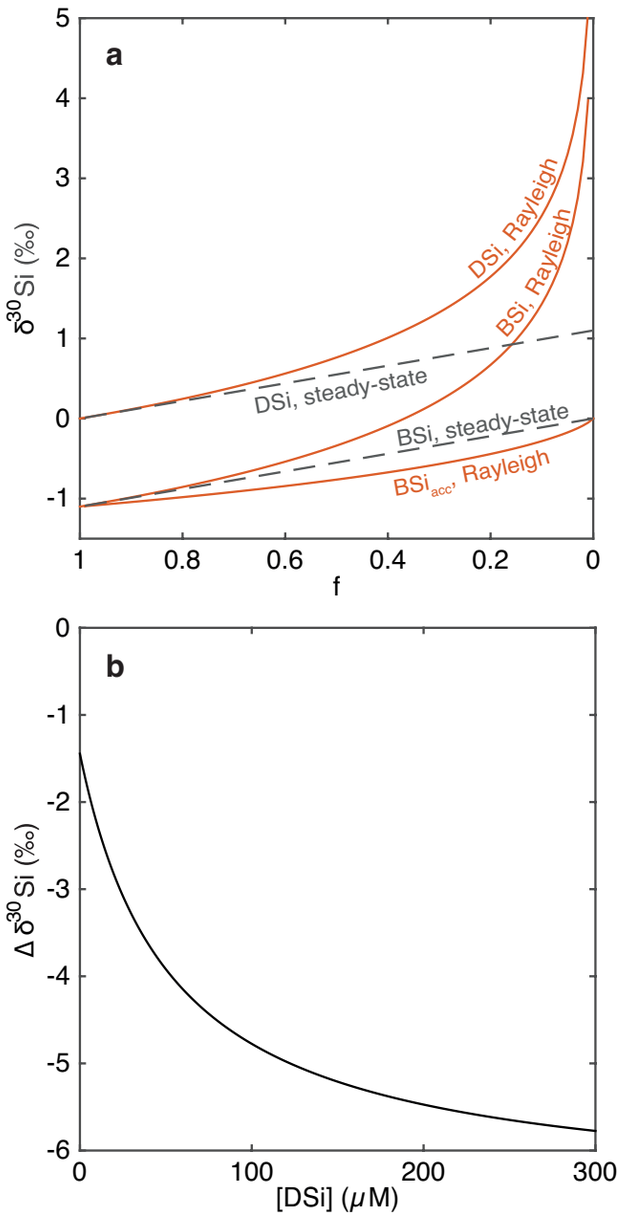

Figure 5: (a) Relationship between DSi and diatom δ^{30}Si following a Rayleigh (red lines) or a steady-state model (gray lines). (b) Relationship between sponge Si isotope fractionation and DSi concentrations.

δ^{30}Si records significant variations in bottom waters DSi concentrations and 2) the drawdown of DSi concentrations is a global phenomenon and is not restricted to certain ocean areas.

In more specific terms, this thesis aimed to:

- Reconstruct DSi concentrations over the Paleogene in the North Atlantic as well as in the Equatorial Pacific by using sponge δ^{30}Si and the established relationship between Si isotope fractionation in sponges and DSi concentrations.
- Provide better constrains on the timing and magnitude of the decrease in marine DSi concentrations during the early Cenozoic.
- Evaluate the impact of relatively rapid climatic perturbations, such as hyperthermals or glacial-interglacial cycles, on the marine Si cycle.

Methods

The analysis of Si isotope ratios requires that the sample be as pure as possible and free of any Si-bearing contamination. This can be achieved by a combination of chemical cleaning, physical separation and handpicking of siliceous microfossils.

Sample preparation

Separation and cleaning of siliceous microfossils from sediment cores must be done without inducing any change to the fossils chemical structure and thus, to their silicon isotopic composition. The separation method used in this thesis exploits the density difference between biosiliceous and detrital material (Morley et al., 2004; Shemesh et al., 1988). Briefly, sediments are cleaned from carbonates and organic matter with hydrochloric acid and hydrogen peroxide. Biogenic silica is separated from detrital material (e.g. clays and other lithogenic silicates) by repeated heavy liquid separation using Sodium Polytungstate (SPT) at a density between 2.1 and 2.3 g/mL. The light fraction, containing BSi, is then collected for handpicking of siliceous microfossils. A sieving step can also be performed to remove fragmented BSi material and ease the handpicking process.

Prior to Si isotope composition analysis, siliceous microfossils samples must be dissolved and purified. Two different chromatographic methods can be used to purify Si solutions. The first one (Engström et al., 2006) uses an anion exchange resin. Si, transformed to an anionic form (silicon hexafluoride, SiF_6^{2-}) beforehand by dissolving BSi in an excess of HF, is retained in the resin and eluted using different acid mixes. This method efficiently separates Si from other anions as well as uncharged

and cationic species, thus minimizing the chance of interferences during Si isotopic composition analysis. The second method (Georg et al., 2006b) is based on an opposite principle. Here, the BSi solutions, dissolved under basic/alkaline conditions, are loaded on a cation exchange resin. Silicon, as well as anionic species, are not retained on the column; this could prove problematic for example with samples containing high sulfate content. Since BSi is composed primarily of SiO_2, the contamination by anionic species remains minimal.

Silicon isotopic composition measurements

Multi-collector mass spectrometers (MC-ICP-MS) successfully resolves polyatomic interferences, mostly due to interference from $^{14}N^{16}O$ on ^{30}Si, during direct measurement of silicon stable isotope abundances (Cardinal et al., 2003). Samples are introduced into a plasma torch in order to be ionized before acceleration in the mass spectrometer. Different masses are monitored simultaneously and the comparison between $\delta^{29}Si$ and $\delta^{30}Si$ can be used to assess the resolution of polyatomic interferences (Fig. 6).

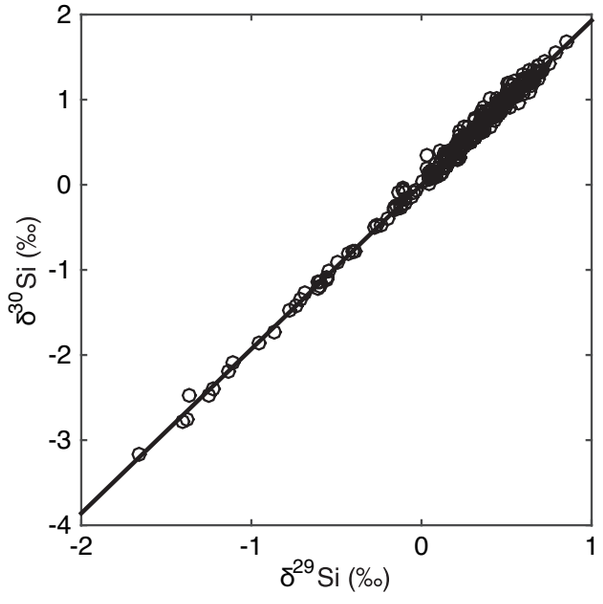

Figure 6: Three-isotopes plot of all the Si isotope determinations from this thesis. Data fall on the expected mass-dependent fractionation line $\delta^{30}Si = 1.93 \times \delta^{29}Si$ (black line; r2= 0.99, n=285).

Most of the $\delta^{30}Si$ values presented in this thesis (Paper I, II and part of paper III) have been measured on a Neptune MC-ICP-MS (Thermo Scientific) at Ifremer (Brest, France). The remaining samples (part of paper III) have been measured on a NuPlasma(II) MC-ICP-MS at the VegaCenter (Stockholm). Details on the running conditions are given in the respective manuscripts. Silicon isotope abundances are most often reported as delta values. Corrections and formulas to calculate delta values from Si isotope ratios are given in Box 1.

Summary of papers

Author contributions are detailed in Table 1.

Paper I

G. Fontorbe, P.J. Frings, C.L. De La Rocha, K.R. Hendry, and D.J. Conley. 2016. **A silicon depleted North Atlantic since the Paleogene: evidence from sponge and radiolarian silicon isotopes**. *Earth and Planetary Science Letters*. In revision.

Paper I presents results of sponge and radiolarian $\delta^{30}Si$ from sediment cores (Blake Nose, Western North Atlantic) covering the early to mid Paleogene. This is the first study presenting radiolarian and sponges $\delta^{30}Si$ from the North Atlantic covering such an extended time period (~30Ma). Using the established relationship between ambient DSi concentration and the magnitude of Si isotope fractionation in siliceous sponges, we demonstrate that the Western North Atlantic was DSi deplete during the Paleocene and Eocene.

This is contrary to previous studies suggesting a drawdown of DSi concentration during the Paleogene. Therefore, we challenge the timing and ubiquity of the decrease of marine DSi concentrations. Our interpretation of a Si deplete North Atlantic since at least 60 Ma is robust to a range of assumptions and uncertainties that are discussed in the manuscript.

Box 1: Si isotopes calculations

The variations in silicon stable isotopes abundances are by convention expressed as delta values. They represent the ratio R, in permil, between a heavy isotope and the lightest one normalised to an international standard:

$$\delta^{x}Si = \left(\frac{R_{sample}}{R_{standard}} - 1 \right) \times 1000$$

where R = $^{x}Si/^{28}Si$, and x is either 29 or 30.

The fractionation – i.e. the ratio of isotopes ratios - between a mother phase A and a daughter phase B can be expressed as :

$$^{x}\alpha_{A-B} = \frac{R_B}{R_A}$$

If $^{x}\alpha_{A\text{-}B} > 1$, the phase B is relatively enriched in heavy isotopes, if $^{x}\alpha_{A\text{-}B} < 1$, the phase B is relatively depleted in heavy isotopes, and if $^{x}\alpha_{A\text{-}B} = 1$, there is no fractionation between the tow phases.

Observed fractionations of silicon isotopes and current precision on the measurements are in the order of a few tenth of permil to a few permil. For better readability, fractionation between two phases is often reported in permil as:

$$^{x}\varepsilon_{A-B} = \left(^{x}\alpha_{A-B} - 1 \right) \times 1000$$

and can be approximated as the difference between two delta values:

$$^{x}\varepsilon_{A-B} \approx \Delta\delta^{x}Si_{A-B} = \delta^{x}Si_{A} - \delta^{x}Si_{B}$$

The measurement of silicon isotopes by MC-ICP-MS is subject to a mass-dependent mass-bias and therefore requires the addition of an internal Mg standard for correction.

$$f_{Mg} = \ln \frac{\left(\frac{^{25}Mg}{^{24}Mg} \right)_{true}}{\left(\frac{^{25}Mg}{^{24}Mg} \right)_{measured}} \div \ln \left(\frac{Mass\,^{25}Mg}{Mass\,^{24}Mg} \right)$$

where “true” is the theoretical ratio of ^{25}Mg and ^{24}Mg, “measured” is the measured ratio, and Mass is the atomic mass of the different isotopes. This correction factor, f_{Mg}, is then applied to the measured Si ratios to give a corrected Si ratio:

$$R_{corrected} = R_{measured} \times \left(\frac{Mass\,^{x}Si}{Mass\,^{28}Si} \right)^{f_{Mg}}$$

Table 1: Author contribution to Papers I to IV.

	Paper I	Paper II	Paper III	Paper IV
Concept and study design	G. Fontorbe D.J. Conley	G. Fontorbe, D.J. Conley	G. Fontorbe, D.J. Conley	P. Frings, D.J. Conley
Laboratory work and analyses	G. Fontorbe	G. Fontorbe	G. Fontorbe, P. Frings	n/a
Data analyses	G. Fontorbe	G. Fontorbe	G. Fontorbe	P. Frings
Discussion of results	G. Fontorbe, P. Frings, D.J. Conley	G. Fontorbe, P. Frings, C.L. De La Rocha, D.J. Conley	G. Fontorbe, P. Frings, D.J. Conley	P. Frings, G. Fontorbe, W. Clymans, C.L. De La Rocha, D.J. Conley
Writing	G. Fontorbe	G. Fontorbe	G. Fontorbe	P. Frings
Comments and feedback	All authors	All authors	All authors	All authors

Additionally, this manuscript discusses the use of radiolarian $\delta^{30}Si$ as a proxy for reconstructing DSi $\delta^{30}Si$ in the upper layer. Results indicate that the top few hundred meters of the North Atlantic during the Paleogene had values similar to the modern one.

Paper II

G. Fontorbe, P.J. Frings, C.L. De La Rocha, K.R. Hendry, and D.J. Conley. 2016. **Enrichment of dissolved silica in the deep Equatorial Pacific during the Eocene-Oligocene**. *manuscript*.

Following on the work presented in Paper I, Paper II explores the changes in radiolarian and sponge $\delta^{30}Si$ from the mid Eocene to the late Oligocene in the Equatorial Pacific. To our knowledge, no study over this time interval from this region has been published yet.

Similarly to that seen in the North Atlantic, radiolarian $\delta^{30}Si$ show values very similar to modern ones. This argues in favor of an upper ocean layer with low concentrations of DSi in the Equatorial Pacific during the mid to late Paleogene. Conversely, sponge $\delta^{30}Si$ decrease significantly around the Eocene-Oligocene boundary. In line with previous studies on sponge $\delta^{30}Si$ during the Eocene-Oligocene boundary, this is attributed to increased DSi concentrations of the bottom waters.

This increase in concentration is consistent with a reorganization of ocean circulation in the Equatorial Pacific, as previously shown in Nd isotope records. We suggest in this manuscript that sponge $\delta^{30}Si$ can provide additional information about ocean circulation, especially on the nutrient content at the sites of the deep waters formation, and complement well established proxies used for reconstructing paleo ocean circulation.

Paper III

G. Fontorbe, P.J. Frings, C.L. De La Rocha, K.R. Hendry, and D.J. Conley. 2016. **Marine silicon cycle response to the Paleocene-Eocene Thermal Maximum.** *manuscript*.

Paper III presents a radiolarian $\delta^{30}Si$ record covering the Paleocene-Eocene Thermal Maximum (PETM). The PETM has been widely studied in terms of carbon and oxygen stable isotopes. Possible mechanisms responsible for the onset of the PETM and its recovery phase are still under debate, and some (especially volcanism/hydrothermalism and weathering of silicate minerals) have the potential to impact several facets of the Si cycle. However, to our knowledge, there are currently no studies focusing on Si cycling during this hyperthermal.

The radiolarian $\delta^{30}Si$ record decreases coincidently with the carbon isotope excursion (CIE) characteristic of the PETM. Therefore, we assessed of the response of Si isotopes in the upper ocean layer, confirming the contribution of Si-related mechanisms during the PETM.

A simple box-model was used to investigate the sensitivity of surface ocean silicon isotopes to changes in fluxes of hydrothermal Si inputs and changes in the Si isotopic composition of riverine inputs. Although the model cannot integrate all the processes involved during the PETM, it provides useful information on the extent of the changes to be recorded in radiolarian $\delta^{30}Si$.

Paper IV

P.J. Frings, W. Clymans, G. Fontorbe, C.L. De La Rocha, D.J. Conley. 2016. **The continental Si cycle and its impact on the ocean Si isotope budget**. *Chemical Geology 425.*

The last paper presented in this thesis is a synthesis paper on the impact of continental Si inputs to the marine Si isotopic composition. Paper IV reviews published work on Si inputs to the ocean with a focus on their Si isotopic composition, thus providing updated estimates of fluxes and $\delta^{30}Si$ of DSi and particulate Si delivered to the ocean. New provided estimates place the total flux of Si delivered to the ocean at 9.55 Tmol/y with a mean $\delta^{30}Si$ of 0.74‰.

A simple box-model, similar to that in Paper III, was used to estimate the impact of the late Quaternary glacial-interglacial transitions on the delivery of Si and its isotopic composition. Results show that a transition from a glacial continental Si cycle to an interglacial one can drive changes in oceanic $\delta^{30}Si$ of comparable magnitude and rate of that recorded in siliceous microfossils. Changes are related to 1) a drier and colder climate, 2) changes in sea level and area of exposed continental shelves, 3) extent of glaciation, and 4) vegetation changes.

Discussion

On the marine DSi concentrations during the Paleogene

As stated in the introduction section, the only narrative of the evolution of DSi concentrations predicts a large decrease of oceanic DSi concentrations starting during the Cretaceous and finishing at the end of the Paleogene with DSi deplete surface waters as it is observed today (Maliva et al., 1989; Siever, 1991). However, tom my knowledge, no studies have attempted to quantitatively reconstruct oceanic DSi concentrations during this time interval.

Paper I and II shed more light on this subject. A decrease as large as described in the classic narrative should be visible in sponge $\delta^{30}Si$. It is counter intuitive to imagine higher DSi concentrations in the surface layer than in the deep layer of the ocean. Since modern DSi concentrations in the North Atlantic are significantly low compared to the other ocean basins, we can hypothesize that if the putative decrease in surface DSi in the surface waters was a ubiquitous phenomenon, it also impacted the deeper waters of the North Atlantic. As an example, a shift of DSi concentrations in the bottom waters from ~100

to ~20µM should be recorded in sponge $\delta^{30}Si$ by an increase of ~2‰, taking into account minor change in ocean $\delta^{30}Si$ (Hendry and Robinson, 2012).

Our sponge $\delta^{30}Si$ record from the North Atlantic presented in Paper I does not show this feature. Instead, the $\delta^{30}Si$ is rather stable over the entire studied period and has no extensive increase in sponge $\delta^{30}Si$ (and therefore a decrease in DSi concentration). The reconstructed DSi concentrations are low, similar to what can be seen in today's ocean (Garcia et al., 2014). This suggests that the putative drawdown of DSi concentrations in the surface waters caused by the proliferation of diatoms is not ubiquitous and/or predates the Paleogene.

On the other hand, our sponge $\delta^{30}Si$ record from the Equatorial Pacific, presented in Paper II, shows a decrease in sponge $\delta^{30}Si$ values around the Eocene-Oligocene transition. According to a previous study by Egan et al. (2013), the decrease in sponge $\delta^{30}Si$ values can be interpreted as an increase in DSi concentrations. This is also challenging the narrative towards decreasing global DSi concentrations. The increase in DSi concentrations in the Equatorial Pacific is discussed further in the next section.

The work presented in Paper I and II emphasize the necessity to re-evaluate our conceptual view of the evolution of DSi concentrations in the ocean over geologic timescales. However, the perspective of such studies is hindered by the fact that older sediments have either been subducted below the continental crust (Müller et al., 2008) or have been exposed on land and undergone diagenetic processes altering their Si isotopic composition (Tatzel et al., 2015).

On the control of DSi distribution over geological time scales

Modern oceanic DSi distribution is widely controlled by the oceanic overturning circulation and biological precipitation of BSi in the surface waters (de Souza et al., 2014). During the Paleogene, the position of landmasses was significantly different from the modern world (Fig. 7). Consequently, circulation of water masses and formation of deep waters were also affected. For example, no deep-water connection existed between the Atlantic and Pacific basin during the Paleogene (e.g. Thomas et al., 2008). This raises questions about the distribution of Si under different ocean circulation conditions.

This aspect of the Si cycle is tackled in Paper II, where our sponge $\delta^{30}Si$ record shows a decrease associated with increased DSi concentrations at depth. This decrease in sponge $\delta^{30}Si$ in consistent with a shift in bottom water Nd isotopic signatures in the Equatorial Pacific (e.g. Thomas et al., 2014; Thomas et al., 2008). Briefly, Nd isotopes from various materials in sediment can be used to track sources and mixing of deep waters. The Nd isotope records show an increased influence of deep-waters from the Southern Ocean moving northwards towards the Equatorial Pacific versus deep-waters formed in the North Pacific (Thomas et al., 2014; Thomas et al., 2008). This is a result of the opening of the Tasman gateway strengthening the formation of deep-waters in the Pacific Sector of the Southern Ocean.

In addition to the insights on ocean circulation and water masses mixing provided by Nd isotopes, the variation in sponge Si isotopic composition provides information on the DSi content at the locus of deep-water formation and extent of regenerated Si. Thus, we suggest that the Equatorial Pacific was dominated by water formed in the North Pacific with low DSi concentrations prior to ~37 Ma after which the source of deep-waters switched to the Southern Ocean were surface waters were DSi replete, similar to what we see today.

We suggest that during the Paleogene, the main control on DSi distribution was already ocean circulation. Moreover, DSi concentrations in the Equatorial Pacific during the Paleogene never reached values as high as today. We hypothesize that the increase of DSi concentrations in the Pacific was gradual, starting during the mid Eocene, with the modern day situation attained when the Antarctic Circumpolar Current was established with the complete subsidence of the Antarctic land bridges.

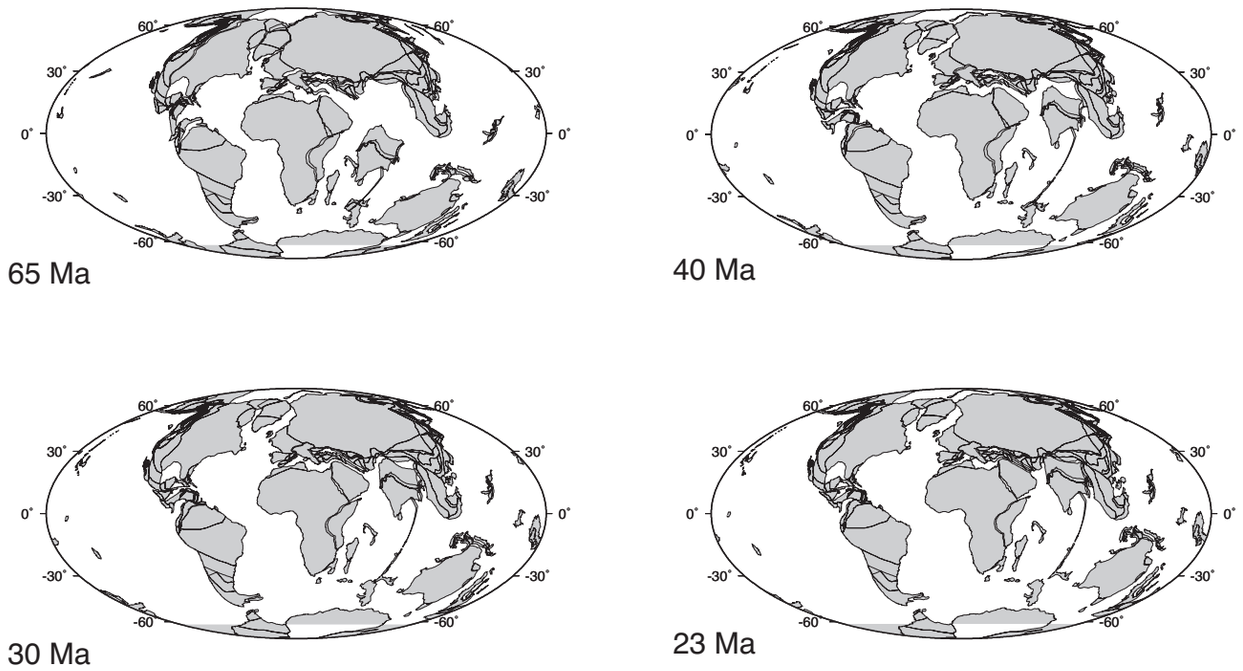

Figure 7: Paleogeographic reconstruction from the early Paleocene to the late Oligocene. Maps generated from the Ocean Drilling Stratigraphic Network Plate Tectonic Reconstruction (http://www.odsn.de/odsn/services/paleomap/paleomap.html)

On the sensitivity of Si cycle to rapid climate change

Perturbations of the marine Si cycle on millennial timescales have been investigated with regards to glacial-interglacial cycles, most often via the analysis of diatom $\delta^{30}Si$ (e.g. Abelmann et al., 2015; Ehlert et al., 2013; Hendry et al., 2014; Maier et al., 2013). Diatom $\delta^{30}Si$ is most often used to estimate the degree of Si utilization in the euphotic layer. Hence, these estimations of the variations in Si utilization are based on the assumption that surface water $\delta^{30}Si$ does not vary and therefore that variations in diatom $\delta^{30}Si$ are solely the results of increased siliceous productivity.

In Paper IV, we used a simple box model with a Monte-Carlo approach to parameterization to estimate the impact of changing the magnitude and $\delta^{30}Si$ of Si input fluxes to the ocean. The process impacting the most the isotopic composition of surface waters is changes in river $\delta^{30}Si$, with estimated changes ranging from -1.00 to +0.05‰. A change in the order of 0.50‰ in riverine DSi input is enough to approach the variability recorded in siliceous microfossils. Taking into account the changes in surface water $\delta^{30}Si$ caused by variations of the riverine DSi $\delta^{30}Si$ would tend to reduce the extent of change in DSi utilization required to explain the observed glacial-interglacial cyclicity in BSi $\delta^{30}Si$. We therefore recommend that future studies on biosiliceous paleoproductivity should take into account the potential variations caused by changes in riverine inputs.

To my knowledge, no peer-reviewed study has ever addressed the variations of marine Si isotopes over early Cenozoic hyperthermals. Several studies invoke increased weathering of silicate minerals as a potential mechanism for the decrease of temperatures via the removal of CO_2 from the atmosphere (e.g. Wieczorek et al., 2013). For the first time, this thesis shows variations of radiolarian $\delta^{30}Si$ coeval with the carbon isotopic excursion during the PETM. Using a box model similar to that of Paper IV, we show that this variation can be explained by changes in riverine $\delta^{30}Si$ and therefore provide information on the potential contribution of chemical weathering of silicate minerals to the waning phase of the PETM.

Conclusions and perspectives

The outcome of this thesis has improved our understanding regarding the evolution of marine Si cycling during the Cenozoic. Most importantly, my studies suggest that we need to reconsider our conceptual view of the variations of oceanic DSi concentrations over the Cenozoic, especially during the Paleogene, where it has previously been hypothesized that DSi concentrations should have decreased due to the proliferation of diatoms. This thesis does not corroborate this hypothesis.

The studies presented here suggest that low DSi concentrations have existed in the surface ocean since at least the early Paleogene, challenging the timing, ubiquity and magnitude of the putative drawdown of marine DSi concentration. This work also emphasizes distribution of Si and its isotopes in the ocean is controlled (on large spatial and time scales) primarily by ocean circulation and continental inputs.

The silicon isotopic composition of siliceous microfossils has proven to be a robust way to get insights on the evolution of Si cycling over a range of timescales. However, this research area is still at an early stage, and therefore, needs further investigation and refinement.

- First of all, we need to increase the number of available records from different ocean basins. For example, sponge and radiolarian $\delta^{30}Si$ record from the Equatorial Indian Ocean spanning the early to mid Cenozoic could provide information on the impact of the subduction of the Indian plate under the Asian plate, and the disappearance of the Tethys Ocean on the physical circulation of waters and distribution of DSi concentrations in the Pacific. The results of such a study could be merged with studies investigating the morphological changes in radiolarian tests in the equatorial waters (e.g. Lazarus et al., 2009) and shed light on the factors influencing the decrease in radiolarian silicification.

- This thesis also calls for better constraints on the extent of silicon isotope fractionation in radiolarians. Although absolute fractionation factors might be difficult to obtain due to the difficulty of successfully maintaining radiolarian cultures, relative species-dependent studies are achievable. By collecting radiolarians from a restricted marine sediment interval (e.g. a few centimetres), we can assume that individual radiolarians were subject to similar environmental conditions during their growth. Radiolarians are widespread and diverse amongst marine sediment archives; therefore, selective analyses of the Si isotopic composition from a range of species would provide a relative Si isotope fractionation. If little or no species-dependent fractionation were found, this would emphasize the fact that selecting a bulk radiolarian community is sufficient to investigate changes in Si cycling. Otherwise, the presence of inter-species differences would suggest that mono-specific samples must be analyzed separately to best reconstruct facets of past Si cycling.

- I recommend that more investigations on the variations of marine silicon isotopes during the early Cenozoic hyperthermals should be conducted. Since the PETM is the largest amplitude hyperthermal it should be the first to be inspected. Combining analyses of siliceous microfossils from different basins and of various proximities to the continents has the potential to provide information of the contribution of hydrothermalism and enhanced weathering of silicate minerals to the different phases of the PETM. For example, if hydrothermalism is triggering the CIE, the response in Si isotopes should be different between ocean basins and depend on the location of the hydrothermal input. During the recovery phase, coastal sites should be more influenced by changes in riverine $\delta^{30}Si$ compared to open-sea sites. Hence, Si isotopes have the potential to contribute to a decades-long debate.

Svensk ammanfattning

Omsättningen av kisel (Si) är en av de viktiga biogeokemiska processerna på jorden. Den lösta formen av Si (DSi) är ett nödvändigt näringsämne för såväl markens som havens ekosystem. Löst kisel kommer från den långsamma kemiska vittringen av kiselmineral. Denna process förbrukar koldioxid och bidrar därför till att reglera jordens klimat genom årmiljonerna. Kisel transporteras huvudsakligen via floder till havet och används där av en mängd olika organismer (t.ex. kiselalger, kiselhaltiga svampdjur, radiolarier (amöbiska encelliga organismer) och kiselflagellater) som fäller ut den lösta kiseln till amorft, biologiskt producerat, kisel (BSi). På så sätt kan biologiska processer påverka exporten av kisel från havsvatten till bottensediment. Medan kunskapen kring den nutida kiselomsättningen och de processer som styr denna har förbättrats i takt med att de oceanografiska mätmetoderna har förfinats så är variationerna i havens kiselkoncentrationer längre tillbaka i jordens historia fortfarande ofullständigt kartlagda.

Denna avhandling syftar till att öka kunskapen om hur den marina kiselomsättningen har förändrats på tidsskalor som sträcker sig från tusentals till miljontals år. För att åstadkomma detta har vi undersökt den isotopiska sammansättning av kisel (uttryckt som $\delta^{30}Si$) i marina kiselhaltiga mikrofossil som tagits fram ur havssediment. Analys av $\delta^{30}Si$ från marina kiselalger, radiolarier och fragment av kiselhaltiga svampdjur är ett kraftfullt verktyg för att kunna klargöra flera olika aspekter i havets kiselomsättning även långt tillbaka i tiden.

På tidsskalor av tusentals år domineras den marina kiselomsättningen främst av variationer i biologisk produktivitet i havens ytvatten och av tillförsel av löst kisel från floder. På tidsskalor av miljontals år så verkar kiselomsättningen framför allt styras av den storskaliga cirkulationen av havsvattnet. Analysen av svampdjurs $\delta^{30}Si$ i den här avhandlingen möjliggjorde en rekonstruktion av koncentrationen löst kisel i bottenvattnet i Nordatlanten och de ekvatoriella delarna av Stilla havet. I motsats till vad som tidigare antagits så tyder våra resultat på att havet inte genomgick en fas av snabbt sjunkande koncentration av löst kisel under Paleogen (perioden för ca 65 till 23 miljoner år sedan). Vi visar att Nordatlanten under Paleogen hade en låg koncentration av löst kisel, ungefär i nivå med dagens koncentration. Koncentrationen av löst kisel i den ekvatoriella delen av Stilla havet är idag högre än i Nordatlanten och har ökat under åtminstone de senaste 35 miljoner åren.

Allt sammantaget så bidrar denna avhandling till att utöka den befintliga kunskapen genom att fylla tidigare luckor i förståelsen kring hur kiselomsättningen i havet har förändrats genom årmiljonerna.

References

Abelmann, A., Gersonde, R., Knorr, G., Zhang, X., Chapligin, B., Maier, E., Esper, O., Friedrichsen, H., Lohmann, G., Meyer, H., 2015. The seasonal sea-ice zone in the glacial Southern Ocean as a carbon sink. Nature communications 6.

Cardinal, D., Alleman, L.Y., de Jong, J., Ziegler, K., André, L., 2003. Isotopic composition of silicon measured by multicollector plasma source mass spectrometry in dry plasma mode. Journal of Analytical Atomic Spectrometry 18, 213-218.

De La Rocha, C., Brzezinski, M.A., DeNiro, M., Shemesh, A., 1998. Silicon-isotope composition of diatoms as an indicator of past oceanic change. Nature 395, 680-683.

De La Rocha, C.L., 2003. Silicon isotope fractionation by marine sponges and the reconstruction of the silicon isotope composition of ancient deep water. Geology 31, 423.

De La Rocha, C.L., Bickle, M.J., 2005. Sensitivity of silicon isotopes to whole-ocean changes in the silica cycle. Marine Geology 217, 267-282.

De La Rocha, C.L., Brzezinski, M.A., DeNiro, M.J., 1997. Fractionation of silicon isotopes by marine diatoms during biogenic silica formation. Geochimica et Cosmochimica Acta 61, 5051-5056.

de Souza, G.F., Slater, R.D., Dunne, J.P., Sarmiento, J.L., 2014. Deconvolving the controls on the deep ocean's silicon stable isotope distribution. Earth and Planetary Science Letters 398, 66-76.

Douthitt, C., 1982. The geochemistry of the stable isotopes of silicon. Geochimica et Cosmochimica Acta 46, 1449-1458.

Egan, K.E., Rickaby, R.E.M., Hendry, K.R., Halliday, A.N., 2013. Opening the gateways for diatoms primes Earth for Antarctic glaciation. Earth and Planetary Science Letters 375, 34-43.

Egan, K.E., Rickaby, R.E.M., Leng, M.J., Hendry, K.R., Hermoso, M., Sloane, H.J., Bostock, H., Halliday, A.N., 2012. Diatom silicon isotopes as a proxy for silicic acid utilisation: A Southern Ocean core top calibration. Geochimica et Cosmochimica Acta 96, 174-192.

Ehlert, C., Grasse, P., Frank, M., 2013. Changes in silicate utilisation and upwelling intensity off Peru since the Last Glacial Maximum – insights from silicon and neodymium isotopes. Quaternary Science Reviews 72, 18-35.

Engström, E., Rodushkin, I., Baxter, D.C., Öhlander, B., 2006. Chromatographic purification for the determination of dissolved silicon isotopic compositions in natural waters by high-resolution multicollector inductively coupled plasma mass spectrometry. Analytical chemistry 78, 250-257.

Frings, P.J., Clymans, W., Fontorbe, G., Christina, L., Conley, D.J., 2016. The continental Si cycle and its impact on the ocean Si isotope budget. Chemical Geology 425, 12-36.

Garcia, H., Locarnini, R., Boyer, T., Antonov, J., Baranova, O., Zweng, M., Reagan, J., Johnson, D., 2014. World Ocean Atlas 2013, Volume 4: Dissolved Inorganic Nutrients (phosphate, nitrate, silicate), S. A. Mishonov Technical Ed, 1-25.

Georg, R.B., Reynolds, B.C., Frank, M., Halliday, A.N., 2006a. Mechanisms controlling the silicon isotopic compositions of river waters. Earth and Planetary Science Letters 249, 290-306.

Georg, R.B., Reynolds, B.C., Frank, M., Halliday, A.N., 2006b. New sample preparation techniques for the determination of Si isotopic compositions using MC-ICPMS. Chemical Geology 235, 95-104.

Georg, R.B., Zhu, C., Reynolds, B.C., Halliday, A.N., 2009. Stable silicon isotopes of groundwater, feldspars, and clay coatings in the Navajo Sandstone aquifer, Black Mesa, Arizona, USA. Geochimica et Cosmochimica Acta 73, 2229-2241.

Hendry, K., Swann, G.E., Leng, M.J., Sloane, H.J., Goodwin, C., Berman, J., Maldonado, M., 2015. Technical Note: Silica stable isotopes and silicification in a carnivorous sponge Asbestopluma sp. Biogeosciences 12, 3489-3498.

Hendry, K.R., Georg, R.B., Rickaby, R.E.M., Robinson, L.F., Halliday, A.N., 2010a. Deep ocean nutrients during the Last Glacial Maximum deduced from sponge silicon isotopic compositions. Earth and Planetary Science Letters 292, 290-300.

Hendry, K.R., Leng, M.J., Robinson, L.F., Sloane, H.J., Blusztjan, J., Rickaby, R.E.M., Georg, R.B., Halliday, A.N., 2010b. Silicon isotopes in Antarctic sponges: an interlaboratory comparison. Antarctic Science 23, 34-42.

Hendry, K.R., Robinson, L.F., 2012. The relationship between silicon isotope fractionation in sponges and silicic acid concentration: Modern and core-top studies of biogenic opal. Geochimica et Cosmochimica Acta 81, 1-12.

Hendry, K.R., Robinson, L.F., McManus, J.F., Hays, J.D., 2014. Silicon isotopes indicate enhanced carbon export efficiency in the North Atlantic during deglaciation. Nature communications 5.

Krabberød, A.K., Bråte, J., Dolven, J.K., Ose, R.F., Klaveness, D., Kristensen, T., Bjørklund, K.R., Shalchian-Tabrizi, K., 2011. Radiolaria Divided into Polycystina and Spasmaria in Combined 18S and 28S rDNA Phylogeny. PLoS ONE 6.

Lazarus, D.B., Kotrc, B., Wulf, G., Schmidt, D.N., 2009. Radiolarians decreased silicification as an evolutionary response to reduced Cenozoic ocean silica availability. Proceedings of the National Academy of Sciences 106, 9333-9338.

Lourens, L.J., Sluijs, A., Kroon, D., Zachos, J.C., Thomas, E., Rohl, U., Bowles, J., Raffi, I., 2005. Astronomical pacing of late Palaeocene to early Eocene global warming events. Nature 435, 1083-1087.

Maier, E., Chapligin, B., Abelmann, A., Gersonde, R., Esper, O., Ren, J., Friedrichsen, H., Meyer,

H., Tiedemann, R., 2013. Combined oxygen and silicon isotope analysis of diatom silica from a deglacial subarctic Pacific record. Journal of Quaternary Science 28, 571-581.

Maliva, R.G., Knoll, A.H., Siever, R., 1989. Secular change in chert distribution: a reflection of evolving biological participation in the silica cycle. Palaios, 519-532.

Morley, D.W., Leng, M.J., Mackay, A.W., Sloane, H.J., Rioual, P., Battarbee, R.W., 2004. Cleaning of lake sediment samples for diatom oxygen isotope analysis. Journal of Paleolimnology 31, 391-401.

Müller, R.D., Sdrolias, M., Gaina, C., Roest, W.R., 2008. Age, spreading rates, and spreading asymmetry of the world's ocean crust. Geochemistry, Geophysics, Geosystems 9.

Nelson, D.M., Tréguer, P., Brzezinski, M.A., Leynaert, A., Quéguiner, B., 1995. Production and dissolution of biogenic silica in the ocean: revised global estimates, comparison with regional data and relationship to biogenic sedimentation. Global Biogeochemical Cycles 9, 359-372.

Opfergelt, S., Burton, K.W., Pogge von Strandmann, P.A.E., Gislason, S.R., Halliday, A.N., 2013. Riverine silicon isotope variations in glaciated basaltic terrains: Implications for the Si delivery to the ocean over glacial–interglacial intervals. Earth and Planetary Science Letters 369-370, 211-219.

Paasche, E., 1973. Silicon and the ecology of marine plankton diatoms. II. Silicate-uptake kinetics in five diatom species. Marine Biology 19, 262-269.

Rosman, K., Taylor, P., 1998. Isotopic compositions of the elements 1997 (Technical Report). Pure and Applied Chemistry 70, 217-235.

Rudnick, R., Gao, S., 2003. Composition of the continental crust. Treatise on geochemistry 3, 1-64.

Schlitzer, R., 2015. Ocean Data View, http://odv.awi.de.

Shemesh, A., Mortlock, R., Smith, R., Froelich, P., 1988. Determination of Ge/Si in marine siliceous microfossils: Separation, cleaning and dissolution of diatoms and radiolaria. Marine Chemistry 25, 305-323.

Siever, R., 1991. Silica in the oceans: Biological-geochemical interplay. Scientists on gaia, 287-295.

Sutton, J.N., Varela, D.E., Brzezinski, M.A., Beucher, C.P., 2013. Species-dependent silicon isotope fractionation by marine diatoms. Geochimica et Cosmochimica Acta 104, 300-309.

Tatzel, M., von Blanckenburg, F., Oelze, M., Schuessler, J.A., Bohrmann, G., 2015. The silicon isotope record of early silica diagenesis. Earth and Planetary Science Letters 428, 293-303.

Thomas, D.J., Korty, R., Huber, M., Schubert, J.A., Haines, B., 2014. Nd isotopic structure of the Pacific Ocean 70-30 Ma and numerical evidence for vigorous ocean circulation and ocean heat transport in a greenhouse world. Paleoceanography 29, 454-469.

Thomas, D.J., Lyle, M., Moore, T.C., Rea, D.K., 2008. Paleogene deepwater mass composition of the tropical Pacific and implications for thermohaline circulation in a greenhouse world. Geochemistry, Geophysics, Geosystems 9.

Treguer, P., Nelson, D.M., Van Bennekom, A.J., DeMaster, D.J., 1995. The silica balance in the world ocean: a reestimate. Science 268, 375.

Treguer, P.J., De La Rocha, C.L., 2013. The world ocean silica cycle. Annual review of marine science 5, 477-501.

Wallace, A.F., Wang, D., Hamm, L.M., Knoll, A.H., Dove, P.M., 2012. Eukaryotic skeletal formation. Fundamentals of Geobiology, 150-187.

Wedepohl, K.H., 1995. The composition of the continental crust. Geochimica et cosmochimica Acta 59, 1217-1232.

Wells, M.L., 2003. The level of iron enrichment required to initiate diatom blooms in HNLC waters. Marine Chemistry 82, 101-114.

Wieczorek, R., Fantle, M.S., Kump, L.R., Ravizza, G., 2013. Geochemical evidence for volcanic activity prior to and enhanced terrestrial weathering during the Paleocene Eocene Thermal Maximum. Geochimica et Cosmochimica Acta 119, 391-410.

Wille, M., Sutton, J., Ellwood, M.J., Sambridge, M., Maher, W., Eggins, S., Kelly, M., 2010. Silicon isotopic fractionation in marine sponges: A

new model for understanding silicon isotopic variations in sponges. Earth and Planetary Science Letters 292, 281-289.

Zachos, J., Pagani, M., Sloan, L., Thomas, E., Billups, K., 2001. Trends, rhythms, and aberrations in global climate 65 Ma to present. Science 292, 686-693.

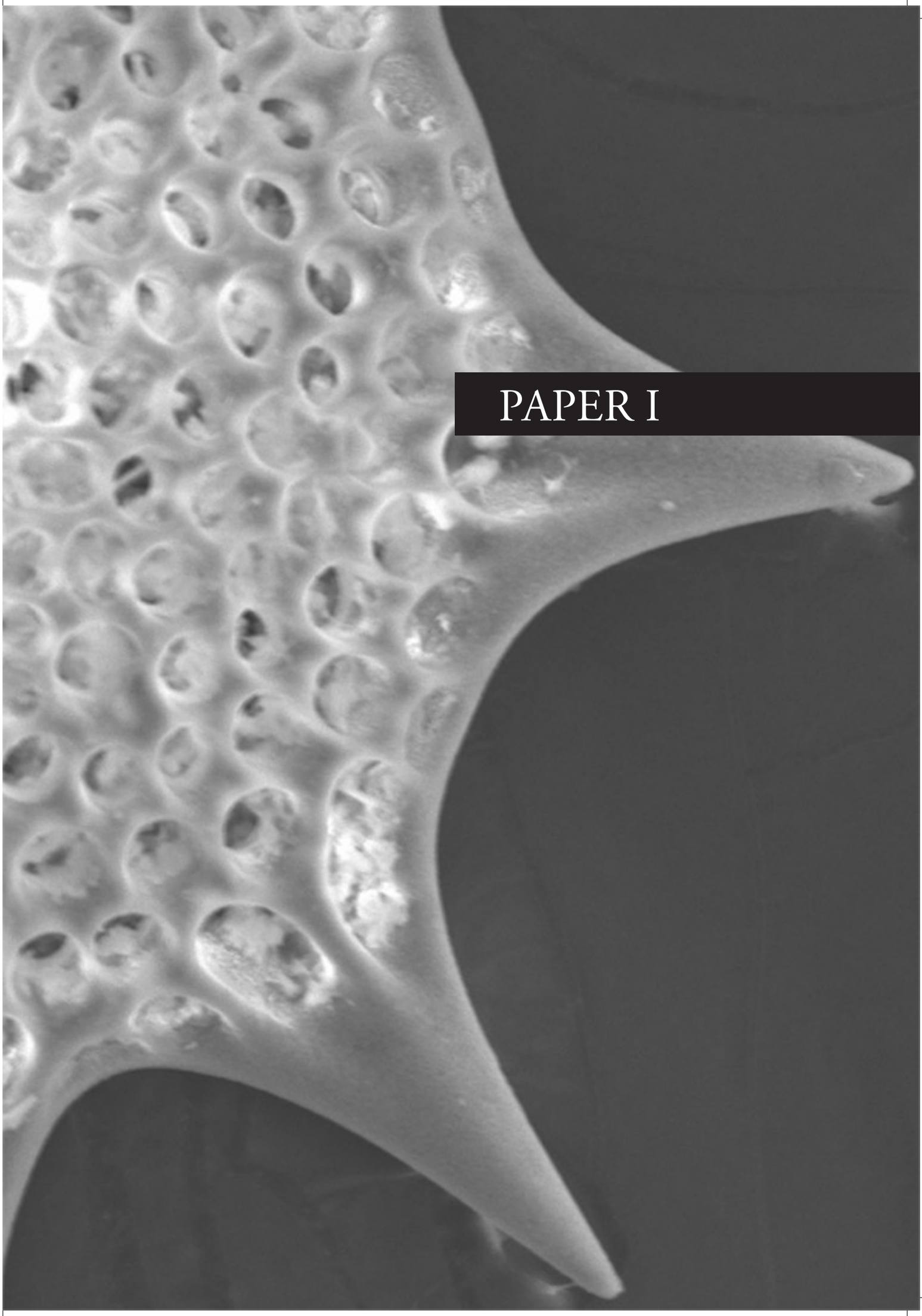

PAPER I

A silicon depleted North Atlantic since the Palaeogene: evidence from sponge and radiolarian silicon isotopes.

Guillaume Fontorbe[a,*], Patrick J. Frings[a], Christina L. De La Rocha, Katharine R. Hendry[b], Daniel J. Conley[a]

[a] Department of Geology, Lund University, Sölvegatan 12, SE-223 62, Lund, Sweden

[b] School of Earth Sciences, University of Bristol, Wills Memorial Building, Queen's Road, Bristol, BS8 1RJ, UK

* corresponding author (guillaume.fontorbe@geol.lu.se)

Abstract

Despite being one of Earth's major geochemical cycles, the evolution of the silica cycle has received little attention and changes in oceanic dissolved silica (DSi) concentration through geologic time remain poorly constrained. Silicon isotope ratios (expressed as $\delta^{30}Si$) in marine microfossils are becoming increasingly recognised for their ability to provide insight into silica cycling. In particular, the $\delta^{30}Si$ of siliceous sponge spicules has been demonstrated to be a useful proxy for past DSi concentrations.

We analysed $\delta^{30}Si$ in radiolarian tests and sponge spicules from the Blake Nose Palaeoceanographic Transect (ODP Leg 171B) spanning the Palaeocene-Eocene (ca. 60 - 30 Ma). Our $\delta^{30}Si$ results range from +0.32 to +1.67‰ and -0.48 to +0.63‰ for the radiolarian and sponge records, respectively.

Using an established relationship between ambient dissolved Si (DSi) concentrations and the magnitude of silicon isotope fractionation in siliceous sponges, we demonstrate that the Western North Atlantic was DSi deplete during the Palaeocene-Eocene throughout the water column, a conclusion that is robust to a range of assumptions and uncertainties. These data can constitute constraints on reconstructions of past-ocean circulation.

Previous work has suggested ocean DSi concentrations were higher than modern ocean concentrations prior to the Cenozoic and has posited a drawdown during the Early Palaeogene due to the evolutionary expansion of diatoms. Our results challenge such an interpretation. We suggest here that if such a global decrease in oceanic DSi concentrations occurred, it must predate 60 Ma.

1. Introduction

On geological time scales, the cycling of silicon (Si) is closely coupled to the climate system. Chemical weathering of silicate rocks converts atmospheric carbon dioxide (CO_2) to a fluvial alkalinity flux that is later precipitated as carbonate minerals in the ocean. This process counteracts a continuous CO_2 input from degassing of the solid Earth and so prevents excessive CO_2 accumulation in the atmosphere (Berner and Caldeira, 1997; Walker et al. 1981). The weathering of silicate rocks also releases solutes into continental ecosystems that will be ultimately transported to the ocean.

Of these solutes, dissolved silica (DSi) is especially important for some marine organisms including diatoms, radiolarians and siliceous sponges that require silica to build their frustules, tests, or skeletons of biogenic silica (BSi). The biological uptake of dissolved silica and the subsequent precipitation as BSi imparts a fractionation to the silicon isotopes, with discrimination against the heavier Si isotopes, resulting in BSi with a lower proportion of the heavier isotopes than the DSi it originated from. Because burial of BSi is by far the main output of silica from the ocean (Tréguer and De La Rocha, 2013), the fractionation during biomineralisation of BSi has a significant influence over the distribution and cycling of silicon isotopes within the ocean.

Silicon isotope ratios (expressed as $\delta^{30}Si$) in marine organisms have proven useful for reconstructions of different facets of the silica cycle, from nutrient use in surface waters (De La Rocha et al., 1998; Egan et al., 2012) to larger spatial and temporal scale changes in the marine silica cycle (De La Rocha, 2003). A recent development has been the use of $\delta^{30}Si$ of siliceous sponge spicules as a proxy for DSi concentrations in the ocean (Hendry and

Robinson, 2012). Advantageously, the degree of Si isotope fractionation by siliceous sponges changes with ambient DSi concentration. This relationship has been used to reconstruct concentrations of DSi in past seawaters by making assumptions about the value of $\delta^{30}Si_{DSi}$, the isotopic composition of the ambient DSi (e.g. Griffiths et al., 2013). This is important, as DSi concentrations of bottom waters - where sponges grow - should be less sensitive to short term or local perturbations. Coupling the use of $\delta^{30}Si$ in sponge spicules to infer DSi concentrations with $\delta^{30}Si$ from other microfossils that instead reflect the $\delta^{30}Si$ of the waters they dwell in could be a profound but as yet relatively unexplored way to infer changes in the relationship between oceanic DSi concentrations, intensity of chemical weathering of silicate rocks and climate over geologic time.

Despite being one of the Earth's most fundamental geochemical cycles, the evolution of the oceanic Si cycle has received little attention. Ocean DSi concentrations over geological time have been estimated using the occurrences and facies distributions of cherts – microcrystalline quartz deposits - to define two endmember situations for the marine Si cycle: i. a Precambrian ocean characterised by saturation of DSi, and ii. the modern ocean characterised by DSi depletion at the surface (Maliva et al., 1989; Siever, 1992). In the absence of silica-secreting organisms, Precambrian DSi concentrations in the ocean must have reached saturation with respect to amorphous, hydrated silica, also known as opal (i.e. concentrations on the order of 1000-1800 μM). Ocean DSi was then brought below opal saturation following the evolution of the first silica-secreting organisms during the Neoproterozoic, with a final, more extreme drawdown towards modern conditions hypothesised in the late Cretaceous to early Cenozoic due to the rise of diatoms (Maliva et al. 1989).

This narrative raises questions about the timing and rate of the transition from a high DSi to a low DSi ocean, and whether it occurred as a single event or a series of stepwise changes. Also open to question is whether the net removal of silica from the ocean occurred because of an oceanwide increase in biologic silica production and export or if it was due to removal restricted to a small number of areas in the ocean. Developing the datasets necessary to answer these questions will further allow investigation into short and longer-term links between climate and the marine silica cycle.

One period to start tackling such questions is the Palaeogene (65.50-23.03 Ma). It encompasses the period of time when the diversification of diatoms is hypothesised to strengthen biological control over the ocean Si cycle (Maliva et al., 1989). Additionally, it allows us to study the behaviour of silicate weathering and the climate system under conditions 4 to 12 °C higher than modern temperatures (Zachos et al., 2001). Here, we investigate the evolution of the ocean Si cycle during the Palaeocene-Eocene as recorded in $\delta^{30}Si$ from siliceous sponge spicules and radiolarian tests in the Western North Atlantic Ocean (ODP Leg 171B). Using a published calibration to constrain ambient DSi concentrations in the deeper waters we show that DSi concentrations in the North Atlantic, which are remarkably low in the modern ocean, were already low during the Palaeocene-Eocene and probably had modern looking isotopic composition. This conclusion is robust to a range of reasonable $\delta^{30}Si$ values for the ambient DSi and adds substantial nuance to previous estimates of palaeo-DSi concentrations in the ocean.

2. Material and Methods

Sample/site description

Samples from five cores (1049A, 1050A, 1051A, 1052A and 1053A) from the Blake Nose Palaeoceanographic Transect (ODP leg 171B; ca. 30°N, 76-77°W) were selected for analysis. Blake Nose is situated on the margin of the Blake Plateau (Fig. 1), where Palaeogene sediments are not extensively covered by more recent material and are topped by manganiferous sand and nodules that prevented post-depositional erosion (Norris et al., 2001). The cores have been drilled along a downslope transect spanning 1300-2700 mbsl. Benson (1978) suggested that Palaeogene sediments

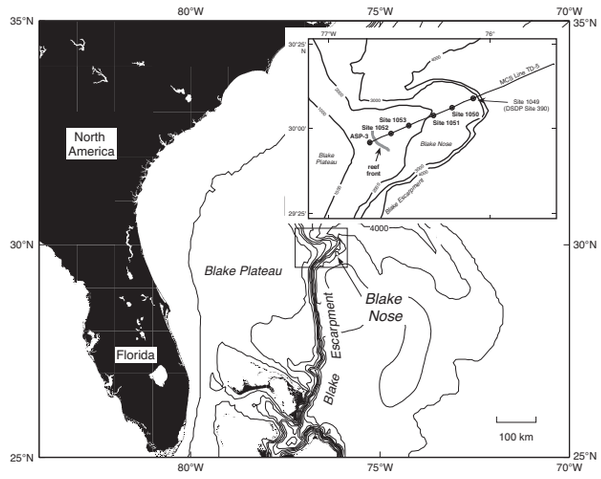

Figure 1: Location of the drill sites in the Western North Atlantic. Modified from Norris et al. (1998).

in this region were deposited at a similar or slightly deeper depth than they are found at present due to minor subsidence, partly compensated for by lower sea levels after the Eocene, although the relative depth differences between the depth of coring sites has remained similar since the time of deposition.

The stratigraphic sequence in the cores is composed for the most part of Eocene carbonate ooze covering claystones from the Palaeocene and constitutes an almost complete sequence of Palaeocene-Eocene sediments. The age model we use derives from a mixture of foraminiferal and radiolarian biostratigraphy and magnetostratigraphy (Norris et al., 1998). Details of the cores and the sampled material can be found in Table 1. Modern day waters in this region are nearly entirely depleted in DSi at the surface, while DSi concentrations increase with depth up to about 30 µM at 3000 mbsl (Garcia et al., 2014). To our knowledge, no data exist for δ^{30}Si of DSi near Blake Nose. Reported values for δ^{30}Si of DSi offshore from Chesapeake Bay (ca. 37˚N, 73˚W) range from +1.5‰ near the surface to +0.9‰ at 3000 m depth, and between +1.2 and +1.5‰ between 1000 and 3000 m depth in the Sargasso Sea (31˚N 58˚W) (De La Rocha et al., 2000).

Sample preparation

Biogenic silica was separated from other sediment fractions following the chemical and physical techniques detailed in Morley et al. (2004). Briefly, a few grams of bulk sediment were cleaned with hydrogen peroxide and hydrochloric acid to remove organic matter and carbonate material. BSi is separated from detrital material such as clays and other lithogenic silicates by repeated heavy liquid separation, using sodium polytungstate (SPT) at a density between 2.1 and 2.3 g/mL. The light fraction, containing the BSi, was then wet-sieved at 53 µm to isolate the larger fraction of BSi and remove the majority of fragmented material.

From this, sponge spicules and radiolarian tests were handpicked under a light microscope to further minimise contamination. Only monoaxonic sponge spicules were collected to avoid the possible difference in silicon isotope fractionation between different types of sponge spicules (Hendry et al. 2015.). It is important to note that given current poor understanding of radiolarian silicon isotope fractionation, we elected to pick the bulk radiolarian sample from the >53 µm fraction. Cleaned and separated BSi fractions were then dissolved in a large excess of HF. The resulting solution was diluted and purified via anion exchange chromatography following Engström et al. (2006) for isotopic analysis.

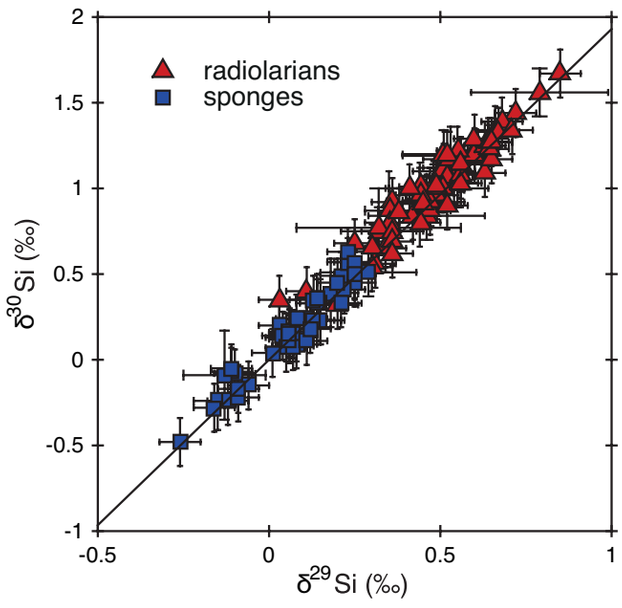

Figure 2: Three-isotope plot of δ^{30}Si and δ^{29}Si values of radiolarian tests (open red triangles) and sponge spicules (solid blue squares). The black line represents the expected mass-dependent fractionation (δ^{30}Si = 1.93 x δ^{29}Si). Vertical and horizontal bars represent external reproducibility (2σ).

Table 1: Hole locations, water depths, sample intervals, approximate sampled age intervals, and number of analysed samples.

Hole	Location	Water depth (mbsl)	Sampled interval (mbsf)	Approx. Age range (Ma)	Number of samples
1049 A	30°08.5436'N 76°06.7312'W	2667.3	33-70	39-50	8
1050 A	30°05.9977'N 76°14.1011'W	2299.8	36-294	41-60	28
1051 A	30°03.1740'N 76°21.4580'W	1982.7	15-610	34-59	27
1052 A	29°57.0906'N 76°37.5966'W	1344.5	20-125	33-40	5
1053 A	29°59.5385'N 76°31.4135'W	1629.5	11-177	36-38	2

Silicon isotope ratios of the purified Si solutions were measured using a multi-collector inductively coupled plasma mass spectrometer (MC-ICPMS, Neptune, Thermo Scientific) at the Pole Spectrometrie Ocean (Ifremer, Brest). The purified Si solutions were diluted to 1 ppm using 1% nitric acid and introduced to the Neptune using an Apex HF desolvator to give a signal intensity of about 25 V on mass 28 at medium resolution. The concentration of HF in the standard (NBS28) and the samples was fixed (~1 mM HF) and the signal intensity matched within 10 %. A matching amount of magnesium (1 ppm) was added to each sample and standard. The beam intensity on masses 28, 29, and 30 for silicon and on masses 25 and 26 for magnesium were monitored for a block of 30 cycles (8s integrations), followed by 5 min of rinse with 1 % HNO_3. The background signal intensity on mass 28 at the end of the rinse was in the order of 1 % of the standard/sample signal intensity.

Si isotope ratios ($^{29}Si/^{28}Si$ and $^{30}Si/^{28}Si$) were corrected for internal mass bias using the Mg internal standard following the method prescribed by Cardinal et al. (2003). These corrected ratios were used to calculate $\delta^{30}Si$ and $\delta^{29}Si$, averaged from two series of bracketed measurements (standard-sample-standard):

$$\delta^{x}Si=(R_{sam}/R_{std} - 1) \times 1000 \quad (1)$$

where R_{sam} and R_{std} are the corrected ratios of $^{x}Si/^{28}Si$ of the sample and the standard respectively.

Values fall on the expected mass-dependent fractionation line (r^2=0.96, n=112; Fig. 2), implying the successful removal of all polyatomic interferences during measurement. Analysis of the secondary standards Diatomite and Big Batch prepared following identical protocols, in a different analytical session, yielded values in good agreement with accepted values (Reynolds et al., 2007; Supplementary Table 2). Long-term precision (expressed as 2σ) based on measurements of multiple NBS28 standards and secondary standards was of ±0.14‰ on $\delta^{30}Si$ and ±0.06‰ on $\delta^{29}Si$.

3. Results

The 65 analysed radiolarian samples cover the period 59.6 to 33.5 Ma, with $\delta^{30}Si$ values ranging from +0.32 to +1.67‰ (mean of +0.99‰) and are consistently more positive than the 47 samples of monoaxonic sponge spicules (-0.48 to +0.63‰, with a mean of +0.17‰) over the same time interval. All data are available in Supplementary Table 1.

Neither the radiolarian nor the sponge $\delta^{30}Si$ record shows a significant trend through time over the entire interval (-0.001‰ per Ma, r^2 = 0.01 for the radiolarian data, and +0.008‰ per Ma with r^2 = 0.06 for the sponge data). However, both datasets contain shorter time scale features, as shown most clearly in a 3-point running average (Fig. 3). In both the radiolarian and the sponge record, there is a positive excursion in $\delta^{30}Si$ between ca. 54 and 50 Ma of 0.7 and 0.5‰, respectively. This excursion is followed, between ca. 50 and 47 Ma, by a drop of 0.7‰ for the radiolarian record and of about 0.25‰ for the sponge record. It is worth noting that the difference in amplitude of the decrease between the

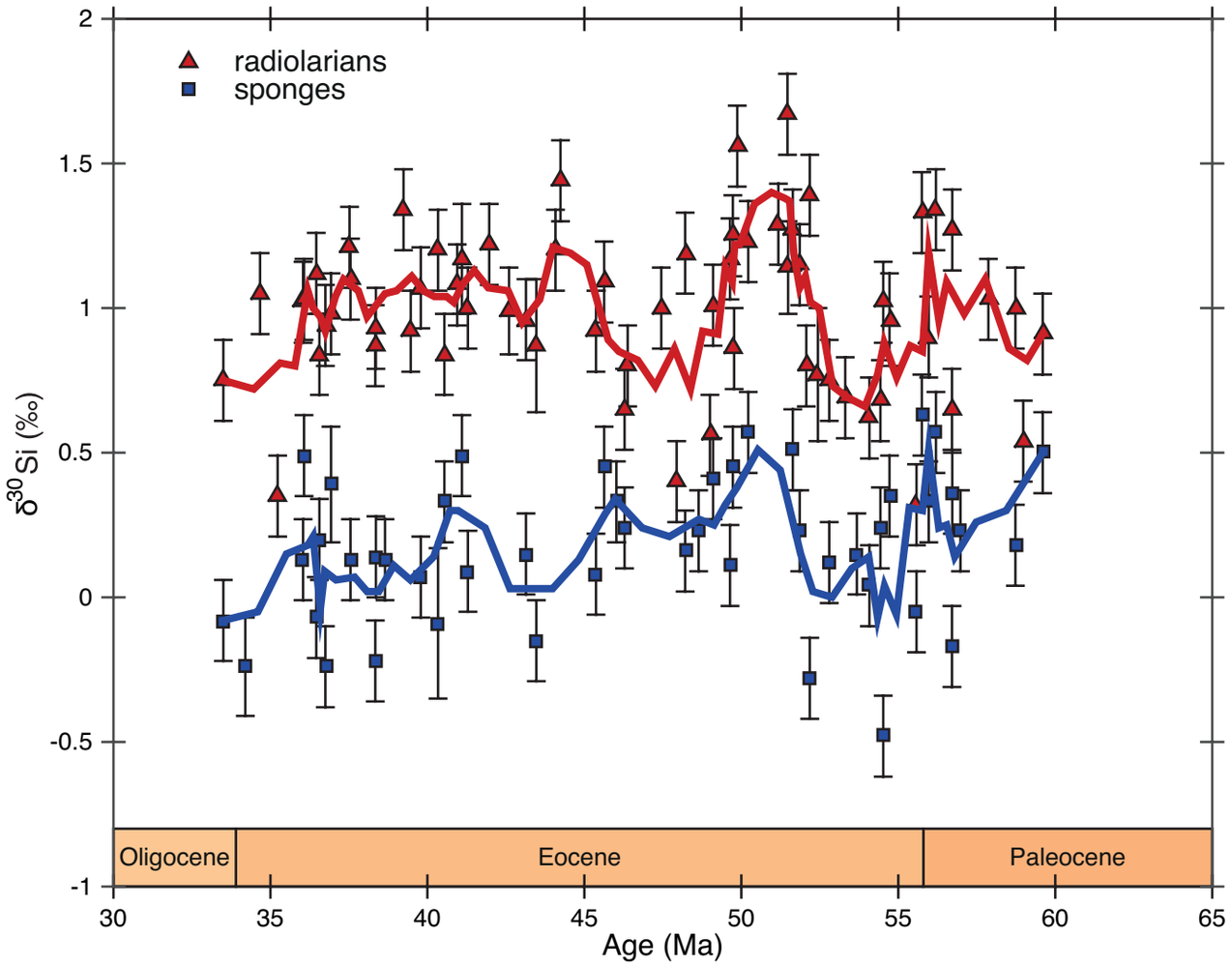

Figure 3: Radiolarian tests (open red triangles) and sponge spicules (solid blue squares) $\delta^{30}Si$ values against sample age. Vertical bars show external reproducibility (2σ). Thick red and blue lines represent the three-points moving average for the radiolarian test and the sponge spicule records, respectively

two records might result from an artefact caused by the lower sampling resolution in the sponge dataset. The radiolarian record may show a second, less pronounced excursion from 47 to 43 Ma, although more samples are needed to confirm this. The sponge record over this interval is too sparse to show any excursion. After 43 Ma, both records appear to be fairly invariant with values of $\delta^{30}Si$ of +1.04 ± 0.05‰ (n=19) for the radiolarian record and +0.10 ± 0.24‰ (n=17) for the sponge spicule record.

The two records also appear to be broadly parallel. Calculation of the offset between radiolarian and sponge spicule $\delta^{30}Si$ over time is possible from paired sponge and radiolarian analyses from the same samples. The typical offset between the records is 0.82 ± 0.29‰ (n=41) and shows no trend with sample age (Fig. 4).

4. Discussion

The reconstruction of ocean DSi concentrations over geological times has only been approached in a semi-quantitative manner. The development of $\delta^{30}Si$ of marine sponge spicules as a proxy for DSi concentrations (Hendry et al., 2010; Wille et al., 2010) has opened the door to longer timescales studies (e.g. Egan et al. 2013). However, a major issue with this approach is the requirement that the silicon isotopic composition of the source DSi must be independently constrained. Here, we utilise the published $\Delta\delta^{30}Si$-[DSi] sponge spicule calibration with a range of reasonable $\delta^{30}Si$ values for the ambient water. In doing so, we provide the first quantitative constraints on DSi concentrations in the deep layer of the Palaeogene Atlantic. Specifically, we address (i) the probable range of DSi concentrations and $\delta^{30}Si$ at our site during the early to mid Palaeogene (section 4.1), (ii) the implications of these estimates in

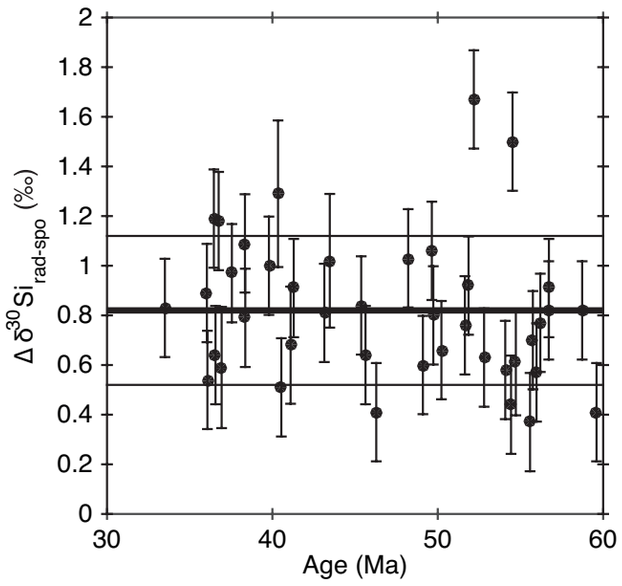

Figure 4: Offset between radiolarian tests and sponge spicules $\delta^{30}Si$ through time. Thick line represents the mean and thin lines show ±1σ.

the context of previous studies (section 4.2) and (iii) what mechanisms may explain the (co-)variation in the radiolarian test and sponge spicule $\delta^{30}Si$ records (section 4.3). Given that we are among the first to apply this new proxy on these timescales, we end by explicitly pre-empting some possible concerns (section 4.4).

4.1 Reconstruction of DSi concentrations and $\delta^{30}Si$.

At a rudimentary level, it is noteworthy how similar the Palaeogene North Atlantic Si cycle as recorded in our sponge and radiolarian $\delta^{30}Si$ records is to the present day North Atlantic.

4.1.1 Surface waters

As with the majority of the global ocean, the modern North Atlantic (i.e. 0 – 60˚ N) is characterised by nearly entirely Si depleted surface waters (upper few hundred metres). The silicon isotope composition of the upper water column (<1000m, encompassing the living habitat of radiolarians) in the Atlantic ranges from +1.00‰ to +2.89‰ (Brzezinski and Jones, 2015; De La Rocha et al., 2000; de Souza et al., 2012). Assuming the fractionation of silicon isotopes during formation of radiolarian tests is ca. -1.5‰ (see section 4.4.4 for a discussion of this assumption), modern radiolarians should have $\delta^{30}Si$ values spanning from -1.0‰ to +1.9‰. No modern data exist, but deglacial (~17ka BP) radiolarians from the north Atlantic (33.7˚N, -57.6˚W) average 1.5‰ (Hendry et al. 2014), and Holocene radiolarians in two cores from the Atlantic sector of the Southern Ocean (49.0˚S, 12.7˚W and 52.6˚S, 4.5˚E) range from -0.45‰ to 1.17‰ (Abelmann et al., 2015). Our Palaeogene radiolarian $\delta^{30}Si$ data broadly overlap with these expectations and measurements, suggesting the $\delta^{30}Si$ of upper water column DSi was similar or perhaps slightly ^{30}Si enriched.

4.1.2 Bottom waters

In contrast to the other ocean basins, the deep waters (>1000m) of the north Atlantic are also relatively Si deplete, ranging from <15μM in e.g. the Labrador Sea or the Iceland Basin, to a maximum of ~60μM in the western equatorial Atlantic (Garcia et al. 2014). In contrast, bottom waters of the Pacific and Indian oceans are consistently >100μM, ranging up to >170μM in the North Pacific. The fundamental reason for this inter-basin gradient is that the modern North Atlantic is a site of deepwater formation, where Si depleted surface water is subducted and drawn southwards. Measurements of $\delta^{30}Si$ in Atlantic waters between 1500 and 2700m (the approximate depth of sponge habitats along the Blake Nose transect) fall between 0.90 – 1.86‰ (De La Rocha et al. 2000; de Souza et al. 2012).

Using modern DSi concentrations and the established relationship between DSi concentration ([DSi]) and the magnitude of siliceous sponge silicon isotope fractionation expressed as (the difference in $\delta^{30}Si$ values of sponges and the source DSi;) (Hendry and Robinson, 2012), we can estimate what $\delta^{30}Si$ value modern sponge spicules at Blake Nose might have. $\Delta\delta^{30}Si_{spo\text{-}DSi}$ has been empirically calibrated on sponge spicules from sediment coretops (Hendry and Robinson, 2012) as:

$$\Delta\delta^{30}Si_{spo\text{-}DSi} = -6.54+270/(53+[DSi]) \quad (2)$$

which can be rearranged to find the DSi concentration of the source water:

$$[DSi] = (270/(\delta^{30}Si_{spo} - \delta^{30}Si_{DSi} + 6.54)) - 53 \quad (3)$$

As captured in equations 2 and 3, the predicted magnitude of fractionation increases

with increasing DSi concentration, ranging from -1.45 to -5.47‰ at 1 to 200 µM. Present-day DSi concentrations around Blake Nose of ca. 15-30 µM at 2500 m depth imply a sponge silicon isotope fractionation ($\Delta\delta^{30}Si$) of in the region of -2.6 to -3.3‰ (cf. equation 2). Combined with the range of $\delta^{30}Si$ values measured in Atlantic waters, this equates to an expected modern sponge silicon isotope composition of ca. -2.4 to -0.6‰, with our best guesses ([DSi] = 20µM, $\delta^{30}Si$ = +1.5‰) equating to a $\delta^{30}Si_{spicule}$ of -1.34‰. To our knowledge, no modern spicules have been measured in the vicinity of Blake Nose, but a record from 300 km to the north has recent (late Holocene) sponge spicules at ca. -1.2 to -1.5‰ (Hendry et al 2014). Our sponge data are consistently heavier, with a mean of +0.17‰. This first-order observation strongly suggests that Palaeogene DSi concentrations at Blake Nose were lower than modern values.

However, as captured in equations 2 and 3, there are two unknowns ([DSi] and $\delta^{30}Si_{DSi}$) and therefore no unique reconstructions of [DSi]. Essentially, our data can be explained by either low-[DSi], low-$\delta^{30}Si$ waters or high-[DSi], high-$\delta^{30}Si$ waters. This already hints at a more likely scenario: in the modern Atlantic (and the ocean as a whole), there is a negative relationship between [DSi] and $\delta^{30}Si_{DSi}$ (De La Rocha et al. 2000; de Souza et al. 2012, 2015; Brzezinski and Jones 2015), making it hard to generate high-DSi, high $\delta^{30}Si$ waters. This is because the main process that increases seawater DSi $\delta^{30}Si$ values (i.e. biological utilisation) also removes DSi, while the reverse is also true: increases in seawater [DSi] tend to lower its $\delta^{30}Si$ (i.e. by opal dissolution). This makes a low-[DSi], high-$\delta^{30}Si$ solution more likely. Nevertheless, we can test the robustness of the interpretation of low-DSi by reconstructing ambient water DSi concentrations with a range of increasingly implausible seawater $\delta^{30}Si$. Shown in Fig. 5a, we perform this exercise with steps in $\delta^{30}Si$ at 0.5‰ to a maximum of 4.5‰, greater than the maximum observed in the modern ocean (+4.4‰ in highly productive, Si-deplete waters in the Peruvian upwelling zone; Grasse et al. 2013). Note that this is almost certainly a gross

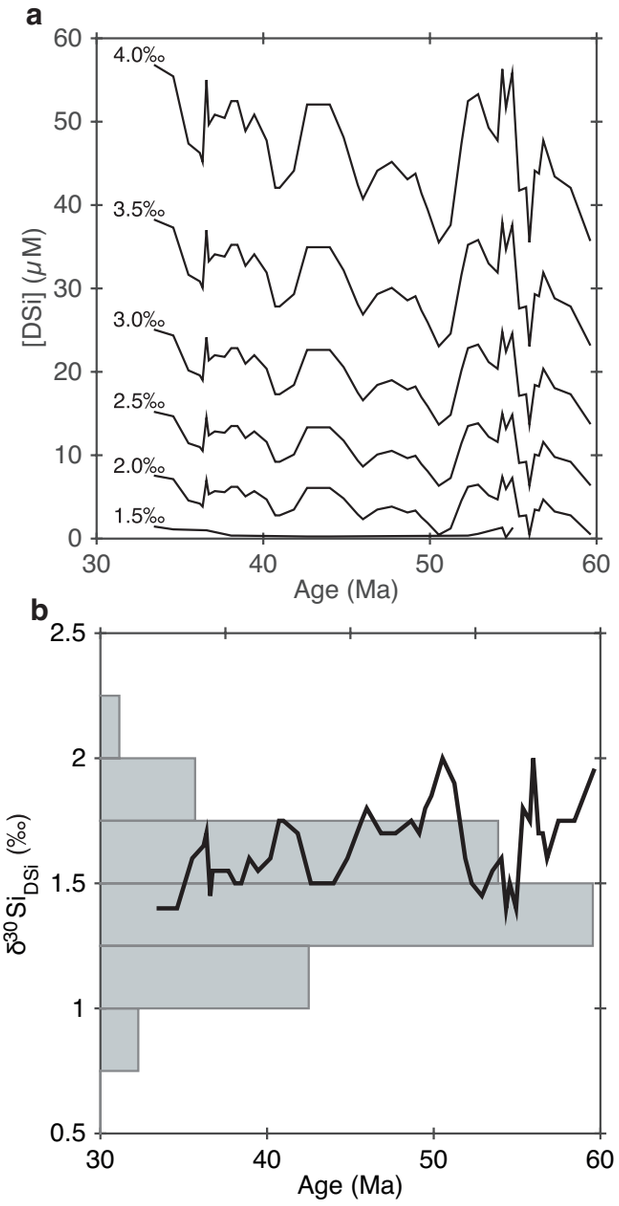

Figure 5: (a) Reconstructed DSi concentrations according to fixed values of $\delta^{30}Si_{DSi}$. (b) Minimum $\delta^{30}Si_{DSi}$ values (black line) required to reconstruct DSi concentrations (i.e. [DSi] > 0 µM). The horizontal histogram represents the modern distribution of $\delta 30Si_{DSi}$ in the Atlantic Ocean below 1000m.

overestimation for bottom water DSi: the highest value to our knowledge for a water mass >1000m depth is 2.2‰ in the Atlantic (De La Rocha et al. 2000), and <1.6‰ in other ocean basins. Maximum predicted DSi concentrations do not exceed 60µM, but generally are <10µM. The point of this exercise is not to precisely define what the DSi concentrations of waters bathing Blake Nose were, but rather to demonstrate that even with improbable inputs, the reconstructed inputs are remarkably low throughout the early Palaeogene relative to those predicted by

earlier work (see discussion below; Maliva et al. 1989).

A second useful outcome of this exercise is that it allows us to define the minimum bottom water $\delta^{30}Si$ value that produces meaningful results (namely [DSi] >0 μM). As shown in Fig 5b, this averages 1.65‰ throughout our study period, and never dips below 1.40‰. This is similar to the range of values seen in the North Atlantic today (Fig. 5b) but given that these are minimum values it implies Palaeogene North Atlantic seawater DSi was slightly more ^{30}Si enriched than the present day.

4.2 Implications of silicon depleted bottom waters at Blake Nose

4.2.1 Extent of silicon depletion

It is first worth considering the extent to which our interpretations can be extrapolated beyond the Blake Nose escarpment itself. We suggest that our results argue for near-global DSi depletion in the surface ocean, and at least in the North Atlantic for deeper waters. The logic behind this conclusion is based on two simple premises. First, that the only way to generate DSi-deplete bottom water is to subduct DSi depleted surface waters, and second, that depletion of DSi from the surface ocean is unlikely to have been a localised phenomenon.

Premise 1 is why North Atlantic Deep Water (NADW) has low [DSi] (<20 μM) and Antarctic Bottom Water (AABW) is DSi replete (~100 μM) (Garcia et al. 2014); NADW derives from low DSi waters while AABW does not. It follows that surface waters at the source of the bottom water (see below) that bathed Blake Nose were DSi depleted, and did not accumulate much DSi by remineralisation. By application of the second premise, the majority of the global surface ocean was also DSi deplete.

Premise 2 can be validated from the modern ocean – with the exception of Fe limited regions like the Southern Ocean, DSi is uniformly low in the surface ocean (<10μM). It is supported by the global distribution of the major groups of silicifying planktonic organisms in the early-mid Palaeogene: both radiolarians and diatoms were ubiquitous, meaning the North Atlantic was not unique. Further support for the extrapolation of our results to the regional scale (for intermediate/deep waters) and the global scale (for surface water) comes from the relative homogeneity within ocean basins with regards to DSi concentrations and the lack of any suitable mechanism for generating and maintaining a gradient of DSi concentrations. For example, from 1500 to 2500m water depth in the north Atlantic DSi varies from 10 to 35 μM, and from 120 to 180 μM, in the North Pacific, i.e. consistency over a large area. This implies that DSi measured (or in our case reconstructed) at a point below the surface ocean can be reasonably extrapolated within the ocean basin in which it occurs.

4.2.2 Implications for evolution of ocean Si cycle on geological timescales

The conclusion that the sponge spicule record robustly yields low DSi concentrations for Blake Nose in the Palaeogene is in contrast to the established narrative. This argues for a transition from ocean DSi concentrations in the region of 1000 μM in the Cretaceous to <100 μM in the late Cenozoic due to the expansion of the diatoms (e.g. Siever 1992). This was originally based on the sedimentary loci of different chert facies (Maliva et al. 1989), and has since found additional support from changes in radiolarian and silicoflagellate silicification (Lazarus et al., 2009; van Tol et al., 2012). Using a simple box model, De La Rocha and Bickle (2005) suggested a diatom-mediated drawdown in DSi could take as little as ~2.5 Ma. If such a decrease occurred in the early Cenozoic, siliceous sponges growing in this time should have shifted from producing highly fractionated (lower $\delta^{30}Si$) to less fractionated (higher $\delta^{30}Si$) spicules (Hendry and Robinson, 2012; Wille et al., 2010) that should produce a highly resolvable decrease in sponge spicule $\delta^{30}Si$ (of a few permil). Such a drop is absent in our data.

It is therefore helpful to look at the assumptions underlying the supposed early Cenozoic DSi drawdown. It is ascribed to the ecological success of diatoms (Maliva et al. 1989), specifically to their ability to produce and export high quantities

of BSi even at low DSi concentrations, and premised on early work that argued for an almost exponential increase in diatom diversity though the Cenozoic (e.g. Small, 1950). However, reconstructing diatom diversity – assuming this is a reasonable proxy for their production – is complicated, and biases can easily be introduced (Kotrc and Knoll, 2015). Most attempts to define diatom diversification to date have used the Neptune database, and different approaches suggest either i) little net Cenozoic change with a slight late-Eocene peak (Cermeño et al., 2015; Rabosky and Sorhannus 2009), ii) a general Cenozoic diversification (Lazarus et al., 2014; Spencer-Cervato, 1999) or iii) general stasis throughout the Cenozoic (Kotrc and Knoll, 2015). While our data cannot eliminate any of these possibilities, they do suggest that if the diatoms truly were responsible for a Cretaceous-Palaeogene DSi drawdown, they had developed the ability to achieve this prior to 60 Ma.

4.2.3 Implications for reconstructions of Palaeogene ocean circulation

Our data provide two new insights. First, the sponge δ^{30}Si record is consistent throughout the depth profile of cores studied (ODP 1049-1052; 1300-2700 m), implying a single water mass was present at all of these sites. Second, they suggest the source of the water did not change during the period studied here (59.6 to 33.5 Ma) - or at least that it coincidentally had a δ^{30}Si-[DSi] pairing that produced similar spicule δ^{30}Si. Therefore, we need to identify a Palaeocene-Eocene source area for the bottom waters at Blake Nose that i) was DSi deplete at the time of formation, and ii) did not accumulate substantial amounts of regenerated DSi as it traveled from the its site of formation to Blake Nose.

Reconstructing the movement of water-masses through time is of considerable interest given the cause-and-effect feedbacks between global climate and ocean circulation. To this end, Nd isotope ratios (expressed as εNd) have been extensively employed. Briefly, this proxy is based on Nd's short residence time and heterogeneous distribution in the ocean, coupled with the fact that different source regions have distinctive εNd values related to the age and lithology of the material being weathered. This means dissolved Nd isotope ratios reflect their source via continental weathering (Lacan et al., 2012), and are transferred to e.g. fish debris early in the diagenetic process (Staudigel et al., 1985), so Nd isotope analysis of leachates from this material reflects εNd of the deep water in the region - and therefore the source of the water mass.

In the early Palaeogene, εNd values of ca. -11 are found at Demerara Rise in the tropical North Atlantic (~9°N, MacLeod et al., 2011). Contemporaneous values from the South Atlantic were more radiogenic (εNd ≈ -8; Via and Thomas, 2006), but Fe-Mn crusts in the waters forming in the Nordic seas had εNd of ~-9 to -11 (O'nions et al., 1998), leading MacLeod et al. (2011) to suggest that the deep waters of the early Cenozoic tropical Atlantic had a North Atlantic source, termed Northern Component Water (NCW). Via and Thomas (2006) had previously demonstrated that water reaching Walvis Ridge (~30°S) began to take on a North Atlantic character early in the Oligocene (~30 Ma), coincident with sedimentological evidence for intensified deep water formation in the North Atlantic (e.g. Davies et al., 2001), suggesting that the evolution of modern North Atlantic Deep Water (NADW) might have proceeded as a two-step process (MacLeod et al., 2011). However, the interpretation of NCW influencing the Equatorial Atlantic during the Palaeogene has been contested on the basis of uncertainties in the εNd values of coeval north Atlantic waters (e.g. Robinson and Vance, 2012). Ocean circulation models (Bice and Marotzke, 2002; Lunt et al., 2010), inferences based on carbon isotope (δ^{13}C) gradients in benthic foraminifera (Borrelli et al., 2014; Corfield and Norris, 1996; Nunes and Norris, 2006) and sedimentological evidence (Mountain and Miller, 1992) also tend to prefer a Southern deep water source for the western North Atlantic for most of the Palaeogene.

Nd isotope evidence from Blake Nose itself is sparse. In the late Cretaceous, prior to our δ^{30}Si records, εNd ≈ -8 (MacLeod et al., 2008) similar to contemporaneous values from the South Atlantic (Robinson et al. 2010) and consistent

with a South Atlantic source through the Central Atlantic Gateway. Two samples from the carbon isotope excursion of the Palaeocene-Eocene Thermal Maximum (PETM; 55.5 Ma) at site 1050 provided εNd of -8.34 and -9.17 (Thomas et al., 2003), also lower than dissolved Nd in the modern Nordic or Labrador seas (Lacan et al., 2012).

Overall, it seems the most likely source of waters bathing Blake Nose during the early-mid Palaeogene derived from the south, though the issue is far from settled. Another intriguing possibility is the presence of a low-latitude, Tethyan deep water mass formed by evaporation-induced density increases, termed Warm Saline Deep Water (WSDW; Norris et al., 2001; Pak and Miller, 1992), which has gained some support from εNd data (Scher and Martin, 2004), although it has proved difficult to reproduce in modelling studies.

The dynamics of water subduction and advection in the Palaeocene-Eocene southern high latitudes were not analogous to present. Prior to the development of the Antarctic Circumpolar Current (ACC) the region was likely dominated by water sinking, while post-ACC, the opening of ocean gateways allowed wind driven upwelling along the Antarctic Divergence, increasing deep water formation in the North Atlantic and setting the scene for the evolution of the modern state of ocean overturning. This led Egan et al. (2013) to posit the presence of a pre-Late Eocene southern overturning loop, causing the poleward advection of nutrient deplete surface waters. The low nutrient status of these surface waters may conceivably have been augmented by the absence of (modern) Fe limitation at high southern latitudes via Fe inputs from an unglaciated Antarctica.

Therefore, the Southern Ocean is a plausible source of bottom water for the Palaeocene-Eocene Blake Nose, if these waters had low [DSi] (Egan et al., 2013). However, previous sponge analysis on ODP core 689 (Southern Ocean, Atlantic sector) spanning the Eocene-Oligocene boundary, though only slightly overlapping with the end of our records (De La Rocha 2003; Egan et al 2013; Fig 3) exhibit δ^{30}Si values about 1.5‰ lower than the Blake Nose record, implying correspondingly greater DSi concentrations (cf. Equations 2-3), which would argue against a southern source for Blake Nose bottom waters. The long travel distance for this water source also suggests that it would accumulate more regenerated DSi than our reconstructions allow, as evidenced by Palaeocene benthic δ^{13}C gradients (Borrelli et al., 2014; Cramer et al., 2009). We therefore favour a Tethyan WSDW, given the much lower distance available for regeneration of DSi from sinking BSi. Extending the Blake Nose sponge δ^{30}Si record forwards, and the Southern Ocean records of De La Rocha (2003) and Egan et al (2013) backwards, would resolve this issue and shed considerable light on the development of the modern Atlantic circulation.

4.3 Co-variation between radiolarian and sponge δ^{30}Si

The radiolarian and sponge δ^{30}Si records behave similarly over the Palaeocene-Eocene (Figs 3 and 4). This is not necessarily an intuitive result: these two groups of silicifiers occupy different environments and have different Si uptake mechanisms, meaning there is little *a priori* reason why they should co-vary. This suggests a major control on both the radiolarian and sponge δ^{30}Si records is the silicon isotope composition of the ambient seawater. The total variability in our sponge spicule and radiolarian records is about 0.5‰ and 0.7‰, respectively, in the smoothed curves (Fig 3). For context, changes in diatom or sponge δ^{30}Si associated with the transition from the last glacial maximum to the Holocene are of similar amplitudes (e.g. Ehlert et al., 2013; recently reviewed in Frings et al., 2016).

Such long-term co-variation can be explained in two ways. The first explanation is a localised shift in δ^{30}Si of both bottom and surface water DSi, related to changes in ocean circulation maintained over several millions of years. The alternative is a whole ocean change in mean δ^{30}Si, related to a change in the average silicon isotopic composition of DSi inputs to the ocean (Frings et al., 2016). Given that the Nd isotope evidence (e.g. Via and Thomas, 2006) does not suggest large-scale reorganisation of Atlantic circulation during the

early Palaeogene, we outline some mechanisms by which the inputs to the ocean Si cycle may have varied.

The largest input of silicon to the ocean is river DSi, which is ultimately derived from the chemical weathering of continental silicate minerals (Tréguer and De La Rocha, 2013) and today has an average $\delta^{30}Si$ value around +1.0 - +1.5‰ (Frings et al., 2016). It is generally accepted that silicate weathering rates are linked to climate, and thus act as a planetary thermostat (Walker et al., 1981). Over long time scales carbon mass-balance imposes the constraint that the consumption of CO_2 via weathering of silicate minerals balances the degassing of CO_2 from the solid Earth (Berner and Caldeira, 1997), assuming silicate weathering is the most important sink in the global C cycle. If this is assumed to be proportional to the seafloor spreading rate - thought to be broadly invariant over the past 180 Ma (Rowley, 2002) - this requires that net CO_2 consumption by silicate weathering rates over the same period have also been relatively consistent, transient changes in the size of the Earth's surficial carbon pool notwithstanding. However, the ratio of fluvial DSi produced to CO_2 consumed is not fixed, and depends both on the cation content of the silicate minerals undergoing weathering, and the congruency of the weathering reactions (i.e. the degree of completeness of the conversion of minerals into solutes). Indeed, because the primary control on river DSi is thought to be the extent of Si incorporated into secondary clay minerals (De La Rocha et al., 2000; Frings et al., 2016), then this provides a simple mechanism for varying the magnitude of the river DSi flux and its silicon isotopic composition: vary the efficiency with which silicate weathering converts the parent minerals to solutes.

Proxy data indicates higher Palaeocene-Eocene atmospheric pCO_2 and temperature reconstructions from marine and terrestrial settings and climate models indicate elevated early Cenozoic warmth (e.g. Zachos et al., 2001). Maintaining a hotter, higher pCO_2 world but with the same CO_2 removal therefore requires that the relationship between pCO_2 and silicate weathering rate differs from todays, i.e. a less efficient continental weathering regime. There is no relationship between weathering rate and river $\delta^{30}Si$, so the impact on the $\delta^{30}Si$ of riverine DSi is hard to predict. A 9‰ Cenozoic increase in ocean lithium isotope ratios (Misra and Froelich, 2012), which are also sensitive to continental weathering congruency, has been interpreted as a global decrease in weathering congruency over the Cenozoic (i.e. a greater proportion of Li tied up in secondary clays, and attributed to lower relief continents mantled with thick, cation-depleted soils (Misra and Froelich, 2012). Although Si isotopes also respond to weathering congruency, it is not clear if have the same sensitivity. Frings et al. (2015) show that the lowland alluvial plain in the Ganges tends to increase river $\delta^{30}Si$, while lowland regions that are more sediment starved tend to produce lower river $\delta^{30}Si$ (e.g. Hughes et al., 2013). Frings et al. (2016) argue that there is enough potential variability in the continental Si cycle to shift ocean $\delta^{30}Si$ by up to 0.8‰ on millennial timescales; the same must be on longer timescales, and so may explain some of the trends apparent in the radiolarian and sponge spicule $\delta^{30}Si$ data. It remains to be understood how the continental Si cycle, including weathering, varied throughout the Cenozoic, especially in the face of various external perturbations. These include periods of extended volcanism and important steps in the evolution of the terrestrial biosphere. Although we have focused on the fluvial DSi flux, a series of hypotheses regarding variations in the other DSi sources to the ocean (chiefly groundwater DSi and atmospheric and fluvial sediment dissolution) could also be constructed (cf. Frings et al., 2016). The salient point here is that changes in mean ocean $\delta^{30}Si$ of >0.5‰, via changes in the magnitude and $\delta^{30}Si$ of the ocean Si inputs, are feasible, and that long-term marine $\delta^{30}Si$ records – especially if and when they become more abundant – offer a novel way to explore the interactions between climate and weathering.

4.4 Alternative explanations

Our interpretation of a Si depleted North Atlantic during the early Cenozoic (section 4.1) and an ocean silicon isotope budget controlled by variations in the inputs (section 4.3) parsimoniously explains all the available observations. However, other interpretations are conceivable. In the following, we briefly explore issues that are known to affect other geochemical proxies hosted in biominerals (namely dissolution/diagenesis, local effects, environment/proxy calibration problems, and ecological effects), and suggest future work where necessary.

4.4.1. Dissolution and diagenesis

The magnitude of Si isotope fractionation associated with dissolution of BSi is unclear. In an initial set of experiments, Demarest et al. (2009) identified a fractionation factor of -0.55‰, i.e. a tendency to discriminate against the release of the heavier isotopes of approximately half the magnitude of the fractionation associated with BSi production by diatoms (De La Rocha et al., 1997). However, later work was unable to reproduce these findings (Wetzel et al. 2014). Core-top diatom BSi δ^{30}Si from the Southern Ocean also agreed well with mixed layer filtered diatom samples, implying little to no effect of dissolution and early diagenesis on opal δ^{30}Si values (Egan et al., 2012), a conclusion supported by water column studies (Fripiat et al. 2011). Similarly, Panizzo et al. (2016) show the absence of silicon isotope fractionation during 1600m of sinking of freshwater diatoms. Both Wetzel et al. (2014) and Demarest et al. (2009) emphasise that a large proportion of the initial BSi is required to dissolve in order that a resolvable isotope fractionation is visible in the residual material, yet our own observations and those of others (Sanfillipo and Blome, 2001; Witkowski et al. 2014) suggest the BSi is excellently preserved. We also note that as dissolution is a surface process, mass-balance requires that any putative fractionation cannot be maintained indefinitely; the outer (^{30}Si enriched) layer will also dissolve, with the net result that the δ^{30}Si of the DSi solubilised will equal that of the original opal.

The ODP shipboard lithostratigraphy indicates the episodic occurrence of porcellanite, particularly in poorly recovered sections in the middle Eocene. Porcellanite is a form of opal-CT, an initial step on the diagenetic pathway of biogenic silica to chert. Tatzel et al. (2015) have shown that this transformation – which proceeds by a dissolution/reprecipitation reaction – is associated with silicon isotope fractionation, the manifestation of which depends on the completeness of transformation. While this is problematic for interpreting δ^{30}Si of cherts, it is unlikely to be an issue for our data: individual microfossils were handpicked and observation by both light microscopy and scanning electron microscopy did not reveal any signs of dissolution or crystallisation. In general, the fact that we observe two distinct and variable populations of δ^{30}Si (i.e. radiolarians and sponges; Fig. X) together in the sediment also argues against any diagenetic overprinting or equilibration. Analysis by X-Ray Diffractometer (XRD) of early Eocene sediments in hole 1051B produces a broad peak characteristic of amorphous silica (Frings, unpublished data). Overall, it is likely artefacts introduced by dissolution or diagenesis are minimal.

4.4.2 Local effects

During at least the middle Eocene, diatom assemblages from hole 1051 (Witkowski et al. 2014) were often dominated by species interpreted as neritic (shallow water), implying considerable offshore transport by surface currents. Diatom taxa with inferred benthic habitats (*Actinoptychus*, *Diplomenora*, *Mastogloia* and *Rhaphoneis*) are also present in 1051 (Witkowski et al. 2014). If the sponge spicules are also being laterally transported, they could be recording a coastal environment signal rather than a deep-water signal, diminishing the scope of our interpretations (section 4.1). Counter to this suggestion, we argue that the inferences of neritic habitats for extinct species are uncertain. For example, the dominant taxa *Paralia*, *Pseudopodosira* and *Rutilaria* are inferred as neritic or tychoplanktonic by Witkowski et al. (2014), yet they frequently occur in the Neptune database in decidedly pelagic settings. We also note that Blake

Nose Eocene benthic foraminifera are typical of paleodepths between 1000-2000m (Borrelli et al. 2014). Extensive input of allochthonous material is also counter to the sedimentology of Blake Nose (Benson 1978), and the absence of substantial amounts of terrestrial siliciclastic material that would indicate large-scale offshore sediment transfer. Further, the benthic diatom taxa reported contribute a very minor fraction of the total assemblage data of Witkowski et al. (2014). We therefore summarise that the evidence for significant post-mortem lateral transport of sponge spicules is limited, and that the $\delta^{30}Si$ signal derives from the reported palaeodepths of the cores (Table 1), not a proximal upslope environment. Future work might seek to verify this through relating sponge assemblages to depth habitats, although the taxonomy of fossil sponges is complicated, and Alvarez et al. (in prep.) argue the majority of siliceous sponges have no real depth preference.

4.4.3 Proxy-environment calibration

The possibility of a relationship between sponge silicon isotope fractionation and ambient DSi concentrations was first posited almost simultaneously by Wille et al. (2010) and Hendry et al. (2010), and expanded on by Hendry and Robinson (2012) who developed the hyperbolic-form calibration of Eqn 2. Current understanding of this relationship attributes it to the ratio of Si influx to Si efflux to and from sponge sclerocyte (spicule forming) cells, both with associated fractionations, and that it is this ratio that is controlled by ambient DSi concentrations (Wille et al. 2010; Hendry and Robinson et al. 2012). As a palaeoceanographic proxy, sponge silicon isotopes are still in their infancy relative to e.g. well-established calcite based proxies, and scientific understanding will undoubtedly become more nuanced. Sponge $\delta^{30}Si$ suffers from the same fundamental limitation as many other (bio)geochemical proxies: we must assume the proxy-environment calibration based on modern sponges from previous studies is valid in the early Cenozoic. Yet we find it unlikely that the basic tenet of the calibration will change. It has been demonstrated that the observed relationship is not driven by temperature, pH, salinity, or the concentration of other nutrients (Hendry and Robinson 2012, Wille et al. 2010). The calibration used here (Eqn 2) is based on coretop spicules, but agrees well with data from living sponges of the classes Demospongiae and Hexactinellida (Hendry and Robinson 2012; Hendry et al. 2010; Wille et al. 2010), the two dominant groups of Si-producing sponges. In sponges, putative sclerocyte cells have been reported in Precambrian fossils (Li et al. 1998), and sponge morphology has been remarkably consistent (Pisera, 2006), arguing for a reasonably consistent relationship between [DSi] and $\Delta\delta^{30}Si$.

4.4.4 Ecological effects on radiolarian Si isotope fractionation

Knowledge regarding silicon isotope fractionation by radiolarians is still at an early stage, partly due to the difficulties involved in successfully culturing radiolarians. Their silicification is poorly understood but thought to occur within a specialised cryptoplasma membrane termed the cytokaymma, which is involved in regulating internal Si concentrations and guiding Si precipitation (Wallace et al., 2012). The extent to which radiolarians have the Si efflux mechanisms that cause Si isotope fractionation to vary with DSi concentration (as in sponges) is unclear. Overall, it seems fractionation should be related only to fractionation during the initial uptake of DSi and its transport into the cell, as is the case with diatoms. This is supported by studies that demonstrate a constant offset (albeit variable between regions) between $\delta^{30}Si$ of diatoms and radiolarians (Abelmann et al., 2015; Hendry et al., 2014). (Note that while it has long been assumed that diatom fractionation is independent of ambient DSi concentrations, compilations of all available data (Hendry and Robinson 2012; Abelmann et al. 2015) suggest there may be a relationship, albeit muted relative to sponges). Thus, in the absence of evidence to the contrary, we assume here that $\delta^{30}Si_{rad}$ reflects the isotopic composition of the source DSi with an offset due to fractionation. Note that this assumption makes little difference to our conclusions regarding ocean Si depletions, which are based on the sponge $\delta^{30}Si$ data.

The actual magnitude of this fractionation is also unknown. Hendry et al. (2014) used an offset of -1.1 to -2.1‰ between radiolarian silica and DSi in the Sargasso Sea, consistent with previous estimates (Egan et al., 2012) in order to model seawater $\delta^{30}Si$ during the most recent Heinrich Stadial (17ka). Abelmann et al. (2015) used a similar range of fractionation of -0.8 to -1.5‰ for their reconstructions based on coretop samples. However, robust data underpinning these values is lacking. Radiolarians dwell in the upper several hundred meters of the water column. Interestingly, the 125-250μm and >250μm size fractions of radiolarians in the deglacial Southern Ocean differ in their silicon isotopic composition by >1‰ (Abelmann et al. 2015). It is unclear what is causing this, although the two most likely suggestions are either that i) the species dominating each size fraction grow at different depths in the water column and/or time of the year, and so tap different sources of DSi and/or ii) the fractionation factor associated with radiolarian BSi production varies with species or growth rate/ ontogeny. More data from paired plankton and water samples and/or culturing experiments are needed to shed light on this.

Conclusions

We have analysed the silicon isotopic composition of the remains of siliceous organisms (radiolarians and sponges) from the Blake Nose escarpment in the western North Atlantic, spanning 60 to 33 Ma. Our study highlights the potential of combining $\delta^{30}Si$ values from sponge spicules and radiolarian tests to infer aspects of the Si cycle in the geological past. Using these data, in particular the sponge δ30Si values, we provide the first quantitative estimates of ocean DSi concentrations in the early Cenozoic. Our results indicate that, contrary to previous work, the North Atlantic was not DSi replete during the Palaeocene-Eocene. We cannot define if and when a drawdown of DSi concentrations occurred in this region of the ocean although it must have occurred prior to 60 Ma. We suggest that the timing and ubiquity of the various steps that have been proposed for the evolution of ocean DSi concentrations since the end of the Precambrian must be reconsidered. The observation of low-DSi waters bathing Blake Nose helps constrain past ocean circulation. Further investigations, primarily on the extent of Si isotope fractionation by radiolarians, as well as from different ocean basins would be beneficial to help put the data in a global context and to begin to elucidate more clearly the linkages between climate and the Si cycle.

Acknowledgements

This work was funded by a grant from the Knut & Alice Wallenberg Foundation to DJC plus support from a LEFEC/CYBER grant ('SiMS') to CDLR. KRH was funded by the Royal Society. We thank Emmanuel Ponzevera at IFREMER and Carolina Funkey at Lund University for laboratory assistance, and Nathalie van der Putten, also at Lund, for providing the necessary equipment for microfossil separation. We thank Damien Cardinal, two anonymous reviewers, and AE Martin Frank for their constructive comments that helped to improve this manuscript.

References

Abelmann, A., Gersonde, R., Knorr, G., Zhang, X., Chapligin, B., Maier, E., Esper, O., Friedrichsen, H., Lohmann, G., Meyer, H., 2015. The seasonal sea-ice zone in the glacial Southern Ocean as a carbon sink. Nature communications 6.

Benson, W.E.S., R. E.; Pastouret, L.; Enos, P.; Freeman, T.; Murdmaa, I. O.; Worstell, P. (editor); Gradstein, F.; Schmidt, R. R.; Weaver, F. M.; Stuermer, D. H., 1978. Initial reports of the Deep Sea Drilling Project.

Berner, R.A., Caldeira, K., 1997. The need for mass balance and feedback in the geochemical carbon cycle. Geology 25, 955.

Bice, K.L., Marotzke, J., 2002. Could changing ocean circulation have destabilized methane hydrate at the Paleocene/Eocene boundary? Paleoceanography 17.

Borrelli, C., Cramer, B.S., Katz, M.E., 2014. Bipolar Atlantic deepwater circulation in the middle-late Eocene: Effects of Southern Ocean gateway openings. Paleoceanography 29, 308-327.

Brzezinski, M.A., Jones, J.L., 2015. Coupling of the distribution of silicon isotopes to the meridional overturning circulation of the North Atlantic Ocean. Deep Sea Research Part II: Topical Studies in Oceanography 116, 79-88.

Cardinal, D., Alleman, L.Y., de Jong, J., Ziegler, K., André, L., 2003. Isotopic composition of silicon measured by multicollector plasma source mass spectrometry in dry plasma mode. Journal of Analytical Atomic Spectrometry 18, 213-218.

Cermeño, P., Falkowski, P.G., Romero, O.E., Schaller, M.F., Vallina, S.M., 2015. Continental erosion and the Cenozoic rise of marine diatoms. Proceedings of the National Academy of Sciences 112, 4239-4244.

Corfield, R.M., Norris, R.D., 1996. Deep water circulation in the Paleocene ocean. Geological Society, London, Special Publications 101, 443-456.

Cramer, B., Toggweiler, J., Wright, J., Katz, M., Miller, K., 2009. Ocean overturning since the Late Cretaceous: Inferences from a new benthic foraminiferal isotope compilation. Paleoceanography 24.

Davies, R., Cartwright, J., Pike, J., Line, C., 2001. Early Oligocene initiation of North Atlantic deep water formation. Nature 410, 917-920.

De La Rocha, C.L., Brzezinski, M.A., DeNiro, M.J., 1997. Fractionation of silicon isotopes by marine diatoms during biogenic silica formation. Geochimica Et Cosmochimica Acta 61, 5051-5056

De La Rocha, C., Brzezinski, M.A., DeNiro, M., Shemesh, A., 1998. Silicon-isotope composition of diatoms as an indicator of past oceanic change. Nature 395, 680-683.

De La Rocha, C.L., 2003. Silicon isotope fractionation by marine sponges and the reconstruction of the silicon isotope composition of ancient deep water. Geology 31, 423.

De La Rocha, C.L., Bickle, M.J., 2005. Sensitivity of silicon isotopes to whole-ocean changes in the silica cycle. Marine Geology 217, 267-282.

De La Rocha, C.L., Brzezinski, M.A., DeNiro, M.J., 2000. A first look at the distribution of the stable isotopes of silicon in natural waters. Geochimica et Cosmochimica Acta 64, 2467-2477.

de Souza, G.F., Reynolds, B.C., Rickli, J., Frank, M., Saito, M.A., Gerringa, L.J.A., Bourdon, B., 2012. Southern Ocean control of silicon stable isotope distribution in the deep Atlantic Ocean. Global Biogeochemical Cycles 26, GB2035..

de Souza, G.F., Slater, R.D., Hain, M.P., Brzezinski, M.A., Sarmiento, J.L., 2015. Distal and proximal controls on the silicon stable isotope signature of North Atlantic Deep Water. Earth and Planetary Science Letters 432, 342-353.

Demarest, M.S., Brzezinski, M.A., Beucher, C.P., 2009. Fractionation of silicon isotopes during biogenic silica dissolution. Geochimica et Cosmochimica Acta 73, 5572-5583.

Egan, K.E., Rickaby, R.E.M., Hendry, K.R., Halliday, A.N., 2013. Opening the gateways for diatoms primes Earth for Antarctic glaciation. Earth and Planetary Science Letters 375, 34-43.

Egan, K.E., Rickaby, R.E.M., Leng, M.J., Hendry, K.R., Hermoso, M., Sloane, H.J., Bostock, H., Halliday, A.N., 2012. Diatom silicon isotopes as a proxy for silicic acid utilisation: A Southern Ocean core top calibration. Geochimica et Cosmochimica Acta 96, 174-192.

Ehlert, C., Grasse, P., Frank, M., 2013. Changes in silicate utilisation and upwelling intensity off Peru since the Last Glacial Maximum – insights from silicon and neodymium isotopes. Quaternary Science Reviews 72, 18-35.

Engström, E., Rodushkin, I., Baxter, D.C., Öhlander, B., 2006. Chromatographic purification for the determination of dissolved silicon isotopic compositions in natural waters by high-resolution multicollector inductively coupled plasma mass spectrometry. Analytical chemistry 78, 250-257.

Frings, P.J., Clymans, W., Fontorbe, G., Christina, L., Conley, D.J., 2016. The continental Si cycle and its impact on the ocean Si isotope budget. Chemical Geology 425, 12-36.

Frings, P.J., Clymans, W., Fontorbe, G., Gray, W., Chakrapani, G.J., Conley, D.J., De La Rocha, C., 2015. Silicate weathering in the Ganges alluvial plain. Earth and Planetary Science Letters 427, 136-148.

Fripiat, F., Cavagna, A.-J., Savoye, N., Dehairs, F., André, L., Cardinal, D., 2011. Isotopic constraints on the Si-biogeochemical cycle of the Antarctic Zone in the Kerguelen area

(KEOPS). Mar. Chem. 123, 11-22.

Garcia, H., Locarnini, R., Boyer, T., Antonov, J., Baranova, O., Zweng, M., Reagan, J., Johnson, D., 2014. World Ocean Atlas 2013, Volume 4: Dissolved Inorganic Nutrients (phosphate, nitrate, silicate), S. A. Mishonov Technical Ed, 1-25.

Grasse, P., Ehlert, C., Frank, M., 2013. The influence of water mass mixing on the dissolved Si isotope composition in the Eastern Equatorial Pacific. Earth and Planetary Science Letters 380, 60-71.

Griffiths, J.D., Barker, S., Hendry, K.R., Thornalley, D.J., Flierdt, T., Hall, I.R., Anderson, R.F., 2013. Evidence of silicic acid leakage to the tropical Atlantic via Antarctic Intermediate Water during Marine Isotope Stage 4. Paleoceanography 28, 307-318.

Hendry, K., Swann, G.E., Leng, M.J., Sloane, H.J., Goodwin, C., Berman, J., Maldonado, M., 2015. Technical Note: Silica stable isotopes and silicification in a carnivorous sponge Asbestopluma sp. Biogeosciences 12, 3489-3498.

Hendry, K.R., Georg, R.B., Rickaby, R.E.M., Robinson, L.F., Halliday, A.N., 2010. Deep ocean nutrients during the Last Glacial Maximum deduced from sponge silicon isotopic compositions. Earth and Planetary Science Letters 292, 290-300.

Hendry, K.R., Robinson, L.F., 2012. The relationship between silicon isotope fractionation in sponges and silicic acid concentration: Modern and core-top studies of biogenic opal. Geochimica et Cosmochimica Acta 81, 1-12.

Hendry, K.R., Robinson, L.F., McManus, J.F., Hays, J.D., 2014. Silicon isotopes indicate enhanced carbon export efficiency in the North Atlantic during deglaciation. Nature communications 5.

Hughes, H.J., Sondag, F., Santos, R.V., André, L., Cardinal, D., 2013. The riverine silicon isotope composition of the Amazon Basin. Geochimica et Cosmochimica Acta 121, 637-651.

Kotrc, B., Knoll, H.A., 2015. Morphospaces and Databases: Diatom Diversification through Time, in: Hamm, C. (Ed.), Evolution of Lightweight Structures: Analyses and Technical Applications. Springer Netherlands, Dordrecht, pp. 17-37.

Lacan, F., Tachikawa, K., Jeandel, C., 2012. Neodymium isotopic composition of the oceans: A compilation of seawater data. Chemical Geology 300, 177-184.

Lazarus, D., Barron, J., Renaudie, J., Diver, P., Türke, A., 2014. Cenozoic planktonic marine diatom diversity and correlation to climate change. PloS one 9, e84857.

Lazarus, D.B., Kotrc, B., Wulf, G., Schmidt, D.N., 2009. Radiolarians decreased silicification as an evolutionary response to reduced Cenozoic ocean silica availability. Proceedings of the National Academy of Sciences 106, 9333-9338.

Li, C.-W., Chen, J.-Y., Hua, T.-E., 1998. Precambrian sponges with cellular structures. Science 279, 879-882.

Lunt, D.J., Valdes, P.J., Jones, T.D., Ridgwell, A., Haywood, A.M., Schmidt, D.N., Marsh, R., Maslin, M., 2010. CO2-driven ocean circulation changes as an amplifier of Paleocene-Eocene thermal maximum hydrate destabilization. Geology 38, 875-878.

MacLeod, K., Londoño, C.I., Martin, E., Berrocoso, Á.J., Basak, C., 2011. Changes in North Atlantic circulation at the end of the Cretaceous greenhouse interval. Nature Geoscience 4, 779-782.

MacLeod, K.G., Martin, E.E., Blair, S.W., 2008. Nd isotopic excursion across Cretaceous ocean anoxic event 2 (Cenomanian-Turonian) in the tropical North Atlantic. Geology 36, 811-814.

Maliva, R.G., Knoll, A.H., Siever, R., 1989. Secular change in chert distribution: a reflection of evolving biological participation in the silica cycle. Palaios, 519-532.

Misra, S., Froelich, P.N., 2012. Lithium isotope history of Cenozoic seawater: changes in silicate weathering and reverse weathering. Science 335, 818-823.

Morley, D.W., Leng, M.J., Mackay, A.W., Sloane, H.J., Rioual, P., Battarbee, R.W., 2004. Cleaning of lake sediment samples for diatom oxygen isotope analysis. Journal of Paleolimnology 31, 391-401.

Mountain, G.S., Miller, K.G., 1992. Seismic and geologic evidence for early Paleogene deepwater circulation in the western North Atlantic. Paleoceanography 7, 423-439.

Norris, R., Klaus, A., Kroon, D., 2001. Mid-Eocene deep water, the late Palaeocene thermal maximum and continental slope mass wasting during the Cretaceous-Palaeogene impact. Geological Society, London, Special Publications 183, 23-48.

Norris, R.D., Kroon, D., Klaus, A., al., e., 1998. Proc. ODP, Init. Repts., 171B: College Station, TX (Ocean Drilling Program).

Nunes, F., Norris, R.D., 2006. Abrupt reversal in ocean overturning during the Palaeocene/Eocene warm period. Nature 439, 60-63.

O'nions, R., Frank, M., Von Blanckenburg, F., Ling, H.-F., 1998. Secular variation of Nd and Pb isotopes in ferromanganese crusts from the Atlantic, Indian and Pacific Oceans. Earth and Planetary Science Letters 155, 15-28.

Pak, D.K., Miller, K.G., 1992. Paleocene to Eocene benthic foraminiferal isotopes and assemblages: Implications for deepwater circulation. Paleoceanography 7, 405-422.

Panizzo, V.N., Swann, G.E.A., Mackay, A.W., Vologina, E., Sturm, M., Pashley, V., Horstwood, M.S.A., 2016. Insights into the transfer of silicon isotopes into the sediment record. Biogeosciences 13, 147-157.

Pisera, A., 2006. Palaeontology of sponges-a review. Canadian Journal of Zoology 84, 242-261.

Rabosky, D.L., Sorhannus, U., 2009. Diversity dynamics of marine planktonic diatoms across the Cenozoic. Nature 457, 183-U173.

Reynolds, B.C., Aggarwal, J., André, L., Baxter, D., Beucher, C., Brzezinski, M.A., Engström, E., Georg, R.B., Land, M., Leng, M.J., 2007. An inter-laboratory comparison of Si isotope reference materials. Journal of Analytical Atomic Spectrometry 22, 561-568.

Robinson, S.A., Murphy, D.P., Vance, D., Thomas, D.J., 2010. Formation of "Southern Component Water" in the Late Cretaceous: Evidence from Nd-isotopes. Geology 38, 871-874.

Robinson, S.A., Vance, D., 2012. Widespread and synchronous change in deeppocean circulation in the North and South Atlantic during the Late Cretaceous. Paleoceanography 27.

Rowley, D.B., 2002. Rate of plate creation and destruction: 180 Ma to present. Geological Society of America Bulletin 114, 927-933.

Sanfilippo, A., Blome, C.D., 2001. Biostratigraphic implications of mid-latitude Palaeocene-Eocene radiolarian faunas from Hole 1051A, ODP Leg 171B, Blake Nose, western North Atlantic. Geological Society, London, Special Publications 183, 185-224.

Scher, H.D., Martin, E.E., 2004. Circulation in the Southern Ocean during the Paleogene inferred from neodymium isotopes. Earth and Planetary Science Letters 228, 391-405.

Siever, R., 1992. The silica cycle in the Precambrian. Geochimica et Cosmochimica Acta 56, 3265-3272.

Small, J., 1950. Quantitative evolution: XVI. Increase of species-number in diatoms. Annals of Botany 14, 91-113.

Spencer-Cervato, C., 1999. The Cenozoic deep sea microfossil record: explorations of the DSDP/ODP sample set using the Neptune database. Palaeontologia electronica 2, 270.

Staudigel, H., Doyle, P., Zindler, A., 1985. Sr and Nd isotope systematics in fish teeth. Earth and Planetary Science Letters 76, 45-56.

Tatzel, M., von Blanckenburg, F., Oelze, M., Schuessler, J.A., Bohrmann, G., 2015. The silicon isotope record of early silica diagenesis. Earth and Planetary Science Letters 428, 293-303.

Thomas, D.J., Bralower, T.J., Jones, C.E., 2003. Neodymium isotopic reconstruction of late Paleocene–early Eocene thermohaline circulation. Earth and Planetary Science Letters 209, 309-322.

Tréguer, P.J., De La Rocha, C.L., 2013. The world ocean silica cycle. Annual review of marine science 5, 477-501.

van Tol, H.M., Irwin, A.J., Finkel, Z.V., 2012. Macroevolutionary trends in silicoflagellate skeletal morphology: the costs and benefits of silicification. Paleobiology 38, 391-402.

Via, R.K., Thomas, D.J., 2006. Evolution of Atlantic thermohaline circulation: Early Oligocene onset of deep-water production in the North Atlantic. Geology 34, 441-444.

Walker, J.C., Hays, P., Kasting, J., 1981. A negative feedback mechanism for the long-term stabilization of the Earth's surface temperature. Journal of Geophysical Research 86, 9776-

9782.

Wallace, A.F., Wang, D., Hamm, L.M., Knoll, A.H., Dove, P.M., 2012. Eukaryotic Skeletal Formation, in: Knoll, A.H., Canfield, D.E., Konhauser, K.O. (Eds.), Fundamentals of Geobiology. John Wiley & Sons, Ltd, Chichester, pp. 150-187.

Wetzel, F., De Souza, G., Reynolds, B., 2014. What controls silicon isotope fractionation during dissolution of diatom opal? Geochimica et Cosmochimica Acta 131, 128-137.

Wille, M., Sutton, J., Ellwood, M.J., Sambridge, M., Maher, W., Eggins, S., Kelly, M., 2010. Silicon isotopic fractionation in marine sponges: A new model for understanding silicon isotopic variations in sponges. Earth and Planetary Science Letters 292, 281-289.

Witkowski, J., Bohaty, S.M., Edgar, K.M., Harwood, D.M., 2014. Rapid fluctuations in mid-latitude siliceous plankton production during the Middle Eocene Climatic Optimum (ODP Site 1051, western North Atlantic). Marine Micropaleontology 106, 110-129.

Zachos, J., Pagani, M., Sloan, L., Thomas, E., Billups, K., 2001. Trends, rhythms, and aberrations in global climate 65 Ma to present. Science 292, 686-693.

Supplementary Table 1: Details of individual samples and secondary reference materials. Values in brackets indicate internal precision when higher than long-term precision.

Hole	Core	Section	Interval (cm)	Depth (mcd)	Age (Ma)	$\delta^{30}Si_{spo}$ (‰)	$\delta^{29}Si_{spo}$ (‰)	$\delta^{30}Si_{rad}$ (‰)	$\delta^{29}Si_{rad}$ (‰)	$\Delta\delta^{30}Si_{rad\text{-}spo}$ (‰)	$\Delta\delta^{29}Si_{rad\text{-}spo}$ (‰)
1049A	4	3	25-27	18.45	39.47	n/a		0.92	0.36		
	4	6	103-105	23.73	40.95	n/a		1.08	0.56		
	5	4	40-42	30.64	42.60	n/a		0.99 (0.15)	0.47 (0.09)		
	6	1	70-72	35.74	44.08	n/a		1.20	0.51 (0.12)		
	6	5	20-22	41.24	45.63	0.45	0.25	1.09	0.63	0.64	0.38
	6	6	10-12	42.64	46.02	0.33	0.14		n/a		
	6	6	140-142	43.94	46.38	n/a		0.80	0.35 (0.07)		
	10	1	105-107	57.43	49.87	n/a		1.56	0.79 (0.20)		
1050A	4	5	90-92	36.02	41.10	0.49	0.25	1.17 (0.19)	0.53 (0.08)	0.70	0.28
	8	2	40-42	72.49	43.47	-0.15	-0.06	0.87 (0.23)	0.35 (0.08)	1.02	0.41
	14	1	11-13	128.87	47.45	n/a		1.00	0.49 (0.15)		
	15	1	120-122	139.56	48.21	0.16	0.06	1.19	0.52 (0.13)	1.03	0.46
	15	6	18-20	145.54	48.64	0.23	0.15		n/a		
	16	3	98-100	151.94	49.10	0.41	0.22	1.01	0.44	0.60	0.22
	17	2	40-42	159.46	49.64	0.11	0.11	1.17	0.65	1.06	0.54
	17	3	18-20	160.74	49.73	0.45	0.20	1.25	0.63	0.80	0.43
	18	1	44-46	168.60	50.22	0.57	0.23	1.23	0.64	0.65	0.41
	19	3	120-122	180.02	51.18	n/a		1.29	0.60		
	19	6	110-112	184.42	51.49	n/a		1.14 (0.16)	0.56		
	20	1	100-102	185.74	51.64	0.51	0.29 (0.14)	1.27	0.64	0.76	0.35
	20	3	110-112	188.84	51.86	0.23	0.15	1.15	0.56	0.91	0.41
	20	5	102-104	191.76	52.07	n/a		0.80	0.44		
	21	4	5-7	197.86	52.44	n/a		0.77 (0.23)	0.32 (0.24)		

	21	7	5-7	202.36	52.80	0.12	0.06	0.75	0.36 (0.09)	0.62	0.30
	23	2	114-116	214.41	53.68	0.15	0.06		n/a		
	23	6	70-72	219.97	54.08	0.04	0.01	0.62	0.36	0.58	0.35
	24	3	60-62	226.15	54.43	0.24	0.08	0.68	0.25	0.45	0.17
	24	6	10-12	230.15	54.72	0.35	0.13	0.96 (0.16)	0.44	0.61	0.31
	26	2	118-120	244.53	55.75	0.63	0.23	1.33	0.67	0.70	0.44
	27	2	30-32	247.65	55.97	0.33	0.21	0.90	0.52	0.58	0.30
	27	4	40-42	250.75	56.20	0.57	0.25	1.34	0.71	0.78	0.46
	28	5	5-7	257.50	56.72	0.36	0.14	1.27	0.65	0.91	0.51
	29	1	64-66	261.69	56.98	0.23	0.13		n/a		
	30	3	50-52	274.15	57.87		n/a	1.03	0.56		
	31	5	98-100	286.09	58.73	0.18	0.12	1.00	0.41	0.82	0.30
	33	4	65-67	298.20	59.60	0.50	0.25	0.91	0.45	0.41	0.20
1051A	3	1	30-32	19.10	34.67		n/a	1.05	0.54		
	6	1	119-121	52.24	36.04	0.13	0.05	1.02	0.48	0.88	0.43
	7	1	59-61	62.29	36.46	-0.07	-0.11	1.12	0.51	1.19	0.62
	8	6	88-90	80.33	36.60	0.49	0.21	1.03	0.55	0.53	0.34
	10	3	20-22	95.36	36.75	-0.24	-0.12	0.94	0.46	1.18	0.58
	12	1	118-120	112.91	37.52		n/a	1.21	0.60		
	14	1	40-42	129.88	38.34	-0.22	-0.09	0.87	0.47	1.09	0.56
	14	1	72-74	130.20	38.36	0.14	0.04	0.93	0.45	0.79	0.41
	16	1	118-120	151.63	39.24		n/a	1.34	0.66		
	17	3	71-73	163.92	39.79	0.07	0.05	1.07	0.52	1.00	0.47
	19	1	80-82	179.48	40.54	0.33	0.15	0.84	0.42	0.51	0.27
	20	6	10-12	197.94	41.29	0.09	0.08	1.00	0.51	0.91	0.43
	22	3	41-43	214.37	41.97		n/a	1.22	0.55		
	25	1	57-59	240.78	43.14	0.15	0.07	0.96	0.49	0.81	0.42

	27	4	92-94	265.97	44.24		n/a		1.44	0.72		
	30	2	9-11	294.06	45.37	0.08		0.07	0.92	0.47 (0.10)	0.84	0.40
	32	2	90-92	314.48	46.28	0.24		0.11	0.65	0.34	0.41	0.23
	36	1	58-60	350.37	47.94		n/a		0.40	0.11		
	38	4	10-12	373.09	49.00		n/a		0.56	0.31		
	40	2	79-81	390.08	49.77		n/a		0.86	0.38		
	44	1	31-33	427.28	51.47		n/a		1.67	0.85		
	45	5	27-29	444.48	52.18	-0.28		-0.16	1.39	0.68	1.67	0.84
	48	2	98-100	470.30	53.31		n/a		0.69	0.36		
	52	1	18-20	498.48	54.52	-0.48		-0.26	1.02	0.49	1.50	0.75
	54	3	132-134	522.20	55.58	-0.05		-0.11	0.32	0.20	0.37	0.31
	57	1	49-51	551.81	56.71	-0.17		-0.09	0.65	0.30	0.82	0.39
	63	2	99-101	603.59	58.98		n/a		0.54	0.30		
1052A	3	5	80-82	23.40	33.50	-0.08		-0.10	0.75	0.32 (0.11)	0.83	0.42
	6	3	30-32	50.92	35.23		n/a		0.35	0.03		
	8	6	130-132	73.27	36.93	0.39 (0.20)		0.18 (0.08)	0.98	0.47	0.59	0.29
	11	4	70-72	99.58	38.65	0.13		0.08		n/a		
	14	1	110-112	124.82	40.34	-0.09 (0.26)		-0.13 (0.12)	1.20 (0.14)	0.60	1.29	0.73
1053A	13	4	80-82	123.98	36.56	0.20		0.03	0.84 (0.13)	0.46 (0.17)	0.64	0.43
	19	1	33-35	170.17	37.55	0.13		0.06	1.10	0.51 (0.09)	0.97	0.45
Mean						0.17		0.07	0.99	0.49	0.82	0.41
St. dev.						0.26		0.13	0.27	0.15	0.29	0.14
Diatomite	n=3					1.20±0.06		0.62±0.06				
Big Batch	n=3					-10.35±0.30		-5.30±0.16				

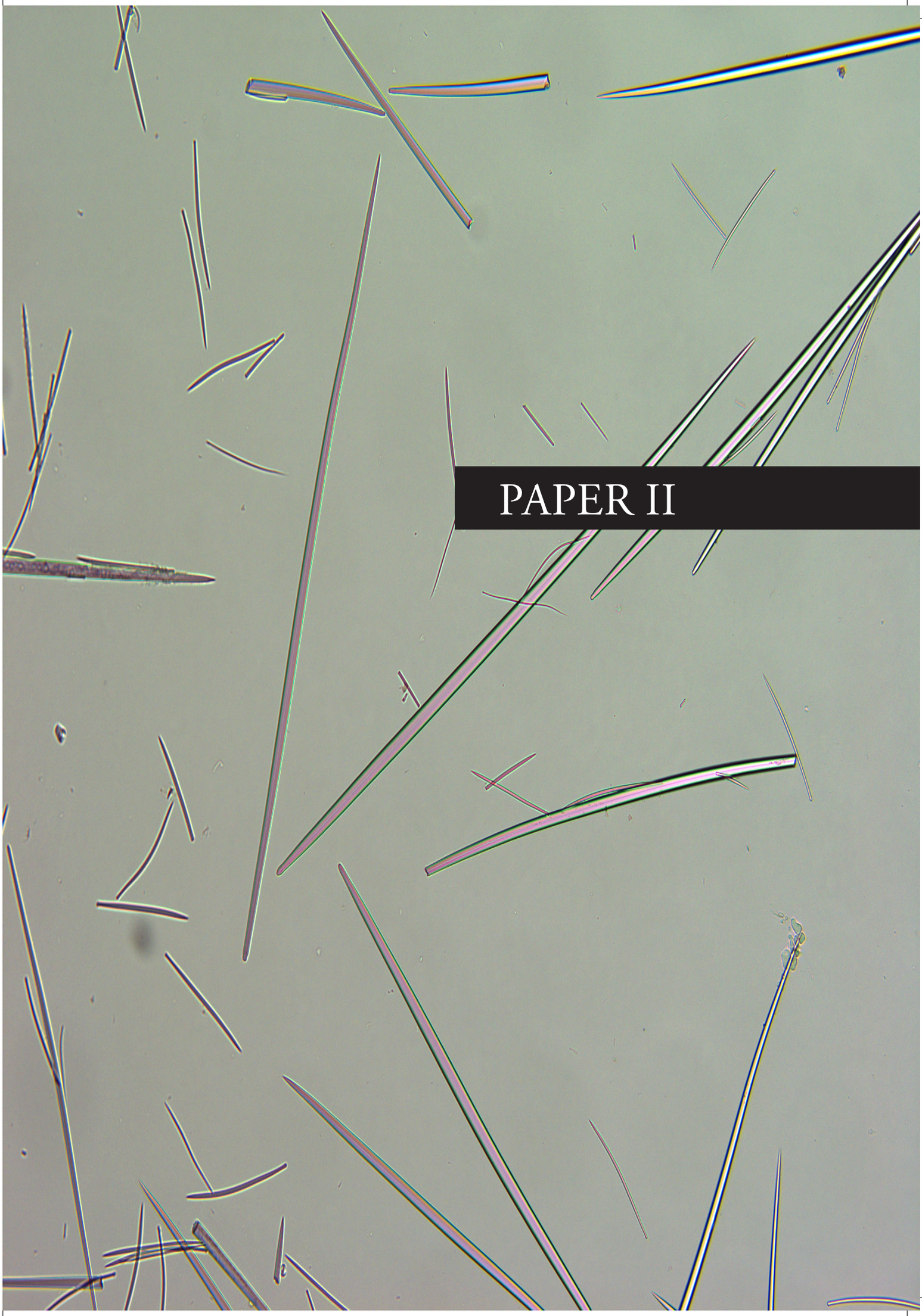

PAPER II

Photo courtesy of Belinda Alvarez

Enrichment of dissolved silica in the deep Equatorial Pacific during the Eocene-Oligocene.

Guillaume Fontorbe[a,*], Patrick J. Frings[a], Christina L. De La Rocha, Katharine R. Hendry[b], Daniel J. Conley[a]

[a] Department of Geology, Lund University, Sölvegatan 12, SE-223 62, Lund, Sweden

[b] School of Earth Sciences, University of Bristol, Wills Memorial Building, Queen's Road, Bristol, BS8 1RJ, UK

* corresponding author(guillaume.fontorbe@geol.lu.se)

Abstract

Silicon isotope ratios (expressed as $\delta^{30}Si$) in marine microfossils can provide insights into silica cycling over geologic time. Here, we used $\delta^{30}Si$ of sponge spicules and radiolarian tests from the Paleogene Equatorial Transect (ODP Leg 199) spanning the Eocene and Oligocene (~50-23 Ma) to reconstruct dissolved silica (DSi) concentrations in deep waters and to examine upper ocean $\delta^{30}Si$. The $\delta^{30}Si$ values range from -3.16 to +0.18‰ and from -0.07 to +1.42‰ for the sponge and radiolarian records, respectively. Both records show a transition towards lower $\delta^{30}Si$ values around 37 Ma. The shift in radiolarian $\delta^{30}Si$ is interpreted as a consequence of changes in the $\delta^{30}Si$ of DSi sourced to the region. The decrease in sponge $\delta^{30}Si$ is interpreted as a transition from low DSi concentrations to higher DSi concentrations, most likely related to the shift towards a solely Southern Ocean source of deep-water in the Pacific during the Paleogene that has been suggested by results from paleoceanographic tracers such as neodymium isotopes and carbon isotopes. Sponge $\delta^{30}Si$, by thus providing relatively direct information about the nutrient content of deep-water, is a useful complement to other tracers of deep-water circulation in the oceans of the past.

1. Introduction

Silicon has three stable isotopes (^{28}Si, ^{29}Si, and ^{30}Si) that can be used to gain insight into silicon cycling in the geologic past. The biological uptake of dissolved silica (DSi) in the surrounding waters and precipitation into biogenic silica (BSi) discriminates against the heavier stable isotopes of silicon (i.e. ^{29}Si and ^{30}Si), resulting in BSi being isotopically lighter than the DSi it is precipitated from (De La Rocha et al., 1997). Si isotope ratios (expressed as $\delta^{30}Si$) in different siliceous marine microfossils can be used to reconstruct different environmental variables related to Si cycling. For example, $\delta^{30}Si$ from diatom frustules can be used to estimate the degree of Si utilization in the surface waters during their growth (Cardinal et al., 2005; Coffineau et al., 2014; De La Rocha et al., 1998; Egan et al., 2012; Varela et al., 2004). Conversely, radiolarians, which are heterotrophs, do not grow in blooms as diatoms and other phytoplankton do. Therefore, radiolarian $\delta^{30}Si$ should more closely track the silicon isotopic composition of the upper couple of hundred meters of the water column (Abelmann et al., 2015; Hendry et al., 2014). Meanwhile, siliceous sponge spicules $\delta^{30}Si$ can be used to estimate DSi concentrations at depth, via a calibrated relationship between DSi concentrations and the magnitude of Si isotope fractionation by sponges (Hendry and Robinson, 2012; Wille et al., 2010).

Such a multifaceted silicon isotope toolkit can be used to investigate the evolution of the oceanic Si cycle, which remains poorly constrained even for relatively recent Earth history, from the late Mesozoic. The customary narrative postulates a permanent transition, starting during the mid Cretaceous to the end of the Paleogene, from a DSi-replete surface ocean, with estimated DSi concentration in the range of 600 to 1100 µM, to DSi-depleted conditions (Maliva et al., 1989; Siever, 1991). This has been attributed to the radiation of diatoms, which have a very high affinity for DSi and are able to precipitate massive amounts of BSi even in surface waters near to DSi depletion.

One aspect missing from the picture is a strong constrain on the timing, duration, and

global synchrony of the transition to low DSi concentration in the surface ocean that exists today. Recently, Fontorbe et al. (in review), used $\delta^{30}Si$ from sponge spicules to reconstruct DSi concentrations in the deep North Atlantic during the Paleocene and Eocene. Their results show that by this time (60 to 30 Ma), concentrations of DSi in the North Atlantic were already low, meaning that the transition to a low silica ocean have to had begun prior the Early Cenozoic.

This leaves open the question of other ocean basins. Were DSi concentrations also already similar to modern ones in all basins during the Paleogene and, if not, how different were they? Today, due to the details of deep-water formation, circulation, and mixing, we observe a significant gradient of DSi concentrations between newly formed and nearly totally DSi depleted (<10 μM) North Atlantic deep water and oldest deep waters of the North Pacific with values of nearly 200 μM. The Paleogene (65.5 to 23.03 Ma), as well as hosting the evolutionary expansion of the diatoms (Rabosky and Sorhannus, 2009), is a period subject to numerous plate tectonic events (e.g. changes in the position of land masses and opening of ocean gateways that impacted ocean circulation), several transient and long-term climatic events (Zachos et al., 2001), and volcanism. During the Paleocene and Early Eocene, the Atlantic and Pacific Oceans were isolated from each other. Formation of deep water potentially took place at high latitudes in both hemispheres in each basin. During the Mid Eocene (ca. 40 Ma), the subsidence of Antarctic land bridges reinforced the formation of deep waters in the Pacific sector of Southern Ocean and ultimately led to the cessation of deep waters in the North Pacific. All these events could have resulted in changes in the delivery of DSi to different region of the ocean, circulation patterns of deep-water, degree of vertical stratification of the water column, and in the overall production and export of biogenic silica on local or even global scales.

To shed more light on this subject, we have analyzed the Si isotopic composition of siliceous sponge spicules - indicative of DSi concentrations in the deeper water column - and radiolarian tests - related to the Si isotopic composition of the upper water column – from sediment cores collected in the Equatorial Pacific (ODP Leg 199) covering the Eocene and Oligocene (ca. 48 to 23 Ma). The $\delta^{30}Si$ of the radiolarian tests show values similar to those reported in the Western North Atlantic during the Paleocene-Eocene (Fontorbe et al., in revision), arguing for similar DSi conditions in the upper waters of both basins. However, the $\delta^{30}Si$ of siliceous sponge spicules in the Pacific notably diverges from the Atlantic values suggesting an increase in DSi concentrations in the deeper waters of the Equatorial Pacific at this time. This shift coincides with large-scale changes in the Pacific Ocean circulation inferred from previous studies (e.g. Thomas et al., 2014; Thomas et al., 2008). Therefore we conclude that $\delta^{30}Si$ can complement other paleocirculation proxies, and is useful both for reconstructing past states of the oceanic silicon cycle, and also for tracking changes in the provenance and characteristics of deep water masses over geologic time.

2. Material and methods

2.1. Site description

A total of 75 samples from ODP sites 1217 through 1221 from the Paleogene Equatorial Transect (ODP leg 199; ca. 7-16°N, 135-143°W, fig 1a) were selected for silicon isotope analysis. The stratigraphic sequence sampled is composed mostly of early Eocene to late Oligocene (ca. 49 to 23Ma) radiolarian and nannofossil oozes. The modern day equatorial Pacific is highly influenced by upwelling that brings deep-waters to the surface, stimulating productivity that results in a band of highly biogenic sedimentation accumulating along and within a narrow band of a couple degrees along the geographical equator. Coupled atmospheric-ocean circulation models have reconstructed Equatorial Pacific upwelling annual intensity during the early Paleogene (Huber, 2002) and showed that drilled sites during ODP Leg 199 were inside the upwelling influenced area during the Paleogene. Figure 1b shows the zone under upwelling influence during the early Paleogene and the approximate paleolocation of the cores.

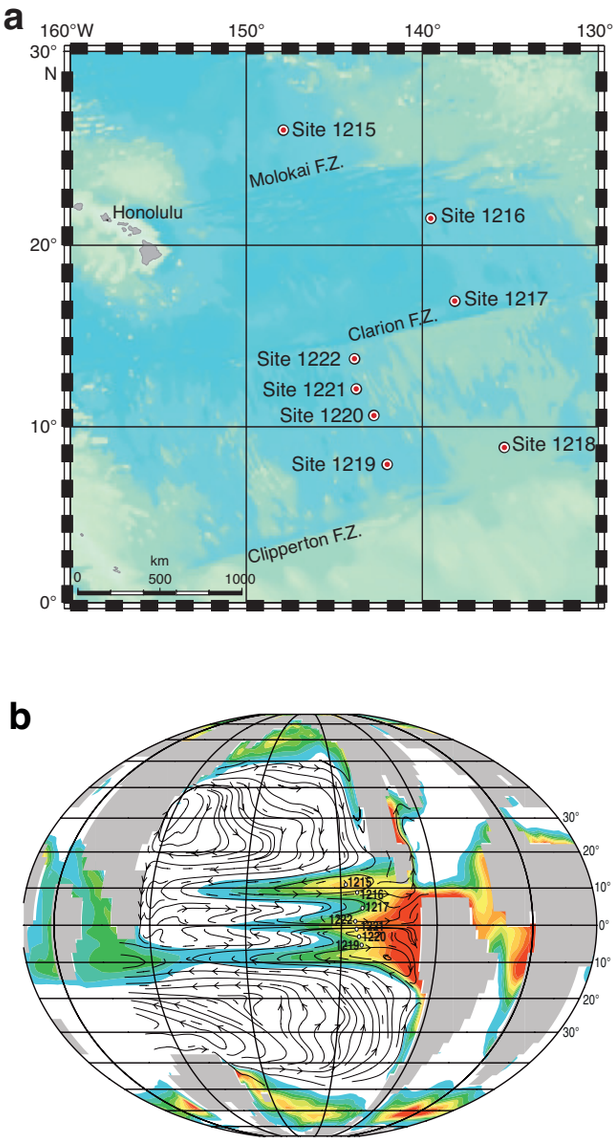

Figure 1: (a) Location of the drill sites from ODP leg 199. (b) Map of the early Paleogene equatorial Pacific upwelling with paleolocation of the drill sites. Red indicates areas of vigorous upwelling, blue/green indicates regions of weak upwelling. Modified from Lyle et al. (2002).

Modern surface DSi concentrations at the loci of sediment deposition during the Paleogene (ca. 5°S-5°N, 130-150°W, fig 1) are low, ranging from ~0 to ~10 µM. The DSi concentration gradually increases with depth up to ~50 µM in the top 500 meters and to over 150 µM in waters deeper than 1000 meters. Measurements of the silicon isotopic composition of DSi in the upper 200 m of the Equatorial Pacific range from +1.2 to +4.4‰, depending on the degree of biological utilization (De Souza et al., 2012; Grasse et al., 2013).

2.2. Sample preparation

Biogenic silica was physically separated from other sediment components such as carbonates and other minerals using standard techniques (Morley et al., 2004). Briefly, sediments were cleaned with hydrochloric acid and hydrogen peroxide to remove carbonates and organic matter. Then BSi was separated from lithogenic silicates and clays by repeated density separation using a sodium polytungstate solution with a density between 2.1 and 2.3 g/mL. The light fraction recovered (i.e. the fraction containing biogenic silica) was wet-sieved at 53µm to remove the majority of fragmented material and isolate larger silica particles like sponge spicules and intact radiolarian tests.

From this cleaned fraction, monoaxonic sponge spicules and radiolarian tests were handpicked under a light microscope to minimize contamination from unwanted particles. For example, the selection of only monoaxonic spicules minimized any potential contribution of spicule type to silicon isotope variations (Hendry et al., 2015). Meanwhile, the radiolarian test samples were picked to represent a bulk radiolarian community. Benefits and caveats induced by the selection of a bulk radiolarian community are discussed further in this article. The separated and handpicked BSi was then dissolved in 0.4M NaOH for a minimum of three days at 100°C, acidified with HNO_3 to pH around 2, and purified chromatographically through a cation exchange resin following Georg et al. (2006) for silicon isotope ratio analysis.

2.3. Silicon isotope analysis

The silicon isotopic composition of the purified Si solutions was determined using a multi-collector inductively coupled plasma mass spectrometer (MC-ICP-MS, Neptune, Thermo Scientific) at the Pole Spectrometrie Ocean (Ifremer, Brest). The Si solutions as well as the standards, diluted to 2ppm using 1% HNO_3, were introduced through an APEX-HF (ESI) desolvator, PFA nebulizer (50µL/min) and an alumina injector. The signal intensity was in the vicinity of 25 V on mass 28 at medium resolution. Following the method prescribed by Cardinal et al.

Table 1: Modern locations, water depths, sampled intervals, approximate age interval, and number of samples for each individual hole sampled.

Hole	Location	Water depth (mbsl)	Sampled interval (mbsf)	Approx. Age range (Ma)	Number of samples
1217 A	16°52.0133'N 138°05.9981'W	5342.1	30-86	33-45	11
1217 B	16°52.0175'N 138°06.0007'W	5342.1	30-84	34-44	12
1218 A	08°53.3667'N 135°22.0002'W	4826.3	77-260	23-41	15
1219 A	7°48.0097'N 142°00.9390'W	5063.3	56-221	24-56	16
1220 A	10°10.6008'N 142°45.4917'W	5217.9	40-114	28-42	8
1221 A	12°01.9987'N 143°41.6514'W	5175.3	10-113	32-48	13

(2003), to correct for internal mass bias, an internal Mg standard with matching concentration (2 ppm) was added to each standard and sample. The beam intensity on masses 28, 29, and 30 for silicon and on masses 25 and 26 for magnesium where monitored for a block of 25 cycles of 15s to calculate corrected isotope ratios, followed by a 1% HNO_3 rinse for 3 min. The beam intensity on mass 28 during the rinse and procedural blanks was approximately <1% of the standards and samples beam intensity.

The silicon isotope ratios are given relative to a standard (NBS28, NIST) as δ^xSi values corresponding to an average of two series of bracketed measurements (i.e. 2 blocks of standard-sample-standard):

$$\delta^x Si=(R_{sam}/R_{std} - 1) \times 1000 \quad (1)$$

where R_{sam} and R_{std} is the corrected ratio of ^{x}Si/^{28}Si of the sample and the standard respectively. Values fall on the expected mass-dependent fractionation line (r^2=0.998, n=105, fig 2), demonstrating the successful removal of polyatomic interferences during measurement. δ^{30}Si analyses on secondary standards Big Batch and Diatomite prepared using identical methods and measured during the same analytical sessions yielded values in agreement with accepted values (Reynolds et al., 2007; Supp. Table 1). Long-term precision (as 2σ) based on measurements of multiple NBS28 standards and secondary standards was of ±0.14‰ on δ^{30}Si and ±0.06‰ on δ^{29}Si.

3. Results

The 75 radiolarian samples covering 23.1 to 47.9 Ma have δ^{30}Si values ranging from -0.07 to +1.42 ‰. The 30 sponge spicule samples, covering this same time interval, have consistently lower values, ranging from -3.16 to +0.18‰. All data are presented in supplementary table 1. The range of δ^{30}Si values for the radiolarian agrees well with previous work on the Paleocene-Eocene Atlantic Ocean (δ^{30}Si from +0.32 to +1.67‰, n=65, Fontorbe et al. in review), and overlap with the upper range of values (-0.90 to 1.17‰) in the Atlantic sector of the Southern Ocean from the past 30ka (Abelmann et al., 2015) and from the Heinrich Stadial 1 (ca. 17ka) in the North Atlantic (+0.73 to +2.00‰, Hendry et al., 2014).

The most notable shift in the radiolarian record is a decrease in δ^{30}Si by roughly 1‰ from ca. 37 to 33 Ma. Similarly, the sponges record shows two distinct steps. The first one falls between 48 and 37 Ma and has δ^{30}Si values of 0 to -1‰,

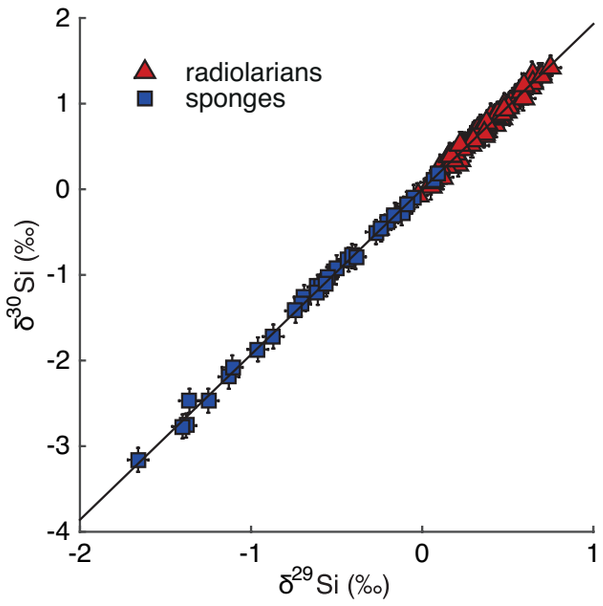

Figure 2: Three-isotope plot ($\delta^{30}Si$ vs $\delta^{29}Si$) of radiolarian tests (red triangles) and sponge spicules (blue squares). The data fall on the the expected mass-dependent fractionation (black line: $\delta^{30}Si = 1.93 \times \delta^{29}Si$, $r^2=0.998$, n=105). Vertical and horizontal bars represent long-term precision (expressed as 2σ).

similar to those of modern sponges living at low DSi concentrations (i.e. [DSi]<25µM) (Hendry and Robinson, 2012; Wille et al., 2010). Following this, there is a transition to lower $\delta^{30}Si$ values (between -1 and -2‰) for the rest of the sponge record (fig. 3). Such values are higher than sponge $\delta^{30}Si$ values published for the Southern Ocean over the Eocene-Oligocene transition (De La Rocha, 2003; Egan et al., 2013) and consistently lower than reported values in the Atlantic Ocean during the Paleocene and Eocene (Fontorbe et al., in revision).

4. Discussion

The number of studies addressing the evolution of the Si cycle over million-year time scales remains limited. More emphasis has been placed on more recent seasonal to millennial variations, and in particular glacial-interglacial periods (e.g. Ehlert et al., 2013; Maier et al., 2013; reviewed in Frings et al. 2016). The narrative of the evolution of DSi concentrations over geologic time scales postulates a transition from a pre-Cretaceous ocean with high DSi concentrations to DSi completed surface waters as it is observed today (Maliva et al., 1989; Siever, 1991). This transition is believed to have occurred from the mid Cretaceous to the end of the Paleogene. Such conclusions are based on the distribution and facies of cherts, a sedimentary diagenetically formed crystalline silica.

The recognition of a relationship between ambient DSi concentrations and the magnitude of sponge Si isotope fractionation (expressed as $\Delta\delta^{30}Si_{spo\text{-}DSi}$) opened the door to quantitative reconstructions of marine DSi concentrations (Hendry and Robinson, 2012; Wille et al., 2010). A recent study (Fontorbe et al., in review) based on sponge $\delta^{30}Si$ suggested that DSi concentrations in the deeper waters of the North Atlantic were already remarkably low and similar to the present day ocean during the Paleocene and Eocene. Using a similar approach, this present study aims to reconstruct DSi concentrations of bottom water as well as the Si isotopic composition of surface to mid-depth waters in the Equatorial Pacific during the Eocene and Oligocene.

4.1 Limitations and uncertainties

The use of radiolarian $\delta^{30}Si$, and to a lesser extent sponge $\delta^{30}Si$, as a proxy to reconstruct aspects of the Si cycle is still at an early stage. Consequently, one has to address the potential influence of factors and processes such as diagenesis, dissolution, and lack of understanding of Si isotope fractionation during the precipitation of radiolarian tests on the sedimentary $\delta^{30}Si$ record.

The first concern that may arise is the impact of diagenetic processes on the $\delta^{30}Si$ records. The transformation of opal-A produced by siliceous organisms to opal-CT via series of dissolution and reprecipitation reaction is associated with fractionation of Si isotopes (Tatzel et al., 2015). The extent of this fractionation depends on the completeness of the transformation. Marin-Carbonne et al. (2014) demonstrated that this process make it difficult to interpret chert $\delta^{30}Si$. However, this is unlikely to impact our data. The handpicking of individual tests and spicules under light microscopy employed in this study, as well as scanning electron microscopy did not reveal any sign of extensive dissolution nor reprecipitation.

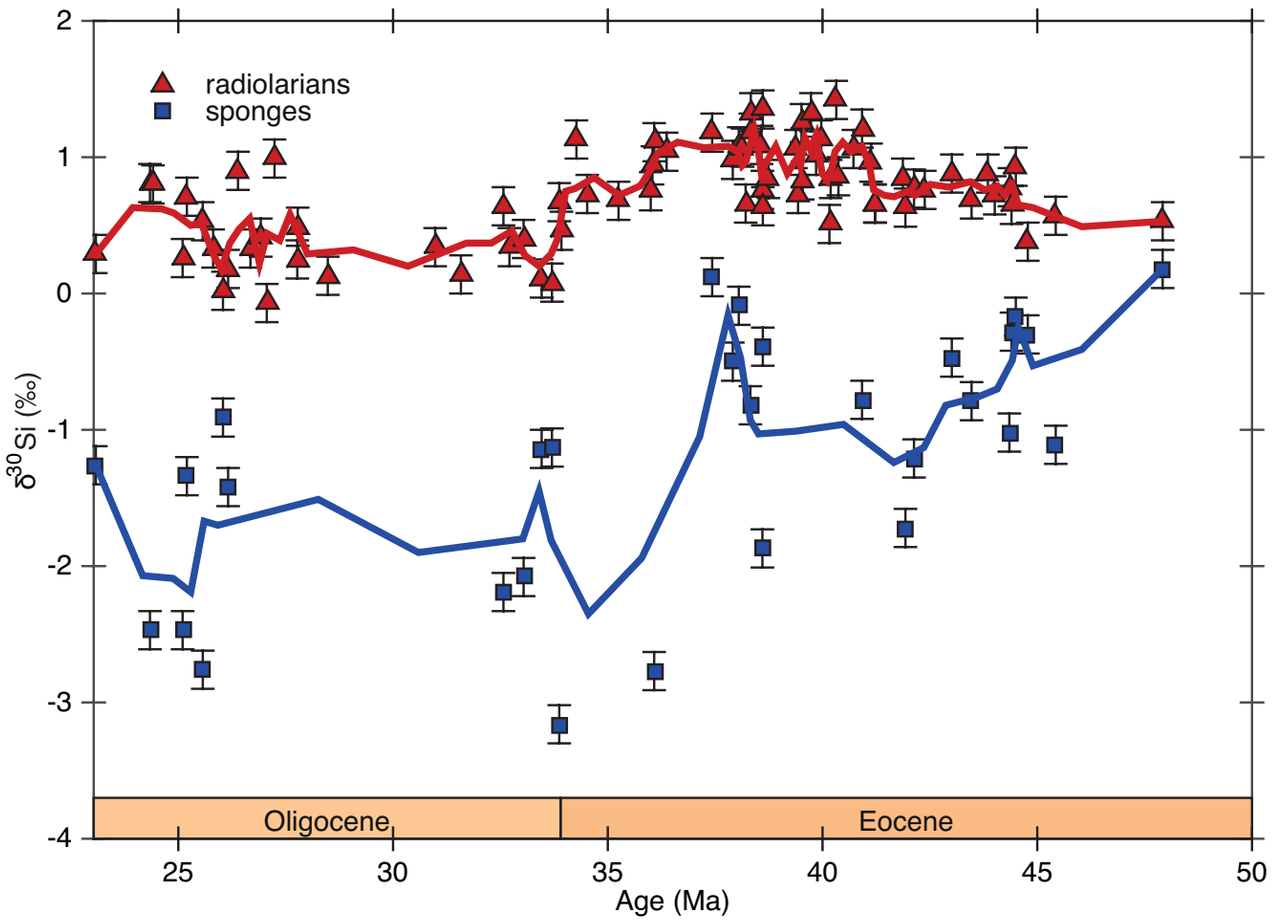

Figure 3: Radiolarian (red triangles) and sponge (blue squares) $\delta^{30}Si$ in the equatorial Pacific during the Eocene and Oligocene. Vertical bars represent 2σ. Thick lines show a 3-points running average.

Moreover, the few occurrences of porcellanite – a form of opal-CT – present in the sediment sequence (Lyle et al., 2002) have intentionally not been sampled during our study. Consequently, it is very unlikely for our sponge and radiolarian $\delta^{30}Si$ records to be affected by artifacts caused by diagenetic processes. Moreover, analyses by X-ray diffractometer on sponge spicules dated from the Eocene/Oligocene boundary extracted from deep-sea sediments in the Atlantic sector of the Southern Ocean (De La Rocha, 2003) suggested that sponge spicules did not undergo diagenetic processes and were solely composed of opal-A.

Another process to consider is the dissolution of BSi and any potential isotopic impact on the residual BSi. Demarest et al. (2009), in a study on diatom BSi dissolution under closed conditions, reported the preferential release of lighter Si isotopes during dissolution with a Si isotope enrichment of -0.55‰ (measured on ^{30}Si). This is significant considering the magnitude of $\delta^{30}Si$ variations observed in BSi from sediment cores covering the Paleogene (this study, Fontorbe et al. (in review), Egan et al. 2013). In a more recent study, Wetzel et al. (2014) did not observe significant Si isotope fractionation during dissolution of diatom opal and argued for the robustness of BSi in the deep sea sedimentary environment against dissolution. Moreover, both studies highlight that a considerable proportion of BSi has to dissolve in order to produce measurable effect on the $\delta^{30}Si$ of the residual opal. As stated in the previous paragraph, our microscopic observations as well as focused studies on the radiolarian fauna (Funakawa et al., 2006; Kamikuri et al., 2005) do not reveal extensive signs of dissolution, corroborating a negligible impact of BSi dissolution on our $\delta^{30}Si$ records.

The study of Si isotope fractionation by radiolarians is hindered partly because no attempts at culture have successfully managed to bring

radiolarians into thir reproductive cycle (Krabberød et al., 2011) that would result in the creation of new radiolarians and thus the silicification of new radiolarian tests. Precipitation of radiolarian tests is though to occur through internal concentration of Si that has been taken up across the outer cell membrane (Wallace et al., 2012). However, the extent of Si efflux mechanisms and relationship to DSi concentration and further impact on measurable Si isotopic fractionation is not yet resolved, although it is expected that fractionation by radiolarians will be analogous to that of other unicellular organisms, such as diatoms, and therefore unaffected by external DSi concentration. Thus, in absence of evidence for a relationship between Si isotope fractionation during the formation of radiolarian test and ambient DSi concentration, we confidently hypothesize that radiolarian $\delta^{30}Si$ reflects the isotopic composition - with a fractionation induced - of the source DSi.

Furthermore, no study on specie-specific Si isotope fractionation, as it has been recently demonstrated for the diatoms (Sutton et al., 2013), exists for radiolarian. Abelmann et al. (2015) demonstrated a difference in radiolarian $\delta^{30}Si$ between two different size fractions (125-250 and >250 μm) as high as 1.5‰. However, they could not attribute this offset to species-specific Si isotope fractionation or to differences in the depth habitat (and hence difference in DSi $\delta^{30}Si$). Our choice of selected all radiolarian species during sample preparation should average out the influence, if any, of species-specific Si isotope fractionation. Thus, although we acknowledge that our radiolarian $\delta^{30}Si$ record has the potential to be biased by shifts in radiolarian species and associated Si isotope fractionation, our data still hold relevant information for reconstructing silicon cycling over geological times.

4.2 Silicon isotopic composition of the surface water

Radiolarians dwell in the upper hundred meters of the water column. Several estimates of silicon isotopic fractionation by radiolarian exist, based on water column and sediment samples. Hendry et al. (2014) used an offset of -1.1 to -2.1‰ between radiolarian silica and DSi in the Sargasso Sea, based on comparison with diatom $\delta^{30}Si$ record during the most recent Heinrich Stadial (15-17 ka). More recently, Abelmann et al. (2015) used a similar if slightly more restrained range of fractionation of -0.8 to -1.5‰ for their reconstructions based on core top analyses. They found that different radiolarian size fractions could have an impact on the absolute $\delta^{30}Si$ values.

We use Abelmann et al.'s (2015) more restrained range of offset between radiolarian silica and seawater ($-1.5 < \Delta\,\delta^{30}Si < -0.8$‰) to reconstruct $\delta^{30}Si$ of DSi during the Paleogene in the Equatorial Pacific. The reconstructed $\delta^{30}Si$ of DSi thus corresponds to the $\delta^{30}Si$ of radiolarian tests to which we add the enrichment factor $\varepsilon_{rad\text{-}DSi}$ (i.e. $\delta^{30}Si_{DSi} = \delta^{30}Si_{rad} + \varepsilon_{rad\text{-}DSi}$), in permil. The reconstructed $\delta^{30}Si$ of DSi varies between +0.97 to +2.70‰, in good agreement with published values for the top hundred meters of the modern Pacific Ocean (De La Rocha et al., 2000; de Souza et al., 2014; Grasse et al., 2013; Reynolds et al., 2006). From this, we suggest that the Si isotopic composition of DSi in the upper ocean layer in the Equatorial Pacific during the Paleogene was similar to what is seen in the present day.

4.3 Reconstruction of DSi concentration in the bottom waters

Si isotopes in sponge spicules can be used to reconstruct DSi concentration (Hendry and Robinson, 2012). The extent of the fractionation between the BSi formed by the precipitation of siliceous sponge spicules and the DSi they originate from is a function of both DSi concentration and $\delta^{30}Si$:

$$\Delta\delta^{30}Si_{spo\text{-}DSi} = -6.54+270/(53+[DSi]) \quad (2)$$

where $\Delta\delta^{30}Si_{spo\text{-}DSi}$ is the fractionation between sponge spicules and seawater (i.e. $\Delta\delta^{30}Si_{spo\text{-}DSi} = \delta^{30}Si_{spo} - \delta^{30}Si_{DSi}$).

In the modern ocean, the $\delta^{30}Si$ of DSi in waters deeper than 1000m ranges from +0.5 to +2‰ (e.g. de Souza et al., 2014). Taking this range into consideration, we may calculate the possible set of DSi concentrations associated with any given the $\delta^{30}Si$ of sponge spicules. Rearranging eq.2 for DSi

concentrations yields:

$$[DSi] = (270/(\delta^{30}Si_{spo} - \delta^{30}Si_{DSi} + 6.54)) - 53 \quad (3)$$

Thus physically possible DSi concentrations reconstructed from the sponge spicules record range from ~0 to ~20-30 µM prior to 37 Ma and from between ~10-20 to 50-70 µM after 37 Ma (fig. 4). The asymptotic structure of the relationship between DSi concentration and sponge Si isotope fractionation limits its accuracy when dealing with high concentrations.

The reconstruction is sensitive at low concentrations of DSi, yielding a relatively precise estimate of DSi $\delta^{30}Si$. But the asymptotic structure of the relationship between DSi concentration and sponge Si isotope fractionation limits its usefulness at high concentrations of DSi. Reconstructions of high concentrations reflect more of the minimum possible concentration as opposed to being an estimate of an exact concentration. But this still provides useful information, especially as there is no other proxy that can be used to make direct estimates of DSi concentrations in the past. Even when taking this caveat into consideration, the record presented here from sponge spicules indicates that concentrations of DSi at depth were lower prior to 37 Ma than they were afterwards. Implications of increasing concentrations during the later half of the Paleogene in the equatorial Pacific are discussed further in section 4.5.

4.4 Results from previous studies

To our knowledge, only two studies have attempted to reconstruct aspects of the silicon cycle during the Paleogene from the variations of Si isotope in marine microfossils. The first study by Fontorbe et al. (in review), investigated the Si isotope variations in sponges and radiolarians over the Paleocene and Eocene periods in the Western North Atlantic Ocean (ODP leg 171B) and argued for an early and mid Paleogene North Atlantic Ocean with relatively low DSi concentrations throughout the entire water column. Even taking into account the entire range of DSi $\delta^{30}Si$ published for modern ocean, including extreme values with high DSi

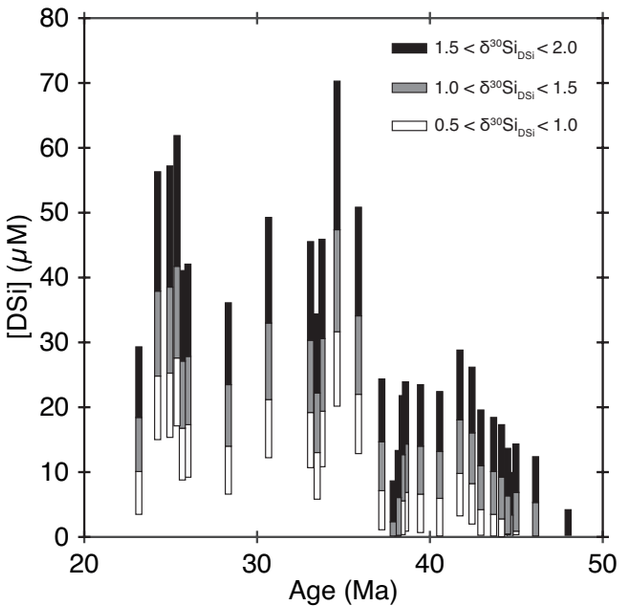

Figure 4: Reconstructed bottom waters DSi concentrations calculated following eq.3, according to three prescribed intervals of $\delta^{30}Si_{DSi.}$ (+0.5 to +1.0‰, white bars; +1.0‰ to +1.5‰, grey bars; +1.5 to +2.0‰, black bars).

$\delta^{30}Si$ (i.e. high $\Delta\delta^{30}Si_{spo\text{-}DSi}$), reconstruction of high DSi concentrations at depth was impossible. The second study, Egan et al. (2013), looked at the isotopic composition of sponge spicules and diatom frustules over the Eocene-Oligocene transition in the Southern Ocean and its Atlantic sector. In that study, sponge spicule $\delta^{30}Si$ decreased by about 1.5‰ over a 5.5 million years interval (37 to 31.5Ma). The timing of this decrease is in good agreement with the timing of subsidence of Southern Ocean land bridges. The opening of the Tasman Gateway and Drake Passage led to a reorganization of Southern Ocean deep-water circulation. Hence, they conclude that this change in ocean circulation resulted in a doubling of DSi concentrations in the studied area. A compilation of our data and previous studies can be found in fig. 5.

4.5 Changes in ocean circulation and DSi distribution

Reconstructions of ocean circulation in the geologic past have been carried out with two major proxies. The first is based on the Nd isotopic composition of seawater, expressed as $\varepsilon_{Nd}(t)$ (the sample $^{143}Nd/^{144}Nd$ ratio normalized to the bulk earth and corrected for age; DePaolo and Wasserburg, 1976). Briefly, the Nd isotopic composition of different water masses

depends on the continental rocks being weathered and draining into ocean basins (e.g. Goldstein et al., 1984). Intermediate and deep-waters get the Nd isotopic composition of the surface waters at the loci of subduction/downwelling. The ε_{Nd} of water masses is modified via mixing with other water masses with different ε_{Nd} value (e.g. Lacan and Jeandel, 2005). Since the oceanic residence time of Nd is relatively short compared to ocean mixing (e.g. Tachikawa et al., 1999), this leads variations in ε_{Nd} within and between ocean basins. Temporal variations of ε_{Nd} at a given location result from changes in ocean circulation and/or water mixing, or from changes in weathering (i.e. changes in Nd delivered to the ocean). Several materials, for example fish debris, foraminiferal calcite, ferromanganese crusts and authigenic ferromanganese, acquire their ε_{Nd} on the seabed and thus record the ε_{Nd} of deep-waters. The Nd isotopic composition of seawater has proven to be a robust proxy to track water masses mixing and circulation over geological time scales and has been successfully applied to reconstruct ocean circulation during the Cenozoic (Frank, 2002 and references therein).

A second method exploits the carbon stable isotopes of carbon (expressed as $\delta^{13}C$) recorded in benthic foraminifera to assess the relative amount of regenerated nutrients present in deep-waters flowing over a given site, as the remineralization of carbon from organic matter should lower the $\delta^{13}C$ of dissolved inorganic carbon (Sexton et al., 2006). Benthic foraminifera, forming their calcium carbonate shell using carbonate in the ambient water, record the isotopic composition of deep-waters. Ocean circulation plays a major role in the distribution of $\delta^{13}C$ at depth. The longer deep-waters travel away from their site of formation, the more potential remineralization of isotopically light carbon (i.e. low $\delta^{13}C$) can influence $\delta^{13}C$ values of deep-waters. Hence, benthic foraminifera can be used to estimate the relative age of deep-waters between different ocean basins.

The Cenozoic records of ε_{Nd}, coupled with ocean circulation models (Lunt et al., 2012; Marshall et al., 1997), suggest there was a reconfiguration of the Pacific Ocean circulation during the Paleogene (Thomas et al., 2014). The significant difference between the Nd isotope composition of North Atlantic and North Pacific deep-waters suggest that deep-waters of the North Atlantic did not make their way into North Pacific via the Caribbean gateway during the Paleogene (Thomas et al., 2003; Thomas et al., 2008). The lack of east-west gradient in ε_{Nd} in the tropical Pacific Ocean during the early Paleogene (Thomas et al., 2008) also suggest insignificant contribution of deep-waters from the Tethys Ocean. Therefore, the early Paleogene Pacific Ocean must be considered as an isolated basin. Prior to ~40-42 Ma, Pacific deep waters were formed both in the North Pacific and in the Pacific sector of the Southern Ocean (the Tasman gateway did not allow deep flow until the early Oligocene, Stickley et al., 2014). After 36 Ma, ε_{Nd} values from ODP Leg 199 exhibit a trend towards less radiogenic values (i.e. decreasing ε_{Nd}) demonstrating greater influence of Southern Ocean deep-waters on the deep equatorial Pacific. This has been attributed to the strengthening of Southern Ocean deep water formation in the Pacific sector due to the progressive deepening of the Tasman gateway as Australia moves farther from Antarctica (Thomas et al., 2008). This interpretation is reinforced by the inter-basinal gradient in $\delta^{13}C$. Over the entire Paleogene, there is no significant offset between $\delta^{13}C$ recorded in benthic foraminifera from different ocean basin, and the $\delta^{13}C$ gradient increases during the mid Miocene (~15 Ma; Cramer et al., 2009). This accentuate the interpretation of a relatively close source of deep-waters to the Pacific either from the North Pacific or from the Pacific sector of the Southern Ocean as deep-waters do not get enough time for expressing measurable changes in $\delta^{13}C$ due to remineralization of organic matter.

Similarly, the sponge $\delta^{30}Si$ values in this study decrease around 37 Ma, which can be most easily explained as an increase in deep-water DSi concentrations, in agreement with previous studies (Egan et al., 2013). As detailed above, Nd isotope records show a transition in the deep-water composition of the equatorial Pacific coincident with the decrease of sponge $\delta^{30}Si$ values. We suggest

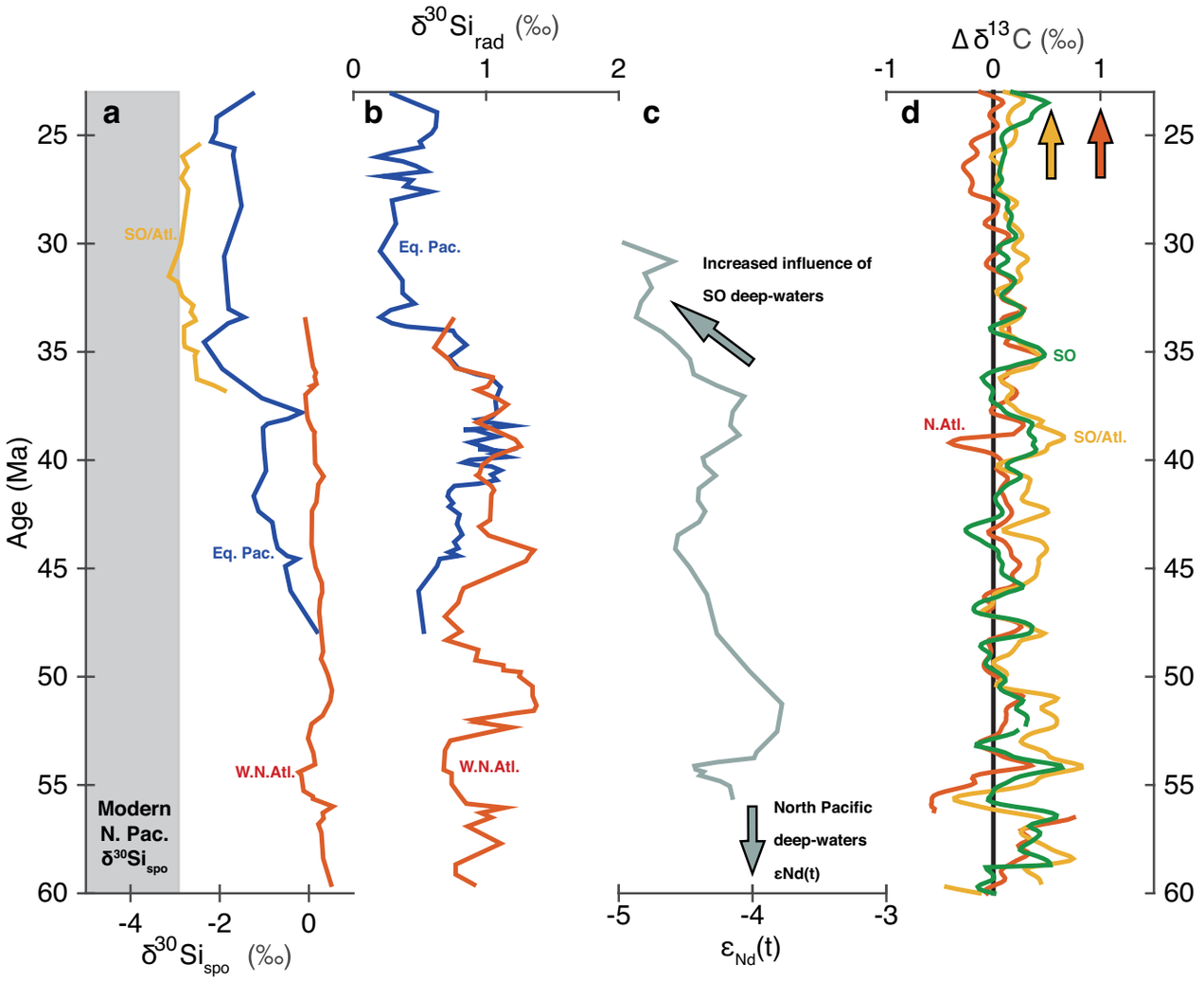

Figure 5: All available Paleogene Si isotope data and literature data for Nd and C isotopic composition from selected sites. (a) Sponge $\delta^{30}Si$ isotope values from the equatorial Pacific (this study, blue line), the Western North Atlantic (red line, Fontorbe et al. in revision) and the Atlantic sector of the Southern Ocean (yellow line, Egan et al. 2013). The gray shaded area highlights modern range of sponge $\delta^{30}Si$ in the North Pacific (Hendry and Robinson, 2012). (b) Radiolarian $\delta^{30}Si$ from the equatorial Pacific (blue line, this study), and the Western North Atlantic (blue line, Fontorbe et al., in revision). (c) Nd isotope data ($\varepsilon_{Nd}(t)$) from ODP leg 199 from Thomas et al. (2008). (d) Basin-specific gradient of $\delta^{13}C$ relative to the North Pacific (red line. North Atlantic; yellow line, Atlantic sector of the Southern Ocean; green line, Southern Ocean). Arrows indicates the modern values of the $\delta^{13}C$ gradient between the North Atlantic (red arrow) and the Atlantic sector of the Southern Ocean (yellow arrow), and the North Pacific. Carbon stable isotope data compiled in Cramer et al. (2009).

here, that sponge $\delta^{30}Si$ provides information complementary to Nd isotopes and $\delta^{13}C$ gradients, two widely applied paleocirculation proxies. Sponge $\delta^{30}Si$ has potential to highlight transition between water masses with highly different nutrient content, although its applicability is lessened when dealing with two or more water masses with similar DSi concentration (see section 4.3). Our data indicates that prior to ~40 Ma, equatorial Pacific deep-waters were influenced by North Pacific deep-waters forming from surface waters with low DSi concentration. Around 37 Ma, the source of deep-water shifted from North Pacific formation to formation in the Southern Ocean where surface waters had significantly higher DSi concentrations. Moreover, considering that the equatorial Pacific was a locus of upwelling during the Paleogene (Huber, 2002), a noticeable change in DSi concentration in the deeper layer should also influence the upper layer. As a general observation, ocean DSi concentrations are negatively correlated to DSi $\delta^{30}Si$ (i.e. high DSi concentrations are associated with low $\delta^{30}Si$ and vice versa). Radiolarian $\delta^{30}Si$ values decrease by about 1‰ between 37 and 34 Ma, which can be

interpreted as changes in the characteristics of the upwelled waters towards deep-waters with lower DSi $\delta^{30}Si$ (and potentially higher DSi concentrations), corroborating the above conclusions.

5. Conclusions

This study emphasizes the complementary use of sponge and radiolarian $\delta^{30}Si$ to reconstruct aspects of changes in ocean circulation as well as facets of the silicon cycle. Our results corroborate previous conclusions based on the reconstruction of Nd isotopic composition of seawater, of changes of ocean circulation in the equatorial Pacific from a source of deep-waters forming in the North Pacific to another source forming in the Southern Ocean. Additionally, the use of sponge $\delta^{30}Si$ provides information about the nutrient content of such water masses. We conclude that the newly formed North Pacific deep-waters had low DSi concentrations whereas the deep-waters formed in the Southern Ocean had significantly higher DSi concentrations.

Acknowledgements

This work was funded by a grant from the Knut & Alice Wallenberg Foundation to DJC. Additional funding for analysis was provided by a grant from the Royal Physiographic Society of Lund tp GF. KRH was funded by the Royal Society. We thank Emmanuel Ponzevera at IFREMER Brest for his support during analyses.

References

Abelmann, A., Gersonde, R., Knorr, G., Zhang, X., Chapligin, B., Maier, E., Esper, O., Friedrichsen, H., Lohmann, G., Meyer, H., 2015. The seasonal sea-ice zone in the glacial Southern Ocean as a carbon sink. Nature communications 6.

Cardinal, D., Alleman, L.Y., de Jong, J., Ziegler, K., André, L., 2003. Isotopic composition of silicon measured by multicollector plasma source mass spectrometry in dry plasma mode. Journal of Analytical Atomic Spectrometry 18, 213-218.

Cardinal, D., Alleman, L.Y., Dehairs, F., Savoye, N., Trull, T.W., André, L., 2005. Relevance of silicon isotopes to Si-nutrient utilization and Si-source assessment in Antarctic waters. Global Biogeochemical Cycles 19, n/a-n/a.

Coffineau, N., De La Rocha, C.L., Pondaven, P., 2014. Exploring interacting influences on the silicon isotopic composition of the surface ocean: a case study from the Kerguelen Plateau. Biogeosciences 11, 1371-1391.

Cramer, B., Toggweiler, J., Wright, J., Katz, M., Miller, K., 2009. Ocean overturning since the Late Cretaceous: Inferences from a new benthic foraminiferal isotope compilation. Paleoceanography 24.

De La Rocha, C., Brzezinski, M.A., DeNiro, M., Shemesh, A., 1998. Silicon-isotope composition of diatoms as an indicator of past oceanic change. Nature 395, 680-683.

De La Rocha, C.L., 2003. Silicon isotope fractionation by marine sponges and the reconstruction of the silicon isotope composition of ancient deep water. Geology 31, 423.

De La Rocha, C.L., Brzezinski, M.A., DeNiro, M.J., 1997. Fractionation of silicon isotopes by marine diatoms during biogenic silica formation. Geochimica et Cosmochimica Acta 61, 5051-5056.

De La Rocha, C.L., Brzezinski, M.A., DeNiro, M.J., 2000. A first look at the distribution of the stable isotopes of silicon in natural waters. Geochimica et Cosmochimica Acta 64, 2467-2477.

De Souza, G., Reynolds, B., Johnson, G., Bullister, J., Bourdon, B., 2012. Silicon stable isotope distribution traces Southern Ocean export of Si to the eastern South Pacific thermocline. Biogeosciences 9, 4199-4213.

de Souza, G.F., Slater, R.D., Dunne, J.P., Sarmiento, J.L., 2014. Deconvolving the controls on the deep ocean's silicon stable isotope distribution. Earth and Planetary Science Letters 398, 66-76.

Demarest, M.S., Brzezinski, M.A., Beucher, C.P., 2009. Fractionation of silicon isotopes during biogenic silica dissolution. Geochimica et Cosmochimica Acta 73, 5572-5583.

DePaolo, D., Wasserburg, G., 1976. Nd isotopic variations and petrogenetic models. Geophysical Research Letters 3, 249-252.

Egan, K.E., Rickaby, R.E.M., Hendry, K.R., Halliday, A.N., 2013. Opening the gateways for diatoms primes Earth for Antarctic glaciation. Earth and Planetary Science Letters 375, 34-43.

Egan, K.E., Rickaby, R.E.M., Leng, M.J., Hendry, K.R., Hermoso, M., Sloane, H.J., Bostock, H., Halliday, A.N., 2012. Diatom silicon isotopes as a proxy for silicic acid utilisation: A Southern Ocean core top calibration. Geochimica et Cosmochimica Acta 96, 174-192.

Ehlert, C., Grasse, P., Frank, M., 2013. Changes in silicate utilisation and upwelling intensity off Peru since the Last Glacial Maximum – insights from silicon and neodymium isotopes. Quaternary Science Reviews 72, 18-35.

Fontorbe, G., Frings, P.J., De La Rocha, C.L., Hendry, K.R., Conley, D.J., in revision. A silicon depleted North Atlantic since the Palaeogene: evidence from sponge and radiolarian silicon isotopes. Earth and Planetary Science Letters.

Frank, M., 2002. Radiogenic isotopes: tracers of past ocean circulation and erosional input. Reviews of geophysics 40.

Funakawa, S., Nishi, H., Moore, T.C., Nigrini, C.A., 2006. Data report: Late Eocene-early Oligocene radiolarians, ODP Leg 199 Holes 1218A, 1219A, and 1220A, central Pacific, In Wilson, P.A., Lyle, M., and Firth, J.V. (Eds.), Proc. ODP, Sci. Results, 199: College Station, TX (Ocean Drilling Program), 1–20, pp. 1-74.

Georg, R.B., Reynolds, B.C., Frank, M., Halliday, A.N., 2006. New sample preparation techniques for the determination of Si isotopic compositions using MC-ICPMS. Chemical Geology 235, 95-104.

Goldstein, S., O'nions, R., Hamilton, P., 1984. A Sm-Nd isotopic study of atmospheric dusts and particulates from major river systems. Earth and Planetary Science Letters 70, 221-236.

Grasse, P., Ehlert, C., Frank, M., 2013. The influence of water mass mixing on the dissolved Si isotope composition in the Eastern Equatorial Pacific. Earth and Planetary Science Letters 380, 60-71.

Hendry, K., Swann, G.E., Leng, M.J., Sloane, H.J., Goodwin, C., Berman, J., Maldonado, M., 2015. Technical Note: Silica stable isotopes and silicification in a carnivorous sponge Asbestopluma sp. Biogeosciences 12, 3489-3498.

Hendry, K.R., Robinson, L.F., 2012. The relationship between silicon isotope fractionation in sponges and silicic acid concentration: Modern and core-top studies of biogenic opal. Geochimica et Cosmochimica Acta 81, 1-12.

Hendry, K.R., Robinson, L.F., McManus, J.F., Hays, J.D., 2014. Silicon isotopes indicate enhanced carbon export efficiency in the North Atlantic during deglaciation. Nature communications 5.

Huber, M., 2002. Straw man 1: A preliminary view of the tropical Pacific from a global coupled climate model simulation of the early Paleogene, Lyle, M., Wilson, PA, Janecek, TR, et al., Proc. ODP, Init. Repts, pp. 1-30.

Kamikuri, S.-i., Nishi, H., Moore, T.C., Nigrini, C.A., Motoyama, I., 2005. 4. Data Report: Late Oligocene and Early Miocene Radiolarians, Sites 1218 and 1219, Central Pacific. In Wilson, P.A., Lyle, M., and Firth, J.V. (Eds.), Proc. ODP, Sci. Results, 199: College Station, TX (Ocean Drilling Program), 1–13.

Krabberød, A.K., Bråte, J., Dolven, J.K., Ose, R.F., Klaveness, D., Kristensen, T., Bjørklund, K.R., Shalchian-Tabrizi, K., 2011. Radiolaria Divided into Polycystina and Spasmaria in Combined 18S and 28S rDNA Phylogeny. PLoS ONE 6, e23526.

Lacan, F., Jeandel, C., 2005. Neodymium isotopes as a new tool for quantifying exchange fluxes at the continent–ocean interface. Earth and Planetary Science Letters 232, 245-257.

Lunt, D.J., Dunkley Jones, T., Heinemann, M., Huber, M., LeGrande, A., Winguth, A., Loptson, C., Marotzke, J., Roberts, C., Tindall, J., 2012. A model–data comparison for a multi-model ensemble of early Eocene atmosphere–ocean simulations: EoMIP. Climate of the Past 8, 1717-1736.

Lyle, M., Wilson, P.A., Janecek, T.R., al., e., 2002. Proc. ODP, Init. Repts., 199: College Station, TX (Ocean Drilling Program).

Maier, E., Chapligin, B., Abelmann, A., Gersonde, R., Esper, O., Ren, J., Friedrichsen, H., Meyer, H., Tiedemann, R., 2013. Combined oxygen and silicon isotope analysis of diatom silica from a deglacial subarctic Pacific record. Journal of Quaternary Science 28, 571-581.

Maliva, R.G., Knoll, A.H., Siever, R., 1989. Secular change in chert distribution: a reflection of

evolving biological participation in the silica cycle. Palaios, 519-532.

Marin-Carbonne, J., Robert, F., Chaussidon, M., 2014. The silicon and oxygen isotope compositions of Precambrian cherts: A record of oceanic paleo-temperatures? Precambrian Research 247, 223-234.

Marshall, J., Adcroft, A., Hill, C., Perelman, L., Heisey, C., 1997. A finite-volume, incompressible Navier Stokes model for studies of the ocean on parallel computers. Journal of Geophysical Research: Oceans 102, 5753-5766.

Morley, D.W., Leng, M.J., Mackay, A.W., Sloane, H.J., Rioual, P., Battarbee, R.W., 2004. Cleaning of lake sediment samples for diatom oxygen isotope analysis. Journal of Paleolimnology 31, 391-401.

Rabosky, D.L., Sorhannus, U., 2009. Diversity dynamics of marine planktonic diatoms across the Cenozoic. Nature 457, 183-186.

Reynolds, B., Frank, M., Halliday, A., 2006. Silicon isotope fractionation during nutrient utilization in the North Pacific. Earth and Planetary Science Letters 244, 431-443.

Reynolds, B.C., Aggarwal, J., André, L., Baxter, D., Beucher, C., Brzezinski, M.A., Engström, E., Georg, R.B., Land, M., Leng, M.J., 2007. An inter-laboratory comparison of Si isotope reference materials. Journal of Analytical Atomic Spectrometry 22, 561-568.

Sexton, P.F., Wilson, P.A., Norris, R.D., 2006. Testing the Cenozoic multisite composite δ18O and δ13C curves: New monospecific Eocene records from a single locality, Demerara Rise (Ocean Drilling Program Leg 207). Paleoceanography 21.

Siever, R., 1991. Silica in the oceans: Biological-geochemical interplay. Scientists on Gaia, 287-295.

Stickley, C.E., Brinkhuis, H., Schellenberg, S.A., Sluijs, A., Röhl, U., Fuller, M., Grauert, M., Huber, M., Warnaar, J., Williams, G.L., 2004. Timing and nature of the deepening of the Tasmanian Gateway. Paleoceanography 19.

Sutton, J.N., Varela, D.E., Brzezinski, M.A., Beucher, C.P., 2013. Species-dependent silicon isotope fractionation by marine diatoms. Geochimica et Cosmochimica Acta 104, 300-309.

Tachikawa, K., Jeandel, C., Roy-Barman, M., 1999. A new approach to the Nd residence time in the ocean: the role of atmospheric inputs. Earth and Planetary Science Letters 170, 433-446.

Tatzel, M., von Blanckenburg, F., Oelze, M., Schuessler, J.A., Bohrmann, G., 2015. The silicon isotope record of early silica diagenesis. Earth and Planetary Science Letters 428, 293-303.

Thomas, D.J., Bralower, T.J., Jones, C.E., 2003. Neodymium isotopic reconstruction of late Paleocene–early Eocene thermohaline circulation. Earth and Planetary Science Letters 209, 309-322.

Thomas, D.J., Korty, R., Huber, M., Schubert, J.A., Haines, B., 2014. Nd isotopic structure of the Pacific Ocean 70-30 Ma and numerical evidence for vigorous ocean circulation and ocean heat transport in a greenhouse world. Paleoceanography 29, 454-469.

Thomas, D.J., Lyle, M., Moore, T.C., Rea, D.K., 2008. Paleogene deepwater mass composition of the tropical Pacific and implications for thermohaline circulation in a greenhouse world. Geochemistry, Geophysics, Geosystems 9.

Varela, D.E., Pride, C.J., Brzezinski, M.A., 2004. Biological fractionation of silicon isotopes in Southern Ocean surface waters. Global Biogeochemical Cycles 18.

Wallace, A.F., Wang, D., Hamm, L.M., Knoll, A.H., Dove, P.M., 2012. Eukaryotic skeletal formation. Fundamentals of Geobiology, 150-187.

Wetzel, F., De Souza, G., Reynolds, B., 2014. What controls silicon isotope fractionation during dissolution of diatom opal? Geochimica et Cosmochimica Acta 131, 128-137.

Wille, M., Sutton, J., Ellwood, M.J., Sambridge, M., Maher, W., Eggins, S., Kelly, M., 2010. Silicon isotopic fractionation in marine sponges: A new model for understanding silicon isotopic variations in sponges. Earth and Planetary Science Letters 292, 281-289.

Zachos, J., Pagani, M., Sloan, L., Thomas, E., Billups, K., 2001. Trends, rhythms, and aberrations in global climate 65 Ma to present. Science 292, 686-693.

Supplementary Table 1: Details of individual samples and secondary reference materials. Uncertainties on $\delta^{x}Si$ values are given as internal measurement precision (1σ)

Hole	Core	Section	Interval (cm)	Depth (mcd)	Age (Ma)	$\delta^{30}Si_{spo}$	1σ	$\delta^{29}Si_{spo}$	1σ	$\delta^{30}Si_{rad}$	1σ	$\delta^{29}Si_{rad}$	1σ
1217A	4	5	80 - 82	30.56	33.46	-1.14	0.03	-0.61	0.02	0.11	0.08	0.07	0.03
	4	6	48 - 50	31.74	33.70	-1.13	0.02	-0.59	0.01	0.08	0.02	0.05	0.02
	7	1	140 - 142	52.92	37.91	-0.5	0.02	-0.27	0.02	0.98	0.07	0.48	0.02
	7	2	140 - 142	54.42	38.21		n/a			0.66	0.03	0.31	0.01
	7	4	40 - 42	56.42	38.61	-0.39	0.03	-0.2	0.04	0.64	0.10	0.31	0.05
	7	6	130 - 132	60.32	39.38		n/a			1.06	0.03	0.55	0.02
	9	2	71 - 73	65.30	40.37		n/a			0.86	0.02	0.40	0.00
	9	5	112 - 114	69.56	41.22		n/a			0.66	0.01	0.36	0.00
	11	1	100 - 102	82.76	43.85		n/a			0.88	0.05	0.46	0.01
	11	3	128 - 130	86.04	44.50	-0.17	0.07	-0.09	0.04	0.93	0.05	0.48	0.05
	11	4	120 - 122	87.46	44.78	-0.3	0.08	-0.16	0.04	0.38	0.02	0.17	0.01
1217B	3	1	92 - 94	32.88	33.92		n/a			0.46	0.04	0.24	0.02
	3	3	92 - 94	35.88	34.52		n/a			0.73	0.02	0.37	0.01
	4	1	92 - 94	43.34	36.00		n/a			0.75	0.13	0.00	0.08
	5	1	91 - 92	50.49	37.43	0.12	0.02	0.07	0.02	1.18	0.10	0.63	0.05
	5	3	104 - 105	53.62	38.05	-0.09	0.02	-0.05	0.02	1.08	0.11	0.55	0.05
	5	5	86 - 87	56.44	38.61		n/a			1.35	0.04	0.64	0.06
	6	1	120 - 122	62.05	39.73		n/a			1.33	0.09	0.70	0.05
	6	3	120 - 122	65.05	40.32		n/a			1.42	0.09	0.75	0.03
	6	5	120 - 122	68.05	40.92	-0.78	0.08	-0.41	0.04	1.21	0.03	0.60	0.02
	7	3	50 - 51	55.02	38.33		n/a			1.33	0.08	0.68	0.04
	7	4	102 - 104	75.40	42.38		n/a			0.76	0.12	0.38	0.07
	8	5	59 - 61	83.59	44.01		n/a			0.72	0.05	0.35	0.01

1218A	9	2	74	-	76	87.20	23.08	-1.26	0.02	-0.69	0.01	0.29	0.04	0.21	0.05
	10	6	103	-	105	104.63	25.10	-2.47	0.03	-1.36	0.01	0.26	0.08	0.14	0.05
	10	7	34	-	36	105.44	25.20	-1.34	0.04	-0.71	0.01	0.71	0.06	0.35	0.03
	11	2	83	-	84	109.43	25.57	-2.76	0.06	-1.38	0.03	0.53	0.08	0.23	0.06
	11	5	65	-	66	113.75	25.81		n/a			0.33	0.11	0.15	0.05
	12	5	53	-	54	124.20	26.39		n/a			0.90	0.04	0.49	0.04
	13	2	35	-	36	129.46	26.68		n/a			0.33	0.04	0.22	0.03
	13	5	19	-	20	133.80	26.92		n/a			0.41	0.03	0.19	0.02
	14	2	49	-	50	139.61	27.24		n/a			0.99	0.04	0.51	0.04
	15	2	4	-	5	149.46	27.78		n/a			0.49	0.05	0.25	0.03
	26	6	32	-	33	268.19	38.74		n/a			0.84	0.07	0.46	0.02
	27	2	55	-	56	272.08	39.54		n/a			0.83	0.04	0.45	0.02
	27	4	56	-	57	275.09	40.16		n/a			0.51	0.10	0.29	0.10
	28	2	54	-	55	279.77	40.72		n/a			1.06	0.11	0.59	0.07
	28	5	60	-	61	284.33	41.13		n/a			0.96	0.06	0.50	0.01
1219A	7	2	110	-	112	58.01	24.34	-2.47	0.04	-1.25	0.02	0.81	0.01	0.42	0.02
	7	3	4	-	5	58.45	24.41		n/a			0.80	0.06	0.41	0.03
	8	2	87	-	88	68.42	26.04	-0.91	0.10	-0.50	0.05	0.02	0.04	0.05	0.03
	8	3	129	-	131	70.34	26.16	-1.42	0.03	-0.74	0.01	0.18	0.02	0.1	0.02
	9	3	138	-	140	84.25	27.06		n/a			-0.07	0.03	-0.03	0.01
	11	1	122	-	124	106.13	28.48		n/a			0.13	0.02	0.08	0.01
	15	2	20	-	21	154.05	31.58		n/a			0.14	0.10	0.12	0.03
	16	6	60	-	62	171.54	32.71		n/a			0.34	0.03	0.18	0.01
	17	3	33	-	35	176.68	33.04	-2.08	0.06	-1.11	0.04	0.4	0.03	0.16	0.02
	19	6	145	-	147	203.78	38.60	-1.87	0.04	-0.96	0.04	0.76	0.03	0.38	0.02
	20	7	42	-	44	214.33	39.85		n/a			1.01	0.02	0.52	0.01
	21	1	137	-	139	217.20	40.19		n/a			0.84	0.02	0.43	0.00

	22	4	108	-	110	231.91	41.93	-1.72	0.07	-0.87	0.04	0.63	0.04	0.36	0.02
	23	6	53	-	55	244.86	43.47	-0.79	0.05	-0.39	0.02	0.69	0.05	0.33	0.01
	24	2	97	-	99	249.80	44.40	-0.28	0.01	-0.12	0.02	0.65	0.05	0.36	0.05
	24	4	110	-	112	252.93	45.43	-1.11	0.02	-0.56	0.01	0.57	0.09	0.3	0.02
1220A	5	2	121	-	123	44.00	27.77		n/a			0.25	0.06	0.11	0.01
	6	6	40	-	42	60.74	30.98		n/a			0.34	0.05	0.17	0.01
	7	5	48	-	50	69.75	32.57	-2.19	0.05	-1.13	0.02	0.64	0.04	0.30	0.00
	8	2	146	-	148	77.10	33.87	-3.16	0.01	-1.66	0.01	0.67	0.01	0.36	0.01
	8	4	73	-	75	79.37	34.27		n/a			1.13	0.01	0.57	0.01
	9	4	60	-	62	89.59	36.08	-2.77	0.06	-1.4	0.03	1.11	0.06	0.57	0.01
	10	5	44	-	46	101.26	38.14		n/a			1.07	0.02	0.55	0.01
	12	7	48	-	50	128.85	41.87		n/a			0.85	0.03	0.43	0.01
1221A	1	7	80	-	82	10.18	35.25		n/a			0.68	0.05	0.36	0.05
	2	4	50	-	51	14.88	36.04		n/a			0.94	0.06	0.48	0.04
	2	5	94	-	95	16.82	36.37		n/a			1.04	0.01	0.53	0.02
	3	4	80	-	82	25.18	38.32	-0.82	0.08	-0.43	0.04	1.18	0.04	0.59	0.02
	3	5	100	-	101	26.88	38.58		n/a			1.09	0.07	0.55	0.03
	4	3	93	-	95	33.81	39.43		n/a			0.73	0.05	0.34	0.02
	4	4	12	-	13	34.50	39.51		n/a			1.25	0.06	0.64	0.02
	4	6	90	-	92	38.28	39.97		n/a			1.13	0.04	0.58	0.04
	5	7	20	-	22	48.58	41.22		n/a			0.66	0.01	0.33	0.02
	6	5	117	-	119	56.05	42.13	-1.21	0.06	-0.61	0.02	0.77	0.00	0.38	0.01
	7	4	80	-	82	63.68	43.01	-0.47	0.06	-0.24	0.05	0.88	0.14	0.44	0.06
	8	6	39	-	41	76.27	44.35	-1.02	0.04	-0.55	0.03	0.78	0.01	0.38	0.02
	12	6	75	-	77	115.13	47.92	0.18	0.02	0.09	0.01	0.53	0.05	0.22	0.02
Big Batch		n=2						-10.37	0.04	-5.31	0.04				
Diatomite		n=2						1.30	0.08	0.66	0.04				

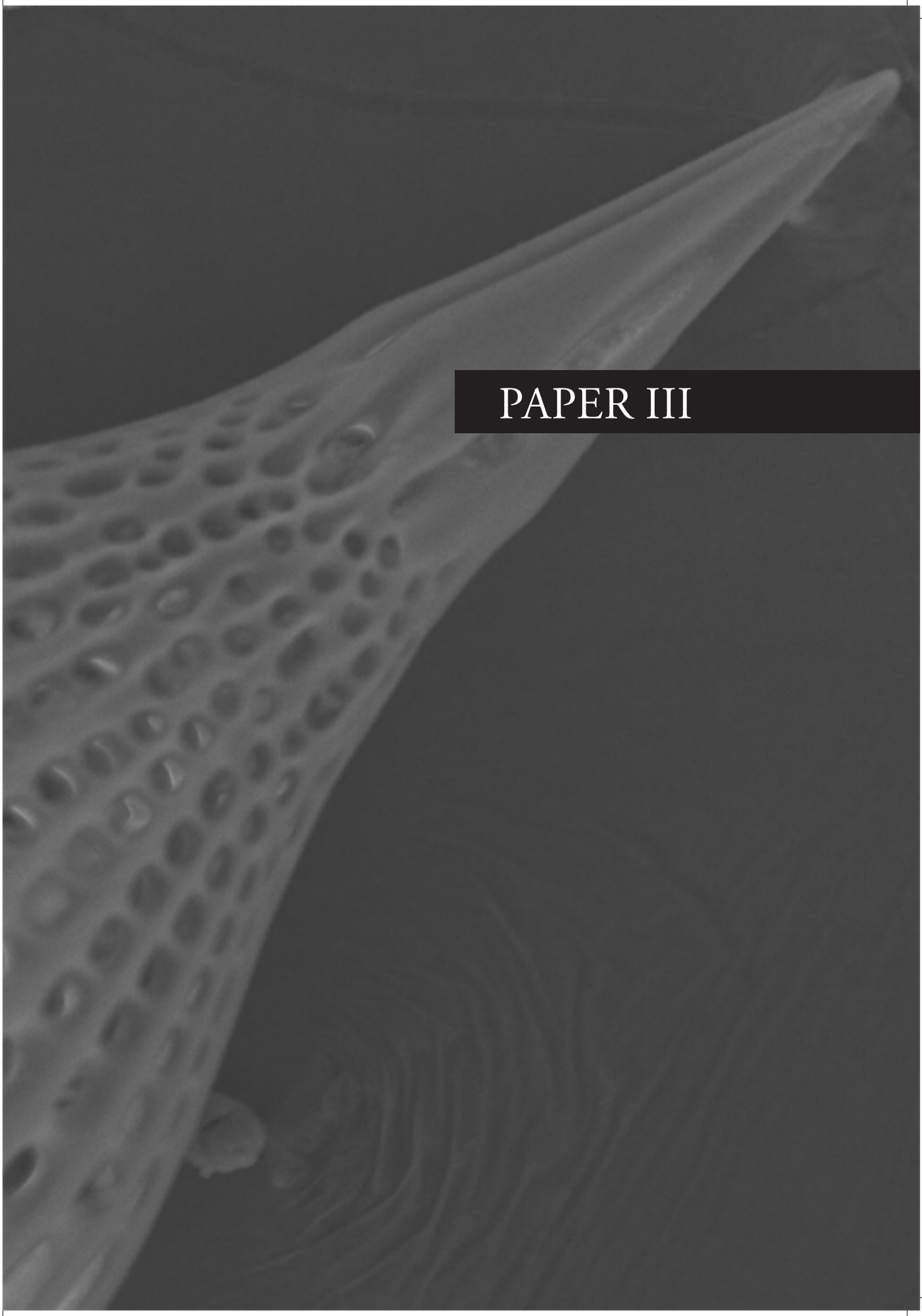

PAPER III

Marine silicon cycle response to the Paleocene-Eocene Thermal Maximum

Guillaume Fontorbe[a,*], Patrick J. Frings[a], Christina L. De La Rocha, Katharine R. Hendry[b], Daniel J. Conley[a]

[a] Department of Geology, Lund University, Sölvegatan 12, SE-223 62, Lund, Sweden

[b] School of Earth Sciences, University of Bristol, Wills Memorial Building, Queen's Road, Bristol, BS8 1RJ, UK

* corresponding author(guillaume.fontorbe@geol.lu.se)

Abstract

The Paleocene Eocene Thermal Maximum (PETM) is a transient period of perturbation of the carbon cycle, occurring about 56 million years ago, marked by a negative carbon isotope excursion (CIE) as well as a rise of global temperatures by several degrees. The CIE results from the fast release of ^{13}C-depleted carbon. While it is widely recognized that the source of carbon is the release of methane from the dissociation of gas hydrates or from the release from carbon rich sediments, the triggers of this release and mechanisms involved during the recovery phase are still heavily debated. Some of these mechansims, e.g. changes in magmatic activity and enhanced weathering of silicate minerals, could potentially impact the marine silicon (Si) cycle. We analyzed the Si isotopic composition (expressed as $\delta^{30}Si$) of radiolarians from the North Altantic (ODP site 1051) covering the PETM. Radiolarian $\delta^{30}Si$ decreases by about 0.75‰ coeval with the CIE. With a simple box model, we investigated the sensitivity of seawater $\delta^{30}Si$ $\delta^{30}Si$ to changes in magmatic and riverine inputs. The amplitude of the shift in $\delta^{30}Si$ is reproducible by combining intrusive volcanism/hydrothermalism processes during the onset of the CIE with enhanced weathering of silicate minerals during the body and recovery phases.

1. Introduction

The early Paleogene is characterized by global warmth, ice-free poles and higher atmospheric CO_2 concentrations ($pCO2$). Short-lived (< 200 ka) periods of extreme warmth and carbon addition termed hyperthermals are superimposed on this already warm climate (Zachos et al., 2001). The most notable of these hyperthermals, termed the Paleocene Eocene Thermal Maximum (PETM), is marked by a negative carbon isotope excursion (CIE) of 2-6‰ recorded synchronously in marine (Kennett and Stott, 1991) and terrestrial archives (Koch et al., 1992). Consequences of the PETM include global temperature increases (bottom water temperatures, reconstructed from the oxygen stable isotope composition ($\delta^{18}O$) of benthic foraminifera, increase by about 5°C; Kennett and Stott, 1991; Thomas and Shackleton, 1996; Zachos et al., 2001), reorganisation of the ocean overturning circulation (e.g. Nunes and Norris, 2006), a changing hydrological cycle (e.g. Tipple et al., 2011), shoaling of the carbonate compensation depth (e.g. Zachos et al., 2005), marine extinction events (e.g. Thomas and Shackleton, 1996) and a drastically altered terrestrial biosphere, among others. The PETM is therefore receiving attention as a possible analogue for the consequences of anthropogenic global warming.

The total duration of the PETM is estimated at ca. 150-220 kyrs based on astronomical cyclostratigraphy (Aziz et al., 2008; Röhl et al., 2003; Röhl et al., 2007), or at 120-220 kyrs based on extraterrestial ^{3}He (Farley and Eltgroth, 2003; Murphy et al., 2010). Conventionally, four phases are recognised. The first consists of pre-CIE conditions, during which both $\delta^{13}C$ and $\delta^{18}O$ gradually decrease (Zachos et al., 2001). The second phase - the CIE onset - is defined as the period between the last sample with pre-CIE values and the one with the most negative values and has been estimated to start between 56.011 and 56.293 Ma (Jaramillo et al., 2010). Estimates of the duration of the onset span 8-23 ka from continental sedimentary sections (e.g. Aziz et al., 2008; Magioncalda et al., 2004) and ca 10 ka from marine carbonates (Zachos et al.,

2005). It is worth noting that in many locations, ocean temperatures as recorded in e.g. $\delta^{18}O$ or the palaeothermometer TEX_{86} appear to start increasing about 3,000-6,000 years before the onset of the CIE (Littler et al., 2014; Sluijs et al., 2007). A CIE 'body' with low and stable $\delta^{13}C$ and $\delta^{18}O$ lasts for about 113 kyrs (McInerney and Wing, 2011; Murphy et al., 2010) and is followed by a recovery in which $\delta^{13}C$ and $\delta^{18}O$ gradually return to pre-CIE values over ~83 kyrs (McInnerney and Wing, 2011; Murphy et al., 2010).

The magnitude of the CIE requires a large quantity of carbon depleted in ^{13}C to be mixed with the exogenic carbon pool. Carbon mass-balance implies that the more ^{13}C depleted the carbon source, the less carbon is required to produce a global CIE of ca. -3‰. With this in mind, the source of this carbon is widely attributed to release of highly ^{13}C deplete, bacterially generated methane ($\delta^{13}C \approx$ -60‰) from the thermal dissociation of sea-floor gas hydrates (Dickens et al., 1997; Dickens et al., 1995; Katz, 1999) or from the thermogenesis of methane via sill emplacement in organic carbon rich marine sediments, producing carbon at approximately -30‰ (Svensen et al. 2004). In addition to the source of the carbon, the mechanism(s) that triggered its release, the amount of carbon released, the timescales involved, and the processes involved in the return to pre-perturbation conditions, are all heavily debated.

Some aspect of the Earth's carbon cycle must have been pushed over a threshold in order to trigger the carbon release, whether from methane hydrates or elsewhere. Many mechanisms have been proposed, including a comet impact (Kent et al., 2003), the crossing of an orbital forcing threshold (e.g. Littler et al., 2014; Lourens et al., 2005; Zachos et al., 2010), and volcanism/hydrothermalism (e.g. Dickson et al., 2015; Larsen et al., 2003; Wieczorek et al., 2013). The recovery phase of the CIE, lasting about 100,000 years (Zachos et al., 2005), saw the stable oxygen and carbon isotopes return to their pre-excursion levels. The recovery must have been achieved by increases in one or both of the two sinks in the long-term carbon cycle, namely i) the burial of organic carbon (e.g. Bowen and Zachos 2010) and ii) the conversion of atmospheric CO_2 to carbonate alkalinity (and hence sedimentary carbonates) via the chemical weathering of silicate minerals. The relative importance of these two processes is uncertain.

Some of these mechanisms will impact the marine silicon (Si) cycle, especially the Si isotopic composition (expressed as $\delta^{30}Si$) of dissolved Si (DSi) in seawater on local to global scales, which means that archives of seawater $\delta^{30}Si$ have a previously unexploited potential to address questions about the likelihood of such mechanisms to have contributed to the environmental perturbations during the PETM. Such an archive is found in the $\delta^{30}Si$ of radiolarians (siliceous zooplankton), which can be used to investigate variations in the $\delta^{30}Si$ of upper water column DSi (Abelmann et al., 2015; Fontorbe et al., in revision; Hendry et al., 2014). Here, we analyzed the Si isotopic composition of radiolarian tests covering the PETM from Blake Nose, Western North Atlantic. The radiolarian $\delta^{30}Si$ record shows a decrease of about 0.75‰ coeval with the CIE. With a simple box model, we investigate the sensitivity of seawater Si isotopes to changes in hydrothermalism and weathering of silicate minerals. The amplitude of the shift in $\delta^{30}Si$ is reproducible by combining intrusive volcanism/hydrothermalism processes during the onset of the CIE with enhanced weathering of silicate minerals during the body and recovery phases.

2. Material and methods

2.1. Sample preparation

Radiolarians have been isolated from sediment from ODP site 1051B (leg 171B; Blake Nose, Western North Atlantic. Site 1051B is known to contain well-preserved siliceous faunas, including abundant radiolarian tests (Sanfilippo and Blome, 2001; Witkowski et al., 2014). The PETM CIE is present in cores 59 and 60, spanning about 512-505 mbsf, and is about 2.5‰ in magnitude (Norris and Rohl 1999; Bains et al. 1999). This period encompassing the PETM in this core has associated age models based on astronomically calibrated cyclostratigraphy

(Norris and Röhl, 1999) and extra-terrestrial ^{3}He (Farley and Eltgroth, 2003).

Briefly, sediments were cleaned using hydrogen peroxide and hydrochloric acid to remove organic matter and carbonate material (Morley et al., 2004). Biogenic silica (BSi) is separated from detrital material by repeated heavy liquid separation using sodium polytungstate (SPT, density 2.1-2.3 g/mL). The light fraction containing BSi was then wet sieved at 53 µm to recover intact radiolarian tests and exclude the majority of fragmented material. The fraction above 53 µm was then freeze-dried and several hundred radiolarian tests per sample were handpicked under a light microscope. The radiolarians picked are well preserved and represent a bulk community (see discussion in Fontorbe et al., in revision).

The separated and handpicked radiolarian tests were dissolved in 0.4 NaOH for a minimum of three days following Hendry et al. (2014), acidified to around pH 2 using HNO_3, and purified chromatographically through a cation exchange resin for silicon isotope ratio analysis (Georg et al., 2006). All reagents were of Suprapur or equivalent grade.

2.2. Silicon isotope analysis

The silicon isotopic composition of the purified Si solutions was determined in two different institutes. During the first session, silicon isotopic compositions were analysed using a Neptune multi-collector inductively coupled plasma mass spectrometer (MC-ICP-MS; Thermo Scientific) at the Pole Spectrometrie Ocean (Ifremer, Brest). Samples and standards solutions were diluted to 2 ppm Si with 1% HNO_3 and introduced to the Neptune through an APEX-HF (ESI). The measured silicon isotope ratios are corrected for internal mass-bias using a Mg internal standard following Cardinal et al. (2003). During the second session, we used a NuPlasma(II) MC-ICP-MS (Nu Instruments Ltd) hosted at the Vegacenter in the Natural History Museum (NRM) in Stockholm, Sweden. The Si solutions were diluted to 1-2.5 ppm using 1% HNO_3, and introduced in wet plasma mode through a glass nebulizer. Instrument settings for both sessions can be found in table 1. Secondary standard analysis on both instruments yields results in good agreement with accepted values (Reynolds et al., 2007) and provide long-term reproducibility of <0.15‰, attesting to the inter-comparability of the two analytical sessions.

Table 1: Instrumental settings, δ^{x}Si 2σ represent the long-term external reproducibility.

Instrument	Neptune	NuPlasma(II)
Plasma mode	dry	wet
Injection line	APEX-HF	glass nebulizer
Resolution	medium	medium
# brackets	2	3
δ^{30}Si 2σ	0.14	0.12
δ^{29}Si 2σ	0.06	0.08

The silicon isotope ratios are expressed relative to a standard (NBS28, NIST RM 8546) as δ^{30}Si, corresponding to an average of several series of bracketed measurements (i.e. blocks of standard-sample-standard):

$$\delta^{x}Si=(R_{sam}/R_{std} - 1) \times 1000 \quad (1)$$

where R_{sam} and R_{std} is the ^{x}Si/^{28}Si ratio of the sample and the standard respectively (after Mg correction, where appropriate). Values fall on the expected mass-dependent kinetic fractionation line (Fig 1), demonstrating the successful removal of polyatomic interferences during measurements.

2.3. Ocean Si cycle box model

A two-box model, developed by De La Rocha and Bickle (2005) and modified by Frings et al. (2016), has been used to investigate the sensitivity of marine silicon isotopes to perturbations to the inputs of Si to the ocean (Fig 2). The model simulates a mass balance between inputs and outputs of Si to the ocean in the euphotic layer and in the rest of the water column.

Briefly, exchange of Si between the surface layer and the bottom layer is achieved by physical upwelling and downwelling, and the sinking and dissolution of BSi. The rate of up/downwelling is calculated to give an ocean mixing timescale of ca. 1000 yrs (De La Rocha and Bickle 2005). BSi is produced in the surface waters following

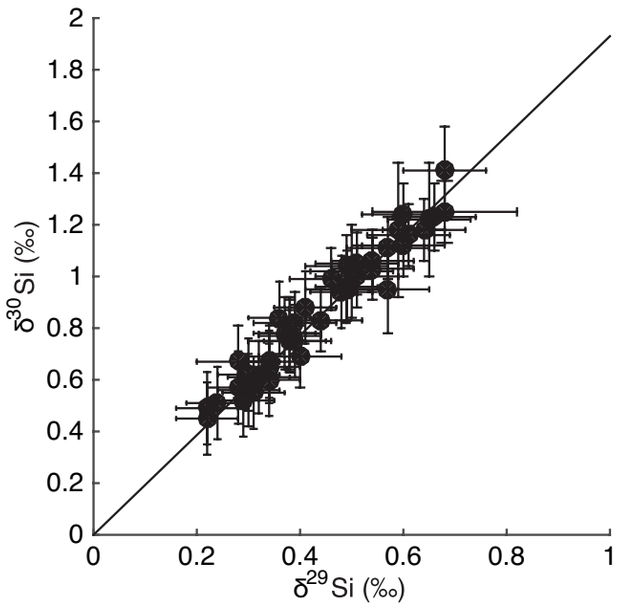

Figure 1: Three-isotope plot of $\delta^{30}Si$ and $\delta^{29}Si$ values of radiolarian tests. The black line represents the expected mass-dependent fractionation ($\delta^{30}Si$ = 1.93 x $\delta^{29}Si$). Vertical and horizontal bars represent external reproducibility (2σ).

Michaelis-Menten kinetics and hence is dependent on DSi concentrations:

$$Prod = (V_{max} \times [DSi])/(K_M + [DSi])$$

where Prod is the annual production of BSi (in mol/y), V_{max} is the maximum rate of BSi production (in mol/y), K_M is half-saturation constant, i.e. the DSi concentration (in mol) at which the production of BSi is half the maximum rate, and [DSi] is the DSi concentration in the surface waters (in mol).

The dissolution rate of BSi is scaled linearly as a function of the degree of DSi undersaturation (Loucaides et al., 2012) and is given as R_{diss} (unitless):

$$R_{diss} = -k \times (1 - [DSi]/[DSi]_{eq})$$

where k is a fitted constant incorporating reactive surface area and intrinsic reactivity, [DSi] is the ambient DSi concentration (in mol) and $[DSi]_{eq}$ is the apparent solubility of BSi in seawater (in mol). The k values are tuned to fit observations of ~3% of BSi production being preserved in marine sediments with about 50% of BSi dissolution taking place in the euphotic layer (De La Rocha and Bickle, 2005; Nelson et al., 1995).

The total dissolution of BSi, $Diss_{surface}$ or $Diss_{deep}$ (in mol), in each box is a function of the residence time of BSi in the given box, R_{diss}, and BSi production:

$$Diss = R_{diss} \times Prod \times D/V$$

where D is the depth of the box (in m) and V is the sinking velocity of particles (in m/y).

The model functions by calculating a mass balance for ^{28}Si and ^{30}Si in each box at each time step *t*:

$$Si_{surface,t+1} = Si_{surface,t} + Upwelling_t - Downwelling_t - Export_t + \Sigma inputs_{surface,t+1}$$

$$Si_{deep,t+1} = Si_{deep,t} - Upwelling_t + Downwelling_t + Diss_{ddep,t} + \Sigma inputs_{deep,t+1}$$

where $\Sigma inputs_{surface}$ is the sum of DSi inputs to the surface layer from rivers, dissolution of suspended particulate matter, dissolution of aeolian dust, and submarine groundwater discharge, while $\Sigma inputs_{deep}$ is the input of DSi to the deep layer via alteration of the oceanic crust, Export is the amount of BSi exported from the surface layer (i.e. Export = Prod - $Diss_{surface}$), and Upwelling and Downwelling are the transfer of DSi between the surface and deep boxes via vertical mixing. The parameters used are given in Table 2.

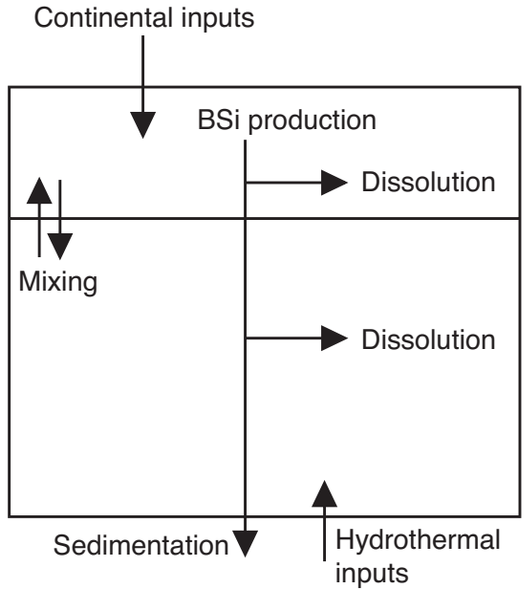

Figure 2: Schematic of the box-model used to investigate the response of marine $\delta^{30}Si$ to changes in Si inputs. From Frings et al. (2016).

Table 2: Fluxes and Si isotopic composition of constant Si inputs and other parameters used in the box model.

Input	Flux (mol/y)	δ^{30}Si (‰)	
SPM	1.9×10^{12}	-0.18	
dust	0.3×10^{12}	-0.65	
groundwater	0.65×10^{12}	0.19	
Parameters	**Value**	**Unit**	**Description**
$^{30}\varepsilon_{BSi\text{-}Dsi}$	-1.1	‰	Fractionation during precipitation of BSi
R_{NBS28}	0.0335320		$^{30}Si/^{28}Si$ ratio in NBS28 standard
V_{max}	500×10^{12}	mol/y	Maximum production rate of BSi
K_M	9×10^{-6}	mol	Half saturation constant
$[DSi]_{eq}$	350×10^{-6}	mol	Apparent solubility
V_{ocean}	1.35×10^{21}	m^3	Total volume of the ocean
$F_{surface}$	0.0263		Fraction of surface ocean
V_{exc}	1.37×10^{18}	m^3/y	Mixing rate between upper and lower boxes
$V_{surface}$	1800	m/y	Sinking velocity in the surface layer
V_{deep}	73000	m/y	Sinking velocity in hte deep layer
K_{surf}	9	mol/y	Dissolution constant in the surface layer (fitted)
K_{deep}	24	mol/y	Dissolution constant in the deep layer (fitted)

3. Results

Using the age-model of Farley and Elgroth (2003), based on the assumption of a constant flux of extra-terrestrial ^{3}He, our 43 radiolarian samples span from ca. -64 to +94 kyrs relative to the onset of the CIE. The silicon isotopic composition of these samples ranges from +0.45 to +1.41‰ (fig 3) and shows a decrease coeval with the decrease of carbon stable isotopes. Prior to the CIE, radiolarian δ^{30}Si values average +1.09‰ (1σ=0.16, n=19). During the onset of the CIE, radiolarian Si isotopic composition decreases by 0.56‰ from 1.10 to 0.54‰ over 18kyrs. We could not recover sufficient radiolarian tests for analysis of δ^{30}Si between 18 and 36kyrs after the onset of the CIE and therefore may not have recovered the full amplitude of the decrease in δ^{30}Si. Combined with the suggestion of a missing sediment section (see discussion) in 1051B, the magnitude and timing of the shift in radiolarian δ^{30}Si must be considered as minimum estimates. From 36 kyrs after the onset of the CIE to the end of the record, radiolarian δ^{30}Si values increase compared to the lowest values during the CIE by about 0.15‰ but do not reach pre-CIE values.

4. Discussion

The radiolarian δ^{30}Si record from ODP site 1051B shows that the marine Si cycle was perturbed during the PETM. This is reflected in the δ^{30}Si record as an excursion towards lower values of about 0.6‰, and occurs simultaneously (within the resolution of our data) with the CIE identified in 1051B by Norris and Röhl (1999) and Bains et al. (1999). The uncertainty about the carbon source, the trigger for its release, and the removal mechanisms has a body of competing hypotheses. We can take these hypotheses and use them to make predictions about the response of the global Si cycle. By comparing these predictions with the δ^{30}Si record we can directly test the hypotheses and provide novel insight into the functioning of the Earth during the PETM.

Amongst the mechanisms proposed to trigger the PETM CIE, one group focuses on the potential for enhanced volcanic activity in the late Paleocene to trigger the release of low δ^{13}C carbon, either directly via contact metamorphism of organic-carbon rich sediments (e.g. Dickens, 2004), or indirectly via climate warming and subsequent destabilisation of deep-sea methane hydrates (e.g.

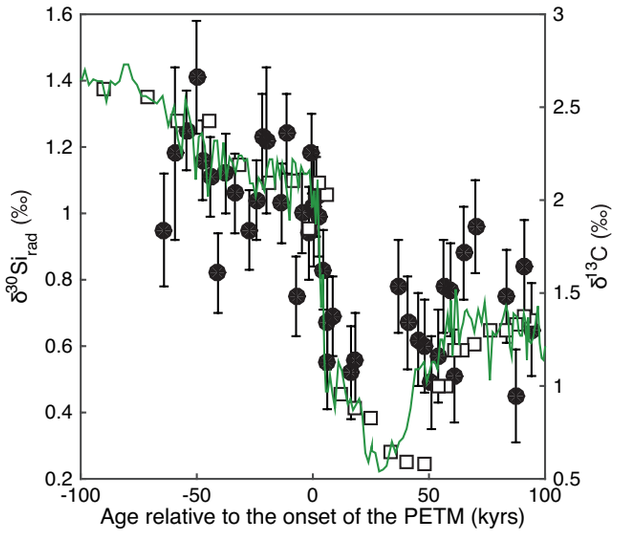

Figure 3: Radiolarian $\delta^{30}Si$ (black circles), low resolution $\delta^{13}C$ (open squares), and high resolution $\delta^{13}C$ (green line) during the PETM. Ages are given relative to the onset of the PETM.

Thomas and Shackleton, 1996). In the modern ocean, DSi that has a magmatic source (i.e. DSi from hydrothermal fluid recirculation) has a very distinct $\delta^{30}Si$ signature (-0.3‰) relative to DSi of continental origin (>1‰). Therefore the scenarios that call for increased volcanic activity would be expected to shift the mean ocean DSi inputs towards lower values. Conversely, the remaining proposed mechanisms (e.g. an orbital threshold, a comet impact) are unlikely to substantially impact the marine Si cycle. The mechanisms that must eventually remove carbon from the exogenic carbon pool make contrasting predictions with regards to their impact on the marine Si cycle. A scenario that focuses on increased marine primary productivity (and therefore organic carbon burial) seems to suggest greater nutrient utilisation, and so may shift seawater DSi towards heavier values. Conversely, enhanced rates of continental silicate weathering could conceivably lower the $\delta^{30}Si$ of river DSi, and thus shift the mean ocean DSi inputs towards lower values. Here, we briefly review arguments for the contribution of volcanism and hydrothermalism to the onset of the PETM, and the consequences of elevated temperature and pCO_2 on the chemical weathering of silicate minerals during the recovery phase. Then, via a simple box model (see section 2.3), we investigate the impact of such mechanisms on the marine $\delta^{30}Si$ over a range of variations in Si input fluxes and $\delta^{30}Si$. The details about the model runs are detailed in the corresponding sections, and summarized in Table 3.

4.1 Extrusive volcanism and hydrothermalism as a trigger of the PETM

Extrusive volcanism during the early stage of the opening of the Greenland-Norwegian Sea has been suggested as a possible trigger of CIE (Schmitz et al., 2004). The release of magmatic CO_2 alone is not a serious contender for explaining the magnitude of the CIE because its $\delta^{13}C$ value is too low (~ -6 to -7‰), so mass balance requires an improbable quantity of carbon to be release over 10kyrs (Dickens et al., 1995). The rate of CO_2 outgassing would represent 25 to 125 times that of estimates of long-term (10kyrs to 1Gyrs) annual discharge (e.g. Leavitt, 1982) and would require over 600 km^3/y of basaltic production, an unprecedented rate in the geological record.

However, outgassing of CO_2 prior to the CIE could have contributed to increasing global temperatures 3 to 6 kyrs before the onset of the PETM, as reconstructed from TEX_{86} (Sluijs et al., 2007) and from benthic foraminifera $\delta^{18}O$ (Littler et al., 2014). Warmer bottom waters could initiate the dissociation of bacterially produced methane hydrates, the stability of which is temperature and pressure dependent (Bralower et al., 1997; Nunes and Norris, 2006; Schmitz et al., 2004; Tripati and Elderfield, 2005). Once initiated, methane hydrate dissociation could then become a self-sustaining process until all sources were depleted. Although absolute ages are difficult to determine, evidence for extrusive volcanism contemporaneous with the PETM is found in the North Atlantic and Arctic region (e.g. Patterson and Francis, 2013; Schmitz et al., 2004).

To test the impact of extrusive volcanism prior to the onset of the CIE on the marine silicon cycle, we used a simple box model (section 2.3) in which we vary the contribution of DSi inputs from magmatic origin to the ocean, and compare the results with radiolarian $\delta^{30}Si$. Radiolarian $\delta^{30}Si$ has been previously used to estimate upper water column

Table 3: Changes of magmatic input fluxes and riverine input $\delta^{30}Si$ used in the different box model runs.

	magmatic input		**riverine input**	
	flux (mol/y)	**δ30Si (‰)**	**flux (mol/y)**	**δ30Si (‰)**
Scenario 1				
pre-CIE	3,000 years prior to the onset, increase by 5-,10-,25-, or 50- fold	-0.30	6.33 x 10^12	1.25
onset of the CIE	0.6 x 10^12	-0.30	6.33 x 10^12	1.25
body of the CIE	0.6 x 10^12	-0.30	6.33 x 10^12	1.25
recovery phase	0.6 x 10^12	-0.30	6.33 x 10^12	1.25
Scenario 2				
pre-CIE	0.6 x 10^12	-0.30	6.33 x 10^12	1.25
onset of the CIE	increase by 5-,10-,25-, or 50- fold	-0.30	6.33 x 10^12	1.25
body of the CIE	0.6 x 10^12	-0.30	6.33 x 10^12	1.25
recovery phase	0.6 x 10^12	-0.30	6.33 x 10^12	1.25
Scenario 3				
pre-CIE	0.6 x 10^12	-0.30	6.33 x 10^12	1.25
onset of the CIE	0.6 x 10^12	-0.30	6.33 x 10^12	linear decrease from 1.25 to 1.25-offset
body of the CIE	0.6 x 10^12	-0.30	6.33 x 10^12	1.25-offset
recovery phase	0.6 x 10^12	-0.30	6.33 x 10^12	linear increase from 1.25-offset to 1.25
Scenario 4				
pre-CIE	0.6 x 10^12	-0.30	6.33 x 10^12	1.25
onset of the CIE	increase by 5-,10-,25-, or 50- fold	-0.30	6.33 x 10^12	linear decrease from 1.25 to 1.25-offset
body of the CIE	0.6 x 10^12	-0.30	6.33 x 10^12	1.25-offset
recovery phase	0.6 x 10^12	-0.30	6.33 x 10^12	linear increase from 1.25-offset to 1.25

DSi $\delta^{30}Si$ (Abelmann et al., 2015; Fontorbe et al., in revision; Hendry et al., 2014). Since we focus on the variation of seawater $\delta^{30}Si$, in all the following model results the radiolarian record is standardised by the mean of the pre-CIE samples (i.e. 1.09‰).

The riverine input is held constant at modern values of 6.33 Tmol/y with a $\delta^{30}Si$ of 1.25‰ (Frings et al., 2016). We prescribe a spike in the input fluxes of DSi from magmatic origin with a constant $\delta^{30}Si$ of -0.30‰ (De La Rocha et al., 2000). DSi fluxes are instantaneously increased by 5-, 10-, 25-, and 50-fold 5 kyrs prior to the onset of the CIE, in line with evidence for pre-PETM warming, and then return to background values of 0.60 Tmol/y (Frings et al., 2016).

The upper water Si isotopic composition responds instantaneously to changes in DSi inputs from magmatic origin and seawater $\delta^{30}Si$ values decrease rapidly (Fig. 4a). Logically, the magnitude of the $\delta^{30}Si$ decrease is related to the magnitude of the increase in DSi fluxes. Seawater $\delta^{30}Si$ decreases by 0.07, 0.15, 0.34, and 0.55‰ for a 5-, 10-, 25-, and 50-fold increase in DSi fluxes for the 5 kyr period, respectively. Variations in seawater DSi $\delta^{30}Si$ resulting from 5- and 10-fold increases would be hard to interpret in sedimentary records, as it falls within measurement precision (here, 0.12 - 0.14‰). A measurable signal would require at least a 25-fold increase of DSi fluxes from magmatic origin. Assuming that degassing fluxes of CO_2 are proportional to the incorporation of magmatic

Si into hydrothermal fluids, this would therefore require a global increase in volcanic CO_2 degassing of 25x. As discussed above, this is improbable.

We argue here, that the influence of extrusive volcanism/hydrothermalism prior to the CIE is either too small to be recorded in radiolarian $\delta^{30}Si$, or had little to no impact on marine Si cycle. Crucially, in this scenario the excursion in $\delta^{30}Si$ should precede the $\delta^{13}C$ excursion.

4.2 Intrusive volcanism and hydrothermalism as a trigger of the PETM

Counter to extrusive volcanism/hydrothermalism, intrusive processes could have had a more direct impact on the onset of the CIE. Several studies have proposed that mantle-derived melts interacting with carbon-rich sediments could have triggered the release of light carbon from the sediment layer (e.g. Storey et al., 2007; Svensen et al., 2004). This is consistent with the development of large-scale hydrothermal complexes in the North Atlantic (e.g. Knox, 1998; Knox, 1996; Schmitz and Pujalte, 2003) and sill intrusions (e.g. Cooper et al., 2007; Storey et al., 2007; Svensen et al., 2010; Svensen et al., 2004).

The rapid intrusion of magmatic fluids (Ledevin et al., 2012) into sediments can easily provide sufficient heat to destabilize gas hydrates and trigger the rapid, if not near-instantaneous, release of methane to the atmosphere. Furthermore, contact metamorphism of carbon-rich sediments generates thermogenic methane (Svensen et al., 2004). Although this is less ^{13}C depleted than methane from gas hydrates (approximately -30‰ vs. -60‰), it is still sufficient to have made a substantial contribution to the CIE. However, the potential impact on the delivery of Si to the ocean is difficult to assess. For intrusive volcanism/hydrothermalism to impact oceanic Si cycling, DSi needs to be released and to diffuse into the water column. Consequently, even with the substantial volume of magmatic rocks comprising the North Atlantic Igneous Province (5-10 x 10^6 km^3; e.g. Eldholm and Grue, 1994; Holbrook et al., 2001; White and McKenzie, 1994), DSi delivery might not increase proportionally.

Here, we test the response of seawater $\delta^{30}Si$ to an increase in DSi from magmatic origin solely from the beginning to the end of the onset of the CIE. Again river inputs of DSi are held constant (6.33 Tmol/y, $\delta^{30}Si$=1.25‰; Frings et al., 2016) while Si input from magmatism increases abruptly at the onset of the PETM by 5-, 10-, 25-, and 50-fold and is maintained over 10 kyrs according to the approximate duration of the onset phase (Zachos et al., 2005). The Si isotopic composition of this Si input is held constant at the value of the bulk silicate earth (≈ -0.30‰)

Similarly to the previous model run (section 4.1), seawater $\delta^{30}Si$ responds instantaneously to changes in Si input from magmatism (Fig 4b). By the end of the 10ka period, seawater $\delta^{30}Si$ decreases by 0.12, 0.23, 0.49, and 0.71‰ for a 5-, 10-, 25-, and 50-fold increase in Si inputs, respectively. The model results from the two largest increases best fit the amplitude and timing of the decrease in radiolarian $\delta^{30}Si$ during the onset of the CIE. Consequently, intrusive magmatism as a trigger of the CIE does not appear to be invalidated by the Si isotope data. However, the recovery phase is not reproduced solely by bringing back the Si inputs of magmatic origin to pre-CIE values. Thus, the recovery phase require additional mechanisms.

4.3 Role of silicate weathering during the recovery phase

During the recovery phase, $\delta^{13}C$ and $\delta^{18}O$ return to their pre-CIE values over ~83 kyrs (Murphy et al., 2010). The recovery phase must have been achieved by long-term carbon sequestration via the removal of atmospheric CO_2 and sequestration of organic and/or inorganic carbon in marine or terrestrial ecosystems. Three mechanisms have been proposed for the drawdown of CO_2 associated with the recovery phase of the PETM: i) increased carbon storage in the terrestrial biosphere (e.g. Beerling, 2000; Bowen and Zachos, 2010)2010, ii) increased marine organic carbon sedimentation (e.g. Bains et al., 2000), and iii) increased weathering of silicate minerals (e.g. Ravizza et al., 2001). Here, we focus on the latter mechanism.

Riverine inputs are by far the largest contributor of DSi to the ocean (Frings et al., 2016; Treguer et al., 1995; Treguer and De La Rocha, 2013), and this DSi derives ultimately from the weathering of silicate minerals. It is thought that the dissolution of silicate minerals is not associated with a Si isotope fractionation, but that the formation of secondary solid phases (mostly clay minerals, but also terrestrial biogenic silica) is. Therefore the Si isotopic composition of river DSi is linked to the weathering congruency (i.e. the degree of completeness of conversion of silicate minerals to solutes). Warmer, wetter catchments tend to display more congruent weathering regimes, as reflected in e.g. their major ion geochemistry. Similarly, because clay minerals preferentially incorporate the lighter Si isotopes, if these begin to be dissolved they will also impact the riverine Si isotopic composition. This is seen today in the lowland regions of the Congo and the Amazon (Cardinal et al. 2010; Hughes et al. 2012). Therefore, higher congruency and greater dissolution of clay minerals are two feasible mechanisms to lower the $\delta^{30}Si$ value of DSi delivered to the surface ocean via rivers. Evidence of enhanced weathering in the North Atlantic and Indian Ocean has been proposed based on Os isotope records (e.g. Ravizza et al., 2001)

We parameterized our box model to investigate the influence of changes in riverine inputs to the ocean. De La Rocha and Bickle (2005), using a similar model, showed that the seawater $\delta^{30}Si$ was insensitive to reasonable changes in riverine DSi fluxes but very sensitive to its $\delta^{30}Si$. Accordingly, we vary solely the $\delta^{30}Si$ values of DSi delivered to the ocean via rivers while keeping the flux constant. We prescribe decreases in the $\delta^{30}Si$ of riverine DSi by 0.10, 0.25, 0.50, and 1.00‰. The timing of these perturbations follows the pattern of $\delta^{13}C$ and $\delta^{18}O$, to account for the dependency of chemical weathering of silicate minerals on climatic conditions. Therefore, in these scenarios, the $\delta^{30}Si$ of riverine DSi decreases linearly during the onset of the CIE over 10kyrs, then is held constant at the lowest value (i.e. initial value - decrease) for the duration of the CIE body (here over 18 kyrs, from 10 to 28 kyrs). During the recovery phase, input $\delta^{30}Si$ increase linearly over 27 kyrs (from 28 to 55 kyrs) before returning to pre-CIE values.

Seawater $\delta^{30}Si$ values decrease gradually by 0.05, 0.13, 0.26, and 0.52‰ with a decrease of riverine $\delta^{30}Si$ input of 0.10, 0.25, 0.50, and 1.00‰ (Fig 4c). The minimum values are attained after ~32 kyrs, shortly after the end of the CIE body. A drop of 1‰ in $\delta^{30}Si$ of riverine DSi best explains the timing of the recovery. Therefore, we assess of the potential contribution of weathering of silicate minerals during the recovery phase of the PETM.

4.4 Combined effect of intrusive magmatism and enhanced weathering

Our model showed that increasing intrusive magmatism by 25- to 50- fold best explains the magnitude of the decrease in radiolarian $\delta^{30}Si$ during the onset of the PETM whereas a decrease is $\delta^{30}Si$ of DSi delivered by rivers best fit the timing of the recovery phase. Lastly, we simulate the combined effect of increased intrusive magmatism and enhanced silicate weathering on the seawater Si isotopic composition. Fluxes of Si from magmatic origin are set to 25- and 50-fold increase according to section 4.2 whereas $\delta^{30}Si$ of riverine DSi inputs are set to a 1‰ decrease according to section 4.3.

The model best explains the radiolarian $\delta^{30}Si$ record when a 25-fold increase in magmatic fluxes is combined with a decrease in river in $\delta^{30}Si$ of 1‰, reproducing both the amplitude during the onset of the PETM and the timing of the recovery phase.

5. Conclusions

In this study, we present the first Si isotope record covering the PETM. The box-model does not account for all the mechanisms proposed to explain the release of ^{13}C depleted carbon during the onset of the CIE, nor the recovery phase of the PETM. However, it provides insights on the conceivable magnitude of changes in volcanism/hydrothermalism and chemical weathering of silicate minerals to explain the shift in radiolarian $\delta^{30}Si$ values coeval with the CIE. We suggest here that high intrusive magmatic activity, releasing thermogenic methane into the exogenic carbon pool during the onset of the PETM, led to increased CO_2 which was

drawn down by enhanced chemical weathering of silicate minerals. We suggest that further studies on Si isotopic composition of siliceous microfossils spanning the PETM should be conducted at various geographical locations and marine settings (coastal and open ocean) to better characterize the response of the Si cycle to hyperthermals.

Acknowledgements

This study was funded by a grant from the Knut and Alice Wallenberg Foundation to DJC. Additional financial support was provided from a grant by the Royal Physiographic Society of Lund to GF. We thank Emmanuel Ponzevera at Ifremer Brest and Melanie Schmitt and Ellen Kooijman at the VegaCenter for their support during analyses.

References

Abelmann, A., Gersonde, R., Knorr, G., Zhang, X., Chapligin, B., Maier, E., Esper, O., Friedrichsen, H., Lohmann, G., Meyer, H., 2015. The seasonal sea-ice zone in the glacial Southern Ocean as a carbon sink. Nature communications 6.

Aziz, H.A., Hilgen, F.J., van Luijk, G.M., Sluijs, A., Kraus, M.J., Pares, J.M., Gingerich, P.D., 2008. Astronomical climate control on paleosol stacking patterns in the upper Paleocene–lower Eocene Willwood Formation, Bighorn Basin, Wyoming. Geology 36, 531-534.

Bains, S., Norris, R.D., Corfield, R.M., Faul, K.L., 2000. Termination of global warmth at the Palaeocene/Eocene boundary through productivity feedback. Nature 407, 171-174.

Beerling, D., 2000. Increased terrestrial carbon storage across the Palaeocene–Eocene boundary. Palaeogeography, Palaeoclimatology, Palaeoecology 161, 395-405.

Bowen, G.J., Zachos, J.C., 2010. Rapid carbon sequestration at the termination of the Palaeocene–Eocene Thermal Maximum. Nature Geoscience 3, 866-869.

Bralower, T., Thomas, D., Zachos, J., Hirschmann, M., Röhl, U., Sigurdsson, H., Thomas, E., Whitney, D., 1997. High-resolution records of the late Paleocene thermal maximum and circum-Caribbean volcanism: Is there a causal link? Geology 25, 963-966.

Cardinal, D., Alleman, L.Y., de Jong, J., Ziegler, K., André, L., 2003. Isotopic composition of silicon measured by multicollector plasma source mass spectrometry in dry plasma mode. Journal of Analytical Atomic Spectrometry 18, 213-218.

Cooper, J.R., Crelling, J.C., Rimmer, S.M., Whittington, A.G., 2007. Coal metamorphism by igneous intrusion in the Raton Basin, CO and NM: implications for generation of volatiles. International Journal of Coal Geology 71, 15-27.

De La Rocha, C.L., Bickle, M.J., 2005. Sensitivity of silicon isotopes to whole-ocean changes in the silica cycle. Marine Geology 217, 267-282.

De La Rocha, C.L., Brzezinski, M.A., DeNiro, M.J., 2000. A first look at the distribution of the stable isotopes of silicon in natural waters. Geochimica et Cosmochimica Acta 64, 2467-2477.

Dickens, G.R., 2004. Global change: Hydrocarbon-driven warming. Nature 429, 513-515.

Dickens, G.R., Castillo, M.M., Walker, J.C.G., 1997. A blast of gas in the latest Paleocene: Simulating first-order effects of massive dissociation of oceanic methane hydrate. Geology 25, 259.

Dickens, G.R., O'Neil, J.R., Rea, D.K., Owen, R.M., 1995. Dissociation of oceanic methane hydrate as a cause of the carbon isotope excursion at the end of the Paleocene. Paleoceanography 10, 965-971.

Dickson, A.J., Cohen, A.S., Coe, A.L., Davies, M., Shcherbinina, E.A., Gavrilov, Y.O., 2015. Evidence for weathering and volcanism during the PETM from Arctic Ocean and Peri-Tethys osmium isotope records. Palaeogeography, Palaeoclimatology, Palaeoecology 438, 300-307.

Eldholm, O., Grue, K., 1994. North Atlantic volcanic margins: dimensions and production rates. Journal of Geophysical Research: Solid Earth 99, 2955-2968.

Farley, K., Eltgroth, S., 2003. An alternative age model for the Paleocene–Eocene thermal maximum using extraterrestrial 3 He. Earth and Planetary Science Letters 208, 135-148.

Fontorbe, G., Frings, P.J., De La Rocha, C.L., Hendry, K.R., Conley, D.J., in revision. A silicon depleted North Atlantic since the Palaeogene: evidence from sponge and radiolarian silicon isotopes. Earth and Planetary Science Letters.

Frings, P.J., Clymans, W., Fontorbe, G., Christina, L., Conley, D.J., 2016. The continental Si cycle and its impact on the ocean Si isotope budget. Chemical Geology 425, 12-36.

Georg, R.B., Reynolds, B.C., Frank, M., Halliday, A.N., 2006. New sample preparation techniques for the determination of Si isotopic compositions using MC-ICPMS. Chemical Geology 235, 95-104.

Hendry, K.R., Robinson, L.F., McManus, J.F., Hays, J.D., 2014. Silicon isotopes indicate enhanced carbon export efficiency in the North Atlantic during deglaciation. Nature communications 5.

Holbrook, W.S., Larsen, H., Korenaga, J., Dahl-Jensen, T., Reid, I.D., Kelemen, P., Hopper, J., Kent, G., Lizarralde, D., Bernstein, S., 2001. Mantle thermal structure and active upwelling during continental breakup in the North Atlantic. Earth and Planetary Science Letters 190, 251-266.

Jaramillo, C., Ochoa, D., Contreras, L., Pagani, M., Carvajal-Ortiz, H., Pratt, L.M., Krishnan, S., Cardona, A., Romero, M., Quiroz, L., Rodriguez, G., Rueda, M.J., de la Parra, F., Moron, S., Green, W., Bayona, G., Montes, C., Quintero, O., Ramirez, R., Mora, G., Schouten, S., Bermudez, H., Navarrete, R., Parra, F., Alvaran, M., Osorno, J., Crowley, J.L., Valencia, V., Vervoort, J., 2010. Effects of rapid global warming at the Paleocene-Eocene boundary on neotropical vegetation. Science 330, 957-961.

Katz, M.E., 1999. The Source and Fate of Massive Carbon Input During the Latest Paleocene Thermal Maximum. Science 286, 1531-1533.

Kennett, J., Stott, L., 1991. Abrupt deep sea warming, paleoceanographic changes and benthic extinctions at the end of the Paleocene.

Kent, D.V., Cramer, B., Lanci, L., Wang, D., Wright, J., Van der Voo, R., 2003. A case for a comet impact trigger for the Paleocene/Eocene thermal maximum and carbon isotope excursion. Earth and Planetary Science Letters 211, 13-26.

Knox, R.B., 1998. The tectonic and volcanic history of the North Atlantic region during the Paleocene–Eocene transition: implications for NW European and global biotic events, Late Paleocene–early Eocene climatic and biotic events in the marine and terrestrial records. Columbia University Press, New York, pp. 91-100.

Knox, R.W.B., 1996. Tectonic controls on sequence development in the Palaeocene and earliest Eocene of southeast England: implications for North Sea stratigraphy. Geological Society, London, Special Publications 103, 209-230.

Koch, P.L., Zachos, J.C., Gingerich, P.D., 1992. Correlation between isotope records in marine and continental carbon reservoirs near the Paleocene Eocene boundary.

Larsen, L.M., Fitton, J.G., Pedersen, A.K., 2003. Paleogene volcanic ash layers in the Danish Basin: compositions and source areas in the North Atlantic Igneous Province. Lithos 71, 47-80.

Leavitt, S.W., 1982. Annual volcanic carbon dioxide emission: an estimate from eruption chronologies. Environmental Geology 4, 15-21.

Ledevin, M., Arndt, N., Cooper, M.R., Earls, G., Lyle, P., Aubourg, C., Lewin, E., 2012. Intrusion history of the Portrush Sill, County Antrim, Northern Ireland: evidence for rapid emplacement and high-temperature contact metamorphism. Geological Magazine 149, 67-79.

Littler, K., Röhl, U., Westerhold, T., Zachos, J.C., 2014. A high-resolution benthic stable-isotope record for the South Atlantic: Implications for orbital-scale changes in Late Paleocene–Early Eocene climate and carbon cycling. Earth and Planetary Science Letters 401, 18-30.

Loucaides, S., Van Cappellen, P., Roubeix, V., Moriceau, B., Ragueneau, O., 2012. Controls on the recycling and preservation of biogenic silica from biomineralization to burial. Silicon 4, 7-22.

Lourens, L.J., Sluijs, A., Kroon, D., Zachos, J.C., Thomas, E., Rohl, U., Bowles, J., Raffi, I., 2005. Astronomical pacing of late Palaeocene to early Eocene global warming events. Nature 435, 1083-1087.

Magioncalda, R., Dupuis, C., Smith, T., Steurbaut, E., Gingerich, P.D., 2004. Paleocene-Eocene carbon isotope excursion in organic carbon and pedogenic carbonate: Direct comparison in a continental stratigraphic section. Geology 32, 553-556.

McInerney, F.A., Wing, S.L., 2011. The Paleocene-Eocene Thermal Maximum: A Perturbation of Carbon Cycle, Climate, and Biosphere with Implications for the Future. Annual Review of Earth and Planetary Sciences 39, 489-516.

Morley, D.W., Leng, M.J., Mackay, A.W., Sloane, H.J., Rioual, P., Battarbee, R.W., 2004. Cleaning of lake sediment samples for diatom oxygen isotope analysis. Journal of Paleolimnology 31, 391-401.

Murphy, B.H., Farley, K.A., Zachos, J.C., 2010. An extraterrestrial 3He-based timescale for the Paleocene–Eocene thermal maximum (PETM) from Walvis Ridge, IODP Site 1266. Geochimica et Cosmochimica Acta 74, 5098-5108.

Nelson, D.M., Tréguer, P., Brzezinski, M.A., Leynaert, A., Quéguiner, B., 1995. Production and dissolution of biogenic silica in the ocean: revised global estimates, comparison with regional data and relationship to biogenic sedimentation. Global Biogeochemical Cycles 9, 359-372.

Norris, R.D., Röhl, U., 1999. Carbon cycling and chronology of climate warming during the Palaeocene/Eocene transition. Nature 401, 775-778.

Nunes, F., Norris, R.D., 2006. Abrupt reversal in ocean overturning during the Palaeocene/Eocene warm period. Nature 439, 60-63.

Patterson, M.V., Francis, D., 2013. Kimberlite eruptions as triggers for early Cenozoic hyperthermals. Geochemistry, Geophysics, Geosystems 14, 448-456.

Ravizza, G., Norris, R.N., Blusztajn, J., Aubry, M.P., 2001. An osmium isotope excursion associated with the Late Paleocene thermal maximum: Evidence of intensified chemical weathering. Paleoceanography 16, 155-163.

Reynolds, B.C., Aggarwal, J., André, L., Baxter, D., Beucher, C., Brzezinski, M.A., Engström, E., Georg, R.B., Land, M., Leng, M.J., 2007. An inter-laboratory comparison of Si isotope reference materials. Journal of Analytical Atomic Spectrometry 22, 561-568.

Röhl, U., Norris, R.D., Ogg, J.G., 2003. Cyclostratigraphy of upper Paleocene and lower Eocene sediments at Blake Nose Site 1051 (western North Atlantic). Geological Society of America Special Papers 369, 567-588.

Röhl, U., Westerhold, T., Bralower, T.J., Zachos, J.C., 2007. On the duration of the Paleocene-Eocene thermal maximum (PETM). Geochemistry, Geophysics, Geosystems 8.

Sanfilippo, A., Blome, C.D., 2001. Biostratigraphic implications of mid-latitude Palaeocene-Eocene radiolarian faunas from Hole 1051A, ODP Leg 171B, Blake Nose, western North Atlantic. Geological Society, London, Special Publications 183, 185-224.

Schmitz, B., Peucker-Ehrenbrink, B., Heilmann-Clausen, C., Åberg, G., Asaro, F., Lee, C.-T.A., 2004. Basaltic explosive volcanism, but no comet impact, at the Paleocene–Eocene boundary: high-resolution chemical and isotopic records from Egypt, Spain and Denmark. Earth and Planetary Science Letters 225, 1-17.

Schmitz, B., Pujalte, V., 2003. Sea-level, humidity, and land-erosion records across the initial Eocene thermal maximum from a continental-marine transect in northern Spain. Geology 31, 689-692.

Sluijs, A., Brinkhuis, H., Schouten, S., Bohaty, S.M., John, C.M., Zachos, J.C., Reichart, G.-J., Damsté, J.S.S., Crouch, E.M., Dickens, G.R., 2007. Environmental precursors to rapid light carbon injection at the Palaeocene/Eocene boundary. Nature 450, 1218-1221.

Storey, M., Duncan, R.A., Swisher, C.C., 2007. Paleocene-Eocene thermal maximum and the opening of the northeast Atlantic. Science 316, 587-589.

Svensen, H., Planke, S., Corfu, F., 2010. Zircon dating ties NE Atlantic sill emplacement to initial Eocene global warming. Journal of the Geological Society 167, 433-436.

Svensen, H., Planke, S., Malthe-Sørenssen, A., Jamtveit, B., Myklebust, R., Eidem, T.R., Rey, S.S., 2004. Release of methane from a volcanic basin as a mechanism for initial Eocene global warming. Nature 429, 542-545.

Thomas, E., Shackleton, N.J., 1996. The Paleocene-Eocene benthic foraminiferal extinction and stable isotope anomalies. Geological Society, London, Special Publications 101, 401-441.

Tipple, B.J., Pagani, M., Krishnan, S., Dirghangi, S.S., Galeotti, S., Agnini, C., Giusberti, L., Rio, D., 2011. Coupled high-resolution marine and terrestrial records of carbon and hydrologic cycles variations during the Paleocene–Eocene Thermal Maximum (PETM). Earth and Planetary Science Letters 311, 82-92.

Treguer, P., Nelson, D.M., Van Bennekom, A.J., DeMaster, D.J., 1995. The silica balance in the world ocean: a reestimate. Science 268, 375.

Treguer, P.J., De La Rocha, C.L., 2013. The world ocean silica cycle. Annual review of marine science 5, 477-501.

Tripati, A., Elderfield, H., 2005. Deep-sea temperature and circulation changes at the Paleocene-Eocene thermal maximum. Science 308, 1894-1898.

White, R., McKenzie, D., 1989. Magmatism at rift zones: the generation of volcanic continental margins and flood basalts. Journal of Geophysical Research: Solid Earth 94, 7685-7729.

Wieczorek, R., Fantle, M.S., Kump, L.R., Ravizza, G., 2013. Geochemical evidence for volcanic activity prior to and enhanced terrestrial weathering during the Paleocene Eocene Thermal Maximum. Geochimica et Cosmochimica Acta 119, 391-410.

Witkowski, J., Bohaty, S.M., Edgar, K.M., Harwood, D.M., 2014. Rapid fluctuations in mid-latitude siliceous plankton production during the Middle Eocene Climatic Optimum (ODP Site 1051, western North Atlantic). Marine Micropaleontology 106, 110-129.

Zachos, J., Pagani, M., Sloan, L., Thomas, E., Billups, K., 2001. Trends, rhythms, and aberrations in global climate 65 Ma to present. Science 292, 686-693.

Zachos, J.C., McCarren, H., Murphy, B., Röhl, U., Westerhold, T., 2010. Tempo and scale of late Paleocene and early Eocene carbon isotope cycles: Implications for the origin of hyperthermals. Earth and Planetary Science Letters 299, 242-249.

Zachos, J.C., Rohl, U., Schellenberg, S.A., Sluijs, A., Hodell, D.A., Kelly, D.C., Thomas, E., Nicolo, M., Raffi, I., Lourens, L.J., McCarren, H., Kroon, D., 2005. Rapid acidification of the ocean during the Paleocene-Eocene thermal maximum. Science 308, 1611-1615.

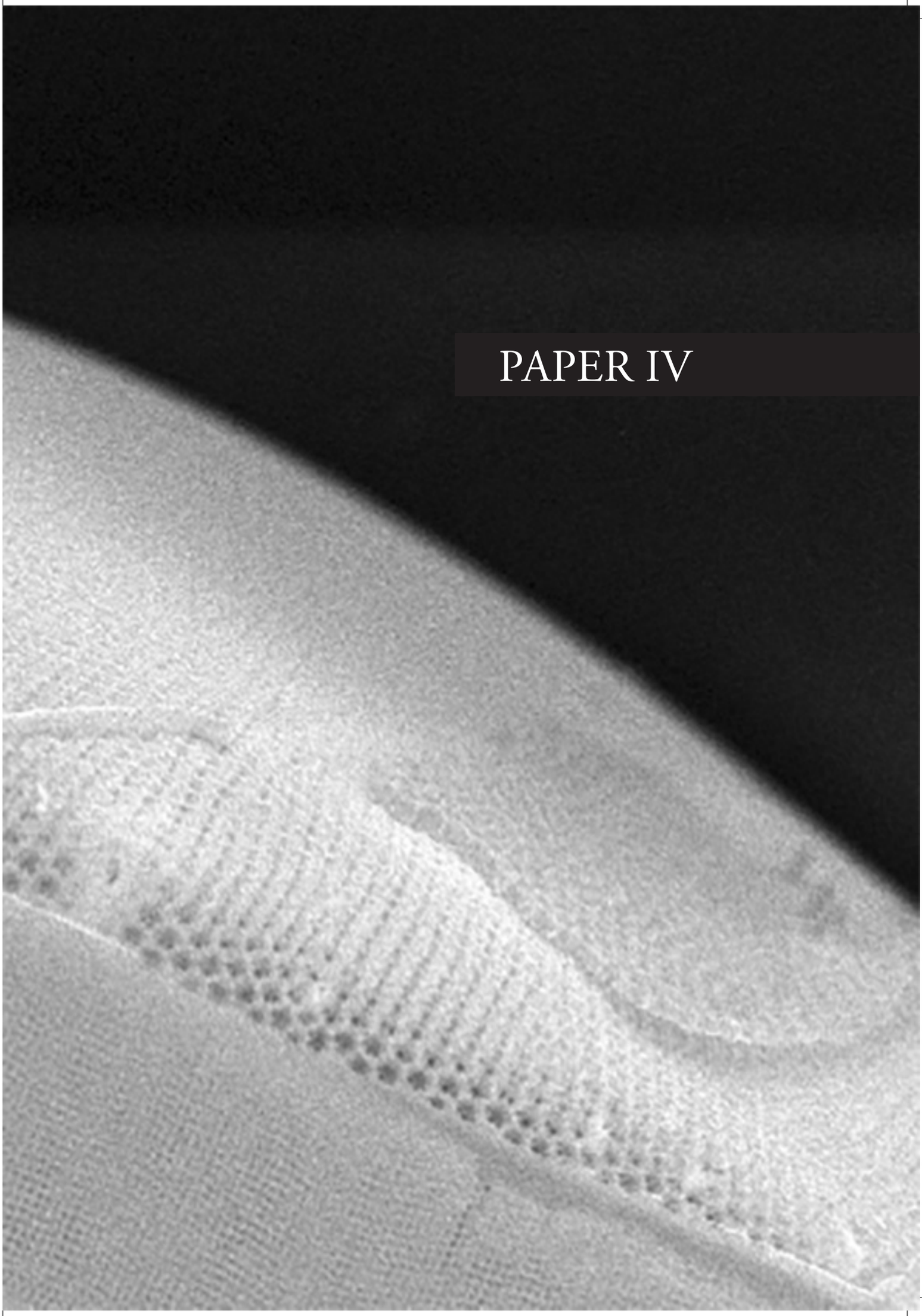
PAPER IV

Photo courtesy of Julia Boutorh

Chemical Geology 425 (2016) 12–36

Contents lists available at ScienceDirect

Chemical Geology

journal homepage: www.elsevier.com/locate/chemgeo

The continental Si cycle and its impact on the ocean Si isotope budget

Patrick J. Frings *, Wim Clymans, Guillaume Fontorbe, Christina L. De La Rocha, Daniel J. Conley

Department of Geology, Lund University, Sweden

ARTICLE INFO

Article history:
Received 16 July 2015
Received in revised form 5 January 2016
Accepted 24 January 2016
Available online 28 January 2016

Keywords:
Global silicon cycle
Biogenic silica
Silicon isotopes
LGM
Palaeoceanography
Biogeochemical cycling

ABSTRACT

The silicon isotope composition of biogenic silica ($\delta^{30}Si_{BSi}$) in the ocean is a function of the $\delta^{30}Si$ of the available dissolved Si (DSi; H_2SiO_4), the degree of utilisation of the available DSi, and, for some organisms, the concentration of DSi. This makes $\delta^{30}Si_{BSi}$ in sediment archives a promising proxy for past DSi concentrations and utilisation. At steady-state, mean $\delta^{30}Si_{BSi}$ must equal a weighted average of the inputs, the majority of which are of continental origin. Variation in the functioning of the continental Si cycle on timescales similar to the residence time of DSi in the ocean (~10 ka) may therefore contribute to downcore variability in $\delta^{30}Si_{BSi}$ on millennial or longer timescales. The direction and magnitude of change in published $\delta^{30}Si_{BSi}$ records over the last few glacial cycles is consistent among ocean basins and between groups of silicifiers. They document glacial values that are typically 0.5 to 1.0‰ lower than interglacial values and together hint at coherent and predictable glacial–interglacial variability in whole-ocean $\delta^{30}Si$ driven by a change in mean $\delta^{30}Si$ of the inputs. In this contribution, we review the modern inputs of DSi to the ocean and the controls on their isotopic composition, and assess the evidence for their variability on millennial-plus timescales.

Today, 9.55×10^{12} mol yr^{-1} DSi enters the ocean, of which roughly 64% and 25% are direct riverine inputs of DSi, and DSi from dissolution of aeolian and riverborne sediment, respectively. The remainder derives from alteration or weathering of the ocean crust. Each input has a characteristic $\delta^{30}Si$, with our current best estimate for a weighted mean being 0.74‰, although much work remains to be done to characterise the individual fluxes. Many aspects of the continental Si cycle may have differed during glacial periods that together can cumulatively substantially lower the mean $\delta^{30}Si$ of DSi entering the ocean. These changes relate to i) a cooler, drier glacial climate, ii) lowered sea level and the exposure of continental shelves, iii) the presence of large continental ice-sheets, and iv) altered vegetation zonation.

Using a simple box-model with a Monte-Carlo approach to parameterisation, we find that a transition from a hypothesised glacial continental Si cycle to the modern Si cycle can drive an increase in whole ocean $\delta^{30}Si$ of comparable rate and magnitude to that recorded in $\delta^{30}Si_{BSi}$. This implies that we may need to revisit our understanding of aspects of the Si cycle in the glacial ocean. Although we focus on the transition from the last glacial, our synthesis suggests that the continental Si cycle should be seen as a potential contributory factor to any variability observed in ocean $\delta^{30}Si_{BSi}$ on millennial or longer timescales.

Contents

* Corresponding author.

http://dx.doi.org/10.1016/j.chemgeo.2016.01.020

1. Introduction

At or near the Earth's surface silicate minerals can be chemically weathered, a process that forms soils, releases solutes and ultimately sustains life. The solutes that are released, including dissolved Si ($Si(OH)_4$; hereafter DSi), enter biogeochemical cycles – the movement of elements through the environment – that end with burial in marine sediments. The global Si cycle is characterised by one relatively discrete sub-cycle on the continents and another in the oceans (Fig. 1). The transfer of Si between the two is essentially unidirectional, so the land-to-ocean Si flux is of interest both as an integrative function of the continental Si cycle and as the chief input for the ocean Si cycle. The purpose of this contribution is (i) to review the fluxes of Si from land to ocean and the mechanisms that determine their magnitude and silicon isotopic composition (δ^{30}Si), (ii) to estimate plausible limits on the magnitude by which these fluxes can vary on millennial or longer timescales, and (iii) to assess the extent to which this variability is propagated to the ocean Si cycle and is visible in palaeoenvironmental archives.

Besides silicon's inherent interest as a major and ubiquitous element, two reasons for studying the Si cycle are commonly put forward. First, the process of chemical weathering of silicate minerals is a key step in the sequestration of atmospheric CO_2 as marine carbonates and hence is a key term in the long-term ('geological') carbon cycle (Walker et al., 1981). The rate of silicate weathering should be related to the concentration of atmospheric CO_2, *via* climatological and biological feedbacks in order to provide the negative feedback necessary to balance the continuous carbon degassing from the solid earth (Berner and Caldeira, 1997). Therefore, understanding the global Si cycle can provide insight to the functioning of Earth's thermostat. Second, DSi is a nutrient for many organisms. For some – notably the diatoms (class: Bacillariophyceae) – it is an essential nutrient. For others, including many vascular plants, DSi provides ecological, physiological or structural benefits (Epstein, 1999; Guntzer et al., 2012; Pilon-Smits et al., 2009). The availability of DSi in aquatic ecosystems controls the amount of siliceous primary productivity (mostly diatoms, which today account for 40% of ocean primary productivity) (Egge and Asknes, 1992). This siliceous production is also a key component of the ocean biological pump, which determines the partitioning of carbon between the deep ocean and the atmosphere on centennial to millennial timescales (De La Rocha, 2006).

This contribution builds on earlier reviews that have explored either the ocean Si budget, but without consideration of a Si isotope perspective (Tréguer et al., 1995; Tréguer and De La Rocha, 2013), or the continental Si isotope cycle (Opfergelt and Delmelle, 2012). It is partly motivated by the proliferation of marine biogenic silica δ^{30}Si records that are conventionally interpreted in terms of palaeonutrient utilisation or water-mass mixing (see Section 2.3). Here, we use our synthesis to advance the hypothesis that these δ^{30}Si records may also reflect changes in the continental Si cycle. This review is structured as follows: first, we provide basic background information on the continental Si cycle (Section 2.1), silicon isotope geochemistry (Section 2.2), and the use and conventional interpretation of downcore fluctuations in δ^{30}Si in marine sediments as a palaeoenvironmental proxy on millennial-plus timescales (Section 2.3). Section 3 summarises the controls on the silicon isotope composition of continental waters. We then report the current state-of-the-art of DSi inputs to the global ocean on a flux-by-flux basis (Section 4), paying close attention to the δ^{30}Si of these

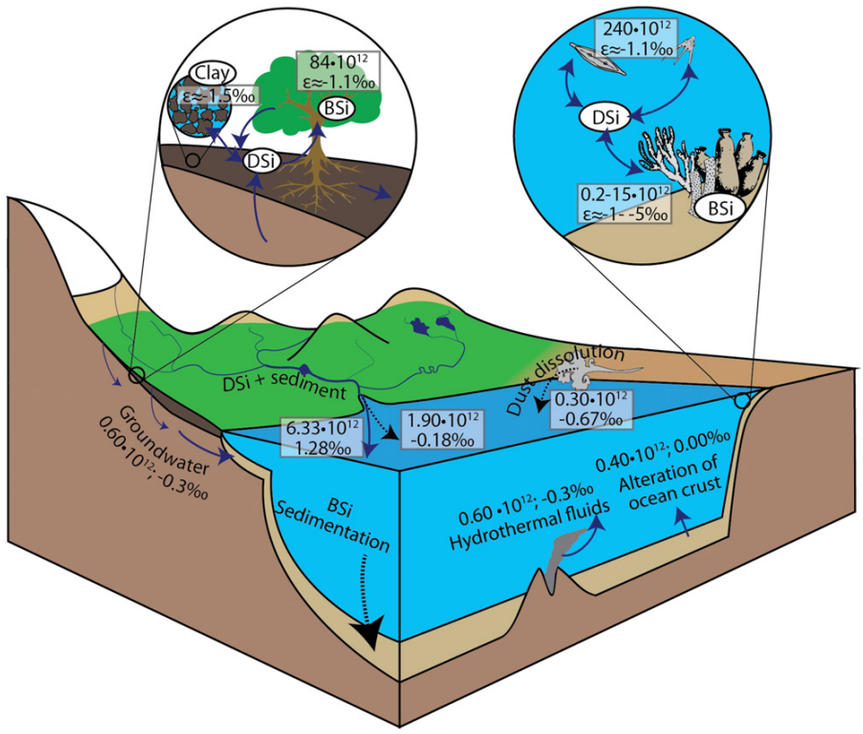

Fig. 1. Cartoon schematic of the modern day global Si cycle. The values show the magnitudes of the fluxes (in 10^{12} mol yr^{-1}) and their associated $\delta^{30}Si$ values (in ‰). Typical fractionations (ε, ‰) associated with production of biogenic silica (BSi) and clay minerals are shown in the inset panels. Dotted lines indicate particulate fluxes; solid lines indicate solute fluxes or transformations. See main text for details.

fluxes. In Section 5, we consider how these fluxes may vary on millennial-plus timescales. Finally, in Section 6, we use a simple box-modelling approach to exploit our synthesis and assess what these variations could mean for the ocean Si cycle, and how this may be recorded in palaeoenvironmental archives.

2. Background

2.1. The continental Si cycle

The key processes in the continental Si cycle are schematised in Fig. 1, and have been reviewed in detail elsewhere (Cornelis et al., 2011). The cycle begins with the release of dissolved silica (DSi) during weathering processes. A fraction may then be transferred directly to the fluvial system, *via* groundwater or soil water flow. A fraction may be incorporated into, or adsorbed onto, secondary phases of variable stability. Finally, a fraction may be utilised by vascular plants that take up DSi and subsequently precipitate it as biogenic silica (BSi) structures termed phytoliths (Carey and Fulweiler, 2012; Massey et al., 2006; Piperno, 2001). Upon litterfall the BSi returns to the soil where it may dissolve, be stored, or be structurally or chemically altered (Barão et al., 2014; Sommer et al., 2006). Ultimately, Si will be lost to the fluvial system as both DSi and eroded particulate Si. BSi, altered BSi and pedogenic silicates can have similar solubilities and reactivities, so the term 'amorphous silica' (ASi) is commonly used instead (Saccone et al., 2007). The net result of continental Si cycling is that in many ecosystems, a soil–plant ASi pool develops that is orders of magnitude larger than the annual release of DSi from primary minerals *via* weathering (Blecker et al., 2006; Clymans et al., 2011; Struyf et al., 2010a). Because of this, it is conceptualised that terrestrial soil–plant systems buffer the release of Si from the continents, at least in some settings (Struyf and Conley, 2012), and that perhaps even a majority of river DSi passes through this buffer before export into the river system (Derry et al., 2005; Struyf et al., 2009). Once in the river system, both biotic and abiotic processes can further modify the Si flux. Lakes and reservoirs provide low-turbidity environments particularly conducive to BSi production by diatoms (Frings et al., 2014a; Lauerwald et al., 2013). In-stream processes and the functioning of floodplains and hyporheic and riparian zones may also be important (Bouwman et al., 2013). Estuaries and deltas constitute a final zone with the capacity to modify river Si fluxes (Milliman and Boyle, 1975; Conley and Malone, 1992; Weiss et al., 2015).

2.2. Low temperature silicon isotope geochemistry

There are three naturally occurring stable isotopes of Si: ^{28}Si, ^{29}Si and ^{30}Si, with atomic masses of 27.97693, 28.97649 and 29.97377 and relative abundances of *ca.* 92.2%, 4.7% and 3.1%, respectively (Ding et al., 2005a). They fractionate during almost all of the low-temperature processes that define the continental and oceanic Si cycles, making them a useful geochemical tracer.

Variations in silicon stable isotope abundances are presented in delta notation as $\delta^{29}Si$ or $\delta^{30}Si$, *i.e.* the deviation in parts per thousand of a given isotope ratio ($^{29}Si/^{28}Si$ or $^{30}Si/^{28}Si$, respectively) from the same ratio in a standard reference material. For Si, this reference material is quartz grains known as NBS28 (RM 8546), and is distributed by the National Institute of Standards (NIST). The isotopic composition ($\delta^{30}Si$, in per mil) of a sample is then:

$$\delta^{x}Si = \left[{}^{R_{sample}}\!/_{R_{standard}} - 1 \right] \times 1000 \quad (1)$$

where R is the ratio of $^{x}Si/^{28}Si$ in the sample and standard, and x is 29 or 30. Differences in Si isotopic composition between two phases can be

caused by isotope fractionation, a process that stems from differences in the masses of the isotopes. Fractionation can result from either kinetic or equilibrium isotope effects and the fractionation of initial (substrate) phase A relative to product phase B is termed the fractionation factor, α:

$$^{x}\alpha_{A-B} = {}^{R_A}/_{R_B}. \quad (2)$$

For Si, α_{A-B} is typically very close to one, and so is also presented in permil as ε:

$$^{x}\varepsilon_{A-B} = 10^3(^{x}\alpha_{A-B}-1). \quad (3)$$

Both kinetic and equilibrium isotope effects stem from mass dependent fractionation, and therefore a plot of δ^{30}Si against δ^{29}Si defines a predictable relationship that is a function of the mass-dependence of the fractionation factors (Young et al., 2002): $^{29}\alpha_{A-B} = (^{30}\alpha_{A-B})^{\beta}$ where β for atomic Si is 0.5092 for kinetic fractionation and 0.5178 for equilibrium fractionation. Generally, kinetic isotope fractionation occurs when the chemical reaction or mass-transfer is unidirectional, and preferentially enriches the product in lighter isotopes. Equilibrium isotope fractionation occurs when chemical reactions are at equilibrium, and tends to partition the heavier isotopes into the phase with a lower energy state. Given the relatively small range of Si isotope fractionations observed at the Earth's surface, the two are essentially indistinguishable at current measurement precision. Deviations from mass-dependency implies mass-independent isotope fractionation, unknown for silicon isotopes during Earth surface processes, so adherence to mass-dependent fractionation is instead more commonly used as an indicator of the successful removal of interferences during measurement.

Some generalisations can be made about the nature of silicon isotope fractionations in the low-temperature environments that characterise the Earth's surface. The tendency is for fractionation associated with the formation of a solid from a solution to favour the incorporation of the lighter isotopes into the new solid, leaving the residual solution enriched in the heavier isotopes (*i.e.* kinetic, not equilibrium isotope fractionations appear to predominate) (De La Rocha et al., 1997, 2000; Opfergelt and Delmelle, 2012; Ziegler et al., 2005a,b). In other words, $\varepsilon_{A-B}<0$ or $\alpha_{A-B}<1$, and is observed in the formation of BSi by diatoms, sponges, radiolarians and plants, and in the formation of secondary minerals (Fig. 2).

Two simple models are commonly used to predict and interpret the evolution of silicon isotope compositions as a function of f_{Si}, the fraction of the available Si in reactant A converted or transferred to product B, with an associated permil enrichment ε_{A-B}. The first model describes the evolution of δ^{30}Si in the reactant and product when a finite-pool of reactant is isolated from fresh sources of Si, and the products do not interact further. In this case, both the residual pool of reactant Si and the pool of produced Si define Rayleigh distillation curves, where the accumulated product, $\delta^{30}Si_B$, is given by:

$$\delta^{30}Si_B = \delta^{30}Si_{A,0} - \left({}^{f_{Si}}/_{1-f_{Si}}\right)\cdot\varepsilon^{30}_{A-B}\cdot\ \ln(f_{Si}) \quad (4)$$

and the residual reactant, $\delta^{30}Si_A$, is given by:

$$\delta^{30}Si_A = \varepsilon^{30}_{A-B}\cdot\ \ln(f_{Si}) \quad (5)$$

where $\delta^{30}Si_{A,0}$ is the isotopic composition of the source Si at time 0 (Mariotti et al., 1981). An alternative model describes the evolution of δ^{30}Si when the production of pool B is at a steady-state with a constant supply of fresh reactant into the system:

$$\delta^{30}Si_B = \delta^{30}Si_{A,0} + \varepsilon^{30}_{A-B}\cdot f_{Si} \quad (6)$$

with the residual reactant Si simply being:

$$\delta^{30}Si_A = \varepsilon^{30}_{A-B}(1-f_{Si}). \quad (7)$$

Eqs. (6) and (7) also apply to a system with a finite pool of Si, in which the reactant and products interact and partition according to f_{Si}. Both models are shown graphically in Fig. 3. The terms 'open' and 'closed' models have been applied to both models, depending on whether the perspective of the reactant or product is taken, and whether the reaction is considered unidirectional or not. For clarity, we refer to the first model (Eqs. (4) and (5)) as a Rayleigh model and the second (Eqs. (6) and (7)) as a steady-state model.

At least 1500 δ^{30}Si determinations, summarised in Fig. 4, have been made on continental material alone, and a similar number on oceanic and extra-terrestrial material. The range of fractionations during low-temperature processes is sufficient to imprint measurable, interpretable and in some cases distinctive δ^{30}Si values on to natural Si bearing phases (Fig. 4). Essentially, this means the stable isotopes of silicon can provide information on Si sources and processes above and beyond that available from simple mass-balance considerations. In this manuscript all

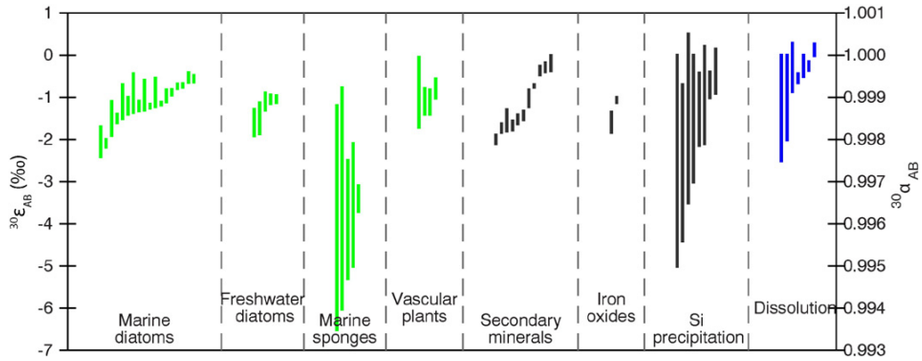

Fig. 2. Summary of published estimates of fractionations associated with the biological or geochemical cycling of Si at the Earth's surface. All fractionations refer to a transformation between a solid phase (product) and a dissolved phase (reactant); the bars represent the range observed in each work. Estimates were obtained from the following sources: *Marine diatoms*: De La Rocha et al. (1997), Sutton et al. (2013), Varela et al. (2004), Cardinal et al. (2005), Reynolds et al. (2006), Beucher et al. (2008), Fripiat et al. (2011), Milligan et al. (2004), De La Rocha et al. (2011), and Egan et al. (2012). *Freshwater (and estuarine) diatoms*: Alleman et al. (2005), Opfergelt et al. (2011), Sun et al. (2013, 2014), and Panizzo et al. (2016). *Marine siliceous sponges*: Hendry and Robinson (2012), Hendry et al. (2010), Wille et al. (2010), and Douthitt (1982). *Vascular plants*: Ding et al. (2005b, 2008), Opfergelt et al. (2006), and Ziegler et al. (2005b). *Secondary minerals*: Ziegler et al. (2005b), Georg et al. (2007a, 2009b), Opfergelt et al. (2010, 2011, 2012), and Basile-Doelsch et al. (2005). *Iron oxides*: Delstanche et al. (2009). (*A*)*Si precipitation*: Geilert et al. (2014, 2015), Oelze et al. (2014, 2015), Roerdink et al. (2015), Ding et al. (2008), Ziegler et al. (2005a), and Li et al. (1995). *Dissolution*: Ziegler et al. (2005a), Frings et al. (2014c), Demarest et al. (2009), Wetzel et al. (2014), and Sun et al. (2014).

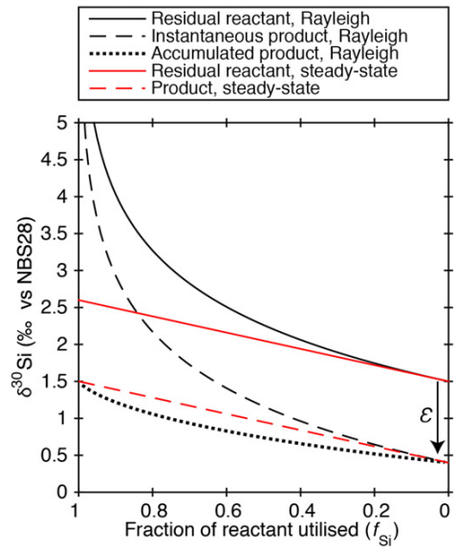

Fig. 3. Schematic showing the evolution of $\delta^{30}Si$ in two fractionation models as Si is converted from one phase to another with an associated fractionation ε. Red lines display the case when there is a steady supply of fresh reactant into the system (with constant $\delta^{30}Si$), *i.e.* the steady-state model. Black lines display the case when there is a finite pool of reactant being converted into a product that has no further interaction, *i.e.* the Rayleigh model. Solid lines indicate the isotopic evolution of the reactant, dashed lines the evolution of the instantaneous product, which is always reactant + ε. The dotted line represents the accumulated (integrated) product of a Rayleigh fractionation model. At $f_{Si} = 1$, all reactant is converted to product, so the product has the composition of the initial solution.

silicon isotope ratios are presented as $\delta^{30}Si$ relative to NBS28, and corrected where necessary from published $\delta^{29}Si$ values assuming a mass-dependency factor of 0.51 (see above). The first measurements were reported relative to the Caltech Rose Quartz Standard (RQS) (*e.g.* Douthitt, 1982), which should produce roughly comparable results since NBS28 and RQS apparently have near-identical Si isotope ratios (Georg et al., 2007b). Early measurements used gas-source mass spectrometers after fluorination of Si to the gaseous SiF_4 (*e.g.* Reynolds and Verhoogen, 1953), but the use of multi-collector inductively-coupled-plasma mass-spectrometry (MC-ICP-MS) is becoming increasingly dominant and can achieve <0.1‰ 2σ external reproducibility (*e.g.* Zambardi and Poitrasson, 2011). The use of a laser-ablation unit attached to a MC-ICP-MS (*e.g.* Steinhoefel et al., 2011) or of secondary ion mass-spectrometry (*e.g.* Basile-Doelsch et al., 2005) are also becoming more prevalent and offer the advantages of in-situ analysis, though they have not reached the precision of solution MC-ICP-MS.

2.3. Silicon isotopes in marine biogenic silica as a palaeoenvironmental proxy

The $\delta^{30}Si$ of biosiliceous remains in marine sediments is being increasingly used as a palaeoceanographic tool (De La Rocha et al., 1998; Hendry et al., 2014). There has been a particular focus on the transition from the last glacial maximum (LGM, *ca.* 21 ka) to the present day and to date, $\delta^{30}Si$ records have been developed from diatoms, sponges or radiolarians from at least 21 cores over the deglacial period (Fig. 5). These records are globally distributed, although more prevalent in the Southern Ocean which plays a large role in the modern day marine silica cycle and where sediments of more than 85 wt.% biogenic silica may be found. They are not straightforward to interpret. The modern day silicon isotope distribution reflects an interplay between biogenic silica production and dissolution, and the physical mixing of the ocean (de Souza et al., 2012, 2014; Reynolds, 2009; Wischmeyer et al., 2003). Together, these combine to produce water masses with relatively distinct DSi concentrations and $\delta^{30}Si$. Deconvolving the effects of one from the other, even when assuming preservational or species-specific biases (vital effects) are negligible (Sutton et al., 2013), becomes tricky.

A conventional interpretation considers changes in $\delta^{30}Si$ of surface-dwelling organisms (diatoms and radiolarians) as reflecting DSi utilisation (De La Rocha et al., 1998; Maier et al., 2013). By considering the pool of DSi from which diatoms and radiolarians precipitate their skeletons as either a finite pool which is not immediately replenished (*i.e.* bloom conditions) or a continuously replenished pool (*i.e.* non-bloom conditions), it is possible to relate the $\delta^{30}Si$ of the product (*i.e.* the BSi) to f_{Si}, the fraction of DSi utilised (Section 2; Fig. 3), assuming $\varepsilon_{DSi-BSi}$ and initial $\delta^{30}Si$ are known. The interpretation is different for siliceous sponges, benthic animals partly comprising the phylum Porifera, that produce skeletons of biogenic silica. The fractionation of silicon isotopes (approximated as the difference between DSi and sponge $\delta^{30}Si$, *i.e.* $\Delta\delta^{30}Si$) by sponges varies as a function of $[DSi]^{-1}$, increasing to an observed maximum magnitude of ${}^{30}\varepsilon_{DSi-BSi} \approx -5‰$ at high (>100 μM) concentrations (Hendry and Robinson, 2012; Wille et al., 2010). Changing $\delta^{30}Si$ of sponge-spicule BSi therefore reflects changes in either ambient DSi concentrations or the isotopic composition of the DSi, or both.

Given that the Si isotope fractionation associated with diatom BSi production is around −1.1‰ (De La Rocha et al., 1997; Sun et al., 2014; Sutton et al., 2013), then large changes in f_{Si} are required to explain the downcore shifts greater than a few tenths of a permil in diatom $\delta^{30}Si$ records, assuming initial $\delta^{30}Si$ remains constant, independent of the model chosen. For example, if the entirety of the change in diatom $\delta^{30}Si$ observed in core MD88-769 (from +1.02‰ to +1.99‰) (Beucher et al., 2007) is attributable to variable palaeoutilisation of DSi, this implies a shift from near-zero DSi usage to near-complete utilisation, assuming a constant diatom fractionation of −1.1‰ (see Fig. 5). These extreme changes strongly suggest other processes must be involved. There is therefore a growing awareness that downcore diatom $\delta^{30}Si$ records can also partly reflect *e.g.* species specific effects (Sutton et al., 2013), water mass mixing or circulation (*e.g.* Beucher et al., 2007) or a whole-ocean change in $\delta^{30}Si$ of DSi (the hypothesis advanced here).

The published marine BSi $\delta^{30}Si$ records, summarised in Fig. 5, show a general increase in $\delta^{30}Si$ from the LGM to the present day superimposed on higher frequency variability. These typically exhibit total variability of 0.5–1.0‰. This pattern of lower glacial $\delta^{30}Si$ to higher interglacial $\delta^{30}Si$ is well recognised and has been documented in the Southern Ocean (De La Rocha et al., 1998; Horn et al., 2011), the eastern equatorial Pacific (Pichevin et al., 2009) and the north Atlantic (Hendry et al., 2014), and has also been shown to be a feature of previous glacial–interglacial cycles (Brzezinski et al., 2002; Ellwood et al., 2010; Griffiths et al., 2013). It also appears to be consistent between benthic and planktic organisms. Given this consistency among ocean-basins, different silicifying organisms, and repeatability across different glacial cycles, coupled with the large changes in DSi utilisation implied (see above), this raises the question to what extent these changes reflect a whole-ocean shift rather than local shifts in palaeoproductivity or nutrient utilisation.

3. What controls $\delta^{30}Si$ of DSi in continental waters?

Many hundreds of individual DSi–$\delta^{30}Si$ determinations from rivers, soil waters, lakes and groundwaters are now available (Fig. 4). This allows a number of results to be generalised:

- River water DSi–$\delta^{30}Si$ is higher than the minerals from which it ultimately derives.
- There is no global relationship between $\delta^{30}Si$ and DSi concentrations (Fig. 6a) (or DSi fluxes where available; Fig. 6b): both positive and negative correlations have been reported from individual systems.
- There is no relationship between $\delta^{30}Si$ and latitude (Fig. 6c).

- Individual sampling stations tend to show seasonal variability of *ca.* 0.5‰ to 1.0‰ with lower values corresponding to high-discharge periods (Fig. 6d).
- River δ^{30}Si tends to increase downstream (Fig. 7).

As a first step, we can probably discount variability inherited directly from the various groups of minerals that collectively constitute 'bedrock.' Although these do exhibit some variability, in particular in shales and other sedimentary rocks (Douthitt, 1982; Savage et al., 2013), they tend to define a limited range of silicon isotope compositions around an upper crustal average of *ca.* −0.25‰ (Fig. 4). Compared to this, the range of values observed in river waters (almost 5‰) is too large to have been imparted from source material variability. We can probably also discount silicon isotope fractionation during the initial solubilisation of Si from the parent material. While a series of dissolution experiments with Hawaiian basalts has demonstrated the preferential initial release of ^{28}Si (Ziegler et al., 2005a), mass-balance dictates that this cannot be maintained indefinitely, and at steady-state progression of weathering into a grain, the ^{30}Si/^{28}Si ratio of Si released must equal that of the grain (Geilert et al., 2015). The complete absence of river DSi of lower δ^{30}Si than bedrock also argues against this. We therefore consider that the range of δ^{30}Si in continental waters predominantly reflects fractionating processes occurring *after* solubilisation from the parent material.

Relatively large Si isotope fractionations are associated with secondary mineral formation, Si adsorption to Fe or Al oxides and biological uptake (summarised in Fig. 2). Note that because both abiotic and biotic processes are associated with similar fractionations, the two are isotopically comparable. For processes in the opposite direction – the dissolution of clay minerals or biogenic silica – the evidence for fractionation is more equivocal (Wetzel et al., 2014) for the reasons discussed above, and has been considered negligible in modelling of isotope behaviour in the weathering zone (Bouchez et al., 2013). Therefore to a first order δ^{30}Si of DSi in continental waters should be a function of i) the degree of net incorporation of solubilised Si into secondary

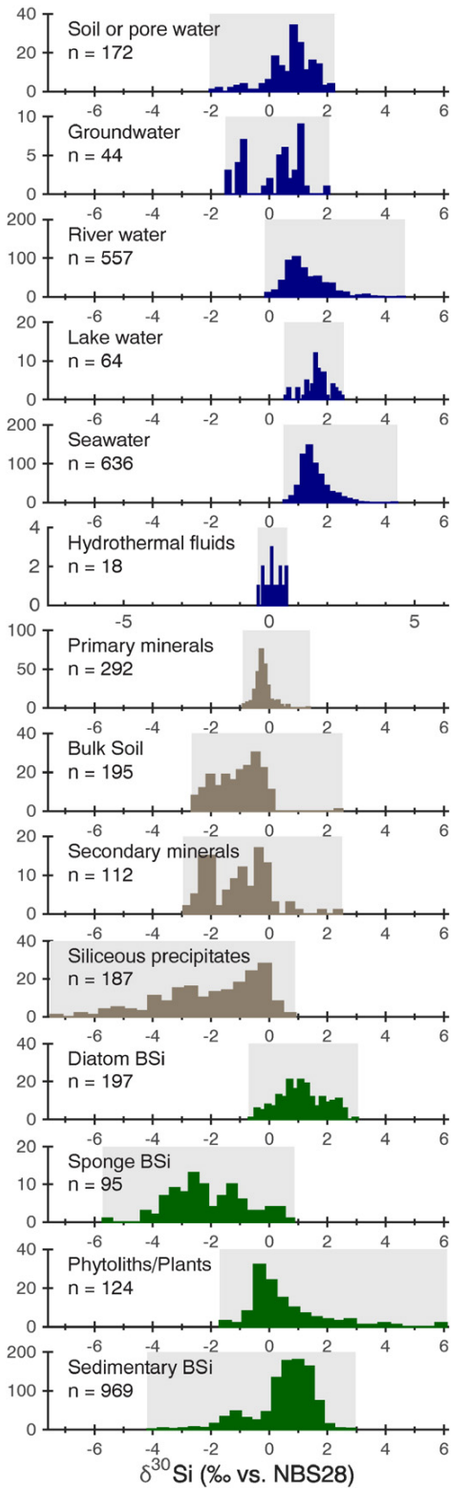

Fig. 4. A compilation of silicon isotope determinations on natural materials. The grey shaded area shows the range of values found in the literature, while the bars show the distribution of these values. Data sources: *Soil and pore waters*: Cornelis et al. (2010), Frings et al. (2014c), Pogge von Strandmann et al. (2012), Pokrovsky et al. (2013), White et al. (2012), Ziegler et al. (2005a,b), and Vandevenne et al. (2015). *Groundwater*: Douthitt (1982), Georg et al. (2009a,b), Opfergelt et al. (2011, 2013), Pokrovsky et al. (2013), Ziegler et al. (2005a,b), and Pogge von Strandmann et al. (2014). *River water*: Alleman et al. (2005), Cardinal et al. (2010), Cockerton et al. (2013), De la Rocha et al. (2000), Delvaux et al. (2013), Ding et al. (2004, 2011), Engström (2009), Engström et al. (2010), Fontorbe et al. (2013), Frings et al. (2014c, 2015), Frings (unpublished data), Georg et al. (2006, 2007a, 2009a), Hughes et al. (2011, 2012, 2013), Opfergelt et al. (2009, 2013), Pokrovsky et al. (2013), Ziegler et al. (2005a,b), and Vandevenne et al. (2015) *Lake water*: Alleman et al. (2005), Opfergelt et al. (2011), and Panizzo et al. (2016). *Seawater*: De La Rocha (unpublished compilation). *Hydrothermal fluids* (*including hot springs*): De La Rocha et al. (2000), Opfergelt et al. (2011, 2013), Douthitt (1982), Geilert et al. (2015), and Ding et al. (1996). *Primary minerals* (*non-exhaustive, includes metamorphic, igneous and sedimentary*): Abraham et al. (2008), Armytage et al. (2011), Basile-Doelsch et al. (2005), Chakrabarti and Jacobsen (2010), Cornelis et al. (2010), Douthitt (1982), Fitoussi and Bourdon (2012), Fitoussi et al. (2009), Frings et al. (2014c), Georg et al. (2007b, 2009b), Opfergelt et al. (2010, 2012), Pokrovsky et al. (2013), Savage et al. (2011, 2013), Steinhoefel et al. (2011), Zambardi et al. (2013), and Ziegler et al. (2005a,b). *Bulk soil*: Bern et al. (2010), Cornelis et al. (2010), Ding et al. (2005b), Opfergelt et al. (2010, 2012), Pogge von Strandmann et al. (2012), Pokrovsky et al. (2013), Steinhoefel et al. (2011), and Ziegler et al. (2005a). *Secondary minerals*: Cornelis et al. (2010, 2014), Ding et al. (1996), Douthitt (1982), Frings et al. (2014c), Georg et al. (2009b), Opfergelt et al. (2010, 2012), Steinhoefel et al. (2011), and Ziegler et al. (2005b). *Siliceous precipitates* (*silcretes, sinters and other precipitates*): Basile-Doelsch et al. (2005), Douthitt (1982), Geilert et al. (2015), and Ding et al. (1996). *Diatom BSi* (*marine and freshwater*): Alleman et al. (2005), Cardinal et al. (2007), De la Rocha et al. (2000), Fripiat et al. (2011), Opfergelt et al. (2011), Panizzo et al. (2016), Varela et al. (2004), and Sun et al. (2013). *Sponge BSi* (*mostly marine*): De La Rocha (2003), Douthitt (1982), Hendry and Robinson (2012), Hughes et al. (2013), and Wille et al. (2010). *Vascular plants/Phyotliths*: Cornelis et al. (2010), Ding et al. (2005b), Douthitt (1982), Engström et al. (2008), Frings et al. (2014c), Hodson et al. (2008), Köster et al. (2009), Opfergelt et al. (2010), Pokrovsky et al. (2013), Steinhoefel et al. (2011), White et al. (2012), and Ziegler et al. (2005b). *Sedimentary BSi*: Cockerton et al. (2015), Douthitt (1982), Frings et al. (2014c), Panizzo et al. (2016), Street-Perrott et al. (2008), Swann et al. (2010), and Sun et al. (2011), plus marine sediments as detailed in Fig. 8.

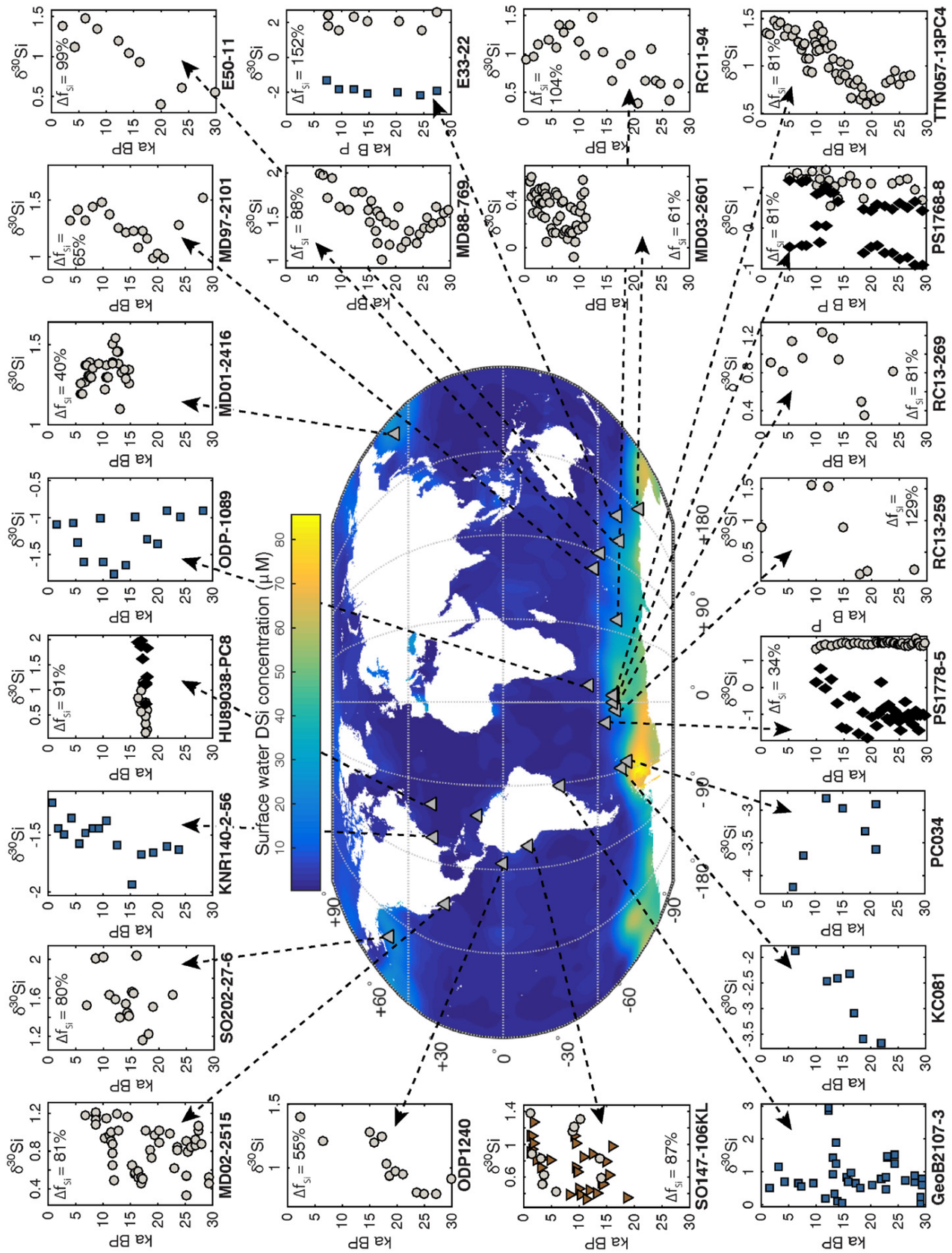
Surface water DSi concentration (µM)
10 20 30 40 50 60 70 80
+90° +60° +30° 0° -30° -60° -90°
-180° -90° 0° +90° +180°
δ30Si
ka BP
E50-11 Δfsi = 99%
E33-22 Δfsi = 152%
RC11-94 Δfsi = 104%
TTN057-13PC4 Δfsi = 81%
MD97-2101 Δfsi = 65%
MD88-769 Δfsi = 88%
MD03-2601 Δfsi = 61%
PS1768-8 Δfsi = 81%
MD01-2416 Δfsi = 40%
RC13-269 Δfsi = 81%
ODP-1089
RC13-259 Δfsi = 129%
HU89038-PC8 Δfsi = 91%
PS1778-5 Δfsi = 34%
KNR140-2-56
PC034
SO202-27-6 Δfsi = 80%
KC081
MD02-2515 Δfsi = 81%
ODP1240 Δfsi = 55%
SO147-106KL Δfsi = 87%
GeoB2107-3

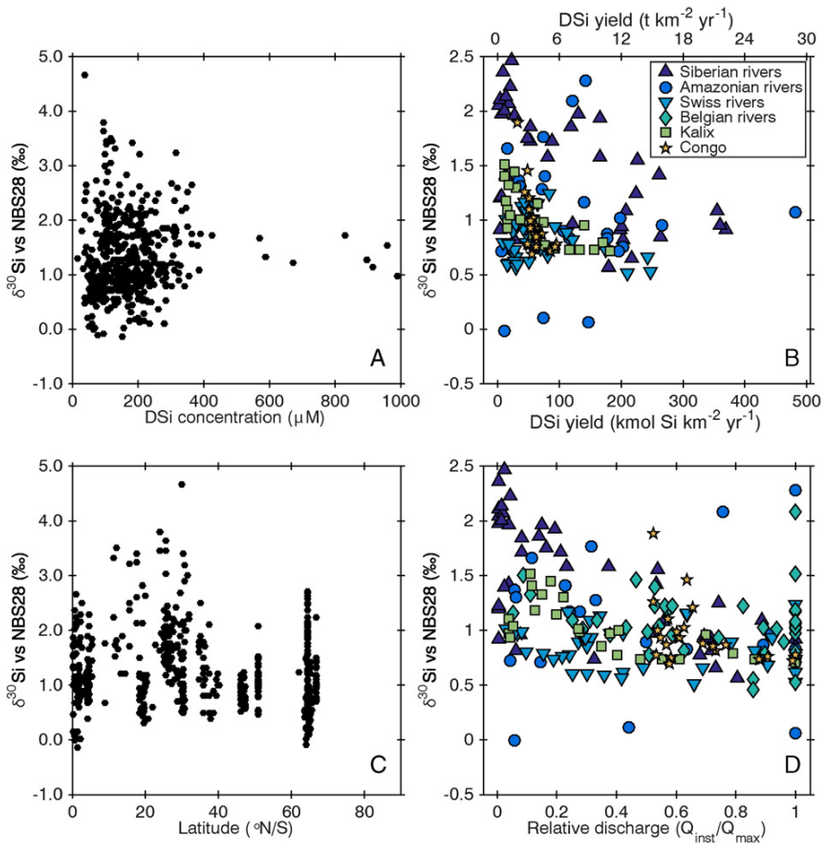

Fig. 6. Variation in δ^{30}Si of river DSi as a function of A: river DSi concentration (μM); B: instantaneous DSi yield (kmol km^{-2} yr^{-1}; the upper axis shows a conversion to t km^{-2} yr^{-1} for convenience); C: latitude (°N or S) and D: Instantaneous discharge (Q_{inst}) normalised to the maximum observed in a given river (Q_{max}).
Data sources as in Fig. 4.

minerals or biogenic silica and ii) the fractionation associated with this (Bouchez et al., 2013). This simple observation explains why all river waters and most soil- and ground-waters are ^{30}Si enriched relative to the DSi released from bedrock: the removal of DSi from solution to these neoformed solid phases preferentially incorporates the lighter ^{28}Si, with permil enrichments ($^{30}\varepsilon_{removal}$) that cluster around −1 to −2‰, though greater fractionations have been reported (Fig. 2).

3.1. Identifying incorporation of Si into secondary phases

Assuming that silicate minerals release Si and other elements stoichiometrically, and if one or more of these elements behaves conservatively in solution, then f_{Si}, the fraction of initially solubilised Si that remains in solution, can be estimated:

$$f_{Si} = {}^{DSi/X_{solution}} \Big/ _{Si/X_{parent}}$$

where $X_{solution}$ and X_{parent} are the concentrations of the normalising element(s) in the dissolved phase and the parent material, respectively. Hughes et al. (2013) used dissolved (Na + K) in the Amazon basin and Georg et al. (2007a) used dissolved Ca in Icelandic rivers. This index reflects weathering *congruency* — an f_{Si} of 1 implies that all Si initially mobilised remains in solution (*i.e.* solute element and isotope ratios identical to that of the parent material), whereas f_{Si} of 0 implies all Si has been removed from solution and incorporated into secondary solids, including biogenic silica. We follow Hughes et al. (2013) and use (Na + K) as normalising elements, with a parent upper crustal Si/(Na + K) molar ratio of 6.7 from Rudnick and Gao (2003), although a value of ~3.5 may be more appropriate, as it discounts the non-reactive quartz component (Hughes et al., 2013). Note that there are several caveats involved in the use of (Na + K) for normalisation, including the assumptions that there are no additional sources other than the silicate bedrock, and that they behave conservatively in solution, which are both commonly invalidated. Additionally, seasonal

Fig. 5. Variation in δ^{30}Si of biogenic silica in marine sediments over the last 30 ka. Data sources as in Fig. 7. Grey circles = diatoms; blue squares = siliceous sponge spicules; black diamonds = radiolarians; brown triangles = bulk biogenic silica. For measurements made on diatom BSi, the required change in utilisation efficiency (Δf_{Si}) is calculated for a case with constant initial δ^{30}Si of DSi, assuming a diatom fractionation of −1.1‰ and a steady-state isotope evolution model. Central map shows the location of marine sediment cores (red dots) referred to in this manuscript, previously studied for variation in δ^{30}Si of biogenic opal in the late Quaternary. Background is the world ocean surface water DSi concentration from Gouretski and Koltermann (2004). Data sources: *Core E50-11*: De La Rocha et al. (1998); *Core GeoB2107–3*: Hendry et al. (2012); *Core HU89038-PC8*: Hendry et al. (2014); *Core KC081*: Hendry et al. (2010); *Core KNR140-2-56GGC*: Hendry et al. (2010); *Core MD01-2416*: Maier et al. (2013); *Core MD01-2515*: Pichevin et al. (2012); *Core MD03-2601*: Panizzo et al. (2014); *Core MD88-769*: Beucher et al. (2007); *Core MD97-2101*: Beucher et al. (2007); *Core MD99-2198*: Griffiths et al. (2013); *Core ODP1240*: Pichevin et al. (2009); *Core ODP1089*: Ellwood et al. (2010); *Core PC034*: Hendry et al. (2010); *Cores PS1778-5 and PS1768-8*: Abelmann et al., 2015; *Core RC11-94*: De La Rocha et al. (1998); *Core RC13-259*: Brzezinski et al. (2002); *Core RC13-269*: De La Rocha et al. (1998); *Core SO147-106KL*: Ehlert et al. (2013); *Core SO202-27-6*: Maier et al. (2016); *Core TTN057-13PC4*: Horn et al. (2011); and *Core E33-22*: Ellwood et al. (2010) and Sutton (2011).

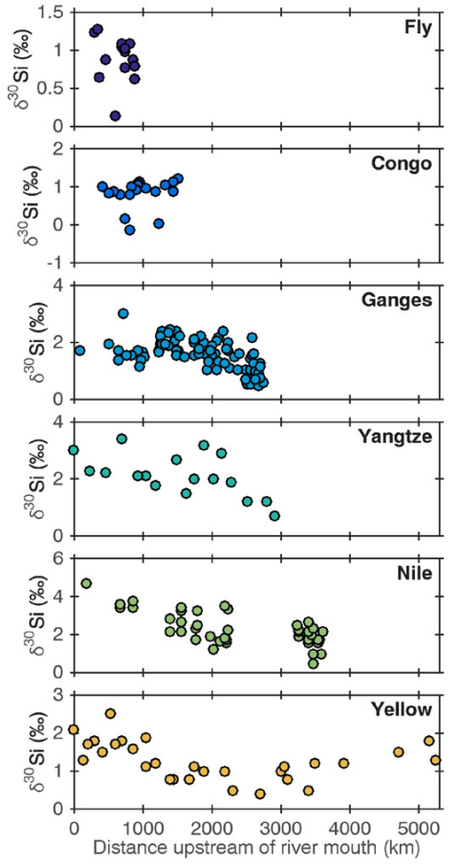

Fig. 7. Longitudinal change in river DSi δ^{30}Si. Fly: Frings (unpublished data); Congo: Cardinal et al. (2010); Ganges: Frings et al. (2015) and Fontorbe et al. (2013); Yangtze: Ding et al. (2011); Nile: Cockerton et al. (2013); Yellow: Ding et al. (2004).

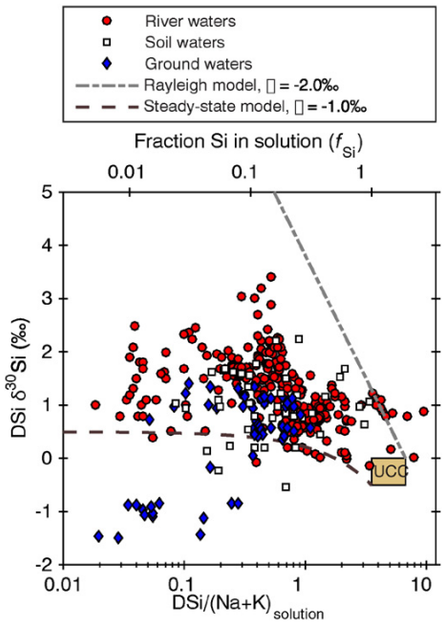

Fig. 8. Range of δ^{30}Si seen in DSi from rivers, porewaters and groundwaters as a function of DSi/(Na + K), a proxy for weathering congruency. The brown box shows an approximate endmember composition of the upper continental crust (UCC) (Rudnick and Gao, 2003; Savage et al., 2013), while the dashed lines show the expected evolution of δ^{30}Si expected as DSi is removed under two simple model scenarios: i) a finite-pool model which produces a Rayleigh distillation curve (*i.e.* a straight line in log-linear space) or ii) an open system (curved line in log-linear space), equivalent to the 'batch reactor' model of Bouchez et al. (2013). These two endmember models provide an envelope of permissible variability for any given system which will likely display behaviour intermediate between the two. The upper x-axis shows a conversion of DSi/(Na + K) to f_{Si}, the fraction of DSi remaining in solution, assuming a starting DSi/(Na + K) of 3.53 after Hughes et al. (2013).
Data sources as in Fig. 4, with additional geochemistry data from Bagard et al. (2011), White et al. (2009), Dowling et al. (2003) and Pogge von Strandmann et al. (2006, 2008) where necessary. Data were corrected for rainwater solute inputs only if available in the original publication.

biological activity can affect DSi concentrations (Conley, 1997; Fulweiler and Nixon, 2005), so the sampling needs to be time-averaged (or at least representative) — a condition rarely met. Finally, the use of a universal $Si/(Na + K)_{parent}$ for all rivers is questionable due to variability in primary mineral cation content.

Despite these caveats, it serves as a starting point for discussion. As plotted in Fig. 8, δ^{30}Si of continental water DSi trends towards higher values as it is progressively removed from solution (*i.e.* moving from right to left). Almost all river waters are accommodated within the envelope defined by the Rayleigh and steady-state fractionation models with molar $Si/(Na + K)_{parent}$ ratios of 3.5 or 6.7, and fractionations of −1‰ and −2‰, respectively. This normalisation procedure suggests that somewhere between 50% and >95% of the Si that is mobilised from parent material is reincorporated into secondary phases (upper x-axis), and that this is a first order control on the variability of silicon isotope ratios in river waters. But beyond this rather crude picture, many questions about the distribution of δ^{30}Si in continental waters remain. Why are soil and ground waters sometimes more negative than the parent material? What causes the large scatter in the evolution of δ^{30}Si as a function of f_{Si}?

In the following we briefly discuss three complicating factors: i) the potential for heterogeneous source material, ii) the potential for variable fractionation factors and iii) mass-balance constraints on the manifestation of isotopic fractionation.

3.1.1. Heterogeneous source material

The above discussion assumed that the parent material is relatively homogenous with regards to its silicon isotope composition. To explain the low (<0‰) values, it may be that the assumption of negligible variation in parent δ^{30}Si is invalid. This is the explanation favoured for low δ^{30}Si (−1.50–1.54‰) groundwater in Arizona (Georg et al., 2009b), the Ganges–Brahmaputra Delta (Georg et al., 2009a) and the Australian Great Artesian Basin (Pogge von Strandmann et al., 2014), where dissolution of (low δ^{30}Si) clay minerals is invoked as a source of low δ^{30}Si DSi.

3.1.2. Variable fractionation factors

Laboratory studies have demonstrated a reaction-rate and temperature dependency of silicon isotope fractionation, as well as a dependency on ambient dissolved Al concentrations (Geilert et al., 2014; Oelze et al., 2014, 2015; Roerdink et al., 2015). They have also demonstrated that instantaneous fractionations between solute and solid can be interpreted within the framework proposed by DePaolo (2011). This framework relates the net isotope fractionation to the ratio of forward and backward reaction rates (R_f and R_b respectively, representing mineral neoformation and (re)dissolution of the solid). These two reactions are associated with kinetic isotope fractionation factors (α_f and α_b), which are normally <1, so both favour the transfer of the light isotope.

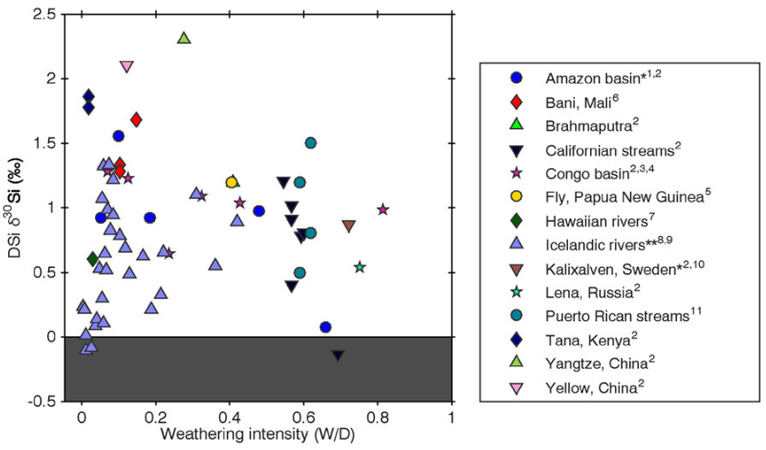

Fig. 9. Variation of δ^{30}Si of river DSi as a function of weathering intensity, as defined by Bouchez et al. (2014), where W refers to the rate of chemical weathering and D to the total (chemical plus physical) denudation rate. At both low and high weathering intensities, there is little silicon isotope fractionation since either close to 0% or close to 100% of Si is exported as solutes, respectively. The grey shaded region indicates the approximate isotopic composition of source material (*i.e. ca.* −0.25‰). *δ^{30}Si as weighted average of annually measured values; all other values are spot samples. **Chemical and physical erosion rates assumed to be captured by instantaneous total dissolved solids (TDS) and total suspended solid (TSS) data, respectively. *δ^{30}Si data sources*: *Amazon*: Hughes et al. (2013); *Brahmaputra*: Georg et al. (2009a) *Californian streams*: De La Rocha et al. (2000); *Congo basin*: Cardinal et al. (2010) and Hughes et al. (2011); *Fly River*: A. Kurtz (unpublished data); *Ganges basin*: Frings et al. (2015); *Hawaiian Rivers*: Ziegler et al. (2005a); *Icelandic rivers*: Opfergelt et al. (2013) and Georg et al. (2007a); *Kalixälven*: Engström et al. (2010); *Lena River*: Engström (2009); *Puerto Rican streams*: Ziegler et al. (2005b); *Tana River*: Hughes et al. (2012); *Yangtze*: Ding et al. (2004); *Yellow*: Ding et al. (2011). Superscripts refer to source of physical and/or chemical denudation rate data: 1: Gaillardet et al. (1997); 2: Milliman and Farnsworth (2011); 3: Dupré et al. (1996); 4: Laraque et al. (2009); 5: A. Kurtz (unpublished data); 6: Picouet et al. (2002); 7: Li (1988); 8: Vigier et al. (2006); 9: Opfergelt et al. (2013); 10: Land et al. (1999); 11: Riebe et al. (2003).

The net reaction rate, R_p is simply $R_f - R_b$, while the apparent fractionation factor, α_p is a function of the two fractionation factors and the ratio of the two reaction rates (see discussion in Oelze et al., 2014). At far-from-equilibrium conditions when $R_p \gg R_b$, the instantaneous $\alpha_p \approx \alpha_f$. Conversely, when R_p is small relative to R_b the reaction is at, or close to, isotopic equilibrium and α_p is equivalent to an equilibrium isotope fractionation factor, α_{eq}.

The magnitude of the equilibrium fractionation factor, α_{eq} between DSi and solid has been experimentally determined at −0.30‰ for Si adsorption onto Al-hydroxides (Oelze et al., 2014) and ~0‰ for amorphous silica precipitation (Roerdink et al., 2015). In the same experiments, the initial (kinetic) silicon isotope fractionations between solution and solid was determined at −1.8 to −3.0‰ (Oelze et al., 2014) and −0.7 to −3.5‰ (Roerdink et al., 2015), demonstrating that for any given process the associated fractionation cannot be assumed constant.

Interestingly, given the long formation times for secondary minerals, and the fact that many river waters are apparently at or close to chemical equilibrium (a prerequisite for isotopic equilibrium), then it might be expected that equilibrium isotope effects (with fractionations close to 0‰) should dominate (Dupuis et al., 2015). The consistently low δ^{30}Si of secondary minerals (Fig. 4) suggests this is not the case. Oelze et al. (2014) resolve this by proposing that the fractionation occurs during the initial Si absorption on Al-hydroxides, that are subsequently converted with no fractionation (no stoichiometric change) to more stable clay minerals *via* hydroxy-aluminosilicate intermediates. Alternatively, the surfaces of the neoformed solids may be at isotopic equilibrium with the surrounding fluids, while the bulk of the solid is protected.

3.1.3. The manifestation of isotopic fractionation

While the two isotope fractionation models in Fig. 6 adequately define the limits of allowable variation in δ^{30}Si of river DSi, no model provides a good fit to the global data. This may result from rivers inherently following either a Rayleigh or a steady-state isotope evolution, the explanation favoured by Hughes et al. (2013) for rivers of the Amazon basin and Georg et al. (2007a) for Icelandic streams. However, there is no reason to expect a given river – which integrates a suite of upstream processes – to correspond to one model. Strictly, the Rayleigh and steady-state models are applicable only to simple scenarios that may rarely be found in nature; the most likely case is an intermediate scenario.

Some rivers do seem to experience isotopic evolution approaching Rayleigh behaviour. The highest river δ^{30}Si values yet observed originate from rivers that flow though dry lowland regions, often with extensive irrigation systems (Cockerton et al., 2013; Ding et al., 2011). In these cases, evapotranspiration water losses can increase DSi concentrations, thereby a) reducing solubilisation of fresh DSi and b) promoting the precipitation and/or preservation of secondary phases, with associated kinetic isotope effects leaving the residual water ^{30}Si enriched. In other words, these systems approximate Rayleigh-type behaviour in that they are isolated from fresh inputs of DSi, while DSi is progressively removed.

Conversely, some rivers have very little isotopic fractionation between parent material and DSi, *i.e.* highly congruent weathering. As shown in Fig. 9, the lowest riverine δ^{30}Si values occur at either end of a weathering *intensity* spectrum, defined as the ratio of chemical erosion, W, to total denudation, D; where $D = W +$ physical erosion, E (Bouchez et al., 2014). At the high-intensity end (W/D near 1), these correspond to black-water rivers in tropical environments with soils that are almost completely desilicified (Cardinal et al., 2010; Hughes et al., 2013). At the low intensity end (W/D near 0), this corresponds to rivers that drain catchments with high physical erosion rates and low sediment residence times (Georg et al., 2006, 2007a). This implies the presence of a degree of equifinality to river δ^{30}Si which is a direct consequence of mass balance. In other words, there can be no observable fractionation if no secondary phases are formed (as in low intensity systems), or if all secondary phases are also re-solubilised (as in high intensity systems). In this way, we can see that a riverine δ^{30}Si value depends not just on the magnitude of the fractionation factor, but also whether the weathering regime permits it. This is broadly consistent with the steady-state isotope mass-balance model presented by Bouchez et al. (2013). This treats the weathering zone as a batch reactor in which the degree of isotopic fractionation observed in waters depends on the ratio of export of fractionated solid (*i.e.* clay or plant residue) to the production of solute from primary minerals.

Table 1
Summary of the modern day inputs of DSi to the global ocean, together with estimates of their Si isotope composition. Previous budgets (mass only) are shown for comparison. TDLR = Tréguer and De La Rocha (2013); T95 = Tréguer et al. (1995); WM83 = Wollast and Mackenzie (1983).

	This compilation					Previous budgets		
	DSi		δ^{30}Si			TDLR	T95	WM83
Flux	$\times 10^{12}$ mol yr^{-1}	±	‰	±‰ (1 sd)	Level of understanding	$\times 10^{12}$ mol yr^{-1}		
River DSi	6.33	0.36	1.25	0.68	OK	6.2 ± 1.8	5.6 ± 0.6	7.25
Estuarine removal	−0.63		+0.10		Poor	−1.5 ± 0.5	−0.6 ± *0.5*	
Dissolution of SPM	1.90	1.00	−0.18	0.25	Poor	1.1 ± 0.2	–	–
Groundwater DSi	0.65	0.54	0.19	0.86	Poor	0.6 ± 0.6	–	–
Dissolution of dust	0.30	0.20	−0.65	0.43	Poor	0.5 ± 0.5	0.5 ± 0.5	–
Hydrothermal fluids	0.60	0.40	−0.30	0.15	Poor	0.6 ± 0.4	0.2 ± 0.1	0.89
Low temperature alteration of oceanic crust	0.40	0.30	0.00	0.5	Poor	1.9 ± 0.7	0.4 ± 0.3	0.36
	9.55	1.31	0.74	0.17		9.4	6.1	8.5

For the majority of rivers that fall between these two weathering regime extremes, the manifestation of silicon isotope fractionation may be dependent on the kinetics of secondary phase formation. In other words, the longer fluids spend in the weathering zone, the longer secondary phases have to precipitate. At greater mean water residence times, clay mineral formation is increased, pushing δ^{30}Si higher. This interpretation is corroborated by δ^{30}Si changes along river longitudinal transects (Cardinal et al., 2010; Cockerton et al., 2013; Ding et al., 2004, 2011; Fontorbe et al., 2013; Hughes et al., 2012; Frings et al., 2015; Fig. 7). These studies show that there is a consistent tendency for δ^{30}Si to increase downstream, presumably as water and sediment residence times increase in the lowland portions of catchments. The greater interaction times implied should increase the degree of secondary mineral neoformation as the limits to clay precipitation (and therefore Si isotope fractionation) are overcome. A similar argument can be made based on the coincidence of the periods of lowest discharge (longest residence times) and highest δ^{30}Si values for annually monitored rivers (Delvaux et al., 2013; Engström et al., 2010; Georg et al., 2006; Hughes et al., 2011, 2013; Pokrovsky et al., 2013; Fig. 5d).

3.2. Outlook: understanding and interpreting δ^{30}Si of DSi in continental waters

Taken altogether, these observations pose problems for modelling and interpreting δ^{30}Si at the Earth surface because interpretation of δ^{30}Si values ultimately depends on an estimate of the fractionation between solution and solid. Yet the magnitude (and perhaps even the sign) of fractionation varies as a function of reaction rate, and the degree to which the fractionation is able to be manifest depends on the completeness of the reaction or transformation. This implies that Si dynamics within individual systems should be rigorously understood before interpretations are made based on silicon isotope ratios. Note also that removal of DSi to biotic (diatoms, vascular plants) or abiotic (clays, Fe-oxides) phases cannot be inferred based on δ^{30}Si of the residual DSi alone.

4. Present-day inputs of DSi to the global ocean

The most important sources of DSi to the global ocean are supplied by the continental fluvial system. Chiefly, these are (i) DSi in rivers and (ii) groundwaters, and (iii) the dissolution of river particulate matter. DSi deriving from these sources must first pass through many fluvial 'filters', including wetlands, lakes, floodplains, estuaries and the coastal zone before reaching the open ocean. Other inputs include (i) the dissolution of aeolian dust and (ii) seafloor weathering and hydrothermal fluid circulation. In this section, the state-of-the-art regarding knowledge of the magnitude and isotopic compositions of the inputs to the ocean are presented (summarised in Table 1). We explore the derivation of each term in the budget and highlight associated uncertainties and knowledge gaps.

4.1. River DSi flux

4.1.1. Magnitude of river DSi flux

The modern river DSi flux is reasonably well constrained. DSi is easily measurable and has limited speciation over the pH range of meteoric waters (Iler, 1979). Global estimates of river DSi fluxes span almost a century (Beusen et al., 2009; Clarke, 1924; Dürr et al., 2011b; Livingstone, 1963) and are surprisingly consistent despite differences in data availability and upscaling procedures. Average river water DSi concentrations are *ca.* 160 μM (9.5 mg l^{-1} SiO_2) (Dürr et al., 2011b). A nutrient export model using a stepwise multiple linear regression approach and developed at the watershed scale (NEWS-DSi) (Beusen et al., 2009) predicts DSi fluxes of 6.33×10^{12} mol yr^{-1} to the coastal ocean, with 2.5–97.5 percentile values at 5.66 and 7.11×10^{12} mol yr^{-1}, respectively. A similar approach (Dürr et al., 2011b) uses essentially the same data but extrapolates at the scale of pre-defined coastal segments to arrive at a similar estimate (6.18×10^{12} mol yr^{-1}), lending further confidence to the NEWS-DSi model, whose output we retain as the best estimate of river DSi fluxes.

4.1.2. δ^{30}Si of river DSi flux

To date, at least 557 δ^{30}Si determinations exist for river water DSi (Fig. 4). These span from −0.14‰ to 4.66‰ with a mean of 1.28‰ (n = 544) and follow a roughly normal distribution (Fig. 4) with a standard deviation of 0.68‰. It is worth noting that seasonal and longitudinal variability in river DSi δ^{30}Si is typically large, on the order of 1.0‰. As noted above δ^{30}Si generally (i) decreases with increasing discharge and (ii) increases with distance downstream. In the absence of many rivers sampled over an annual period near their mouths, we retain the simple mean of 1.28 ± 0.68‰.

4.1.3. The role of estuaries in modulating river Si fluxes

The estimates of sediment and DSi delivery *via* rivers to the ocean are based on sampling of the river freshwater endmember, often a considerable distance upstream of its entrance to the ocean. It is acknowledged that storage of sediment fluxes between gauging stations and the end of the freshwater endmember may perhaps cause global sediment delivery to be overestimated (Allison et al., 1998; Milliman and Farnsworth, 2011). A similar problem exists with DSi as the river passes through the salinity gradient and across a continental shelf to reach the open ocean. Estuarine and other coastal environments are often highly productive, owing to their proximity to continentally sourced nutrients. If this production removes Si and permanently stores it in estuarine or deltaic sediments, then the amount of DSi entering the global ocean will correspondingly decrease. Removal of DSi will be manifest

as non-conservative mixing between the freshwater and saline endmembers (Bien et al., 1958), and can occur biologically (Conley and Malone, 1992) and abiotically (Chou and Wollast, 2006). Diatom blooms in the mixing zone may consume up to 50% of riverine DSi in the Amazon River (DeMaster, 2002) and almost 100% in the Scheldt (Chou and Wollast, 2006), although most of this will be regenerated. Using published transects along salinity gradients, DeMaster (2002) inferred 0.6×10^{12} mol Si yr^{-1} for estuarine Si removal based on the degree of non-conservative mixing, which we use in our budget (Table 1). The global estuarine surface area is ~1.1×10^6 km^2 (Dürr et al., 2011a), implying a sedimentation rate of ~33 g SiO_2 km^{-2} yr^{-1}, close to lake sedimentation rates (Frings et al., 2014a), and lower than the few estuarine BSi accumulation rates found in the literature (60–500 g SiO_2 km^{-2} yr^{-1}) (Colman and Bratton, 2003; Qin et al., 2012; Carbonnel et al., 2013).

Previous ocean Si budgets have included reverse weathering in estuarine or deltaic regions as a discrete loss term (Tréguer et al., 1995; Tréguer and De La Rocha, 2013). The term reverse weathering refers to the formation of authigenic clay minerals in continental margins, and was first proposed to balance ocean element budgets (Mackenzie and Garrels, 1966) — indeed, it is known to be a key sink for many elements. Reverse weathering is thought to occur as a result of the interaction of degraded continental aluminosilicates with ocean porewaters following the approximate reaction scheme: (alumino)silicate + cations + SiO_2 + HCO_3^- = cation-rich aluminosilicate + CO_2 + H_2O. This process occurs in different settings, and has been inferred indirectly from porewater profiles (Mackenzie and Kump, 1995; März et al., 2015; Michalopoulos and Aller, 1995, 2004), observed in situ (Michalopoulos et al., 2000; Presti and Michalopoulos, 2008), or experimentally replicated (Loucaides et al., 2010). It is suggested to account for up to 25% of DSi removed from the ocean (Holland, 2005). However, porewaters of marine sediments are almost exclusively enriched in DSi relative to the overlying water column (März et al., 2015; Ragueneau et al., 2000); the benthic DSi flux across the sediment/water interface is always positive. In this context, reverse weathering should be considered as a diagenetic pathway for BSi (Aller, 2014) that enhances its preservation efficiency, rather than being a sink *per se*.

4.1.4. Isotopic effect of estuarine Si removal

DeMaster (2002) estimated that ~10% of river DSi is sequestered within estuaries today as biogenic silica. If this is associated with a typical fractionation of −1.1‰ (De La Rocha et al., 1997), then the δ^{30}Si of river DSi entering the ocean is shifted towards a higher value by ~0.11‰ due to the presence of an estuarine filter, assuming no fractionation associated with reverse weathering. There is little work available to test this conclusion, and the available studies are equivocal. In the Tana River, Kenya, DSi mixes conservatively along the salinity gradient so there is no Si isotope fractionation (Hughes et al., 2012). In the Lena River delta, DSi is removed along the salinity gradient, but counter to expectations δ^{30}Si also decreases (Engström, 2009), interpreted as mixing with an unidentified ^{30}Si deplete water mass. Conversely, in the Elbe River estuary (Weiss et al., 2015) and the tidal freshwater section of the Scheldt river (Delvaux et al., 2013), DSi concentrations are depleted – presumably by biological activity – and δ^{30}Si of the residual DSi increases as expected, at least during the times of the year in which silicifying organisms grow.

4.2. Dissolution of river particulate matter

4.2.1. Magnitude of DSi flux from dissolution of river particulate matter

River suspended particulate matter (SPM) is predominantly silicate material (Viers et al., 2009), some of which will dissolve in the ocean. Conventionally, river SPM is assumed to dissolve sufficiently slowly that it does not contribute to biological cycling. However, it need be only sparingly reactive to have a large effect (Oelkers et al., 2011; Jeandel and Oelkers, 2015), and recent work suggests that dissolution, desorption or ion-exchange of river SPM in estuaries and the coastal zone is indeed large enough to be a substantial component of ocean elemental or isotope budgets (Gislason et al., 2006; Jeandel et al., 2011; \ et al., 2014; Oelkers et al., 2011). Estimates of the magnitude of the total river particulate flux cluster around 14–20 × 10^9 t yr^{-1} (*e.g.* Milliman and Meade, 1983; Syvitski et al., 2005) with a recent estimate being 19×10^9 t yr^{-1} (Milliman and Farnsworth, 2011). How much of this SPM will dissolve in the ocean? Insight can be gained by considering the amount of BSi carried by rivers, or by simple experimental approaches exploring the interaction of river sediment and seawater.

4.2.1.1. River transport of biogenic silica. Conley (1997) quantified the BSi material carried by rivers at $1.05 \pm 0.20 \times 10^{12}$ mol yr^{-1}, based on a simple extrapolation of surface water samples from a small dataset of 11 rivers. However, with a growing awareness that the conventional measurement protocols (weak alkali leaches, *e.g.* DeMaster, 1981) do not target BSi *per se*, but rather a range of non-crystalline siliceous phases, the term 'amorphous silica' (ASi) is now more prevalent (Barão et al., 2014, 2015), although some fraction of river SPM can indeed be 'true' BSi (Cary et al., 2005; Meunier et al., 2011). Dissolution rates of ASi are greater, by around a factor of 5, in the higher pH and electrolyte concentrations of seawater relative to freshwater (Loucaides et al., 2008, 2012). As a result, the ASi fraction is assumed to dissolve rapidly along the salinity gradient, an assumption generally borne out in studies of estuarine particulate matter (Carbonnel et al., 2013; Lehtimäki et al., 2013; Pastuszak et al., 2008). Frings et al. (2014b) showed that in the Ganges basin, the Si extracted by a conventional weak alkali leaching protocol (DeMaster, 1981) is a relatively consistent fraction (mean $\pm \sigma = 1.2 \pm 0.78$%) of the total sediment load. Extending the calibration dataset to include 415 paired and globally distributed ASi-SPM measurements, Frings (2014) estimated that ~0.6% of global river SPM is 'ASi'. Taking a total SPM flux of 19×10^9 t, this implies that 1.9×10^{12} mol yr^{-1} ASi is carried by rivers.

4.2.1.2. Experimental approaches. Experimental work to investigate the interaction of river sediment and seawater has mostly used riverbed material from basaltic islands (e.g. Jones et al., 2012a,b; Pearce et al., 2013; Oelkers et al., 2011), though Jones et al. (2012b) also used material from the Amazon, Mississippi and Orange rivers. Over the full course of these experiments, only about 0.005 to 0.01% of the Si in the sediment was solubilised. However, given the high solid:solution ratios (*ca.* 1:3), a near-equilibrium concentration was quickly obtained (≪1 month), impeding further dissolution. Focusing on basaltic glass, Morin et al. (2015) confirmed Si dissolution rates increase as a function of salinity. Their experiments were conducted at 90 °C, and based on an extrapolation to 16 °C and assumptions about the quantity of sediment deriving from volcanic islands, they argue 2–8 × 10^{12} mol Si yr^{-1} is released from basaltic glass dissolution alone, broadly equivalent to the river DSi flux. The young, basaltic sediment used in these studies is known to have high dissolution rates (Dupré et al., 2003) but is unlikely to be representative of global river SPM. These problems hamper extrapolation of the results to a global scale — further field or lab-based approaches in granitic or meta-sedimentary terrains are required. Nevertheless, they demonstrate the potential importance of dissolution of terrigenous material, which is reinforced by a mass-balance of the Mediterranean Si cycle that invokes dissolution of 1% of river SPM to close the budget (Jeandel and Oelkers, 2015).

Given that the ASi content of river SPM is of a very similar order of magnitude (see above), this suggests the two approaches at least partially target the same Si. The relevant questions then become: (i) To what extent do the measurement protocols for river ASi reflect the behaviour of river sediment in seawater? (ii) To what extent do the extraction protocols target amorphous silica? and (iii) To what extent is there a discrete ASi pool? These questions require further research. For the time being, we assume that the protocols developed for BSi

analysis (*e.g.* DeMaster, 1981) fortuitously capture the amount of all Si likely to dissolve in seawater – both amorphous and lithogenic – and therefore take a flux of 1.9×10^{12} mol yr^{-1} as the input of DSi to the ocean from terrigenous sediment dissolution, which may need revising upwards if the results of Morin et al. (2015) can be confirmed.

4.2.2. δ^{30}Si of DSi flux from dissolution of river particulate matter

The δ^{30}Si of bulk SPM has been measured only in the Yellow and the Yangtze rivers (Ding et al., 2004, 2011). Both systems have low δ^{30}Si SPM (mean $\pm$ 1 σ = -0.02 ± 0.20‰ and -0.34 ± 0.19‰, respectively). The δ^{30}Si of ASi has never been directly assessed in river sediment, although we can extrapolate from terrestrial ecosystem studies that these phases, whether formed biogenically (*e.g.* diatoms, phytoliths) or inorganically (*e.g.* poorly crystalline aluminosilicates), should tend towards even lower δ^{30}Si (Fig. 4). For now, we take the mean of the Yellow and Yangtze rivers of -0.18 ± 0.25‰ as representing the Si isotopic composition of terrigenous sediment.

4.3. Submarine groundwater discharge (SGD)

4.3.1. Magnitude of DSi flux from submarine groundwater discharge

It has long been recognised that the discharge of water from groundwater directly into the ocean may be a significant term ecologically, chemically and volumetrically (Johannes, 1980). Even if the flow rates are low, integrated over the entire length of a shoreline and combined with the generally higher solute concentrations in groundwater, SGD fluxes can be important (Moore, 1996). There is some confusion regarding the definition of submarine groundwater discharge. It is generally taken to mean any flow of water out across the seafloor, and so includes both the terrestrially derived freshwater endmember and a much larger recycled seawater component (Burnett et al., 2006). Here, we restrict ourselves to the component that derives directly from terrestrial infiltration of meteoric waters, although if the recirculating component interacts substantially with continental silicates it could be an important and completely unexplored term in the global Si cycle. The patchy and variable nature of this water flux has made it difficult to quantify (Burnett et al., 2006). Nevertheless, significant regional inputs of DSi from SGD have been demonstrated in *e.g.* the Mediterranean (Rodellas et al., 2015; Weinstein et al., 2011), the Bay of Bengal (Georg et al., 2009a) and from volcanic islands (Schopka and Derry, 2012).

To our knowledge, the only global estimates of the SGD contribution to the ocean Si budget are 0.4 and 0.6×10^{12} mol DSi yr^{-1} to the oceans, or approximately 6–10% of the river DSi flux (Laruelle et al., 2009; Tréguer and De La Rocha, 2013). These are based on the product of a total SGD of 2000 km^3 yr^{-1} (adapted from Slomp and Van Cappellen, 2004) and an arbitrarily assigned groundwater DSi concentration of 200 or 340 μM. Building on this approach, we note that estimates of the volume of SGD (Slomp and Van Cappellen, 2004; Knee and Paytan, 2011; Burnett et al., 2006; Taniguchi et al., 2002) range from 0.1 to 10% of the global river flux (which is approximately 37×10^3 km^3 yr^{-1}; Dai and Trenberth, 2002). These estimates are commonly based on global water budgets, with SGD being the residual of the other terms, such that the propagated uncertainty is of the same order of magnitude as the flux itself. Nonetheless, a consensus seems to be developing for a total flux of approximately 5% of river discharge, *i.e.* 1850 km^3 yr^{-1}, which we retain as the total SGD water flux with an uncertainty of $\pm$ 50%.

We now turn our attention to the 'mean' groundwater DSi concentration. To our knowledge, no systematic survey of global groundwater geochemistry is available. A geochemical survey of 1785 European bottled waters yields a mean $\pm$ 1σ DSi concentration of 319 $\pm$ 285 μM (Birke et al., 2010). Querying the database maintained by the USGS (the 'National Water Information System'/'Water Quality Samples for the Nation') for all well data in the USA, for measurements made in 2014, yields mean $\pm$ 1σ DSi concentration of 380 $\pm$ 250 μM (n = 2081). Based on 2640 datapoints from regional datasets, mostly from the continental United States, Davis (1964) suggested a median concentration for groundwater DSi of 300 μM. We take the mean of the USGS data of 380 $\pm$ 250 μM as representing the concentration of DSi in groundwater inputs to the ocean. Combining this with the total volume of SGD flow, we obtain a total SGD DSi flux of 0.65 $\pm$ 0.54×10^{12} mol yr^{-1}, or about 10% of the river DSi flux.

4.3.2. δ^{30}Si of DSi flux from submarine groundwater discharge

The range of δ^{30}Si reported for groundwater DSi is large (Fig. 4) and spans from -0.15‰ to $+1.34$‰ at various depths in the Bengal Basin (Georg et al., 2009a), from $+0.35$‰ to $+1.01$‰ for Icelandic springs (Opfergelt et al., 2011), from -1.42 to $+0.56$‰ along a 100 km flowpath in a sandstone aquifer in Arizona (Georg et al., 2009b) and from -1.50 to -0.85‰ in the Great Artesian Basin, Australia (Pogge von Strandmann et al., 2014). Isolated values of $+0.3$‰, $+0.5$‰ and $+0.7$‰ have also been reported in Hawaiian systems (Ziegler et al., 2005a,b), and up to $+2.07$‰ in a Siberian permafrost landscape (Pokrovsky et al., 2013). Unsurprisingly, given the diversity of systems and processes, there is no relationship between groundwater DSi concentration and δ^{30}Si. We therefore take the mean of the 44 published values (Fig. 4) of $+0.19$‰, with a range of 0.9‰, as representing the δ^{30}Si of groundwater DSi inputs to the ocean.

4.4. DSi inputs from dissolution of atmospheric dust

4.4.1. Magnitude of DSi flux from dissolution of aeolian dust

Existing estimates of DSi inputs from aeolian dust are essentially back-of-the-envelope calculations based on deposition rates and estimates of the fraction liable to dissolve as a function of residence time in the water column. All global Si budgets to date (Laruelle et al., 2009; Tréguer et al., 1995; Tréguer and De La Rocha, 2013) take a value of 0.5×10^{12} mol Si yr^{-1}. How realistic is this value?

Somewhere between 500 and 5000×10^{12} g dust yr^{-1} is currently entrained into the atmosphere (Engelstaedter et al., 2006), of which 134 to 910×10^{12} g yr^{-1} is deposited in the oceans (Duce et al., 1991; Jickells et al., 2005). This is mostly in the form of wet deposition, *i.e.* scavenged by precipitation, although gravitational ('dry') settling of larger particles may be important in nearshore environments (Prospero and Arimoto, 2008). If the composition of the upper continental crust (Rudnick and Gao, 2003) reflects the composition of mineral dust, some 67% is SiO_2. In other words, somewhere between 1.5 and 10.2×10^{12} mol Si yr^{-1} is deposited on the ocean surface.

Anywhere between <1% to more than 10% may potentially dissolve (Guerzoni et al., 1999; Tegen and Kohfeld, 2006), and a single value is hard to prescribe given regional differences in source composition, particle size, etc. Ridgwell et al. (2002) take a solubility of 6.6% for their model study, and Maring and Duce (1987) estimated up to 8–10% of Al contained in aerosol aluminosilicates would dissolve in seawater within 60 h. Using values of 1.5% to 5% for the fraction of dust which dissolves reasonably reproduce the distribution of global surface-ocean dissolved Al (Gehlen et al., 2003; Han et al., 2008; Measures and Vink, 2000). Si and Al co-occur as aluminosilicates, so assuming the same solubility for Si as Al (*i.e.* 1.5 to 5%, while acknowledging they have different fates in solution), provides DSi inputs from aerosol dissolution of 0.023 to 0.50×10^{12} mol Si yr^{-1}, so the Tréguer and De La Rocha (2013) estimate (0.5×10^{12} mol yr^{-1}) is probably an upper bound. Clearly, the two key terms in this derivation (dust deposition rates and Si solubility) need much better quantification.

4.4.2. δ^{30}Si of DSi flux from dissolution of aeolian dust

In the absence of direct measurements, there are two means of identifying the silicon isotope composition of aeolian dust. The mean of published bulk soil δ^{30}Si determinations (Fig. 4), equal to -1.08 ± 0.77‰ (n = 195), may suffice if soils can be considered broadly representative of the sources of dust to the ocean. Alternatively, the Pleistocene loess samples analysed by Savage et al. (2013) provide a mean of $-0.22 \pm$

0.07‰ (n = 13), and a similar value of −0.2‰ provided plausible results in an endmember analysis of Si sources in the glacial East Philippines Sea (Xiong et al., 2015). However, loess deposits tend to be towards the larger end of the dust size spectrum (Muhs, 2013), while the long-range transport particles that enter the marine realm may be smaller clays that tend towards lower δ^{30}Si values. We therefore take a value intermediate between soils and loess of −0.65‰, but suggest that it should be empirically determined in future.

4.5. Non-continental sources of DSi

Interaction between seawater and ocean basalts is an important control on seawater chemistry on geological timescales (Staudigel, 2014). Seawater flows through the permeable upper oceanic crust, where it may be heated by residual heat. Alkalinity, cations and DSi can derive from the reactions that occur. Compiling the available literature, Tréguer and De La Rocha (2013) estimate that the high temperature, axial component of fluid recirculation introduces 0.2–0.8 × 10^{12} mol Si yr^{-1}, and the low temperature ridge component 0–0.15 × 10^{12} mol Si yr^{-1}. We retain this estimate, in total *ca.* 0.6 ± 0.4 × 10^{12} mol DSi yr^{-1} from hydrothermal systems. This DSi probably has an initial δ^{30}Si value of −0.4 to −0.2‰, based on two samples collected at the East Pacific Rise by the submersible Alvin at ~300 °C and 11–15 mM DSi (De La Rocha et al., 2000), but this may change as the expelled fluid cools and becomes supersaturated, inducing silica precipitation. Whether or not precipitation of silica in such a process is important and if it is associated with isotope fractionation is unclear. The siliceous sinter deposits associated with hydrothermal or hot spring systems tend to be ^{30}Si depleted (Douthitt, 1982; Ding et al., 1996), implying the presence of an associated fractionation, perhaps as large as −4.4‰ (Geilert et al., 2015) although the effect on the residual DSi will depend on the proportion of the fluid DSi that is precipitated.

DSi can also be supplied from weathering of seafloor basalt, although the distinction between solutes deriving from hydrothermal fluid circulation and basalt weathering is ultimately arbitrary. Tréguer et al. (1995) included low-temperature alteration in their budget at 0.4 ± 0.3 × 10^{12} mol yr^{-1}, which can be traced to Maynard (1976) and Wolery and Sleep (1976) who invoked basalt alteration to balance ocean elemental budgets. Based on benthic DSi efflux rates, Tréguer and De La Rocha (2013) updated this value to 1.9 × 10^{12} mol DSi yr^{-1}, but including dissolution of terrestrial lithogenic material which we separated above. We therefore retain the earlier Tréguer et al. (1995) estimate of 0.4 ± 0.3 × 10^{12} mol yr^{-1}. Its δ^{30}Si value is also uncertain: secondary aluminosilicates are common in altered seafloor basalts, confirming that alteration is incongruent and therefore probably associated with Si isotope fractionation. We provisionally take 0.0 ± 0.5‰, but note that high and low-temperature hydrothermal fluids are probably isotopically distinct. It should be highlighted that DSi fluxes deriving from oceanic basalt are perhaps the most poorly understood and unconstrained in the global Si cycle.

4.6. Synthesis of DSi inputs to the global ocean

Based on the above, a total annual input of DSi to the modern ocean can be calculated at 9.55 ± 1.30 × 10^{12} mol with a flux-weighted δ^{30}Si of 0.74 ± 0.17‰ (Table 1). To our knowledge, this is the first estimate of the ocean δ^{30}Si budget. Note that of the component fluxes, few are known to a reasonable degree of precision. Uncertainties are hard to prescribe given the limited data availability. The total ocean volume is ~1.3 × 10^{21} l. According to the gridded climatology of Gouretski and Koltermann (2004), there is an average DSi concentration of 88 μmol kg^{-1} (or *ca.* 85 μmol/l^{-1}), for a total mass 112 × 10^{15} mol. For total inputs of 9.55 × 10^{12} mol yr^{-1} the estimated residence time for dissolved Si in the global ocean, defined as inventory/input, is just under 12,000 years. This is towards the lower end of previous estimates that cluster around 15,000 to 20,000 years (Broecker and Peng, 1982; Laruelle et al., 2009; Quinby-Hunt and Turehian, 1983; Sarmiento and Gruber, 2006; Tréguer et al., 1995). These typically have a similar total inventory of DSi; the smaller residence time derived here is a result of more inputs being considered and is consistent with that calculated by Tréguer and De La Rocha (2013) (~10,000 years).

5. Potential for variability in continent-ocean Si fluxes

If we understand the parameters that control the magnitude and isotopic composition of the Si fluxes to the ocean, we can use this understanding to place limits on how much Si fluxes to the ocean may vary. Given the *ca.* 12 ka residence time of Si in the ocean (Section 5), perturbations to the inputs must occur on similar timescales to affect ocean Si cycling (Richter and Turekian, 1993), so we focus on the processes that affect continental Si cycling over these timescales.

The world at the Last Glacial Maximum (LGM, *ca.* 21 ka BP) differed greatly to the modern world. Climate was generally cooler and drier and large ice sheets existed at high latitudes in both hemispheres. As a consequence, sea level was lower, newly exposing land surfaces and the distribution of terrestrial vegetation was drastically altered. In the following, we evaluate how each of these four main changes (climate, ice sheet extent, sea-level and vegetation zonation) may have altered the magnitude and isotopic composition of land-to-ocean Si fluxes. The aim of this exercise is to define plausible ranges that land-to-ocean Si fluxes may have varied within. These ranges can then be used to create scenarios of change in global land-to-ocean Si fluxes that act as inputs to a simple model to evaluate the timescales and magnitudes of whole-ocean δ^{30}Si response to a variable continental Si cycle.

5.1. Impact of glacial climate on land-to-ocean Si fluxes

5.1.1. Impact of glacial climate on the river DSi flux and δ^{30}Si

The river DSi flux is the single largest input to the ocean, but inferring potential variability on glacial–interglacial (G–IG) timescales is difficult, partly because the parameters controlling DSi fluxes are not well understood and are probably compensatory to some degree (Kump and Alley, 1994). The flux, and its associated δ^{30}Si, can vary in two ways:

1. *Via* changes in the rate of DSi release from primary minerals (*i.e.* the silicate weathering rate) and the weathering style, including changes associated with the exposure of continental shelf during sea-level lowstands and subglacial weathering.
2. *Via* changes in continental Si cycling, particularly the presence and efficiency of continental Si sinks (Billen et al., 1991; Meybeck and Vörösmarty, 2005).

What controls DSi mobilisation from bedrock? First-order controls on silicate-weathering rates include temperature, water availability and lithology, plus the tectonic parameters that affect the exposure of new material (West et al., 2005). These parameters control *e.g.* the degree of soil development, physical erosion rates, catchment hydrology and ecosystem structure which may be more direct determinants of silicate weathering rates. In practise, this makes it hard to predict how silicate-weathering rates may have varied over G–IG cycles. As Kump and Alley (1994) note, intuition is of little help because of the multiple interacting and counteracting controls.

We consider that the river DSi flux has been relatively invariant (±20%) since the LGM. This premise is based on modelling of river DSi fluxes using lithology-specific runoff–Si flux relationships (Jones et al., 2002; Gibbs and Kump, 1994; Munhoven, 2002). This work has demonstrated that a decrease in Si fluxes resulting from *e.g.* lower continental precipitation was largely balanced by increased fluxes from newly-exposed continental shelf. It is also consistent with interpretations of G–IG records of Pb stable isotopes in oceanic ferromanganese crusts (Foster and Vance, 2006), high-precision radiogenic ^{87}Sr/^{86}Sr ratios in foraminifera (Mokadem et al., 2015) and cosmogenic ^{10}Be/^{9}Be

ratios in ocean authigenic sediments and ferromanganese crusts (von Blanckenburg et al., 2015). These independent lines of evidence all suggest that the continental weathering fluxes have not substantially varied over the late Quaternary glacial–interglacial cycles; we make the simplifying assumption that the same is true for DSi fluxes.

However, the δ^{30}Si of the river DSi flux might be more variable. River DSi δ^{30}Si primarily reflects weathering congruency (Section 3, Fig. 6), so if this could be inferred or reconstructed it can constrain the magnitude of any change in river δ^{30}Si. Qualitatively, we suggest that the river DSi at the LGM likely had a lower associated δ^{30}Si. Dosseto et al. (2015) present an increase in lithium isotope ratios of 7‰ in clays in Himalayan fluvial terraces since the LGM, attributed to a corresponding decrease in weathering congruency. This is relevant because mass-balance dictates that the residual solutes should follow a similar trend (*cf.* Fig. 2), and the Si and Li isotope systems are thought to behave similarly (Opfergelt et al., 2013; Pogge von Strandmann et al., 2012), so glacial river DSi should also have lower δ^{30}Si. Note that no similar studies exist for silicon isotopes: there is clear potential for the δ^{30}Si of secondary minerals in *e.g.* fluvial terraces, floodplain deposits or deltaic sediments to provide useful insight into palaeo-weathering dynamics. Mechanistically, lower glacial river δ^{30}Si may result from (i) reduced catchment fluid and/or sediment residence times, (ii) lower temperatures acting to lower rates of secondary mineral formation *via* a reduction in the rate constants of precipitation or (iii) the greater relative formation of 2:1 clays over 1:1 clays, which tends to be associated with a smaller magnitude of fractionation (Opfergelt et al., 2012). Altogether, these can act to reduce the total magnitude of clay formation (increase weathering congruency), and therefore reduce the expression of Si isotope fractionation during glacials. We suggest a conservative reduction of 0.2 ± 0.25‰ of river DSi at the LGM relative to today.

5.1.2. Impact of glacial climate on the dust flux and δ^{30}Si

Marine and terrestrial sediments and ice-cores from both poles consistently show increased dust accumulation rates over the LGM (Muhs, 2013). Glacial dust fluxes have received attention for their potentially important role as a source of nutrients (particularly Fe or Si) to regions of the oceans where (siliceous) primary production is currently limited by lack of these nutrients (Harrison, 2000; Jickells et al., 2005; Martin, 1990). Due to expanded dust production areas, greater entrainment capabilities (drier soils and higher winds) and greater transport capacity due to less efficient washout (Muhs, 2013; Tegen and Kohfeld, 2006), total dust input to the glacial ocean was 2–10 times higher than modern deposition rates. We assume that even if loci of dust production are variable, the solubility and mean isotopic composition (*i.e.* −0.67 ± 0.45; Table 1) of the dust as estimated above are invariant.

5.1.3. Impact of glacial climate on the river sediment flux and δ^{30}Si

The boundary conditions that control river sediment export (*e.g.* temperature, precipitation, glacial activity and basin area) change over glacial cycles. Using U-series disequilibria, Dosseto et al. (2010) argue that sediment storage times in the Murrumbidgee River catchment, Australia, reached a minimum at the LGM due to the lack of stabilising influence from vegetation. Some larger rivers have sediment deliveries buffered by their alluvial plains on timescales as long as Quaternary glacial cycles (Métivier and Gaudemer, 1999), although this does not apply to all large rivers (Clift and Giosan, 2014). Even small mountain catchments can buffer sediment delivery on millennial timescales (Blöthe and Korup, 2013), introducing inertia into river system sediment fluxes. Glaciers and ice-sheets produce large amounts of finely ground glacial flour, but the extent to which this contributes to enhanced sediment fluxes rather than providing for a potential post-glacial pulse (Vance et al., 2009) is unclear. Modelling studies in both the Po River basin, northern Italy (Kettner and Syvitski, 2009), and the Waipaoa River, New Zealand (Upton et al., 2013), driven by temperature, precipitation, catchment size and an index of erodability suggest enhanced LGM fluxes relative to modern (preindustrial) fluxes. Overall, we consider that the net sediment load carried by rivers at the LGM was between 1 and 2× modern (preindustrial) values. We make the simplifying assumption that the percentage of this sediment liable to dissolve was a constant fraction, and we assume no post-glacial sediment pulses or lags, and that it had a constant δ^{30}Si.

5.2. Impact of continental ice-sheets on land-to-ocean Si fluxes

Subglacial and periglacial silicate weathering is different in style to subaerial weathering. Analysis of subglacial streams shows that silicate weathering tends to be more congruent, as evidenced by high Ge/Si (approaching the Ge/Si ratio of bedrock) and elemental stoichiometries (Tranter, 2005), and tends to be driven by acidity not sourced from atmospheric carbon (Anderson, 2005; Wadham et al., 2010). The few investigations of DSi δ^{30}Si in glaciated catchments (Georg et al., 2007a; Opfergelt et al., 2013) show that these tend to be low δ^{30}Si rivers that approach the parent material isotopic composition. Therefore, a world with increased sub- or peri-glacial solute generation could perhaps be expected to introduce low δ^{30}Si DSi. Opfergelt et al. (2013) found a difference in δ^{30}Si of 0.8‰ between glaciated and non-glaciated catchments in Iceland and estimated a net decrease in river δ^{30}Si of 0.12‰ due to the presence of the high-latitude ice sheets, mountain ice-caps and valley glaciers, which we retain here.

5.3. Impact of lowered sea-level on land-to-ocean Si fluxes

At the LGM, global eustatic sea levels were approximately 130 m lower as a result of water storage in the polar ice caps (Lambeck et al., 2014). This may affect the inputs to the global ocean and ocean Si cycling in at least three ways: i) a reduction in the 'fluvial filtering' of land to ocean fluxes, ii) the exposure of new land surface to subaerial weathering and remobilisation of 'old' BSi, with an associated reduction in the area of continental shelf available for neritic BSi sedimentation, and iii) alteration to groundwater flow dynamics.

5.3.1. DSi and the fluvial filter: alluvial plains, estuaries and lakes

The land-to-ocean DSi flux must pass through a series of biogeochemically reactive systems – wetlands, lakes, estuaries, etc. – that act as a 'fluvial-filter' (Billen et al., 1991; Meybeck and Vörösmarty, 2005). The base level of a river system is the lowest level to which it can be subaerially eroded, usually sea level. In response to a sea-level change and therefore a channel shortening or lengthening, a river network can aggrade or incise to adjust towards a new equilibrium profile, although the nature of the adjustment depends on shelf and channel gradients, sediment supply, stream power, etc. A full discussion of fluvial responses to base-level change is beyond the scope of this paper (reviews can be found in Blum and Törnqvist, 2000 and Schumm, 1993). However, we speculate that water/sediment interaction times in alluvial plains were lower at the LGM because of the lowered base-level, a suggestion advanced previously (Lupker et al., 2013).

In the Ganges basin today, rivers partially or completely draining the alluvial plain have DSi δ^{30}Si (typically >2‰) consistently and substantially higher than rivers draining solely the Himalaya (around 1‰) (Fontorbe et al., 2013; Frings et al., 2015). The silicon isotope composition (1.69‰) at the most downstream point reflects a conservative mixing of the upstream tributaries, meaning the presence of alluvial plain derived DSi pushes the δ^{30}Si of exported DSi higher by around 0.7‰ in the Ganges. As suggested above, δ^{30}Si from alluvial plain streams are high because sediment/water interaction times are sufficiently long to promote clay formation. If the interaction time between sediment and water is reduced, then we can speculate that secondary mineral formation will be reduced, with a correspondingly lower exported δ^{30}Si. We speculate that this could cause the mean river DSi δ^{30}Si to decrease by up to 0.2‰.

Lakes also act as biogeochemical reactors, converting some fraction of inflowing DSi into BSi and burying it in their sediments (Frings et al., 2014a; Harrison et al., 2012). This retention must shift δ^{30}Si of the residual DSi higher (Frings et al., 2014a; Hughes et al., 2012). Two global estimates of the magnitude of DSi retention in lakes arrived at similar values of ~25% of the river DSi flux (Frings et al., 2014a; Harrison et al., 2012), meaning that δ^{30}Si of river DSi is about 0.2‰ higher than in a hypothetical lake-free world, assuming a BSi production fractionation of −1.1‰ (Fig. 2). Many lakes today are glacial relics (Hutchinson, 1957), formed by glacial scouring or in dead-ice pits. This implies that during glacial periods there were fewer lakes and less DSi retention, so therefore less fractionation, perhaps compounded by decreased productivity (and therefore less efficient retention) in cooler climates. Overall, a reduced lake sink may constitute a further lowering of fluvial δ^{30}Si by *ca.* 0.1‰ in glacial periods.

Estuaries provide a final example of how a less efficient fluvial filter may have altered river Si fluxes on millennial timescales. Estuaries are of interest since they are features of periods of transgressive sea level (Weiss et al., 2015; Kennett, 1982). If these environments are acting as efficient particle or solute filters today (Section 4.1.3), we can expect them to behave differently (*i.e.* a much reduced filtering capacity) during the LGM sea level lowstand when river discharge into the ocean was mostly direct (Kennett, 1982). Taking the estimated isotopic impact of estuarine DSi retention (~0.1‰; Section 4.1.4), a near cessation of estuarine Si filtering associated with more direct riverine discharge to the ocean could conceivably lower the net δ^{30}Si of river DSi entering the open ocean by ~0.1‰ — assuming a BSi production fractionation of −1.1‰ (Fig. 2).

5.3.2. Exposure of continental shelf

BSi accumulation rates on continental shelves are high (~1.8×10^{12} mol yr^{-1}) because of high production rates (due to proximity to continental nutrients) and higher preservation efficiencies (due to shorter water column residence time and higher sedimentation rates) (DeMaster, 2002). This means that there are massive pools of BSi that could potentially become available to subaerial weathering during sea level lowstands. The δ^{30}Si of this is unknown; we speculate it could alter the mean δ^{30}Si of river DSi by ±0.1‰.

5.3.3. Potential modification of submarine groundwater discharge at the LGM

A lowering of base level both allows for greater freshwater storage in continental aquifers (Adkins et al., 2002) and increases the hydraulic gradient, which may be expected to increase the glacial submarine groundwater discharge (SGD) flux relative to today. To our knowledge, this has never been quantified. Global precipitation was lower at the LGM, but rates of evaporation also declined, meaning discharge remained relatively constant (Kump and Alley, 1994; Jones et al., 2002). However, it is possible that the partitioning of this discharge between SGD and rivers changed. We incorporate this into our scenarios whereby a glacial SGD increase of between 1 and 2× modern values is counterbalanced by a decrease in river runoff of the same magnitude; the δ^{30}Si of SGD is held constant.

5.4. Impact of altered vegetation zonation on land-to-ocean Si fluxes

At the LGM, there was a general equatorward contraction in the zonation of vegetation communities towards lower altitudes and latitudes, and an expansion of grasslands at both low and high latitudes (Harrison and Prentice, 2003). Given that distinctive Si cycles exist in these biomes, could this play a role? It is unclear to what extent there are systematic differences in silicate weathering rates beneath various biomes. In the absence of clear evidence, we assume that the latitudinal contraction and expansion of vegetation ranges characteristic of the Quaternary glacial cycles was not associated with a net change in the rate of the solubilisation of Si from bedrock at a global scale beyond that included in our ±20% DSi flux range (Section 5.1.1).

Vegetation pattern changes might alter the DSi exported from catchments *via* a change in Si cycling at an ecosystem level (Conley and Carey, 2015). The ratio of export of fractionated material to initial solubilisation from bedrock is a key control on the silicon isotope composition of river water (Section 3; Bouchez et al., 2013). Therefore if a larger fraction of the total Si exported is detrital biogenic opal or other secondary (alumino)silicates then the degree of fractionation relative to bedrock of the residual DSi should be more pronounced. Vegetation and its associated fungal and bacterial communities are key players in soil/clay formation; it is likely that some biomes are more efficient at producing secondary solids than others, but we are currently unable to evaluate this. Related, some ecosystems may export more Si as biogenic Si. Two lines of evidence suggest that this is not an important mechanism of change over G–IG cycles. Firstly, the biogenic component is generally a small fraction of the total of secondary Si phases produced and exported, which tend to be dominated by clay minerals (Section 3). Secondly, an assumption inherent in the preceding discussion (Section 5.2) is that the majority of BSi carried by rivers dissolves upon entry to seawater, such that it can have minimal net effect on the δ^{30}Si of Si delivered to the ocean.

A final mechanism whereby vegetation zonation may alter land-to-ocean Si fluxes is through transient changes in the size of the ecosystem Si pool. Although our understanding of terrestrial Si cycling is still in its infancy (Conley, 2002; Struyf and Conley, 2012), some aspects are reasonably well established. We know that terrestrial ecosystems develop a pool of Si in the soil–plant system that is composed of biogenic silica (BSi; mostly phytoliths) and its diagenetic products together with amorphous Si phases formed purely pedogenically (Barão et al., 2015; Sommer et al., 2006), and that this pool is isotopically distinct, being depleted in the heavy ^{30}Si (Cornelis et al., 2010, 2011; Vandevenne et al., 2015). We know that just considering the upper portion of a soil profile, this pool can be orders of magnitude larger than the annual Si export from a system (Struyf et al., 2010a,b). It has recently been estimated at 8250×10^{12} mol, *i.e.* ~1000 × annual DSi export (Laruelle et al., 2009) and ~100 × annual BSi production by terrestrial vegetation (Carey and Fulweiler, 2012). Finally, we know that the size of this pool varies among different ecosystems (summarised in Alfredsson et al., 2015), such that when land-cover changes the pool will aggrade or be depleted to reach a new steady state commensurate with the rate of input and the recycling efficiency (Clymans et al., 2011; Struyf et al., 2010b). There is therefore the potential for a transient increase or decrease in river DSi fluxes and/or associated changes in δ^{30}Si as the pool aggrades or depletes. At local scales, the build-up or depletion of this soil–plant ASi pool may be key in interpreting lacustrine δ^{30}Si records (Street-Perrott et al., 2008; Swann et al., 2010). One key unknown relates to the timescale of adjustment to a new steady-state. Although

Table 2
Summary of plausible changes to the magnitude and/or Si isotopic composition of dissolved Si inputs to the ocean, for the LGM relative to today.

Altered flux	Mechanism for alteration	Change in associated DSi flux	Change in associated δ^{30}Si (‰)
River DSi	Altered weathering regimes	±20%	−0.45 to +0.05
	Subglacial weathering		−0.15 to 0
	Lesser lake Si retention		−0.10 to 0
	Less alluvial plain interaction		−0.10 to 0.1
	Remobilisation of continental shelf BSi deposits		−0.10 to 0
	Reduced estuarine filter	0–10%[a]	−0.10 to 0[a]
	Net:	−20 to +30%	−1.00 to +0.05
Dust	Greater dust generation; less efficient continental rainout	2–10×	Constant
River SPM	Increased glacial flour production, less vegetation stabilisation	1–2×	Constant
SGD	Greater groundwater flow due to greater hydraulic head	1–2×	Constant

[a] Assumed to co-vary.

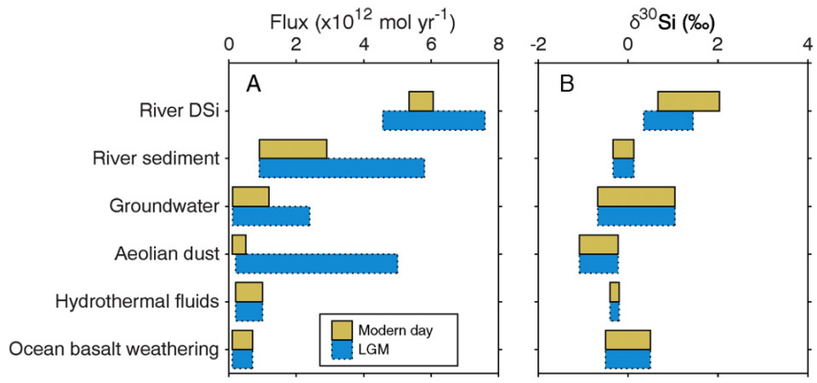

Fig. 10. A visual depiction of potential changes in the magnitudes (A) and δ^{30}Si (B) of DSi fluxes to the ocean between modern day (brown boxes) and LGM (blue boxes with dotted outline). The figure emphasises that the most likely mechanism of alterating the glacial ocean Si cycle is *via* a change in the relative importance of the individual fluxes, rather than *via* a change in their δ^{30}Si.

there is little evidence available, estimates of adjustment times span decadal to centennial timescales (Conley et al., 2008; Clymans et al., 2011; Struyf et al., 2010b), less than the multi-millennial perturbations required to impact the whole-ocean Si cycle. This can also be viewed in another, simpler way: the estimate of the size of the continental ASi pool (*i.e.* 8.25×10^{15} mol) is 'only' about 7% of the ocean DSi inventory (112×10^{15} mol) — too small to impact ocean δ^{30}Si on long timescales.

5.5. Synthesis of potential changes

A summary of these mechanisms for change, together with estimates of their impact on the Si flux magnitude and isotope composition, is presented in Table 2 and graphically in Fig. 10. Overall, this review suggests that the total inputs of DSi to the ocean have declined slightly from the LGM to today, and that the weighted δ^{30}Si of these inputs may have been up to 1‰ lower at the LGM, larger than the changes envisaged by previous work (Opfergelt et al., 2013; Georg et al., 2009a).

6. Manifestation of continental variability in the ocean Si cycle

Simple mass-balance calculations suggest that changes of >0.50‰ in river DSi δ^{30}Si alone are necessary to approach the level of variability observed in BSi (0.5 to 1‰). The synthesis above suggests changes of this magnitude are plausible, especially when considered in tandem with changing dust and groundwater fluxes and a reduced fluvial filter efficiency. If our analysis (Table 2) is correct in suggesting that a net change in the input weighted δ^{30}Si of ≥0.5‰ is plausible, then how rapidly is this observed in the ocean sediment record? Two studies have touched on this question before. One did not consider a time dependent aspect (Opfergelt et al., 2013). The second (Georg et al., 2009a) used a two-box model to resolve the time dependency and concluded that while δ^{30}Si of BSi did change, the magnitude and speed of this change was insufficient to be of interest. However, they considered only a variable SGD flux and held all other parameters constant.

Models of varying complexity have been used to investigate aspects of the ocean Si cycle. The simplest models have a limited number of boxes (De La Rocha and Bickle, 2005; Yool and Tyrrell, 2003, 2005; Laruelle et al., 2009; Bernard et al., 2010; de Souza et al., 2012; Reynolds,

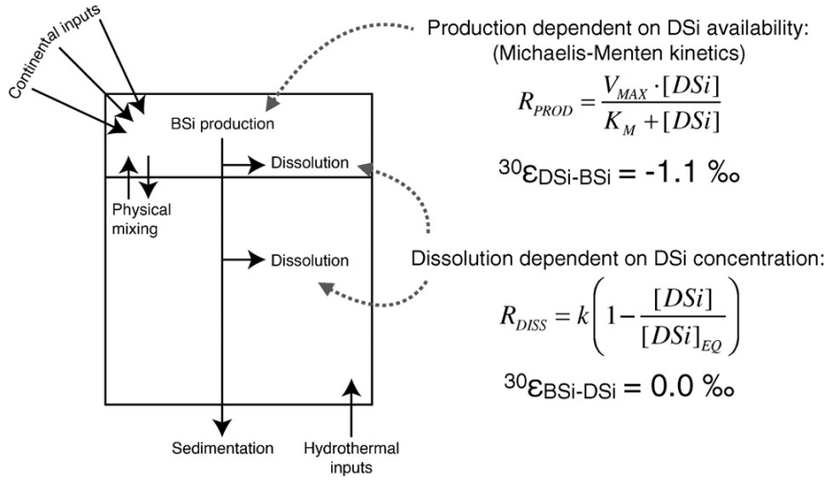

Fig. 11. Schematic of box model used to test ocean response to perturbations to input fluxes, showing both mass fluxes and associated fractionations, modified from De La Rocha and Bickle (2005). DSi inputs are prescribed independently into both the upper euphotic box (riverine, aeolian, and groundwater fluxes) and the deep ocean box (hydrothermal fluid recirculation). Si is transferred between the boxes by biological production, settling and dissolution, and physical mixing (upwelling and downwelling). See main text for more details.

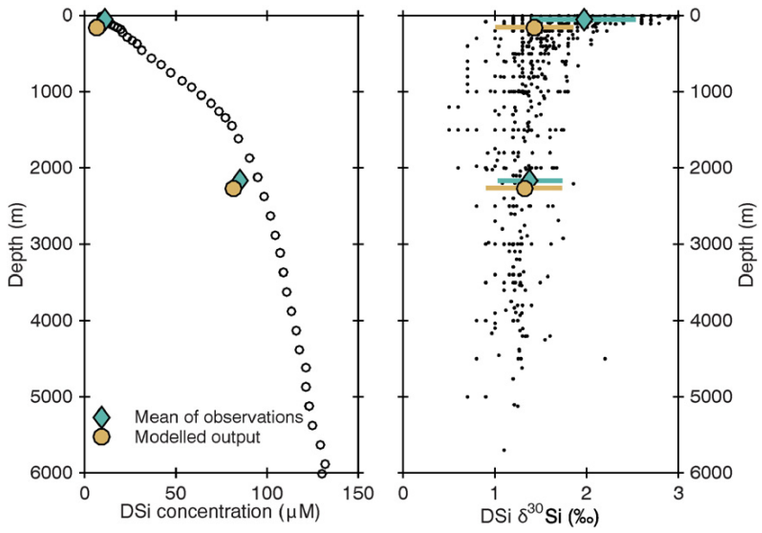

Fig. 12. Comparison of model output (brown circles) for the present day (parameters as in Table 1 and Supplementary data) with observational data (black dots, means given as green diamonds). DSi data averaged by depth from the global climatology of Gouretski and Koltermann (2004). Ocean δ^{30}Si data from literature compilation from all ocean basins (CDLR, unpublished compilation).

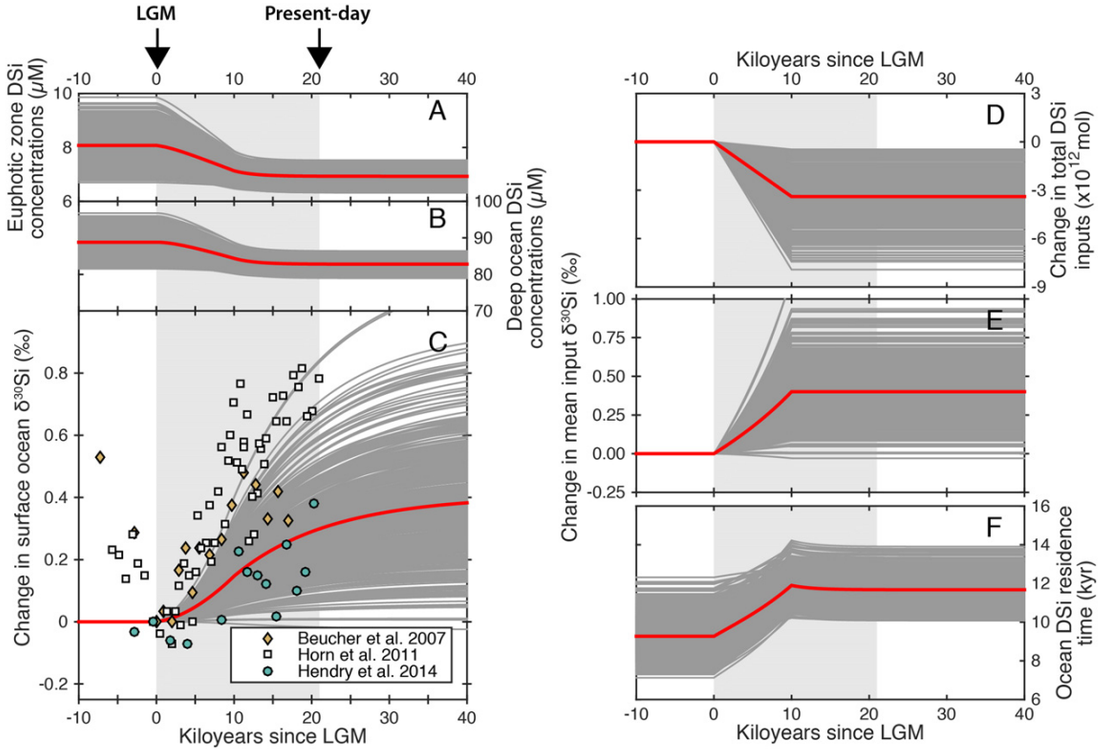

Fig. 13. Potential impact of changing land-to-ocean Si fluxes on millennial timescales on ocean Si cycling, as simulated by a two-box model. All results generated using 500 iterations (each light grey line represents one iteration), each representing one ensemble of input parameters randomly selected from the range of plausible values in Tables 1 and 2. See main text for details. A: Change in surface-water (upper 100 m) DSi concentrations in response to imposed input changes. B: Change in deep ocean (below 100 m) DSi concentrations in response to imposed input changes. C: Isotopic response of surface ocean DSi. Each iteration is standardised to a LGM baseline derived from a 50,000 yr spin-up period, in order to show the contrast between simulated glacial and modern oceans. Three representative downcore δ^{30}Si profiles from the sub-Antarctic Indian Ocean (Beucher et al. (2007), the Southern Ocean (Horn et al., 2011) and the North Atlantic (Hendry et al., 2014) are shown for comparison, also standardised to the δ^{30}Si of the sample nearest 21 ka, with the published age-models used as provided. D: Change in the sum of all input fluxes ($\times 10^{12}$ mol yr^{-1}), standardised to each iteration's LGM value. E: Change in the weighted mean δ^{30}Si of all DSi inputs to the ocean, standardised to each iteration's LGM value. F: Modelled Si residence time in the global ocean (total DSi inventory/annual DSi inputs).

2009; Nelson et al., 1995; Sutton et al., 2010; Ridgwell et al., 2002). More complex ocean general circulation models (GCMs) have also proved extremely insightful (*e.g.* Bernard et al., 2011; Wischmeyer et al., 2003), but simple box models have the advantage that many ensembles of input parameters can be tested to robustly assess model sensitivity and identify magnitudes and timescales of change.

Here, we use a simple two-box model modified from De La Rocha and Bickle (2005). The aim of this model is not to reproduce the exact response of the ocean Si cycle to perturbations but rather to assess the magnitude and timescales characteristic of ocean Si responses, and potential visibility in sedimentary record of changes to input fluxes. The model is modified slightly from that described in De La Rocha and Bickle (2005) and shown in Fig. 11. This simple approach captures the key features of the modern ocean Si cycle (Fig. 13), namely lower DSi, higher δ^{30}Si surface waters and higher DSi, lower δ^{30}Si deep waters, with a total DSi residence time (mass/inputs) of ~12 ka. The main modifications from the original De La Rocha and Bickle (2005) model are the incorporation of a DSi concentration dependency of BSi production and dissolution. The model and its parameterisation are described more fully in the Supplementary data. We use multiple model iterations with different flux parameterisations to allow us to assess model sensitivity and to account for our poor knowledge of modern DSi fluxes and even poorer knowledge of the palaeo-fluxes. (See Fig. 10.)

Both the magnitude and the isotopic composition of the input fluxes are varied over the course of a model run. For each iteration, values for the modern input fluxes and δ^{30}Si are randomly chosen from within the values and uncertainties given in Table 1. The LGM input values are then defined as a function of their deviation from the modern values, selected randomly from within the estimates in Table 2. The model is then spun-up to near equilibrium (50,000 model years) with the LGM values, then run from this baseline for a further 50,000 years, with all changes from LGM values to modern values conservatively assumed to occur progressively over a 10 ka deglacial period, *i.e.* assuming a monotonic climate transition. A series of sensitivity tests described in the Supplementary data demonstrate that the results described below are robust to changes in parameterisation.

6.1. Box model results

When the prescribed changes (Table 2, Fig. 10) are imposed on the model-ocean, BSi production and dissolution adjust on the timescale of ocean mixing (1000 years) to maintain steady-state and keep the sedimentation of BSi equal to the total DSi inputs. Because of this, from the LGM to the modern day, the residence time of DSi, BSi production and dissolution fluxes, preservation efficiency and DSi concentrations were all relatively invariant. Fig. 13a–b shows the change in modelled DSi concentrations from each LGM iteration to a modern day value. These small changes observed, despite relatively large changes to the input fluxes, demonstrate a relative insensitivity of the marine Si cycle to perturbations. Feedbacks between production and dissolution act to ensure that the total inventory of Si in the ocean is relatively insensitive to input fluxes, a conclusion corroborated by previous work (Ridgwell et al., 2002).

In contrast, the δ^{30}Si of ocean DSi, and therefore the BSi produced from it, exhibits relatively large changes and takes multiple Si residence times (>40,000 years) to reach steady-state. The results presented in Fig. 13c shows the modelled change in δ^{30}Si of surface ocean DSi over a 50,000 yr simulation, standardised to the baseline ("LGM") value for each iteration. Note that because δ^{30}Si of BSi in the model is approximately a constant offset (*i.e.* −1.1‰) from the surface ocean DSi, and because we prescribe no fractionation during dissolution (Wetzel et al., 2014), the δ^{30}Si of BSi buried in marine sediments produces identical results. Likewise, including a fractionation during dissolution only affects the absolute δ^{30}Si values of the buried BSi, not the relative trends (see Supplementary data). The δ^{30}Si of deep-ocean DSi is similarly offset from the surface ocean DSi. In the 20,000 model years from LGM to present, δ^{30}Si of surface ocean DSi (or BSi) changes by between ~0.0 and 0.8‰, depending on the suite of input values chosen. This is a similar magnitude of total change, and at a similar rate, as measured in sedimentary BSi δ^{30}Si (Figs. 5 and 13). The results suggest that diatom δ^{30}Si does not necessarily reflect simply palaeoutilisation of DSi or the other factors invoked to explain downcore δ^{30}Si changes, including water-mass mixing or species-specific effects (Sutton et al., 2013). Instead, diatom δ^{30}Si since the LGM potentially represents both these factors *and* a variable δ^{30}Si of whole-ocean DSi.

Many of the parameter ensembles in Fig. 13 show little change, while some exhibit change in δ^{30}Si of up to 0.8‰. This differences are primarily due to the difference in importance the randomised parameter selection ascribes to the dust, SPM and SGD fluxes. Because the LGM values are defined relative to the modern values, the scenarios that call for values of dust, river sediment and groundwater fluxes towards the higher end of their possible values (Table 1) are especially sensitive to changes in their magnitude. Because these fluxes have distinctively low δ^{30}Si relative to river DSi, this implies that they could be key controls, and overlooked, controls on the ocean Si isotope budget, particularly in the glacial ocean. Yet these fluxes, together with the fluxes of DSi from seafloor alteration, remain understudied. Their magnitudes and isotopic compositions are often based on tenuous assumptions or extrapolations (Section 4). This is a knowledge gap that would be relatively simple to address, and could be a future research priority.

The intention of this exercise is to demonstrate the potential for whole ocean shifts in δ^{30}Si of DSi rapid enough to be relevant for interpretation of downcore δ^{30}Si-BSi over glacial–interglacial cycles. Many processes cannot be incorporated. For example, the model clearly cannot capture the complexities of ocean circulation and the spatial distribution of marine DSi and δ^{30}Si, which is also a contributory factor to downcore δ^{30}Si records (Hendry and Brzezinski, 2014). Future research could focus on better constraining the magnitude of fluctuations in Si fluxes and isotopic compositions, and on more mechanistic modelling of the ocean Si cycle. Nevertheless, with a reasonable range of input parameters, our synthesis suggests that the continental Si cycle is directly responsible for somewhere between 10 and 100% of the well-established LGM-modern trend observed in marine δ^{30}Si records (Fig. 10). Importantly, the higher frequency (*i.e.* sub-millennial) variability, which is a feature of many records (*e.g.* Hendry et al., 2014; Hendry et al., 2016; Horn et al., 2011) is *not* explainable by such a whole-ocean mechanism and must instead reflect internal ocean circulation or productivity dynamics.

6.2. Implications of whole-ocean changes in δ^{30}Si of DSi

Any whole-ocean, long-term trend in DSi δ^{30}Si driven by a variable continental cycle should be detrended from BSi records before interpretation of palaeo-nutrient utilisation. As an example of an application of δ^{30}Si of BSi to palaeoenvironmental questions that may require reinterpretation, we highlight the issue of explaining changes in G–IG atmospheric CO_2. An outstanding question in the geosciences is the cause of the *ca.* 100 ppmv lower CO_2 concentrations at the LGM relative to the preindustrial world (Sigman and Boyle, 2000). As the largest carbon reservoir at the Earth's surface, the ocean must be involved in sequestering atmospheric carbon in the deep ocean during glacial periods, although a compelling explanation has thus far been elusive. One body of work has focused on increased siliceous productivity as a contributory mechanism (*e.g.* Harrison, 2000; Brzezinski et al., 2002; Matsumoto et al., 2002; see Hendry and Brzezinski, 2014 for a review). Testing these hypotheses hinges on demonstrating whether, and where, siliceous productivity increased at the LGM, and so downcore silicon isotope records (Fig. 5) have been an important part of evaluating these hypotheses. Accounting for the existence of a whole-ocean trend would tend to lessen the difference in DSi utilisation recorded in diatom δ^{30}Si between the LGM and modern oceans. In general, this weakens support for the family of hypotheses that invoke biosiliceous

productivity shifts as a mechanism to alter atmospheric CO_2, though it should be noted that these hypotheses often require upwelling/circulation changes not resolvable at a global scale (Hendry and Brzezinski, 2014).

Quantifying such a whole ocean trend should be a research priority, and could be achieved *via* two approaches. First, *via* more sophisticated modelling approaches than that employed here, perhaps driven by reconstructions of river DSi δ^{30}Si inferred from river delta sedimentary records, improved dust deposition fields, etc. Second, *via* measurements of δ^{30}Si over a glacial–interglacial cycle from an archive/proxy sensitive to whole-ocean δ^{30}Si changes, but insensitive to changing DSi concentration or utilisation. We suggest such an archive may be found in deep-sea siliceous sponges between 30° and 60° N in the Pacific. Here, DSi concentrations are among the highest observed in the global ocean (~170 μM), owing to its location at the end of the thermohaline 'conveyor belt.' Water here is among the oldest in the global ocean, and has had the longest time to accumulate regenerated Si from dissolution of BSi produced in surface waters (Sarmiento and Gruber, 2006). Because the relationship between siliceous sponge silicon isotope fractionation and ambient DSi concentrations plateaus at high DSi (Section 2.3), sponges consistently bathed in ≫100 μM DSi should exhibit more-or-less constant fractionation, meaning any variability must reflect instead changes in δ^{30}Si of the ambient DSi.

7. Conclusions and future directions

The fluxes of Si from land to ocean provide the majority of Si for the ocean Si cycle, and they are variable in terms of both magnitude and isotopic composition. While the ~12 ka residence time of DSi in the modern ocean buffers it against external forcing on short timescales, persistent changes to the inputs over millennia could theoretically produce a whole-ocean δ^{30}Si shift. Indeed, the consistency among different ocean basins of changes in δ^{30}Si from biogenic silica (BSi) over the last few glacial cycles hints at such a shift. These records document somewhere between 0.5 and 1‰ variability between low glacial δ^{30}Si and higher interglacial δ^{30}Si, which is classically interpreted in terms of palaeoproductivity. Given that the majority of all Si in the ocean originally derives from the continents, at least some of this variation may in fact reflect varying continental processes. A glacial continental Si cycle likely differs from the modern one, and we suggest that many processes operating together can cumulatively lower the mean δ^{30}Si of Si entering the ocean by up to 1‰. These include alterations to the rate and style of continental silicate weathering, less efficient continental and estuarine filtering of river fluxes, and increased dust and groundwater fluxes. A simple box-model suggests that these changes, prescribed gradually over the entire deglaciation, can produce a whole ocean δ^{30}Si increase of comparable rate, magnitude and timing to that recorded in sedimentary BSi. If correct, this implies that we may need to revisit some interpretations of the glacial–ocean Si cycle. It also suggests that the continental Si cycle should not be neglected when interpreting pre-Quaternary long-term $\delta 30Si_{BSi}$ records from marine sediment records (Fontorbe et al., in review; Egan et al., 2013).

However, many aspects of the modern and the palaeo-Si cycles need to be better constrained. We still have only a poor understanding of the magnitude of most inputs of Si to the global ocean, and an even poorer understanding of the controls on their isotopic composition. Only when these are better understood will we be able to improve the estimates of the direction and magnitude of change over the glacial–interglacial cycles that characterise the late Quaternary. Future research could take a three-pronged approach of measuring, modelling and reconstructing:

1. *Measuring*. What are the modern inputs of DSi to the ocean? In particular, DSi from dissolution of aeolian dust and river sediment (particularly non-basaltic terrains), DSi from alteration of the oceanic crust (high and low temperature), and DSi from submarine groundwater discharge, all need better constraining. The role of estuaries and the coastal zone *sensu lato*, in scavenging river Si fluxes also needs better quantification.
2. *Modelling*. Especially of the potential role for both transient and persistent impacts of terrestrial vegetation on river Si fluxes, and more sophisticated ocean response models.
3. *Reconstructing*. Interrogation of well chosen archives can provide useful information. For example, detrital clays in sedimentary archives seem well placed to inform about continental weathering rates and intensities, while sponge spicules from some sites in the global ocean may document long-term whole-ocean δ^{30}Si changes.

Acknowledgements

This research was funded by the Knut & Alice Wallenberg Foundation and the Swedish Research Council (2010–4696 and 2014–5910). We thank Kate Hendry for helpful comments on an earlier version of this manuscript, and Paul Savage and an anonymous reviewer for providing useful, constructive and insightful reviews.

Appendix A. Supplementary data

Supplementary data to this article can be found online at http://dx.doi.org/10.1016/j.chemgeo.2016.01.020.

References

Abraham, K., Opfergelt, S., Fripiat, F., Cavagna, A.J., de Jong, J.T.M., Foley, S.F., Andre, L., Cardinal, D., 2008. delta Si-30 and delta Si-29 determinations on USGS BHVO-1 and BHVO-2 reference materials with a new configuration on a Nu plasma multi-collector ICP-MS. Geostand. Geoanal. Res. 32, 193–202.

Abelmann, A., Gersonde, R., Knorr, G., Zhang, X., Chapligin, B., Maier, E., Esper, O., Friedrichsen, H., Lohmann, G., Meyer, H., Tiedemann, R., 2015. The seasonal sea-ice zone in the glacial Southern Ocean as a carbon sink. Nat. Commun. 6.

Adkins, J.F., McIntyre, K., Schrag, D.P., 2002. The salinity, temperature, and δ^{18}O of the Glacial Deep Ocean. Science 298, 1769–1773.

Alfredsson, H., Hugelius, G., Clymans, W., Stadmark, J., Kuhry, P., Conley, D.J., 2015. Amorphous silica pools in permafrost soils of the Central Canadian Arctic and the potential impact of climate change. Biogeochemistry 1–19.

Alleman, L.Y., Cardinal, D., Cocquyt, C., Plisnier, P.D., Descy, J.P., Kimirei, I., Sinyinza, D., Andre, L., 2005. Silicon isotopic fractionation in Lake Tanganyika and its main tributaries. J. Great Lakes Res. 31, 509–519.

Aller, R.C., 2014. 8.11 — Sedimentary diagenesis, depositional environments, and benthic fluxes. In: Turekian, H.D.H.K. (Ed.), Treatise on Geochemistry, second ed. Elsevier, Oxford, pp. 293–334.

Allison, M., Kuehl, S., Martin, T., Hassan, A., 1998. Importance of flood-plain sedimentation for river sediment budgets and terrigenous input to the oceans: insights from the Brahmaputra–Jamuna River. Geology 26, 175–178.

Anderson, S.P., 2005. Glaciers show direct linkage between erosion rate and chemical weathering fluxes. Geomorphology 67, 147–157.

Armytage, R., Georg, R., Savage, P., Williams, H., Halliday, A., 2011. Silicon isotopes in meteorites and planetary core formation. Geochim. Cosmochim. Acta 75, 3662–3676.

Bagard, M.-L., Chabaux, F., Pokrovsky, O.S., Viers, J., Prokushkin, A.S., Stille, P., Rihs, S., Schmitt, A.-D., Dupré, B., 2011. Seasonal variability of element fluxes in two Central Siberian rivers draining high latitude permafrost dominated areas. Geochim. Cosmochim. Acta 75, 3335–3357.

Barão, L., Clymans, W., Vandevenne, F., Meire, P., Conley, D.J., Struyf, E., 2014. Pedogenic and biogenic alkaline-extracted silicon distributions along a temperate land-use gradient. Eur. J. Soil Sci. 65, 693–705.

Barão, L., Vandevenne, F., Clymans, W., Frings, P., Ragueneau, O., Meire, P., Conley, D.J., Struyf, E., 2015. Alkaline-extractable silicon from land to ocean: a challenge for biogenic silicon determination. Limnol. Oceanogr. Methods 13, 329–344.

Basile-Doelsch, I., Meunier, J.D., Parron, C., 2005. Another continental pool in the terrestrial silicon cycle. Nature 433, 399–402.

Bern, C.R., Brzezinski, M.A., Beucher, C., Ziegler, K., Chadwick, O.A., 2010. Weathering, dust, and biocycling effects on soil silicon isotope ratios. Geochim. Cosmochim. Acta 74, 876–889.

Bernard, C.Y., Durr, H.H., Heinze, C., Segschneider, J., Maier-Reimer, E., 2011. Contribution of riverine nutrients to the silicon biogeochemistry of the global ocean — a model study. Biogeosciences 8, 551–564.

Bernard, C.Y., Laruelle, G.G., Slomp, C.P., Heinze, C., 2010. Impact of changes in river fluxes of silica on the global marine silicon cycle: a model comparison. Biogeosciences 7, 441–453.

Berner, R.A., Caldeira, K., 1997. The need for mass balance and feedback in the geochemical carbon cycle. Geology 25, 955–956.

Beucher, C.P., Brzezinski, M.A., Crosta, X., 2007. Silicic acid dynamics in the glacial sub-Antarctic: implications for the silicic acid leakage hypothesis. Glob. Biogeochem. Cycles 21.

Beucher, C.P., Brzezinski, M.A., Jones, J.L., 2008. Sources and biological fractionation of silicon isotopes in the Eastern Equatorial Pacific. Geochim. Cosmochim. Acta 72, 3063–3073.
Beusen, A.H.W., Bouwman, A.F., Dürr, H.H., Dekkers, A.L.M., Hartmann, J., 2009. Global patterns of dissolved silica export to the coastal zone: results from a spatially explicit global model. Glob. Biogeochem. Cycles 23, GB0A02.
Bien, G., Contois, D., Thomas, W., 1958. The removal of soluble silica from fresh water entering the sea. Geochim. Cosmochim. Acta 14, 35–54.
Billen, G., Lancelot, C., Meybeck, M., Mantoura, R., Martin, J.-M., Wollast, R., 1991. N, P and Si retention along the aquatic continuum from land to ocean. Ocean Margin Processes in Global Change 1. John Wiley & Sons, pp. 19–44.
Birke, M., Reimann, C., Demetriades, A., Rauch, U., Lorenz, H., Harazim, B., Glatte, W., 2010. Determination of major and trace elements in European bottled mineral water — analytical methods. J. Geochem. Explor. 107, 217–226.
Blecker, S.W., McCulley, R.L., Chadwick, O.A., Kelly, E.F., 2006. Biologic cycling of silica across a grassland bioclimosequence. Glob. Biogeochem. Cycles 20, GB3023.
Blöthe, J.H., Korup, O., 2013. Millennial lag times in the Himalayan sediment routing system. Earth Planet. Sci. Lett. 382, 38–46.
Blum, M.D., Törnqvist, T.E., 2000. Fluvial responses to climate and sea-level change: a review and look forward. Sedimentology 47, 2–48.
Bouchez, J., Gaillardet, J., von Blanckenburg, F., 2014. Weathering intensity in lowland river basins: from the Andes to the Amazon mouth. Procedia Earth Planet. Sci. 10, 280–286.
Bouchez, J., von Blanckenburg, F., Schuessler, J.A., 2013. Modeling novel stable isotope ratios in the weathering zone. Am. J. Sci. 313, 267–308.
Bouwman, A.F., Bierkens, M.F.P., Griffioen, J., Hefting, M.M., Middelburg, J.J., Middelkoop, H., Slomp, C.P., 2013. Nutrient dynamics, transfer and retention along the aquatic continuum from land to ocean: towards integration of ecological and biogeochemical models. Biogeosciences 10, 1–22.
Broecker, W., Peng, T., 1982. Tracers in the sea. Lamont-Doherty Geol. Obs., Palisades, NY (690 pp.).
Brzezinski, M.A., Pride, C.J., Franck, V.M., Sigman, D.M., Sarmiento, J.L., Matsumoto, K., Gruber, N., Rau, G.H., Coale, K.H., 2002. A switch from $Si(OH)(4)$ to NO_3^- depletion in the glacial Southern Ocean. Geophys. Res. Lett. 29.
Burnett, W.C., Aggarwal, P.K., Aureli, A., Bokuniewicz, H., Cable, J.E., Charette, M.A., Kontar, E., Krupa, S., Kulkarni, K.M., Loveless, A., Moore, W.S., Oberdorfer, J.A., Oliveira, J., Ozyurt, N., Povinec, P., Privitera, A.M.G., Rajar, R., Ramessur, R.T., Scholten, J., Stieglitz, T., Taniguchi, M., Turner, J.V., 2006. Quantifying submarine groundwater discharge in the coastal zone via multiple methods. Sci. Total Environ. 367, 498–543.
Carbonnel, V., Vanderborght, J.-P., Lionard, M., Chou, L., 2013. Diatoms, silicic acid and biogenic silica dynamics along the salinity gradient of the Scheldt estuary (Belgium/The Netherlands). Biogeochemistry 113, 657–682.
Cardinal, D., Gaillardet, J., Hughes, H.J., Opfergelt, S., André, L., 2010. Contrasting silicon isotope signatures in rivers from the Congo Basin and the specific behaviour of organic-rich waters. Geophys. Res. Lett. 37, L12403.
Cardinal, D., Savoye, N., Trull, T.W., Dehairs, F., Kopczynska, E.E., Fripiat, F., Tison, J.L., Andre, L., 2007. Silicon isotopes in spring Southern Ocean diatoms: large zonal changes despite homogeneity among size fractions. Mar. Chem. 106, 46–62.
Cardinal, D., Alleman, L.Y., Dehairs, F., Savoye, N., Trull, T.W., André, L., 2005. Relevance of silicon isotopes to Si-nutrient utilization and Si-source assessment in Antarctic waters. Glob. Biogeochem. Cycles 19, GB2007.
Carey, J.C., Fulweiler, R.W., 2012. The terrestrial silica pump. PLoS One 7, e52932.
Cary, L., Alexandre, A., Meunier, J.D., Boeglin, J.L., Braun, J.J., 2005. Contribution of phytoliths to the suspended load of biogenic silica in the Nyong basin rivers (Cameroon). Biogeochemistry 74, 101–114.
Chakrabarti, R., Jacobsen, S.B., 2010. Silicon isotopes in the inner solar system: implications for core formation, solar nebular processes and partial melting. Geochim. Cosmochim. Acta 74, 6921–6933.
Chou, L., Wollast, R., 2006. Estuarine silicon dynamics. In: Ittekkot, D., Unger, C., Humborg, C., Tac An, N. (Eds.), The Silicon Cycle: Human Perturbations and Impacts on Aquatic Systems. Scope vol. 66, pp. 93–120.
Clarke, A., 1924. Data of Geochemistry. fifth ed. USGS, Washington (841 pp.).
Clift, P., Giosan, L., 2014. Sediment fluxes and buffering in the post-glacial Indus Basin. Basin Res. 26, 369–386.
Clymans, W., Struyf, E., Govers, G., Vandevenne, F., Conley, D.J., 2011. Anthropogenic impact on biogenic Si pools in temperate soils. Biogeosciences 8, 2281–2293.
Cockerton, H.E., Street-Perrott, F.A., Leng, M.J., Barker, P.A., Horstwood, M.S.A., Pashley, V., 2013. Stable-isotope (H, O, and Si) evidence for seasonal variations in hydrology and Si cycling from modern waters in the Nile Basin: implications for interpreting the Quaternary record. Quat. Sci. Rev. 66, 4–21.
Cockerton, H.E., Street-Perrott, F.A., Barker, P.A., Leng, M.J., Sloane, H.J., Ficken, K.J., 2015. Orbital forcing of glacial/interglacial variations in chemical weathering and silicon cycling within the upper White Nile basin, East Africa: stable-isotope and biomarker evidence from Lakes Victoria and Edward. Quat. Sci. Rev. 130, 57–71.
Colman, S.M., Bratton, J.F., 2003. Anthropogenically induced changes in sediment and biogenic silica fluxes in Chesapeake Bay. Geology 31, 71–74.
Conley, D.J., 1997. Riverine contribution of biogenic silica to the oceanic silica budget. Limnol. Oceanogr. 42, 774–777.
Conley, D.J., 2002. Terrestrial ecosystems and the global biogeochemical silica cycle. Glob. Biogeochem. Cycles 16, 1121.
Conley, D.J., Likens, G.E., Buso, D.C., Saccone, L., Bailey, S.W., Johnson, C.E., 2008. Deforestation causes increased dissolved silicate losses in the Hubbard Brook Experimental Forest. Glob. Chang. Biol. 14, 2548–2554.
Conley, D.J., Malone, T.C., 1992. The annual cycle of dissolved silicate in Chesapeake Bay: implications for the production and fate of phytoplankton biomass. Mar. Ecol. Prog. Ser. 81, 121–128.
Conley, D.J., Carey, J.C., 2015. Biogeochemistry: silica cycling over geologic time. Nat. Geosci. 8, 431–432.
Cornelis, J.T., Weis, D., Lavkulich, L., Vermeire, M.-L., Delvaux, B., Barling, J., 2014. Silicon isotopes record dissolution and re-precipitation of pedogenic clay minerals in a podzolic soil chronosequence. Geoderma 235–236, 19–29.
Cornelis, J.T., Delvaux, B., Cardinal, D., Andre, L., Ranger, J., Opfergelt, S., 2010. Tracing mechanisms controlling the release of dissolved silicon in forest soil solutions using Si isotopes and Ge/Si ratios. Geochim. Cosmochim. Acta 74, 3913–3924.
Cornelis, J.T., Delvaux, B., Georg, R.B., Lucas, Y., Ranger, J., Opfergelt, S., 2011. Tracing the origin of dissolved silicon transferred from various soil–plant systems towards rivers: a review. Biogeosciences 8, 89–112.
Dai, A., Trenberth, K.E., 2002. Estimates of freshwater discharge from continents: latitudinal and seasonal variations. J. Hydrometeorol. 3, 660–687.
Davis, S.N., 1964. Silica in streams and ground water. Am. J. Sci. 262, 870–891.
De La Rocha, C.L., 2003. Silicon isotope fractionation by marine sponges and the reconstruction of the silicon isotope composition of ancient deep water. Geology 31, 423–426.
De La Rocha, C.L., 2006. The biological pump. Oceans Mar. Geochem. 6, 83–112.
De La Rocha, C.L., Bickle, M.J., 2005. Sensitivity of silicon isotopes to whole-ocean changes in the silica cycle. Mar. Geol. 217, 267–282.
De La Rocha, C.L., Brzezinski, M.A., DeNiro, M.J., 1997. Fractionation of silicon isotopes by marine diatoms during biogenic silica formation. Geochim. Cosmochim. Acta 61, 5051–5056.
De La Rocha, C.L., Brzezinski, M.A., DeNiro, M.J., 2000. A first look at the distribution of the stable isotopes of silicon in natural waters. Geochim. Cosmochim. Acta 64, 2467–2477.
De La Rocha, C.L., Brzezinski, M.A., DeNiro, M.J., Shemesh, A., 1998. Silicon-isotope composition of diatoms as an indicator of past oceanic change. Nature 395, 680–683.
De La Rocha, C.L., Bescont, P., Croguennoc, A., Ponzevera, E., 2011. The silicon isotopic composition of surface waters in the Atlantic and Indian sectors of the Southern Ocean. Geochim. Cosmochim. Acta 75, 5283–5295.
de Souza, G.F., Reynolds, B.C., Rickli, J., Frank, M., Saito, M.A., Gerringa, L.J.A., Bourdon, B., 2012. Southern Ocean control of silicon stable isotope distribution in the deep Atlantic Ocean. Glob. Biogeochem. Cycles 26, GB2035.
de Souza, G.F., Slater, R.D., Dunne, J.P., Sarmiento, J.L., 2014. Deconvolving the controls on the deep ocean's silicon stable isotope distribution. Earth Planet. Sci. Lett. 398, 66–76.
Delstanche, S., Opfergelt, S., Cardinal, D., Elsass, F., André, L., Delvaux, B., 2009. Silicon isotopic fractionation during adsorption of aqueous monosilicic acid onto iron oxide. Geochim. Cosmochim. Acta 73, 923–934.
Delvaux, C., Cardinal, D., Carbonnel, V., Chou, L., Hughes, H.J., André, L., 2013. Controls on riverine $\delta^{30}Si$ signatures in a temperate watershed under high anthropogenic pressure (Scheldt — Belgium). J. Mar. Syst. 128, 40–51.
Demarest, M.S., Brzezinski, M.A., Beucher, C.P., 2009. Fractionation of silicon isotopes during biogenic silica dissolution. Geochim. Cosmochim. Acta 73, 5572–5583.
DeMaster, D.J., 1981. The supply and accumulation of silica in the marine-environment. Geochim. Cosmochim. Acta 45, 1715–1732.
DeMaster, D.J., 2002. The accumulation and cycling of biogenic silica in the Southern Ocean: revisiting the marine silica budget. Deep-Sea Res. II Top. Stud. Oceanogr. 49, 3155–3167.
DePaolo, D.J., 2011. Surface kinetic model for isotopic and trace element fractionation during precipitation of calcite from aqueous solutions. Geochim. Cosmochim. Acta 75, 1039–1056.
Derry, L.A., Kurtz, A.C., Ziegler, K., Chadwick, O.A., 2005. Biological control of terrestrial silica cycling and export fluxes to watersheds. Nature 433, 728–731.
Ding, T., Jiang, M.S., Wan, D., Li, Y., Li, J., Song, H., Liu, Z., Yao, X., 1996. Silicon Isotope Geochemistry. Geological Publishing House, Beijing, China (125 pp.).
Ding, T., Wan, D., Bai, R., Zhang, Z., Shen, Y., Meng, R., 2005a. Silicon isotope abundance ratios and atomic weights of NBS-28 and other reference materials. Geochim. Cosmochim. Acta 69, 5487–5494.
Ding, T., Wan, D., Wang, C., Zhang, F., 2004. Silicon isotope compositions of dissolved silicon and suspended matter in the Yangtze River, China. Geochim. Cosmochim. Acta 68, 205–216.
Ding, T.P., Gao, J.F., Tian, S.H., Wang, H.B., Li, M., 2011. Silicon isotopic composition of dissolved silicon and suspended particulate matter in the Yellow River, China, with implications for the global silicon cycle. Geochim. Cosmochim. Acta 75, 6672–6689.
Ding, T.P., Ma, G.R., Shui, M.X., Wan, D.F., Li, R.H., 2005b. Silicon isotope study on rice plants from the Zhejiang Province, China. Chem. Geol. 218, 41–50.
Ding, T.P., Tian, S.H., Sun, L., Wu, L.H., Zhou, J.X., Chen, Z.Y., 2008. Silicon isotope fractionation between rice plants and nutrient solution and its significance to the study of the silicon cycle. Geochim. Cosmochim. Acta 72, 5600–5615.
Dosseto, A., Vigier, N., Joannes-Boyau, R., Moffat, I., Singh, T., Srivastava, P., 2015. Rapid response of silicate weathering rates to climate change in the Himalaya. Geochem. Perspect. Lett. 1, 10–19.
Dosseto, A., Hesse, P., Maher, K., Fryirs, K., Turner, S., 2010. Climatic and vegetation control on sediment dynamics during the last glacial cycle. Geology 38, 395–398.
Douthitt, C.B., 1982. The geochemistry of the stable isotopes of silicon. Geochim. Cosmochim. Acta 46, 1449–1458.
Dowling, C.B., Poreda, R.J., Basu, A.R., 2003. The groundwater geochemistry of the Bengal Basin: weathering, chemsorption, and trace metal flux to the oceans. Geochim. Cosmochim. Acta 67, 2117–2136.
Duce, R.A., Liss, P.S., Merrill, J.T., Atlas, E.L., Buat-Menard, P., Hicks, B.B., Miller, J.M., Prospero, J.M., Arimoto, R., Church, T.M., Ellis, W., Galloway, J.N., Hansen, L., Jickells, T.D., Knap, A.H., Reinhardt, K.H., Schneider, B., Soudine, A., Tokos, J.J., Tsunogai, S., Wollast, R., Zhou, M., 1991. The atmospheric input of trace species to the world ocean. Glob. Biogeochem. Cycles 5, 193–259.

Dupré, B., Dessert, C., Oliva, P., Goddéris, Y., Viers, J., François, L., Millot, R., Gaillardet, J., 2003. Rivers, chemical weathering and Earth's climate. Compt. Rendus Geosci. 335, 1141–1160.

Dupré, B., Gaillardet, J., Rousseau, D., Allègre, C.J., 1996. Major and trace elements of river-borne material: the Congo Basin. Geochim. Cosmochim. Acta 60, 1301–1321.

Dupuis, R., Benoit, M., Nardin, E., Méheut, M., 2015. Fractionation of silicon isotopes in liquids: the importance of configurational disorder. Chem. Geol. 396, 239–254.

Dürr, H.H., Laruelle, G.G., van Kempen, C.M., Slomp, C.P., Meybeck, M., Middelkoop, H., 2011a. Worldwide typology of nearshore coastal systems: defining the estuarine filter of river inputs to the oceans. Estuar. Coasts 34, 441–458.

Dürr, H.H., Meybeck, M., Hartmann, J., Laruelle, G.G., Roubeix, V., 2011b. Global spatial distribution of natural riverine silica inputs to the coastal zone. Biogeosciences 8, 597–620.

Egan, K.E., Rickaby, R.E.M., Leng, M.J., Hendry, K.R., Hermoso, M., Sloane, H.J., Bostock, H., Halliday, A.N., 2012. Diatom silicon isotopes as a proxy for silicic acid utilisation: a Southern Ocean core top calibration. Geochim. Cosmochim. Acta 96, 174–192.

Egan, K.E., Rickaby, R.E.M., Hendry, K.R., Halliday, A.N., 2013. Opening the gateways for diatoms primes Earth for Antarctic glaciation. Earth Planet. Sci. Lett. 375, 34–43.

Egge, J.K., Asknes, D.L., 1992. Silicate as regulating nutrient in phytoplankton competition. Mar. Ecol. Prog. Ser. 83, 281–289.

Ehlert, C., Grasse, P., Frank, M., 2013. Changes in silicate utilisation and upwelling intensity off Peru since the Last Glacial Maximum—insights from silicon and neodymium isotopes. Quat. Sci. Rev. 72, 18–35.

Ellwood, M.J., Wille, M., Maher, W., 2010. Glacial silicic acid concentrations in the Southern Ocean. Science 330, 1088–1091.

Engelstaedter, S., Tegen, I., Washington, R., 2006. North African dust emissions and transport. Earth Sci. Rev. 79, 73–100.

Engström, E., 2009. Fractionation of the stable silicon isotopes studied using MC-ICP-MS. Department of Chemical Engineering and Geosciences. Luleå University of Technology, Luleå.

Engström, E., Rodushkin, I., Ingri, J., Baxter, D.C., Ecke, F., Osterlund, H., Ohlander, B., 2010. Temporal isotopic variations of dissolved silicon in a pristine boreal river. Chem. Geol. 271, 142–152.

Engström, E., Rodushkin, I., Ohlander, B., Ingri, J., Baxter, D.C., 2008. Silicon isotopic composition of boreal forest vegetation in Northern Sweden. Chem. Geol. 257, 250–259.

Epstein, E., 1999. Silicon. Annu. Rev. Plant Physiol. Plant Mol. Biol. 50, 641–664.

Fitoussi, C., Bourdon, B., 2012. Silicon isotope evidence against an enstatite chondrite Earth. Science 335, 1477–1480.

Fitoussi, C., Bourdon, B., Kleine, T., Oberli, F., Reynolds, B.C., 2009. Si isotope systematics of meteorites and terrestrial peridotites: implications for Mg/Si fractionation in the solar nebula and for Si in the Earth's core. Earth Planet. Sci. Lett. 287, 77–85.

Fontorbe, G., De La Rocha, C.L., Chapman, H.J., Bickle, M.J., 2013. The silicon isotopic composition of the Ganges and its tributaries. Earth Planet. Sci. Lett. 381, 21–30.

Fontorbe, G., Frings, P.J., De La Rocha, C.L., Hendry, K.R., Conley, D., 2016. A silicon depleted North Atlantic since the Palaeogene: evidence from sponge and radiolarian silicon isotopes. Earth Planet. Sci. Lett. (in review).

Foster, G.L., Vance, D., 2006. Negligible glacial–interglacial variation in continental chemical weathering rates. Nature 444, 918–921.

Frings, P., Clymans, W., Jeppesen, E., Lauridsen, T., Struyf, E., Conley, D., 2014a. Lack of steady-state in the global biogeochemical Si cycle: emerging evidence from lake Si sequestration. Biogeochemistry 117, 255–277.

Frings, P.J., 2014. Integrating Fluvial Processes into the Global Si Cycle. Department of Geology. Lund University, Lund, p. 161.

Frings, P.J., Clymans, W., Conley, D.J., 2014b. Amorphous silica transport in the Ganges Basin: implications for Si delivery to the oceans. Procedia Earth Planet. Sci. 10, 271–274.

Frings, P.J., Clymans, W., Fontorbe, G., Gray, W., Chakrapani, G.J., Conley, D.J., De La Rocha, C.L., 2015. Silicate weathering in the Ganges alluvial plain. Earth Planet. Sci. Lett. http://dx.doi.org/10.1016/j.epsl.2015.06.049.

Frings, P.J., De La Rocha, C., Struyf, E., van Pelt, D., Schoelynck, J., Hudson, M.M., Gondwe, M.J., Wolski, P., Mosimane, K., Gray, W., Schaller, J., Conley, D.J., 2014c. Tracing silicon cycling in the Okavango Delta, a sub-tropical flood-pulse wetland using silicon isotopes. Geochim. Cosmochim. Acta 142, 132–148.

Fripiat, F., Cavagna, A.-J., Savoye, N., Dehairs, F., André, L., Cardinal, D., 2011. Isotopic constraints on the Si-biogeochemical cycle of the Antarctic zone in the Kerguelen area (KEOPS). Mar. Chem. 123, 11–22.

Fulweiler, R.W., Nixon, S.W., 2005. Terrestrial vegetation and the seasonal cycle of dissolved silica in a southern New England coastal river. Biogeochemistry 74, 115–130.

Gaillardet, J., Dupre, B., Allegre, C.J., Négrel, P., 1997. Chemical and physical denudation in the Amazon River Basin. Chem. Geol. 142, 141–173.

Gehlen, M., Heinze, C., Maier-Reimer, E., Measures, C., 2003. Coupled Al–Si geochemistry in an ocean general circulation model: a tool for the validation of oceanic dust deposition fields? Glob. Biogeochem. Cycles 17.

Geilert, S., Vroon, P.Z., Roerdink, D.L., Cappellen, P.V., van Bergen, M.J., 2014. Silicon isotope fractionation during abiotic silica precipitation at low temperatures: inferences from flow-through experiments. Geochim. Cosmochim. Acta 142, 95–114.

Geilert, S., Vroon, P.Z., Keller, N.S., Gudbrandsson, S., Stefánsson, A., van Bergen, M.J., 2015. Silicon isotope fractionation during silica precipitation from hot-spring waters: evidence from the Geysir geothermal field, Iceland. Geochim. Cosmochim. Acta 164, 403–427.

Georg, R.B., Reynolds, B.C., Frank, M., Halliday, A.N., 2006. Mechanisms controlling the silicon isotopic compositions of river waters. Earth Planet. Sci. Lett. 249, 290–306.

Georg, R.B., Reynolds, B.C., West, A.J., Burton, K.W., Halliday, A.N., 2007a. Silicon isotope variations accompanying basalt weathering in Iceland. Earth Planet. Sci. Lett. 261, 476–490.

Georg, R.B., Halliday, A.N., Schauble, E.A., Reynolds, B.C., 2007b. Silicon in the Earth's core. Nature 447, 1102–1106.

Georg, R.B., West, A.J., Basu, A.R., Halliday, A.N., 2009a. Silicon fluxes and isotope composition of direct groundwater discharge into the Bay of Bengal and the effect on the global ocean silicon isotope budget. Earth Planet. Sci. Lett. 283, 67–74.

Georg, R.B., Zhu, C., Reynolds, B.C., Halliday, A.N., 2009b. Stable silicon isotopes of groundwater, feldspars, and clay coatings in the Navajo Sandstone aquifer, Black Mesa, Arizona, USA. Geochim. Cosmochim. Acta 73, 2229–2241.

Gibbs, M.T., Kump, L.R., 1994. Global chemical erosion during the last glacial maximum and the present — sensitivity to changes in lithology and hydrology. Paleoceanography 9, 529–543.

Gislason, S.R., Oelkers, E.H., Snorrason, Á., 2006. Role of river-suspended material in the global carbon cycle. Geology 34, 49–52.

Gouretski, V., Koltermann, K.P., 2004. WOCE global hydrographic climatology. Ber. BSH 35, 1–52.

Griffiths, J.D., Barker, S., Hendry, K.R., Thornalley, D.J.R., van de Flierdt, T., Hall, I.R., Anderson, R.F., 2013. Evidence of silicic acid leakage to the tropical Atlantic via Antarctic Intermediate Water during Marine Isotope Stage 4. Paleoceanography 28, 307–318.

Guerzoni, S., Molinaroli, E., Rossini, P., Rampazzo, G., Quarantotto, G., De Falco, G., Cristini, S., 1999. Role of desert aerosol in metal fluxes in the Mediterranean area. Chemosphere 39, 229–246.

Guntzer, F., Keller, C., Meunier, J.-D., 2012. Benefits of plant silicon for crops: a review. Agron. Sustain. Dev. 32, 201–213.

Han, Q., Moore, J.K., Zender, C., Measures, C., Hydes, D., 2008. Constraining oceanic dust deposition using surface ocean dissolved Al. Glob. Biogeochem. Cycles 22.

Harrison, J.A., Frings, P.J., Beusen, A.H.W., Conley, D.J., McCrackin, M.L., 2012. Global importance, patterns, and controls of dissolved silica retention in lakes and reservoirs. Glob. Biogeochem. Cycles 26, GB2037.

Harrison, K.G., 2000. Role of increased marine silica input on paleo-pCO_2 levels. Paleoceanography 15, 292–298.

Harrison, S.P., Prentice, C.I., 2003. Climate and CO_2 controls on global vegetation distribution at the last glacial maximum: analysis based on palaeovegetation data, biome modelling and palaeoclimate simulations. Glob. Chang. Biol. 9, 983–1004.

Hendry, K.R., Brzezinski, M.A., 2014. Using silicon isotopes to understand the role of the Southern Ocean in modern and ancient biogeochemistry and climate. Quat. Sci. Rev. 89, 13–26.

Hendry, K.R., Robinson, L.F., 2012. The relationship between silicon isotope fractionation in sponges and silicic acid concentration: modern and core-top studies of biogenic opal. Geochim. Cosmochim. Acta 81, 1–12.

Hendry, K.R., Georg, R.B., Rickaby, R.E.M., Robinson, L.F., Halliday, A.N., 2010. Deep ocean nutrients during the Last Glacial Maximum deduced from sponge silicon isotopic compositions. Earth Planet. Sci. Lett. 292, 290–300.

Hendry, K.R., Robinson, L.F., Meredith, M.P., Mulitza, S., Chiessi, C.M., Arz, H., 2012. Abrupt changes in high-latitude nutrient supply to the Atlantic during the last glacial cycle. Geology 40, 123–126.

Hendry, K.R., Robinson, L.F., McManus, J.F., Hays, J.D., 2014. Silicon isotopes indicate enhanced carbon export efficiency in the North Atlantic during deglaciation. Nat. Commun. 5.

Hodson, M.J., Parker, A.G., Leng, M.J., Sloane, H.J., 2008. Silicon, oxygen and carbon isotope composition of wheat (*Triticum aestivum* L.) phytoliths: implications for palaeoecology and archaeology. J. Quat. Sci. 23, 331–339.

Holland, H.D., 2005. Sea level, sediments and the composition of seawater. Am. J. Sci. 305, 220–239.

Horn, M.G., Beucher, C.P., Robinson, R.S., Brzezinski, M.A., 2011. Southern Ocean nitrogen and silicon dynamics during the last deglaciation. Earth Planet. Sci. Lett. 310, 334–339.

Hughes, H.J., Bouillon, S., André, L., Cardinal, D., 2012. The effects of weathering variability and anthropogenic pressures upon silicon cycling in an intertropical watershed (Tana River, Kenya). Chem. Geol. 308–309, 18–25.

Hughes, H.J., Sondag, F., Cocquyt, C., Laraque, A., Pandi, A., Andre, L., Cardinal, D., 2011. Effect of seasonal biogenic silica variations on dissolved silicon fluxes and isotopic signatures in the Congo River. Limnol. Oceanogr. 56, 551–561.

Hughes, H.J., Sondag, F., Santos, R.V., André, L., Cardinal, D., 2013. The riverine silicon isotope composition of the Amazon Basin. Geochim. Cosmochim. Acta 121, 637–651.

Hutchinson, G.E., 1957. A treatise on limnology. Georgraphy, Physics and Chemistry vol. 1. John Wiley & Sons.

Iler, R.K., 1979. Chemistry of Silica — Solubility, Polymerization, Colloid and Surface Properties and Biochemistry. John Wiley & Sons.

Jeandel, C., Oelkers, E.H., 2015. The influence of terrigenous particulate material dissolution on ocean chemistry and global element cycles. Chem. Geol. 395, 50–66.

Jeandel, C., Peucker-Ehrenbrink, B., Jones, M.T., Pearce, C.R., Oelkers, E.H., Godderis, Y., Lacan, F., Aumont, O., Arsouze, T., 2011. Ocean margins: the missing term in oceanic element budgets? EOS Trans. Am. Geophys. Union 92.

Jickells, T.D., An, Z.S., Andersen, K.K., Baker, A.R., Bergametti, G., Brooks, N., Cao, J.J., Boyd, P.W., Duce, R.A., Hunter, K.A., Kawahata, H., Kubilay, N., laRoche, J., Liss, P.S., Mahowald, N., Prospero, J.M., Ridgwell, A.J., Tegen, I., Torres, R., 2005. Global iron connections between desert dust, ocean biogeochemistry, and climate. Science 308, 67–71.

Johannes, R., 1980. Ecological significance of the submarine discharge of groundwater. Mar. Ecol. Prog. Ser. 3, 365–373.

Jones, I.W., Munhoven, G., Tranter, M., Huybrechts, P., Sharp, M.J., 2002. Modelled glacial and non-glacial HCO_3^-, Si and Ge fluxes since the LGM: little potential for impact on

atmospheric CO_2 concentrations and a potential proxy of continental chemical erosion, the marine Ge/Si ratio. Glob. Planet. Chang. 33, 139–153.
Jones, M.T., Gislason, S.R., Burton, K.W., Pearce, C.R., Mavromatis, V., Pogge von Strandmann, P.A.E., Oelkers, E.H., 2014. Quantifying the impact of riverine particulate dissolution in seawater on ocean chemistry. Earth Planet. Sci. Lett. 395, 91–100.
Jones, M.T., Pearce, C.R., Oelkers, E.H., 2012. An experimental study of the interaction of basaltic riverine particulate material and seawater. Geochim. Cosmochim. Acta 77, 108–120.
Jones, M.T., Pearce, C.R., Jeandel, C., Gislason, S.R., Eiriksdottir, E.S., Mavromatis, V., Oelkers, E.H., 2012. Riverine particulate material dissolution as a significant flux of strontium to the oceans. Earth and Planetary Science Letters 355 (356), 51–59.
Kennett, J.P., 1982. Marine Geology. Prentice-Hall, New Jersey (752 pp.).
Kettner, A.J., Syvitski, J.P.M., 2009. Predicting discharge and sediment flux of the Po River, Italy since the Last Glacial Maximum. Analogue and Numerical Modelling of Sedimentary Systems: From Understanding to Prediction. Wiley-Blackwell, pp. 171–189.
Knee, K.L., Paytan, A., 2011. Submarine groundwater discharge: a source of nutrients, metals, and pollutants to the Coastal Ocean. In: Wolanski, E., McLusky, D. (Eds.), Treatise on Estuarine and Coastal Science. Academic Press, Waltham, pp. 205–233.
Köster, J.R., Bol, R., Leng, M.J., Parker, A.G., Sloane, H.J., Ma, J.F., 2009. Effects of active silicon uptake by rice on ^{29}Si fractionation in various plant parts. Rapid Commun. Mass Spectrom. 23, 2398–2402.
Kump, L., Alley, R.B., 1994. Global chemical weathering on glacial time scales. Material Fluxes on the Surface of the Earth, pp. 46–60.
Lambeck, K., Rouby, H., Purcell, A., Sun, Y., Sambridge, M., 2014. Sea level and global ice volumes from the Last Glacial Maximum to the Holocene. Proc. Natl. Acad. Sci. 111, 15296–15303.
Land, M., Ingri, J., Öhlander, B., 1999. Past and present weathering rates in Northern Sweden. Appl. Geochem. 14, 761–774.
Laraque, A., Bricquet, J.P., Pandi, A., Olivry, J.C., 2009. A review of material transport by the Congo River and its tributaries. Hydrol. Process. 23, 3216–3224.
Laruelle, G.G., Roubeix, V., Sferratore, A., Brodherr, B., Ciuffa, D., Conley, D.J., Dürr, H.H., Garnier, J., Lancelot, C., Le Thi Phuong, Q., Meunier, J.D., Meybeck, M., Michalopoulos, P., Moriceau, B., Ní Longphuirt, S., Loucaides, S., Papush, L., Presti, M., Ragueneau, O., Regnier, P., Saccone, L., Slomp, C.P., Spiteri, C., Van Cappellen, P., 2009. Anthropogenic perturbations of the silicon cycle at the global scale: key role of the land-ocean transition. Glob. Biogeochem. Cycles 23, GB4031.
Lauerwald, R., Hartmann, J., Moosdorf, N., Dürr, H.H., Kempe, S., 2013. Retention of dissolved silica within the fluvial system of the conterminous USA. Biogeochemistry 112, 637–659.
Lehtimäki, M., Tallberg, P., Siipola, V., 2013. Seasonal dynamics of amorphous silica in Vantaa River Estuary. SILICON 5, 35–51.
Li, Y., Ding, T., Wan, D., 1995. Experimental study of silicon isotope dynamic fractionation and its application in geology. Chin. J. Geochem. 14, 212–219.
Li, Y.-H., 1988. Denudation rates of the Hawaiian islands by rivers and Groundwaters1. Pac. Sci. 42.
Livingstone, D.A., 1963. Chapter G: chemical composition of rivers and lakes. In: Fleischer, M. (Ed.), Data of Geochemistry. USGS, Washington.
Loucaides, S., Cappellen, P., Roubeix, V., Moriceau, B., Ragueneau, O., 2012. Controls on the recycling and preservation of biogenic silica from biomineralization to burial. SILICON 4, 7–22.
Loucaides, S., Michalopoulos, P., Presti, M., Koning, E., Behrends, T., Van Cappellen, P., 2010. Seawater-mediated interactions between diatomaceous silica and terrigenous sediments: results from long-term incubation experiments. Chem. Geol. 270, 68–79.
Loucaides, S., Van Cappellen, P., Behrends, T., 2008. Dissolution of biogenic silica from land to ocean: role of salinity and pH. Limnol. Oceanogr. 53, 1614–1621.
Lupker, M., France-Lanord, C., Galy, V., Lavé, J., Kudrass, H., 2013. Increasing chemical weathering in the Himalayan system since the Last Glacial Maximum. Earth Planet. Sci. Lett. 365, 243–252.
Mackenzie, F.T., Garrels, R.M., 1966. Chemical mass balance between rivers and oceans. Am. J. Sci. 264, 507–525.
Mackenzie, F.T., Kump, L.R., 1995. Reverse weathering, clay mineral formation, and oceanic element cycles. Science 270, 586–587.
Maier, E., Chapligin, B., Abelmann, A., Gersonde, R., Esper, O., Ren, J., Friedrichsen, H., Meyer, H., Tiedemann, R., 2013. Combined oxygen and silicon isotope analysis of diatom silica from a deglacial subarctic Pacific record. J. Quat. Sci. 28, 571–581.
Maring, H.B., Duce, R.A., 1987. The impact of atmospheric aerosols on trace metal chemistry in open ocean surface seawater, 1. aluminum. Earth Planet. Sci. Lett. 84, 381–392.
Maier, E., Méheust, M., Abelmann, A., Gersonde, R., Chapligin, B., Ren, J., Stein, R., Meyer, H., Tiedemann, R., 2015. Deglacial subarctic Pacific surface water hydrography and nutrient dynamics and links to North Atlantic climate variability and atmospheric CO2. Paleoceanography 30 2014PA002763.
Mariotti, A., Germon, J.C., Hubert, P., Kaiser, P., Letolle, R., Tardieux, A., Tardieux, P., 1981. Experimental determination of nitrogen kinetic isotope fractionation: some principles; illustration for the denitrification and nitrification processes. Plant Soil 62, 413–430.
Martin, J.H., 1990. Glacial–interglacial CO_2 change: the iron hypothesis. Paleoceanography 5, 1–13.
März, C., Meinhardt, A.K., Schnetger, B., Brumsack, H.J., 2015. Silica diagenesis and benthic fluxes in the Arctic Ocean. Mar. Chem. 171, 1–9.
Massey, F.P., Ennos, A.R., Hartley, S.E., 2006. Silica in grasses as a defence against insect herbivores: contrasting effects on folivores and a phloem feeder. J. Anim. Ecol. 75, 595–603.
Matsumoto, K., Sarmiento, J.L., Brzezinski, M.A., 2002. Silicic acid leakage from the Southern Ocean: a possible explanation for glacial atmospheric pCO(2). Glob. Biogeochem. Cycles 16.
Maynard, J.B., 1976. The long-term buffering of the oceans. Geochim. Cosmochim. Acta 40, 1523–1532.
Measures, C., Vink, S., 2000. On the use of dissolved aluminum in surface waters to estimate dust deposition to the ocean. Glob. Biogeochem. Cycles 14, 317–327.
Métivier, Gaudemer, 1999. Stability of output fluxes of large rivers in South and East Asia during the last 2 million years: implications on floodplain processes. Basin Res. 11, 293–303.
Meunier, J.-D., Braun, J.-J., Riotte, J., Kumar, C., Sekhar, M., 2011. Importance of weathering and human perturbations on the riverine transport of Si. Appl. Geochem. 26, S360–S362 (Supplement).
Meybeck, M., Vörösmarty, C., 2005. Fluvial filtering of land-to-ocean fluxes: from natural Holocene variations to Anthropocene. Compt. Rendus Geosci. 337, 107–123.
Michalopoulos, P., Aller, R.C., 1995. Rapid clay mineral formation in Amazon delta sediments — reverse weathering and oceanic elemental cycles. Science 270, 614–617.
Michalopoulos, P., Aller, R.C., 2004. Early diagenesis of biogenic silica in the Amazon delta: alteration, authigenic clay formation, and storage. Geochim. Cosmochim. Acta 68, 1061–1085.
Michalopoulos, P., Aller, R.C., Reeder, R.J., 2000. Conversion of diatoms to clays during early diagenesis in tropical, continental shelf muds. Geology 28, 1095–1098.
Milligan, A.J., Varela, D.E., Brzezinski, M.A., Morel, F., 2004. Dynamics of silicon metabolism and silicon isotopic discrimination in a marine diatom as a function of pCO(2). Limnol. Oceanogr. 49, 322–329.
Milliman, J.D., Boyle, E., 1975. Biological uptake of dissolved silica in the Amazon River estuary. Science 189, 995–997.
Milliman, J.D., Farnsworth, K.L., 2011. River Discharge to the Coastal Ocean: A Global Synthesis. Cambridge University Press, Cambridge.
Milliman, J.D., Meade, R.H., 1983. World-wide delivery of river sediment to the oceans. J. Geol. 91, 1–21.
Mokadem, F., Parkinson, I.J., Hathorne, E.C., Anand, P., Allen, J.T., Burton, K.W., 2015. High-precision radiogenic strontium isotope measurements of the modern and glacial ocean: limits on glacial–interglacial variations in continental weathering. Earth Planet. Sci. Lett. 415, 111–120.
Moore, W.S., 1996. Large groundwater inputs to coastal waters revealed by ^{226}Ra enrichments. Nature 380, 612–614.
Morin, G.P., Vigier, N., Verney-Carron, A., 2015. Enhanced dissolution of basaltic glass in brackish waters: impact on biogeochemical cycles. Earth Planet. Sci. Lett. 417, 1–8.
Muhs, D.R., 2013. The geologic records of dust in the Quaternary. Aeolian Res. 9, 3–48.
Munhoven, G., 2002. Glacial–interglacial changes of continental weathering: estimates of the related CO_2 and HCO_3^- flux variations and their uncertainties. Glob. Planet. Chang. 33, 155–176.
Nelson, D.M., Tréguer, P., Brzezinski, M.A., Leynaert, A., Quéguiner, B., 1995. Production and dissolution of biogenic silica in the ocean: revised global estimates, comparison with regional data and relationship to biogenic sedimentation. Glob. Biogeochem. Cycles 9, 359–372.
Oelkers, E.H., Gislason, S.R., Eiriksdottir, E.S., Jones, M., Pearce, C.R., Jeandel, C., 2011. The role of riverine particulate material on the global cycles of the elements. Appl. Geochem. 26, S365–S369 (Supplement).
Oelze, M., von Blanckenburg, F., Bouchez, J., Hoellen, D., Dietzel, M., 2015. The effect of Al on Si isotope fractionation investigated by silica precipitation experiments. Chem. Geol. 397, 94–105.
Oelze, M., von Blanckenburg, F., Hoellen, D., Dietzel, M., Bouchez, J., 2014. Si stable isotope fractionation during adsorption and the competition between kinetic and equilibrium isotope fractionation: implications for weathering systems. Chem. Geol. 380, 161–171.
Opfergelt, S., Burton, K.W., Pogge von Strandmann, P.A.E., Gislason, S.R., Halliday, A.N., 2013. Riverine silicon isotope variations in glaciated basaltic terrains: implications for the Si delivery to the ocean over glacial–interglacial intervals. Earth Planet. Sci. Lett. 369–370, 211–219.
Opfergelt, S., Cardinal, D., André, L., Delvigne, C., Bremond, L., Delvaux, B., 2010. Variations of δ^{30}Si and Ge/Si with weathering and biogenic input in tropical basaltic ash soils under monoculture. Geochim. Cosmochim. Acta 74, 225–240.
Opfergelt, S., Cardinal, D., Henriet, C., Draye, X., André, L., Delvaux, B., 2006. Silicon isotopic fractionation by banana (*Musa* spp.) grown in a continuous nutrient flow device. Plant Soil 285, 333–345.
Opfergelt, S., de Bournonville, G., Cardinal, D., André, L., Delstanche, S., Delvaux, B., 2009. Impact of soil weathering degree on silicon isotopic fractionation during adsorption onto iron oxides in basaltic ash soils, Cameroon. Geochim. Cosmochim. Acta 73, 7226–7240.
Opfergelt, S., Delmelle, P., 2012. Silicon isotopes and continental weathering processes: assessing controls on Si transfer to the ocean. Compt. Rendus Geosci. 344, 723–738.
Opfergelt, S., Eiriksdottir, E., Burton, K., Einarsson, A., Siebert, C., Gislason, S., Halliday, A., 2011. Quantifying the impact of freshwater diatom productivity on silicon isotopes and silicon fluxes: Lake Myvatn, Iceland. Earth Planet. Sci. Lett. 305, 73–82.
Opfergelt, S., Georg, R.B., Delvaux, B., Cabidoche, Y.M., Burton, K.W., Halliday, A.N., 2012. Silicon isotopes and the tracing of desilication in volcanic soil weathering sequences, Guadeloupe. Chem. Geol. 326–327, 113–122.
Panizzo, V., Crespin, J., Crosta, X., Shemesh, A., Massé, G., Yam, R., Mattielli, N., Cardinal, D., 2014. Sea ice diatom contributions to Holocene nutrient utilization in East Antarctica. Paleoceanography 29, 328–343.
Panizzo, V.N., Swann, G.E.A., Mackay, A.W., Vologina, E., Sturm, M., Pashley, V., Horstwood, M.S.A., 2016. Insights into the transfer of silicon isotopes into the sediment record. Biogeosciences 13, 147–157.

Pastuszak, M., Conley, D.J., Humborg, C., Witek, Z., Sitek, S., 2008. Silicon dynamics in the Oder estuary. Baltic Sea. Journal of Marine Systems 73, 250–262.
Pearce, C.R., Jones, M.T., Oelkers, E.H., Pradoux, C., Jeandel, C., 2013. he effect of particulate dissolution on the neodymium (Nd) isotope and Rare Earth Element (REE) composition of seawater. Earth and Planetary Science Letters 369 (370), 138–147.
Pichevin, L., Reynolds, B., Ganeshram, R., Cacho, I., Pena, L., Keefe, K., Ellam, R., 2009. Enhanced carbon pump inferred from relaxation of nutrient limitation in the glacial ocean. Nature 459, 1114–1117.
Pichevin, L., Ganeshram, R.S., Reynolds, B.C., Prahl, F., Pedersen, T.F., Thunell, R., McClymont, E.L., 2012. Silicic acid biogeochemistry in the Gulf of California: insights from sedimentary Si isotopes. Paleoceanography 27, PA2201.
Picouet, C., Dupré, B., Orange, D., Valladon, M., 2002. Major and trace element geochemistry in the upper Niger river (Mali): physical and chemical weathering rates and CO_2 consumption. Chem. Geol. 185, 93–124.
Pilon-Smits, E.A.H., Quinn, C.F., Tapken, W., Malagoli, M., Schiavon, M., 2009. Physiological functions of beneficial elements. Curr. Opin. Plant Biol. 12, 267–274.
Piperno, D.R., 2001. Phytoliths. In: Smol, J.P., Birks, H.J.B., Last, W.M. (Eds.), Tracking Environmental Change Using Lake SediментsTerrestrial, Algal and Siliceous Indicators volume 3. Kluwer, London, pp. 235–252.
Pogge von Strandmann, P.A., Burton, K.W., James, R.H., van Calsteren, P., Gíslason, S.R., Mokadem, F., 2006. Riverine behaviour of uranium and lithium isotopes in an actively glaciated basaltic terrain. Earth Planet. Sci. Lett. 251, 134–147.
Pogge von Strandmann, P.A.E., Burton, K.W., James, R.H., van Calsteren, P., Gislason, S.R., Sigfússon, B., 2008. The influence of weathering processes on riverine magnesium isotopes in a basaltic terrain. Earth Planet. Sci. Lett. 276, 187–197.
Pogge von Strandmann, P.A.E., Opfergelt, S., Lai, Y.-J., Sigfússon, B., Gislason, S.R., Burton, K.W., 2012. Lithium, magnesium and silicon isotope behaviour accompanying weathering in a basaltic soil and pore water profile in Iceland. Earth Planet. Sci. Lett. 339–340, 11–23.
Pogge von Strandmann, P.A.E., Porcelli, D., James, R.H., van Calsteren, P., Schaefer, B., Cartwright, I., Reynolds, B.C., Burton, K.W., 2014. Chemical weathering processes in the Great Artesian Basin: evidence from lithium and silicon isotopes. Earth Planet. Sci. Lett. 406, 24–36.
Pokrovsky, O.S., Reynolds, B.C., Prokushkin, A.S., Schott, J., Viers, J., 2013. Silicon isotope variations in Central Siberian rivers during basalt weathering in permafrost-dominated larch forests. Chem. Geol. 355, 103–116.
Presti, M., Michalopoulos, P., 2008. Estimating the contribution of the authigenic mineral component to the long-term reactive silica accumulation on the western shelf of the Mississippi River Delta. Cont. Shelf Res. 28, 823–838.
Prospero, J., Arimoto, R., 2008. Atmospheric transport and deposition of particulate material to the oceans. Encyclopedia of Ocean Sciences, pp. 248–257.
Qin, Y.-C., Weng, H.-X., Jin, H., Chen, J., Tian, R.-X., 2012. Estimation of authigenic alteration of biogenic and reactive silica in Pearl River estuarine sediments using wet-chemical digestion methods. Environ. Earth Sci. 65, 1855–1864.
Quinby-Hunt, M.S., Turehian, K.K., 1983. Distribution of elements in sea water. *EOS* Trans. Am. Geophys. Union 64, 130.
Ragueneau, O., Treguer, P., Leynaert, A., Anderson, R.F., Brzezinski, M.A., DeMaster, D.J., Dugdale, R.C., Dymond, J., Fischer, G., Francois, R., Heinze, C., Maier-Reimer, E., Martin-Jezequel, V., Nelson, D.M., Queguiner, B., 2000. A review of the Si cycle in the modem ocean: recent progress and missing gaps in the application of biogenic opal as a paleoproductivity proxy. Glob. Planet. Chang. 26, 317–365.
Reynolds, B.C., 2009. Modeling the modern marine delta Si-30 distribution. Glob. Biogeochem. Cycles 23.
Reynolds, B.C., Frank, M., Halliday, A.N., 2006. Silicon isotope fractionation during nutrient utilization in the North Pacific. Earth Planet. Sci. Lett. 244, 431–443.
Reynolds, J.H., Verhoogen, J., 1953. Natural variations in the isotopic constitution of silicon. Geochim. Cosmochim. Acta 3, 224–234.
Richter, F.M., Turekian, K.K., 1993. Simple models for the geochemical response of the ocean to climatic and tectonic forcing. Earth Planet. Sci. Lett. 119, 121–131.
Ridgwell, A.J., Watson, A.J., Archer, D.E., 2002. Modeling the response of the oceanic Si inventory to perturbation, and consequences for atmospheric CO_2. Glob. Biogeochem. Cycles 16.
Riebe, C.S., Kirchner, J.W., Finkel, R.C., 2003. Long-term rates of chemical weathering and physical erosion from cosmogenic nuclides and geochemical mass balance. Geochim. Cosmochim. Acta 67, 4411–4427.
Rodellas, V., Garcia-Orellana, J., Masqué, P., Feldman, M., Weinstein, Y., 2015. Submarine groundwater discharge as a major source of nutrients to the Mediterranean Sea. Proc. Natl. Acad. Sci. 12 (13), 3926–3930.
Roerdink, D.L., van den Boorn, S.H., Geilert, S., Vroon, P.Z., van Bergen, M.J., 2015. Experimental constraints on kinetic and equilibrium silicon isotope fractionation during the formation of non-biogenic chert deposits. Chem. Geol. 402, 40–51.
Rudnick, R.L., Gao, S., 2003. 3.01 — Composition of the continental crust. In: Holland, H.D., Turekian, K.K. (Eds.), Treatise on Geochemistry. Pergamon, Oxford, pp. 1–64.
Saccone, L., Conley, D.J., Koning, E., Sauer, D., Sommer, M., Kaczorek, D., Blecker, S.W., Kelly, E.F., 2007. Assessing the extraction and quantification of amorphous silica in soils of forest and grassland ecosystems. Eur. J. Soil Sci. 58, 1446–1459.
Sarmiento, J.L., Gruber, N., 2006. Ocean Biogeochemical Dynamics. PUP, Princeton (503 pp.).
Savage, P.S., Georg, R.B., Williams, H.M., Burton, K.W., Halliday, A.N., 2011. Silicon isotope fractionation during magmatic differentiation. Geochim. Cosmochim. Acta 75, 6124–6139.
Savage, P.S., Georg, R.B., Williams, H.M., Halliday, A.N., 2013. The silicon isotope composition of the upper continental crust. Geochim. Cosmochim. Acta 109, 384–399.
Schopka, H.H., Derry, L.A., 2012. Chemical weathering fluxes from volcanic islands and the importance of groundwater: the Hawaiian example. Earth Planet. Sci. Lett. 339, 67–78.
Schumm, S., 1993. River response to baselevel change: implications for sequence stratigraphy. J. Geol. 279–294.
Sigman, D.M., Boyle, E.A., 2000. Glacial/interglacial variations in atmospheric carbon dioxide. Nature 407, 859–869.
Slomp, C.P., Van Cappellen, P., 2004. Nutrient inputs to the coastal ocean through submarine groundwater discharge: controls and potential impact. J. Hydrol. 295, 64–86.
Sommer, M., Kaczorek, D., Kuzyakov, Y., Breuer, J., 2006. Silicon pools and fluxes in soils and landscapes — a review. J. Plant Nutr. Soil Sci. 169, 310–329.
Staudigel H. 2014. 4.16 — Chemical fluxes from hydrothermal alteration of the oceanic crust. In: H. D. H. K. Turekian (Ed.), Treatise on Geochemistry (Second edition). Elsevier, Oxford, pp. 583–606.
Steinhoefel, G., Breuer, J., von Blanckenburg, F., Horn, I., Kaczorek, D., Sommer, M., 2011. Micrometer silicon isotope diagnostics of soils by UV femtosecond laser ablation. Chem. Geol. 286, 280–289.
Street-Perrott, F.A., Barker, P.A., Leng, M.J., Sloane, H.J., Wooller, M.J., Ficken, K.J., Swain, D.L., 2008. Towards an understanding of late Quaternary variations in the continental biogeochemical cycle of silicon: multi-isotope and sediment-flux data for Lake Rutundu, Mt Kenya, East Africa, since 38 ka BP. J. Quat. Sci. 23, 375–387.
Struyf, E., Conley, D.J., 2012. Emerging understanding of the ecosystem silica filter. Biogeochemistry 107, 9–18.
Struyf, E., Mörth, C.-M., Humborg, C., Conley, D.J., 2010a. An enormous amorphous silica stock in boreal wetlands. J. Geophys. Res. Biogeosci. 115, G04008.
Struyf, E., Smis, A., Van Damme, S., Garnier, J., Govers, G., Van Wesemael, B., Conley, D.J., Batelaan, O., Frot, E., Clymans, W., Vandevenne, F., Lancelot, C., Goos, P., Meire, P., 2010b. Historical land use change has lowered terrestrial silica mobilization. Nat. Commun. 1, 129.
Struyf, E., Smis, A., Van Damme, S., Meire, P., Conley, D., 2009. The global biogeochemical silicon cycle. SILICON 1, 207–213.
Sun, X., Andersson, P., Humborg, C., Gustafsson, B., Conley, D.J., Crill, P., Mörth, C.-M., 2011. Climate dependent diatom production is preserved in biogenic Si isotope signatures. Biogeosciences 8, 3491–3499.
Sun, X., Andersson, P.S., Humborg, C., Pastuszak, M., Mörth, C.-M., 2013. Silicon isotope enrichment in diatoms during nutrient-limited blooms in a eutrophied river system. J. Geochem. Explor. 132, 173–180.
Sun, X., Olofsson, M., Andersson, P.S., Fry, B., Legrand, C., Humborg, C., Mörth, C.-M., 2014. Effects of growth and dissolution on the fractionation of silicon isotopes by estuarine diatoms. Geochim. Cosmochim. Acta 130, 156–166.
Sutton, J.N., Ellwood, M.J., Maher, W.A., Croot, P.L., 2010. Oceanic distribution of inorganic germanium relative to silicon: germanium discrimination by diatoms. Glob. Biogeochem. Cycles 24.
Sutton, J.N., Varela, D.E., Brzezinski, M.A., Beucher, C.P., 2013. Species-dependent silicon isotope fractionation by marine diatoms. Geochim. Cosmochim. Acta 104, 300–309.
Sutton, J.N., 2011. Germanium/silicon and silicon isotope fractionation by marine diatoms and sponges and utility as tracers of silicic acid utilization. Australian National University.
Swann, G.E.A., Leng, M.J., Juschus, O., Melles, M., Brigham-Grette, J., Sloane, H.J., 2010. A combined oxygen and silicon diatom isotope record of Late Quaternary change in Lake El'gygytgyn, North East Siberia. Quat. Sci. Rev. 29, 774–786.
Syvitski, J.P.M., Vorosmarty, C.J., Kettner, A.J., Green, P., 2005. Impact of humans on the flux of terrestrial sediment to the global coastal ocean. Science 308, 376–380.
Taniguchi, M., Burnett, W.C., Cable, J.E., Turner, J.V., 2002. Investigation of submarine groundwater discharge. Hydrol. Process. 16, 2115–2129.
Tegen, I., Kohfeld, K.E., 2006. Atmospheric transport of silicon. SCOPE 66, 81.
Tranter, M., 2005. Geochemical weathering in glacial and proglacial environments. In: Drever, J.I. (Ed.), Surface and Ground Water, Weathering, and Soils. Elsevier, London, pp. 189–205.
Tréguer, P., Nelson, D.M., Vanbennekom, A.J., DeMaster, D.J., Leynaert, A., Queguiner, B., 1995. The silica balance in the world ocean — a reestimate. Science 268, 375–379.
Tréguer, P.J., De La Rocha, C.L., 2013. The world ocean silica cycle. Annu. Rev. Mar. Sci. 5.
Upton, P., Kettner, A.J., Gomez, B., Orpin, A.R., Litchfield, N., Page, M.J., 2013. Simulating post-LGM riverine fluxes to the coastal zone: the Waipaoa River system, New Zealand. Comput. Geosci. 53, 48–57.
Vance, D., Teagle, D.A.H., Foster, G.L., 2009. Variable quaternary chemical weathering fluxes and imbalances in marine geochemical budgets. Nature 458, 493–496.
Vandevenne, F.I., Delvaux, C., Hughes, H.J., André, L., Ronchi, B., Clymans, W., Barão, L., Cornelis, J.-T., Govers, G., Meire, P., Struyf, E., 2015. Landscape cultivation alters δ^{30}Si signature in terrestrial ecosystems. Sci. Rep. 5.
Varela, D.E., Pride, C.J., Brzezinski, M.A., 2004. Biological fractionation of silicon isotopes in Southern Ocean surface waters. Glob. Biogeochem. Cycles 18.
Viers, J., Dupre, B., Gaillardet, J., 2009. Chemical composition of suspended sediments in world rivers: new insights from a new database. Sci. Total Environ. 407, 853–868.
Vigier, N., Burton, K.W., Gislason, S.R., Rogers, N.W., Duchene, S., Thomas, L., Hodge, E., Schaefer, B., 2006. The relationship between riverine U-series disequilibria and erosion rates in a basaltic terrain. Earth Planet. Sci. Lett. 249, 258–273.
von Blanckenburg, F., Bouchez, J., Ibarra, D.E., Maher, K., 2015. Stable runoff and weathering fluxes into the oceans over Quaternary climate cycles. Nat. Geosci. 8, 538–542.
Wadham, J.L., Tranter, M., Skidmore, M., Hodson, A.J., Priscu, J., Lyons, W.B., Sharp, M., Wynn, P., Jackson, M., 2010. Biogeochemical weathering under ice: size matters. Glob. Biogeochem. Cycles 24, GB3025.
Walker, J.C.G., Hays, P.B., Kasting, J.F., 1981. A negative feedback mechanism for the long-term stabilization of Earth's surface-temperature. J. Geophys. Res. Oceans Atmos. 86, 9776–9782.
Weinstein, Y., Yechieli, Y., Shalem, Y., Burnett, W.C., Swarzenski, P.W., Herut, B., 2011. What is the role of fresh groundwater and recirculated seawater in conveying nutrients to the Coastal Ocean? Environ. Sci. Technol. 45, 5195–5200.

s, A., De La Rocha, C., Amann, T., Hartmann, J., 2015. Silicon isotope composition of dissolved silica in surface waters of the Elbe Estuary and its tidal marshes. Biogeochemistry 1–19.
t, A.J., Galy, A., Bickle, M., 2005. Tectonic and climatic controls on silicate weathering. Earth Planet. Sci. Lett. 235, 211–228.
zel, F., de Souza, G.F., Reynolds, B.C., 2014. What controls silicon isotope fractionation during dissolution of diatom opal? Geochim. Cosmochim. Acta 131, 128–137.
:e, A.F., Schulz, M.S., Stonestrom, D.A., Vivit, D.V., Fitzpatrick, J., Bullen, T.D., Maher, K., Blum, A.E., 2009. Chemical weathering of a marine terrace chronosequence, Santa Cruz, California. Part II: Solute profiles, gradients and the comparisons of contemporary and long-term weathering rates. Geochim. Cosmochim. Acta 73, 2769–2803.
:e, A.F., Vivit, D.V., Schulz, M.S., Bullen, T.D., Evett, R.R., Aagarwal, J., 2012. Biogenic and pedogenic controls on Si distributions and cycling in grasslands of the Santa Cruz soil chronosequence, California. Geochim. Cosmochim. Acta 94, 72–94.
e, M., Sutton, J., Ellwood, M.J., Sambridge, M., Maher, W., Eggins, S., Kelly, M., 2010. Silicon isotopic fractionation in marine sponges: a new model for understanding silicon isotopic variations in sponges. Earth Planet. Sci. Lett. 292, 281–289.
hmeyer, A.G., De La Rocha, C.L., Maier-Reimer, E., Wolf-Gladrow, D.A., 2003. Control mechanisms for the oceanic distribution of silicon isotopes. Glob. Biogeochem. Cycles 17.
ery, T.J., Sleep, N.H., 1976. Hydrothermal circulation and geochemical flux at mid-ocean ridges. J. Geol. 249–275.
ast, R., Mackenzie, F.T., 1983. The Global Cycle of Silica. In: Aston, S.R. (Ed.), Silicon geochemistry and biochemistry. Academic Press, London, pp. 39–76.
Xiong, Z., Li, T., Algeo, T., Doering, K., Frank, M., Brzezinski, M.A., Chang, F., Opfergelt Crosta, X., Jiang, F., Wan, S., Zhai, B., 2015. The silicon isotope composition *Ethmodiscus rex* laminated diatom mats from the tropical West Pacific: implicati for silicate cycling during the Last Glacial Maximum. Paleoceanography 30 (803–823 (2015PA002793).
Yool, A., Tyrrell, T., 2003. Role of diatoms in regulating the ocean's silicon cycle. Gl Biogeochem. Cycles 17.
Yool, A., Tyrrell, T., 2005. Implications for the history of Cenozoic opal deposition fro quantitative model. Palaeogeogr. Palaeoclimatol. Palaeoecol. 218, 239–255.
Young, E.D., Galy, A., Nagahara, H., 2002. Kinetic and equilibrium mass-dependent isot fractionation laws in nature and their geochemical and cosmochemical significar Geochim. Cosmochim. Acta 66, 1095–1104.
Zambardi, T., Poitrasson, F., Corgne, A., Méheut, M., Quitté, G., Anand, M., 2013. Silicon i tope variations in the inner solar system: implications for planetary formation, difl entiation and composition. Geochim. Cosmochim. Acta 121, 67–83.
Zambardi, T., Poitrasson, F., 2011. Precise Determination of Silicon Isotopes in Silic Rock Reference Materials by MC-ICP-MS. Geostandards and Geoanalytical Resea 35, 89–99.
Ziegler, K., Chadwick, O.A., Brzezinski, M.A., Kelly, E.F., 2005a. Natural variations of δ^{3} ratios during progressive basalt weathering, Hawaiian Islands. Geochim. Cosmoch Acta 69, 4597–4610.
Ziegler, K., Chadwick, O.A., White, A.F., Brzezinski, M.A., 2005b. δ^{30}Si systematics in a g nitic saprolite, Puerto Rico. Geology 33, 817–820.